Cascade profiling of the ubiquitin-proteasome system in cancer

Anastasiia Rulina

Communauté
UNIVERSITÉ Grenoble Alpes

THÈSE

Pour obtenir le grade de
DOCTEUR DE L'UNIVERSITÉ GRENOBLE ALPES
Spécialité : **Biodiversite du Developpement Oncogenese**
Arrêté ministériel : 7 août 2006

Présentée par
Anastasiia Rulina

Thèse dirigée par **Maxim Balakirev**

préparée au sein du **Laboratoire BIOMICS**
dans **l'École Doctorale Chimie et Sciences du Vivant**

Profilage en cascade du système ubiquitine-protéasome dans le cancer

Thèse soutenue publiquement le **«17/12/2015»**,
devant le jury composé de :
M. Damien ARNOULT
Docteur CR1, CNRS, Rapporteur
M. Matthias NEES
Professor Adjunct, University of Turku, Rapporteur
M. Philippe SOUBEYRAN
Docteur, INSERM, Membre
Mme. Jadwiga CHROBOCZEK
Directeur de recherche DR1, CNRS, Membre
M. Xavier GIDROL
Directeur de laboratoire, CEA, Président du jury
M. Maxim BALAKIREV
Docteur, CEA, Membre, Directeur de Thèse

Я посвящаю эту научную работу моей маме, Рулиной Людмиле Михайловне, с любовью и благодарностью.

Мне всегда везло с людьми, которые давали мне вдохновение и любовь для занятий биологией, но именно ты заложила во мне те качества, которые помогли мне пройти весь путь от начала и до конца. И Именно твоя поддержка, в любых моих начинаниях давали мне ощущение «твердой земли под ногами».

ACKNOWLEDGEMENTS

First and foremost, I would like to thank my supervisor, **Maxim Balakirev** for guiding me throughout the thesis. Your expertise and endless enthusiasm helped me to work on this complicated subject. During these 3 years you were always there to discuss and share experience, and I hope I have learned the most I could from you.

I would like to express gratitude to all the members of the laboratory, who helped me with the technical part of my thesis. Thank you to **Patricia Obeid** for introducing me to siRNA screens, as well as for data acquisition and analysis. It was a great pleasure and luck for me to work with such a hard-working, experienced and enthusiastic person. **Laurent Guyon**, thank you for your job! Your deep and comprehensive data analysis was just priceless for this dissertation. I would also like to thank **Frederic Mittler** for cell culture, recent Western Blots and IF; **Sophie Gerbaud** for performing EdU tests and recent IF images; **Frederic Kermarreck** for qPCRs; **Eric Sulpice** for helping with FACS analysis. Also I want to show my appreciation to **Amandine Pitaval** for explaining immunofluorescence microscopy to me and to **Vincent Haguet** for performing Wound Healing Assay. I am grateful to the members of my "Comité de suivi de thèse" - **Jadwiga Chroboczek** and **François Berger** for their time and useful advice in the course of the project.

I would like to say "merci" to **Nicole Assard**. It was a pleasure to share working space with you! I appreciate so much your friendliness and positive attitude, as well as accuracy and professionalism. Thanks to the **Eric Sulpice and Stephanie Combe's** team for moral support and useful advice about science and personal life. I am also grateful to our wonderful secretary, **Patricia Leclyese** for helping with the millions of administrative questions I had.

I would like to thank **my mother** – you have always been a constant source of support. Thanks to all **my friends in Grenoble** for all the good days we spent together – without you it would be so boring here! Special thanks to **Dolega Monika, Brasouskaya Daria, Fefelova Anastasiia, Ilaria Vitulano** and **Komarynets Olga** for the best support during these times. Thank you, **Arnaud Lemelle** for all the loving, patience and care you give me.

MOTIVATION AND CONTEXT

According to the American Cancer Society, the prostate cancer (PCa) is the most frequent malignancy in men. After lung cancer, the PCa is the second leading oncological cause of death. Despite many years of research, the main current treatments are still surgery, radiation and androgen deprivation therapy. The androgen ablation ultimately leads to the development of a more advanced, hormone-refractory (castration-resistant) form of prostate cancer, which responds poorly to standard chemotherapy and is considered to be terminal. It is evident that there is an urgent need for the discovery of alternative targets and the development of new therapeutic approaches for prostate cancer treatment.

The design of new therapeutic agents against prostate cancer depends critically on our knowledge of the molecular mechanisms of cancer origin and progression. In 2007 the term “non-oncogene addiction” was proposed by Elledge and co-authors to explain the increased dependency of cancer cells on the function of normal genes. The phenomenon is based on increased cellular stresses experienced by cancer cells (mitotic, proteotoxic, metabolic, etc.), making them more dependent on stress support systems. Among these, the ubiquitin-proteasome system (UPS), as a major mediator of key cellular functions, represents a perfect model for a loss-of-function screen to search for potential drug targets based on non-oncogene addiction.

This work was carried out in the Biomics laboratory, which is specialized in functional genome-wide screens and biomarker discovery targeting prostate cancer. In the course of the project, we applied a novel systematic approach to the loss-of-function screen of the UPS. Our strategy was to employ the cascade organization of the UPS and its hierarchical mode of function. Compared to standard genome-wide screens, this "cascade profiling" results in a rather compact and more targeted screen, which facilitates hits identification. Using this approach we have identified components of UPS potentially important for prostate cancer cell viability.

LIST OF ABBREVIATIONS

2D/3D – two dimensional/three dimensional
7-AAD – 7-Aminoactinomycin D
a.a. – amino acid
ADAMs – A-disintegrin-and-metalloproteinases
AIDS – acquired immune deficiency syndrome
AJs – adherens junctions
AKT – v-Akt murine thymoma viral oncogene homolog 1
AMACR - alpha-methylacyl-coa racemase
AR – androgen receptor
ATCC - American Type Culture Collection
ATG12 – autophagy 12
ATG8 – autophagy 8
ATM – ataxia telangiectasia mutated
bp – base pair
BPH – benign prostatic hyperplasia
BRCA – breast cancer
BSA – bovine serum albumin
CAND1 – cullin-associated and neddylation-dissociated 1
Caspase – cysteine-aspartic proteases
CHD1 – chromodomain helicase DNA binding protein 1
ChSM – DMEM supplemented with the charcoal/dextran stripped FBS
c-Myc – v-Myc avian myelocytomatosis viral oncogene homolog
COP1 – constitutive photomorphogenesis protein 1 homolog
CR – castration resistant
CRL – Cullin-RING-Ligase
CUL1-7 – cullins 1-7
DAPI – 4'6-diamidino-2-phenylindole
DDR – DNA-damage response
DHT - 5α-dihydrotestosterone
DMEM – Dulbecco's Modified Eagle's Medium
DMSO – dimethyl sulfoxide
DNA – deoxyribonucleic acid
DSB – double stranded breaks
dsRNA – double-stranded RNA
DUB – deubiquitylating enzyme
E1 – ubiquitin-activating enzymes
E2 – ubiquitin-conjugating enzymes
E3 – ubiquitin-protein ligases
EdU – 5'-ethyl-2'-deoxyuridine
EGFR – epidermal growth factor receptor
EMT – epithelial-to-mesenchymal transition
ERG – ETS-related gene
ETS – v-Ets avian erythroblastosis virus E26 oncogene homolog 1
ETV1-5 - Ets variants 1-5
FACS – fluorescent activated cell sorting
FAK – focal adhesion kinase
FAs – focal adhesions
FAT10 – HLA-F adjacent transcript 10
FAU – Finkel-Biskis-Reilly murine sarcoma virus (FBR-MuSV) ubiquitously expressed
FBS – fetal bovine serum
GS – Gleason Score
gSD – global Standard Deviation
HIF1α – hypoxia-inducible factor-1 alpha
IRS-1 - insulin receptor substrate 1
ISG15 – interferon-stimulated gene product of 15 kDa
IκB – inhibitor of NF-κB
LAP – leukemia associated protein
Lys – lysine
MDM2 – mouse double minute 2, human homolog of; p53-binding protein

miRNA – micro RNA
mRNA – messenger RNA
MSMB – microseminoprotein, Beta-
MW – molecular weight
NAE – NEDD8 activating enzyme E1 subunit 1
NEDD8 – neural precursor cell expressed, developmentally down-regulated 8
NF-κB – nuclear factor kappa B
NKX3-1 – NK3 Homeobox 1
nt – nucleotide
Opti-MEM – reduced serum modification of eagle's minimum essential media
p21 – cyclin-dependent kinase inhibitor 1A
p27 – cyclin-dependent kinase inhibitor P27
p53 – tumor protein p53
PBS – phosphate buffered saline
PBS – phosphate-buffered saline
PCa – prostate cancer
PCA3 – prostate cancer antigen 3
PDGFRβ – platelet-derived growth factor receptor, beta polypeptide
PFA – paraformaldehyde
PHD – plant homeo domain
PI3K – phosphoinositide 3-kinase
PIN – prostatic intraepithelial neoplasia
PSA – prostate specific antigen
PSMA – prostate-specific membrane antigen
PTEN – phosphatase and tensin homolog
Rb – retinoblastoma 1
RBR – ring between ring
RBX1/2 - RING-box 1/2, E3 Ubiquitin Protein Ligase
RdRP – RNA-dependent RNA-polymerase
RING – Really Interesting New Gene
RISC – RNA-induced silencing complex
RLC – RISC loading complex
RNA – ribonucleic acid
RNAi – RNA interference
siRNA – small interfering RNA
SPOP – speckle-type POZ protein
StdM – DMEM supplemented with standard FBS
SUMO – small ubiquitin-like modifier
TGFβ – transforming growth factor beta
TICs – tumor-initiating cells
TJs – tight junctions
TMPRSS2 – transmembrane protease, serine 2
TMPRSS2:ERG – genetic fusion of TMPRSS2 and ERG genes
Ub – Ubiquitin
UFM1 – ubiquitin-fold modifier 1
ULM – Ubiquitin-like modifiers
UPS – Ubiquitin-proteasome system
URM1 – for ubiquitin-related modifier 1
UTR – untranslated region
WB – Western Blot
Wnt – wingless-type MMTV integration site family

TABLE OF CONTENT

LITERATURE REVIEW

CHAPTER 1. PROSTATE CANCER

While in developing countries respiratory infections and AIDS are the most mortal diseases, in developed countries, medicine and technology allow people to overcome these health problems and live longer, which make heart disease and cancer the leading causes of death (http://www.who.int/). Prostate cancer (PCa) is the most often diagnosed malignancy (1 in 6 men is diagnosed with PCa during their lifetime) and the second leading cause of death from cancers (Jemal *et al*., 2011; Siegel *et al*., 2012; Stewart & Wild, 2014). Despite high incidence of PCa, the prognosis is usually positive – only 1 of 100 men will have progression to an aggressive form during the 5 years following diagnosis, and the best treatment option in this case – is watchful waiting. Nevertheless, in some patients PCa progresses to terminal disease with extremely fast metastasis that requires intensive therapy. Apart from that, current treatment options (radio-, chemo- and androgen-deprivation therapy) ultimately lead to the development of more advanced forms of prostate cancer - castration-resistant and metastatic PCa. Metastatic cancer is considered to be incurable and only 1/3 of patients with metastatic PCa survives the 5 years following diagnosis. Better understanding of prostate cancer biology would allow clinicians to distinguish relatively indolent forms of prostate cancer from aggressive ones. In our research we are searching for proteins involved in the viability of prostate cancer cells thus giving an insight in prostate cancer biology. In this chapter I describe: (I) epidemiology of prostate cancer, (II) major biomarkers that clinicians currently use to determine disease stage and prognosis, and (III) the prevalent mutation in prostate cancer, TMPRSS:ERG, and its influence on prostate cancer development.

1.1 STRUCTURE AND FUNCTION OF PROSTATE

The prostate is a little (3 cm diameter, about 20 grams) auxiliary exocrine gland of the male reproductive system located in the anteroinferior part of the pelvis where it encloses the urethra and bladder neck. An adult human prostate consists of 3 concentric zones (transition/periurethral, central, peripheral), and an anterior fibro-muscular zone (Figure 1). The majority of cancers are found in the peripheral zone of the prostate, the transition zone in the second place, and almost none in the central zone (De Marzo *et al*.,

2007). In contrast, benign prostatic hyperplasia (BPH), a common nonmalignant condition found in older men, arises mostly from the transition zone. The prostate is both a glandular and muscular body. About a half of the volume of the prostate is taken up by 30-50 small glands (usually thin branching tubules), forming wedge-shaped slices draining into the urethra. The second half of the gland is distributed evenly between fibro-elastic stroma and randomly orientated smooth muscle bundles that help expel semen during ejaculation and form the involuntary urethral sphincter (Shen & Abate-Shen C., 2010).

At the histological level, the glandular epithelium of the prostate is mainly pseudostratified, comprising tall columnar luminal cells, basal and neuroendocrine cells. Tall columnar cells express high levels of androgen receptor (AR), and are responsible for the secretory functions of the prostate. They are controlled by the endocrine system and respond by the production of unique complex of secretions involved in the fertilization of the egg. Basal cells, comprising about 10% of prostatic epithelium, are almost devoid of secretory products. They lie on the basal membrane and are wedged between columnar cells. It is believed that these cells function as stem cells and are ancestors of luminal cells (Merk *et al.*, 1982; Shen & Abate-Shen, 2010). Finally, neuroendocrine cells are singular cells producing growth-support secretions (Davis, 1987; Abrahamsson & Lilja, 1989).

There is a large variety of types of sensory nerve receptors in the prostate: Vater-Pacini corpuscles (lamellar bodies), Krause's end bulb, etc. An extensive network of nerve ganglia and nodes around the prostate is so large that relatively small pathological changes often lead to severe disorder. Nerve fibers are connected with other nerves of the pelvic organs, primarily with the bladder, seminal vesicles, rectum, vas deferens, and corpus cavernosum. The close interweaving of the pelvic nerves may facilitate the transmission of stimuli (e.g., inflammation) to other pelvic organs. Because of this effect, various disorders of pelvic organs often induce uniform symptoms (Molochkov & Ilyin, 1998).

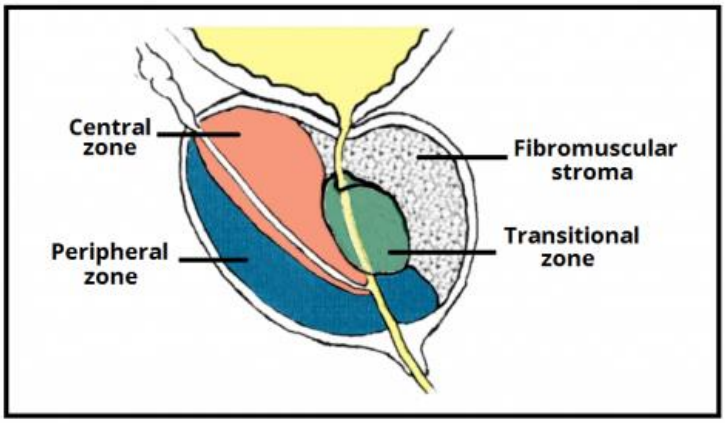

Figure 1. Structure of the prostate. http://teachmeanatomy.info/pelvis/the-male-reproductive-system/prostate-gland/

1.2 EPIDEMIOLOGY OF PROSTATE CANCER

The main risk factors for the development of prostate cancer are: aging, family history, race (for African-Americans this type of cancer is diagnosed more frequently and more often leads to death), hormonal changes, genetic mutations and lifestyle (Reiter & de Kernion, 2002). The prevalent form (95%) of prostate cancer is adenocarcinoma originating from columnal cells in the acini and glandular part of the ducts. Other categories of prostate cancer – such as ductal adenocarcinoma, mucinous carcinoma, and signet ring carcinoma – are extremely rare.

As it was mentioned before, PCa is one of the most often diagnosed malignancies in men. Since the introduction of prostate specific antigen (PSA) screening, the rates of prostate cancer mortality and incidence began to stabilize and then decline since 1990s. PCa incidence decreases 2.4% per year, and the number of PCa-related deaths declines by 3.4% per year (Figure 2). Despite high incidence of this type of cancer, the prognosis is usually positive: PCa is usually confined within the gland and progresses slowly. The percentage of patients surviving 5 years comprises 98.9% (Edwards *et al*., 2014). Nonetheless, long-term survival is not as good, because the main treatments often lead to the development of highly aggressive metastatic form of PCa (Elledge, 2010).

The clinical course of localized untreated prostate cancer is still unclear. Progression of the disease to the metastatic form within 10-15 years following diagnosis is not frequent (5% of all PCa cases according to American Cancer Society), but the further follow-up has shown that even primarily indolent localized prostate cancer can proceed to a more aggressive form, invading surrounding tissues and giving metastases in the lymph nodes and the bones as the major sites (McNeal JE, 1992). To prevent

overtreatment, it is necessary to understand the prolonged natural history of the disease (McNeal, 1969; McNeal, 1992; Johansson *et al*., 2004; Shen MM & Abate-Shen C., 2010).

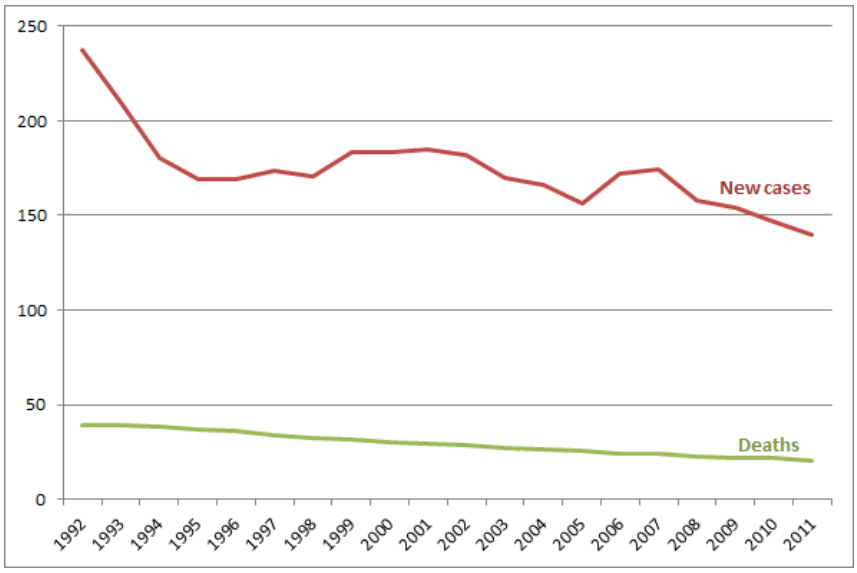

Figure 2. Number of new cases and deaths from prostate cancer per 100,000. Figure from Edwards *et al*., 2014

Therapeutic decisions based on correct diagnosis and accurate staging of prostate cancer is critically important for the fate of the patient. Early diagnosis of prostate cancer includes three main options: (1) measurement of PSA in blood, (2) digital rectal examination and (3) ultrasound-guided transrectal biopsy of the prostate with further immunostaining for specific markers (anti-p63, cytokeratin 5 and 14). The most important prognosis factors are the initial (pre-therapeutic) level of total serum PSA and the Gleason score (G2-G10, discussed below in more details). Patients are also diagnosed by the status of their primary tumors, from organ-confined to fully invasive (T1–T4), with or without lymph node involvement (N0 or N1), and the presence and degree of distant metastases (M0 and M1a–c). Prostate cancer is often preceded by a stage of pre-cancer, and timely identification of this condition significantly helps to determine prognosis and treatment. To date, Prostatic Intraepithelial Neoplasia (PIN) remains as the only well-proven preneoplastic condition with clinical significance (Armah & Parwani1, 2008; Shen & Abate-Shen, 2010).

For early diagnosed organ-confined prostate cancer current treatment options include watchful waiting, surgery (radical prostatectomy) and radiotherapy - external or brachytherapy (implantation of radioactive “seeds”). This type of PCa is curable with very good survival and cure rates, but the disease relapses in approximately 25% of patients. Nevertheless, choice of treatment option is very questionable – localized cancer

rarely progresses to a fatal form and some patients receive overtreatment while others die during prostatectomy. For more malignant forms, combined therapy regimens (brachytherapy, hormone therapy and chemotherapy) are applied specifically according to the disease's stage, patient's age and personal choice. In the case of advanced cancer, these regimens are usually followed or substituted by androgen deprivation therapy (chemical or surgical castration), which initially will reduce tumor burden, but inevitably leads to the development of a more destructive form of prostate cancer - androgen-independent (or castration-resistant, CR-PCa) prostate cancer (Bardan *et al*., 2007; Shen & Abate-Shen, 2010). This recurrent disease has a median survival rate of less than 2 years. For CR prostate cancer, the only approved therapy is with docetaxel and provides a modest survival benefit of 2 to 3 months.

To explain the emergence of CR-cancer, Isaacs and Coffey proposed that androgen withdrawal results in the natural selection of the androgen-refractory cells initially present in heterogeneous prostate tumor (Isaacs & Coffey, 1981). Indeed, several observations suggest that prostate tumor-initiating cells (TICs) do not express androgen receptor (AR) (Gu *et al.*, 2007; Kasper, 2009). In addition, prostate neuroendocrine cells, which have been implicated in CR-PCa, are androgen-independent (Cindolo *et al.*, 2007). Despite this evidence, however, it is widely established that in the majority of CR tumors, AR remains the key driver of cancer progression. Notably, castration-resistant tumors express AR as well as AR target genes such as PSA, indicating that pathway activity is intact (Gregory *et al.*, 1998). Androgen ablation has been shown to select for TIC clones with aberrant, androgen-independent AR signaling (Wang & Shen, 2011). This arises through a variety of mechanisms, including mutations that change AR function, inactivation of tumor suppressors, activation of oncogenes, increase in autocrine stimulation, and rearrangement of cell signaling pathways (Knudsen & Penning, 2010; Feldman & Feldman, 2001). As a result, in CR malignant cells, AR executes a transcriptional program distinct from that in androgen-responsive cells resulting in increased cell survival and androgen-independent growth (Wang *et al.*, 2009).

It should be noted that in more than 50% of metastatic prostate tumors AR is not mutated (Heinlein & Chang, 2004; Knudsen & Penning, 2010). This suggests that the aberrant function of AR in androgen-refractory cells results mainly from the changed cellular context, i.e. a variety of cellular factors, which define and complement AR activity in CR prostate cancer. Comparative genomic analysis of prostate cancer, CR tumors and normal prostate cells has revealed numerous genetic alterations and abnormal

gene expression profiles in cancer cells (Varambally *et al*, 2005; Taylor *et al*, 2010; Berger *et al*, 2011). However, though very valuable for cancer classification and prognosis, genomic data tell less about molecular mechanisms of prostate cancer progression. A complete understanding of cancer biology requires knowledge of principal actors regulating protein interactions and activities.

1.3 SIGNIFICANT PROGNOSTIC FACTORS

2.3.1 Gleason score

To assess the prognosis of patients, clinicians use Gleason Score based on the architecture of the prostate glands and the relationship between the tumor cells and the surrounding stromal tissue. The Gleason grading system has five levels of tumor progression, grade 1 being the least aggressive, while grade 5 is the most anaplastic. Usually, prostate tumors are not homogenous. Gleason Score is a sum of Gleason grades of the two most typical tumor samples. Thus, it can range from 2 (1 +1) to 10 (5 +5) (Bardan *et al*., 2007).

In general, the higher the Gleason Score, the more "malignant" the tumor is. However, this rule should be used wisely. Generally, the patients with GS $\geq$ 7 means a greater risk for the patient and that it should be treated intensively. Nevertheless, some studies using surrogate end points have shown that the prognosis of GS 7 cancers varies considerably (Stark *et al*., 2009). On the other hand, tumors with GS below 4 are considered to be indolent and almost never progress to the advanced stage, thus the best treatment option in this case – local therapy and watchful waiting. However, after universal introduction of routine PSA diagnostics, it became clear that small fraction of these “indolent” tumors could progress rapidly and require immediate treatment. Consequently, the major clinical challenge is the current inability to readily distinguish between indolent and aggressive tumors in prostate cancer patients with a low Gleason Score (Shen & Abate-Shen, 2010).

2.3.2 Prostate specific antigen

PSA is an organ-specific marker produced by a healthy prostate, and released into the blood only in the case of impairment of normal prostate architecture (Lilja *et al*., 2008). Thus, while the blood PSA is not a sign of a certain disease or condition, its increased level can indicate the presence of a destructive disease, such as adenoma or

tumor. This helps to diagnose and monitor PCa progression. PSA in blood serum exists in three forms: free, associated with either α-1-antichymotrypsin or with α-2-macroglobulin. Two forms of PSA are routinely used in diagnostics: free and α-1-antichymotrypsin-binded, which add up to a "total PSA". In healthy conditions, PSA is present in serum at a very low level, which is age-dependent:

40-49 years - 2.5 ng/ml

50-59 years - 3.5 ng/ml

60-69 years - 4.5 ng/ml

Over 70 years - 6.5 ng/ml

Nevertheless, it has been shown that some PCa cases can exist at normal level of PSA (Thompson *et al*., 2004). Men with increased PSA level (10 ng/ml) are recommended for prostate biopsy to verify the presence of cancer. To make a decision about biopsy in these cases, when serum PSA level is below 10 ng/ml, the ratio of free PSA to total PSA becomes crucial: prostate cancer was shown to be associated with the formation of protein-bound PSA. “PSA velocity” (the rate of PSA increase) and PSA density (the ratio of PSA to prostate volume) are also important prognostic factors (Carter, 2006).

2.3.2 Other potential biomarkers

Routine PSA screening provides a 20% mortality reduction, because it helps in early detection of clinically unapparent, localized tumors with a low GS. However, the clinical course of localized untreated prostate cancer is still unclear. Progression to the metastatic form in 10-15 years following diagnosis is not frequent, but a further follow-up has shown that even primarily indolent localized prostate cancer can proceed to a more aggressive form. To prevent overtreatment, it is necessary to understand the prolonged natural history of the disease. In order to improve specificity and sensitivity of detection, many efforts are being made to identify novel biomarkers. Some of them are already at early stages of development and are being evaluated in clinical trials (Duskova & Vesely, 2014). Examples of such biomarkers are PCA3, PSMA, AMACR, MSMB, etc. One of the promising urine biomarkers is TMPRSS2:ERG fusion transcripts. In contrast to PSA, which often gives false-negative and false-positive results, TMPRSS2:ERG appears only in malignant conditions, which greatly increases the specificity of the test. Some other researchers show the efficiency of a multiplexed approach, where the set of markers is followed simultaneously that make detection more sensitive and specific. These

prominent results could be adjusted for clinical use and would increase the efficiency of routing testing for prostate cancer (Rubin, 2012).

1.4 REARRANGMENTS OF ETS (E26 TRANSFORMATION SPECIFIC) TRANSCRIPTION FACTORS

Localized prostate cancer usually contains histologically and genetically distinct areas and thus is regarded as multifocal malignancy. In contrast, despite phenotypical differences of metastases in diverse sites, genomic analysis demonstrates their clonal origin. During the last few decades, there has been an accumulation of data on molecular alterations in PCa, shedding light on the mechanisms of prostate cancer initiation and progression. The frequent characteristic mutations have been identified, which include: (1) ETS-rearrangements found in more than half of prostate cancer cases (discussed in details below); (2) mutations of SPOP component of cullin-RING E3 Ub-ligase complex, which are present in up to 15 % of PCa cases; (3) deletion of CHD1 gene (substrate recognition component of the transcription regulatory histone acetylation complex SAGA) found in up to 15 % of PCa cases. There are also some other less frequent mutations/deletions/rearrangements involving PTEN, AR, NKX3-1, p27, p53, Rb and etc. (Tomlins *et al.*, 2005; Shen & Abate-Shen, 2010; Yoshimoto *et al*, 2012; Wyatt *et al.*, 2014; Yadav *et al.*, 2015).

The ETS (E26 transformation-specific) family of transcription factors includes 30 proteins unified by the presence of evolutionarily-conserved ETS domain responsible for DNA binding. Also, they contain an N-terminal regulatory domain. The ETS family of proteins participates in the regulation of many key cellular processes including proliferation, differentiation and apoptosis. In prostate cancer, rearrangements that activate ERG, ETV1, ETV4 and ETV5 members of the ETS family have been identified (John *et al*., 2012; Kumar-Sinha *et al.*, 2008; Tomlins *et al.*, 2005; Tomlins *et al.*, 2007b). The most frequently rearranged gene in prostate cancer is ERG (ETS related gene) (Tomlins *et al*., 2005). Under normal conditions ERG is constitutively expressed in endothelial cells where it regulates angiogenesis and endothelial apoptosis by affecting expression of many genes, including eNOS, HO-1, ICAM-2, VE-cadherin, von Willebrand's Factor, etc. (Birdsey *et al*., 2008; Nikolova-Krstevski *et al*., 2009). The major ETS translocation in PCa is TMPRSS2:ERG. TMPRSS2 is a prostate specific, androgen responsive transmembrane serine protease (Figure 3). TMPRSS2:ERG fusion leads to the ERG expression under control of androgen sensitive promoter elements of

TMPRSS2 (St John *et al*., 2012). There are multiple other 5' fusion partners of the ETS family in PCa (Figure 3).

Interestingly, these chromosomal rearrangements may be caused by AR function. Studies in androgen-responsive LNCaP cells have shown that AR binding induces chromosomal proximity between the TMPRSS2 and ERG loci that can lead, upon DNA damage, to the formation of TMPRSS2:ERG fusions. In addition, androgen signaling recruits topoisomerase II to AR-binding sites, leading to the induction of double-stranded breaks even in the absence of genotoxic stress (Shen MM & Abate-Shen C, 2010). Thus, ETS fusions could be induced in cells, which, initially, do not harbor these translocations. Combined treatment of prostate cancer LNCaP cells or non-cancerous PNT2 cells with DHT and γ-irradiation leads to the appearance of cells with ETS rearrangements (Lin *et al*., 2009; Mani *et al*., 2009; Bastus *et al*., 2010; Chiu *et al*., 2012). Unfortunately, the fate of these cells has not been followed, and there is no data on whether this rearrangement gives some survival advantages to the cells.

TMPRSS2:ERG is most likely a driver mutation in prostate cancer. The first piece of evidence is the enrichment of this translocation during cancer progression. TMPRSS2:ERG fusion is found only in 20% of prostatic intraepithelial neoplasia (PIN) lesions (Tomlins *et al.*, 2008), and in up to 50% of confined cancers (Taylor *et al*., 2010), suggesting that this rearrangement is often acquired after cancer initiation, or, instead, it is an early event in cancer development and predisposes cells to progression to malignant state (Tomlins *et al*., 2005). The second piece of evidence comes from molecular biology: the appearance of this translocation in prostatic cells results in overproduction of various N-truncated ERG isoforms (Figure 4). ERG, in its turn, causes transcriptional activation of oncogenic pathways including Wnt/β-catenin, NF-κB, c-MYC and disruption of AR-dependent signaling (Birdsey *et al*., 2015; Yu *et al*., 2010; Sun *et al*., 2008; Wang *et al*., 2011). This could lead to the development of PIN but is not sufficient to produce invasive adenocarcinoma (Klezovitch *et al*., Tomlins *et al*., 2008; Zong *et al*., 2009). Additional factors (e.g., AKT activation, enhanced AR signaling and PTEN loss resulting in aberrant phosphoinositide 3-kinase (PI3K) pathway) are required for the development of prostate cancer (Carver *et al*., 2009; Sowalsky *et al*., 2013; Krohn *et al*., 2014).

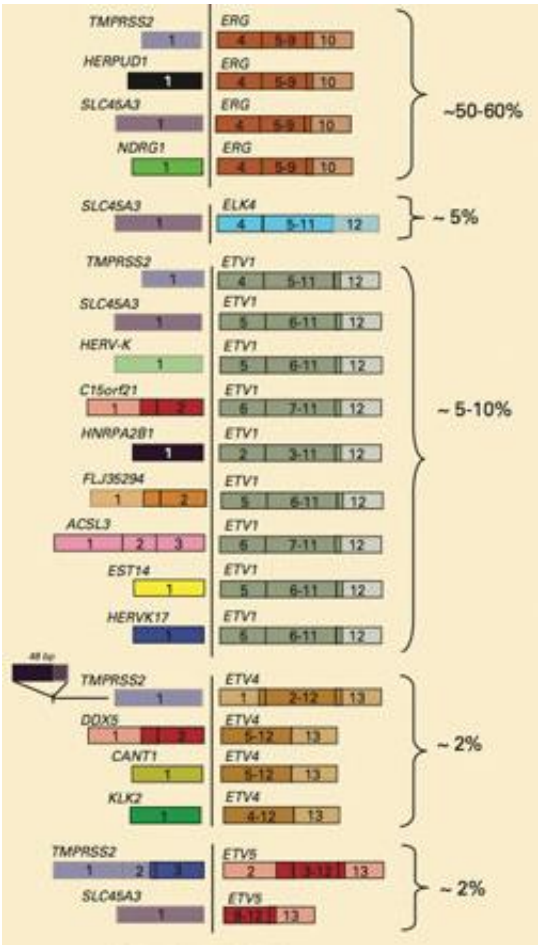

Figure 3. ETS rearrangements. This diagram represents all published ETS-fusions grouped by ETS members. http://oncofusion.com/pipelines/erg-inhibitors/

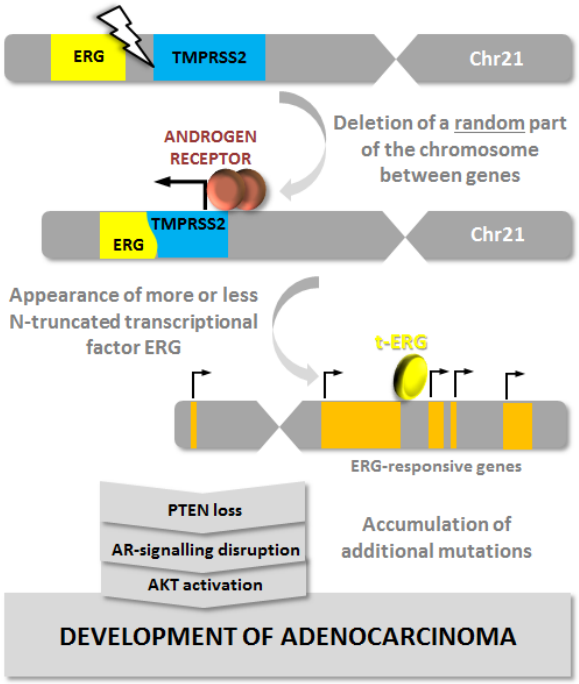

Figure 4. ETS fusions in prostate cancer. Fusion places transcriptional factor ERG (or any other ETS family member, i.e. ETV1, ETV4, and ETV5) under the control of AR-responsive promoter that results in overproduction of more or less N-truncated ERG protein. ERG, in its turn, activates its own transcriptional program. Acquisition of additional mutations (e.g., loss of PTEN) leads to the development of prostate cancer.

The third piece of evidence comes from follow-up studies. Most studies following the natural history of the disease show strong correlation between the presence of TMPRSS2:ERG fusion and cancer progression to more aggressive forms, metastases and a reduced survival rate (Demichelis *et al*., 2007; Attard *et al*., 2008; Hägglöf *et al*., 2014; Berg *et al*., 2014). Interestingly, expression of ERG protein has been shown to correlate with markers previously associated with bad prognosis, such as PDGFRβ, hyaluronan, Caveolin-1 and von Willebrand factor (Hägglöf *et al*., 2014). Unfortunately, none of these studies addressed the clinical outcome of different TMPRSS2:ERG isoforms, while in *in vivo* cancer models different isoforms were shown to have antagonistic behavior (Rastogi *et al*., 2014). However, the T1E4 isoform (fusion of 1st exon of TMPRSS2 with 4th exon of ERG) seems to be the most frequent and clinically relevant. A study, published in 2011 by Markert and colleagues, takes into account several molecular signatures, including TMPRSS2:ERG, and shows that the presence of this translocation is associated with poor prognosis, even though the most aggressive phenotype is defined as stem cell-like with P53−/PTEN− genotype (Markert *et al*., 2011).

High incidence of these gene fusions in prostate cancer and their cancer-driving behavior makes them attractive drug targets. However, direct inhibition of ERG protein does not give expected results: inhibition of ERG expression in VCaP cells diminishes invasiveness, but has no effect on the viability of the cells (Tomlins *et al*., 2008). Another study on VCaPs has shown a slight decrease of cell proliferation under ERG-deprived conditions, but only where a high concentration of siRNA was used (starting from 50 nM), despite that the decrease of ERG protein level starts from 2.5 nM concentration (Urbinati *et al*., 2015). Thus, this effect on viability could be due to some off-target effects. Hence, targeted therapy might benefit from using pathways altered in ERG-expression tumors (Chatterjee *et al*., 2015; Mancarella *et al*., 2015) or identification of ERG-specific non-oncogene addiction.

CHAPTER 2. UBIQUITIN-PROTEASOME SYSTEM (UPS)

In this thesis we describe siRNA screening of the ubiquitin-proteasome system (UPS) and ubiquitin-like modifiers (ULMs) pathways to identify individual components required for the functioning of PCa cells. We chose to investigate UPS and ULMs pathways because of the previous success of proteasome inhibitors in the treatment of tumors. It should be noted, that despite the documented anti-cancer effect, proteasome inhibition is generally toxic and, thus, may be detrimental for healthy cells. We wanted to benefit from targeting individual components of UPS or ULM, which could make therapy more selective toward tumor cells. Our screens and subsequent validation experiments using a small molecule inhibitor of neddylation revealed that the inhibition of the components of the CRL/NEDD8 pathway can have a complex outcome on the viability of PCa cells. In this chapter I describe the organization and function of the UPS, and of the CRL/NEDD8 pathway as a part of the UPS.

2.1 UBIQUITIN AND UBIQUITIN-LIKE MODIFIERS

It has been estimated that bacteria with an average genome size of few thousands genes produces about 250,000 individual proteins packed so tight that the space between them does not exceed a few molecules of water. Most likely, the eukaryotic cell has more or less the same level of compaction (Petsko & Ringe, 2004). The cell interior is extremely crowded, but also very mobile: the proteins are separated into different compartments and organelles with permanent exchange between them. Complexity is increased by a flow of newly synthesized proteins and their constant degradation. In such a crowded and mobile environment, precise regulation of protein function is essential to avoid chaos. Protein function *in vivo* can be regulated at transcriptional level via control of gene expression. Other levels of control include regulation of translation, post-translational modification, localization of the protein, covalent or noncovalent binding of effector molecules, and the lifetime of the active protein (Petsko & Ringe, 2004; Cooper, 2000).

Although it was known that, despite the exergonic nature of peptide-bond cleavage protein, degradation is energy-dependent and proteins have different life-time, for many decades protein degradation was believed to be non-specific and thus was never

really studied (Ravid & Hochstrasser, 2008). At that time lysosome-mediated protein degradation was the only pathway known, in accordance with this paradigm. The discovery of the ubiquitin-proteasome system made a revolution and was awarded by the Nobel Prize in Chemistry in 2004. Specific labeling of intracellular proteins, by small protein ubiquitin (Ub), which targets them for degradation by a multienzymatic complex called the proteasome, was identified as the main function of this system. Later it was shown that ubiquitination also has regulatory functions and does not necessarily lead to the degradation of proteins (Glickman & Ciechanover, 2002; Herrmann *et al*., 2007). Ubiquitin, a highly conserved, 76-amino acid protein, is ubiquitously present in eukaryotes, but absent in the Eubacteria and the Archaea. Characterization of ubiquitin was followed by the discovery that it is a member of a group of protein tags, which share similar structure and mechanism of attachment. Ubiquitin and Ubiquitin-Like Modifiers (ULMs) have a similar three-dimensional core structure, the β-grasp fold, but otherwise are distinct (Figure 5). There are 17 known ubiquitin-like proteins (UBLs) belonging to nine phylogenetically distinct classes (Table 1): NEDD8 (RUB for bacteria and plants), SUMO (for small ubiquitin-like modifier), ATG8 (for autophagy 8) and ATG12, Ufm1 (for ubiquitin-fold modifier1), URM1 (for ubiquitin-related modifier 1), ISG15 (interferon-stimulated gene product of 15 kDa), FAT10 (HLA-F adjacent transcript 10), FAU and a diverse assortment of proteins which harbor structurally related folds fused translationally to other domains (Watson *et al.*, 2011; Hochstrasser, 2009; Vierstra, 2012).

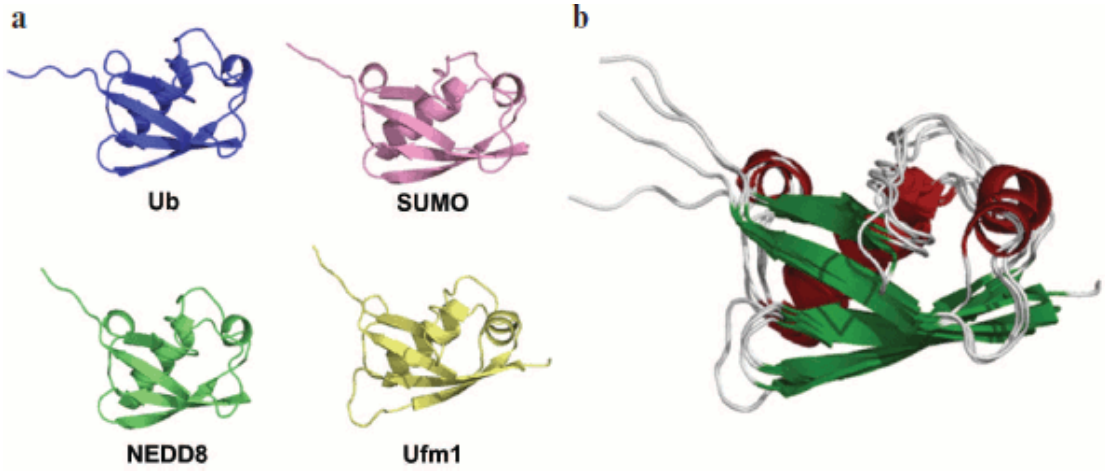

Figure 5. Characteristic ubiquitin-fold. a. Ribbon representation of 3D fold of Ub and ULMs. b. Superposition of their 3D-folds. Figure from Sorokin at al., 2009

Table 1. Known ULMs (modified figure from Hochstrasser, 2009). E1 and E2 - enzymes, involved in modification of proteins with a given modifier: E1 – Ub-activating enzyme, E2 – Ub-conjugase (discussed in details below in 2.2 UPS MACHINERY)

Modifier	Identity with Ub (%)	E1	E2	Roles
Ub	100	UBA1 & UBA6	>30	Multiple, including protein homeostasis, cell receptor signaling, endocytic trafficking, transcriptional regulation and cell cycle progression
NEDD8	59	Uba3/NAE1	UBE2M & UBE2F	Activation of cullin-based E3s
SUMO	18	SAE1/UBA2	Ubc9	Multiple, including protein stability and localization, transcriptional regulation and cell cycle progression
Atg12	5	Atg7	Atg10	ATG5–ATG12 conjugate forms complex with ATG16 that functions as an E3 ligase for autophagic vesicle formation
Atg8	8	Atg7	Atg3	Autophagic vesicle formation
Urm1	~0	UBA4 dimer	–	Antioxidant pathways; tRNA uracil thiolation
ISG15	32/37	UBA7	UBE2H	Antiviral functions; possibly cell growth and differentiation
UFM1	14	UBA5 dimer	UFC1	Unknown
FAU	38	–	–	Regulation of immune response
FAT10	32/40	Uba6	USE1	Antiviral functions

2.2 UPS MACHINERY

Ubiquitin and ULM became attached to target molecule in multistep reaction. More time will be given to the description of the machinery and organization of the ubiquitin-ligation pathway, but the principles are the same for other modifiers.

Ubiquitin is conjugated to target proteins by the formation of an iso-peptide bond between the C-terminal carboxyl group of ubiquitin and a lysine side-chain of the target protein. Ub can also be attached by peptide bond to the N-terminus of the protein. This process, termed ubiquitylation, occurs through a cascade reaction and requires three classes of enzymes: ubiquitin-activating enzymes (E1), ubiquitin-conjugating enzymes (E2), and ubiquitin-protein ligases (E3) (Figure 6). E1 activates ubiquitin by forming a high-energy thiol ester bond between an E1 active site-located cysteine and a C-terminal glycine of ubiquitin in a reaction that requires the hydrolysis of ATP. Activated ubiquitin is then transferred to a specific Cys residue of one of ~30 E2s via a thioester linkage. The E3 ubiquitin ligases (E3s) recruit ubiquitin-loaded E2s, recognize specific substrates, and facilitate (or directly catalyze) ubiquitin transfer to either the Lys residues (in most cases) or the N terminus of their molecular targets with the formation of (iso-) peptide bonds. E3s are the key determinants of substrate specificity and are capable of recognizing a few or multiple substrates through specific degradation signals. A single E2 may function with multiple E3s (and *vice versa*) to provide specificity in a combinatorial way. To date, >500 E3s have been identified. There are several mechanistically distinct classes of E3 enzymes: many of these E3s contain the Homologous to E6-associated protein (E6-AP) Carboxy Terminal (**HECT**) domain or the Really Interesting New Gene (**RING**) finger domain. Recently, four RING-like domains, the **U-box**, the Leukemia Associated Protein (**LAP**) finger proteins, the Plant Homeo Domain (**PHD**) and the Ring Between Ring fingers (**RBR**)-domain family, have also been shown to have E3 activity (Figure 7) (Bernassola *et al.*, 2008; Deshaies & Joazeiro, 2009; Chen *et al*, 2006; Metzger *et al.*, 2012; Eisenhaber *et al*., 2007).

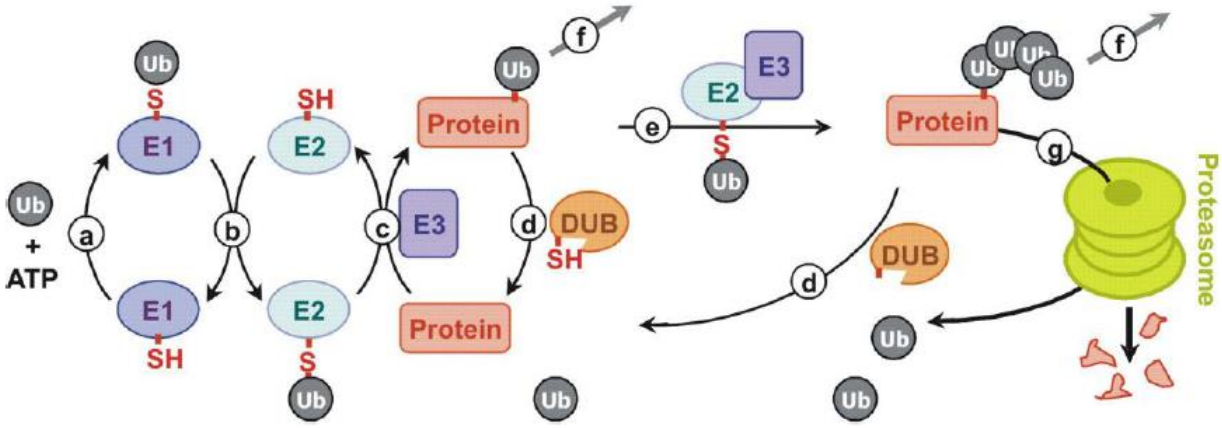

Figure 6. Enzymatic cascade of UPS. (a) Activation of Ub-moiety by activating enzyme (E1) in energy-dependent reaction. (b) Transthiolesterification reaction between E1 and E2 (conjugating enzyme). (c) E3 ubiquitin ligase transfer Ub from E2~Ub thioester on target protein. (d) Ubiquitin mark can be eliminated by deubiquitylating enzymes (DUBs). Monoubiquitylated substrate can then acquire additional Ub moieties in the form of multiple single attachments (not shown) or an ubiquitin chain (e). After depending on the nature of the chain protein can change its function (common for mono- multi-ubiquitylation and also for poly-Lys63-cahains) (f) or undergo proteasomal degradation (typical for the Lys48 chains (g). Modified figure from Deshaies & Joazeiro, 2009

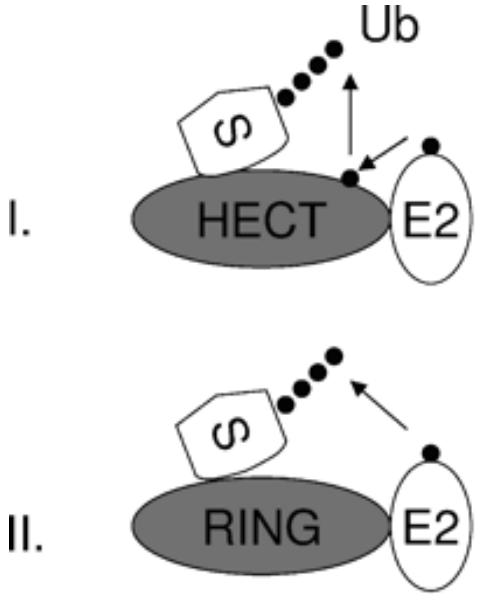

Figure 7. Classification of E3 ubiquitin ligases by mechanism of action. Two major types of E3 are illustrated. The PHD domain, LAP and U-box E3 have the similar mechanism as RING-ligases. S, substrate of an E3. I. For HECT-ligases, ligation involves an obligate thioester intermediate with the active-site cysteine of the E3. II. Ring-ligases mediate the direct transfer of ubiquitin from E2 to substrate. Modified figure from Chen *et al*., 2006

The fate of ubiquitylated proteins is determined by its nature (mono-, multi- or poly-ubiquitylation) and the type of isopeptide linkage of Ub (chains formed through lysine 6, 11, 27, 29, 33, 48, 63 or mixed are found *in vivo* and seem to target proteins to different fates). Monoubiquitylation and the formation of multiubiquitin chains by isopeptide bonds other than Lys48, such as Lys6, Lys29/33 and Lys63, perform both proteolytic as well as regulatory function. Poly-ubiquitylation through Lys48 represents a standard signal for proteasome-mediated degradation (Bernassola *et al*., 2008). Lys63-poly-ubiquitin chains are involved in protein/protein interaction important for kinase signaling activation, receptor endocytosis, protein trafficking, and DNA damage repair (Wertz *et al.*, 2004). Lys6 and Lys11 polyubiquitin linkages have been identified *in vivo*, and their accumulation correlates with the pathogenesis in neurodegenerative disorders (Bernassola *et al*., 2008). In addition, recently discovered linear polyubiquitylation through Methionine (Met1) is involved in nuclear factor-κB signaling and cell death, and dysfunctions in linear ubiquitylation underlie chronic inflammation (Iwai *et al., 2014*).

Like many other dynamic posttranslational protein modification, ubiquitylation is a reversible process. Ub cleavage is performed by deubiquitylating proteins (DUBs). The human genome encodes for nearly 100 Ub-specific DUBs, divided in six families: the UCH, USP, OTU, MJD, MCPIP and JAMM families (Reyes-Turcu *et al.*, 2009).

2.3 PROSTATE CANCER & UPS

The UPS conjugation pathways have multiple essential biological roles. Even if we focus our attention only on cancer-related processes of UPS, the variety of downstream effects is extraordinary (Table 2). Ubiquitin-mediated proteasomal degradation controls cell-cycle progression, protein quality control, signal transduction, and circadian rhythms. The non-proteolytic way of regulation is applied to membrane trafficking, control of genome integrity, and the assembly of signaling complexes (Hochstrasser, 2009). ULM also regulates multiple biological functions. For example, SUMO plays an important role in DNA repair and maintenance of genome stability (Bergink & Jentsch, 2004; Nagai et al., 2011). NEDD8 regulates the Ub-pathway and degradation of some individual proteins including p53. ISG15 modification is part of the cellular response to infection and inflammation (Hochstrasser, 2009). In this light it is not surprising that their function, and often malfunction, are important factors in various human pathogenesis, including numerous cancer types, cardiovascular diseases and neurodegenerative disorders.

Table 2. Biological roles of UPS in cancer.

Process	Deregulated UPS components	Substrates	Cancer-related features
Cell cycle	E3-RING: SCF/Skp2, SCF/Fbw7, APC/C, SCF/b-TrCP, COP1; E3-HECT: HACE1, E6AP; DUB: USP17L2, USP2, USP13, USP7, BAP1	Cyclins, securin, p27, Emi1/2, p53, Rb...	Loose cell cycle control, accelerated proliferation, genomic instability
Control of genome integrity	E3-RING: BRCA1/2, BARD1, FANCL, Hdm2, Hdmx, PARC, PIRH2; E3-HECT: HUWE1, EDD: DUB: USP1, USP28	CTIP, PCNA, TopBP1, PR, ERα, p53...	Defective DNA repair, bypassing DNA damage checkpoint, increasing rate of mutations, inhibition of apoptosis
Apoptosis	E3-RING: Hdm2, Hdmx, PARC, PIRH2, IAPs; E3-HECT: E6AP, WWP1, HUWE1, Itch; DUB: USP7, USP9X, USP2	p53, Bcl2 family, I-kB, Notch1...	Inhibition of apoptosis, increasing cell survival, resistance to radiation and chemotoxic stress
Cell signaling : common pathways	E3-RING: APC, AXIN, SCF/b-TrCP, Cbls, SCF/Roc1, TRAFs, SCF/Keap1; E3-HECT: Smurfs, Nedd4; DUB: USP7, USP4, USP15, CYLD, A20	Components of NF-kB/Bcl3, Wnt, PTEN/PI3K/Akt, TGF-b pathways...	Growth stimulation by an autocrine mechanism (independence on endo- and paracrine signals), inhibition of senescence, differentiation and apoptotic pathways
Cell signaling : membrane trafficking	E2L: TSG101, E3-RING: Cbls, Hakai, VHL, Hdm2; E3-HECT: Nedd4 family; DUB: USP8, USP18	Receptor tyrosine kinases/ growth factor receptors, E-caderin...	Defective endocytosis/ recycling of both signaling and adhesion receptors, overcoming contact inhibition, epithelial-mesenchymal transition (EMT), cell invasion and metastasis
Cell signaling : hypoxia response	E3-RING: VHL, Siah2, KLHL20; DUB: USP20	HIF-1a, VHL, PML....	Shifting metabolism from oxidative phosphorylation to glycolysis ("Warburg effect"or "aerobic glycolysis"), stimulation of agiogenesis, enhanced cell motility and invasion

In prostate cancer, E3 ubiquitin ligase adaptor SPOP (speckle-type POZ protein) is probably the most often deregulated component of UPS. It is specifically down-regulated or mutated in 10-15% of all PCa cases, but not in other types of cancer suggesting tissue-specific mechanism of action (García-Flores *et al*., 2014). Indeed, it was shown that the wt-SPOP protein provides ubiquitylation and degradation of androgen receptor, while mutant isoforms lack this activity (An *et al*., 2014). Moreover, *SPOP* mutation is associated with genomic instability (Boysen *et al*., 2015). Interestingly, mutation of *SPOP* and the presence of *TMPRSS2:ERG* translocation are mutually exclusive events (Berger *et al*., 2011). COP1 (constitutive photomorphogenesis protein 1 homolog) is another tumor suppressor E3-RING gene, which is frequently affected by loss-of-function mutations in cancer (Migliorini *et al.*, 2011). This Ub-ligase controls degradation of such oncoproteins as c-Jun and ETS transcription factor Etv1. In the majority of prostate cancers ETS factors are overproduced because of TMPRSS2:ETS gene fusions (Tomlins *et al.*, 2008). Interestingly, truncated Etv1 encoded by prostate cancer translocation TMPRSS2:ETV1 lacks the critical COP1 binding motifs and is

fiftyfold more stable than wild-type Etv1 (Vitari *et al.*, 2011). As a result, almost all clinically-relevant translocations result in COP1-insensitive Etv1, implying that COP1 loss-of-function confers a selective advantage to prostate cancer cells. In contrast to COP1, the gene for E3-HECT Ub-ligase WWP1 is frequently amplified in prostate cancer. WWP1 induces degradation of several components of the TGFβ pathway as well as the Klf5 protein. The latter is one of the key tumor suppressor transcription factors, which are down-regulated in PCa (Chen *et al.*, 2007). Mutations of some UPS genes have been associated with elevated incidence of sporadic cancer as well as with hereditary prostate cancer. For example, the risk of prostate cancer is increased two- to fourfold in men with BRCA1/2 mutations (Agalliu *et al.*, 2009). These tumor suppressor genes code for E3-RING Ub-ligases, which control DNA repair as well as G2/M and DNA replication checkpoints. The most frequent mutations result in truncated BRCA proteins, which have lost E3-ligase activity.

The global alterations of UPS in prostate cancer can also be seen on the protein level. Immunostaining of prostate tissues reveals that upon cancer progression sub-cellular localization of Ub-conjugates is shifted from the nucleus to the cytoplasm (Bataineh & Habbal, 2006). This may result from the accumulation of Ub-rich cytoplasmic protein aggregates caused by defective protein synthesis and degradation. Indeed some UPS components implicated in protein quality control are specifically downregulated in PCa (Tomlins *et al.*, 2007b; Lapointe *et al.*, 2004). Other ULMs also demonstrate global changes in conjugation and intracellular localization. For example, both SUMO and ISG15 pathways are upregulated in PCa cells (Moschos *et al.*, 2010; Kiessling *et al.*, 2009), while the NEDD8 pathway is believed to be significantly inhibited (Meehan *et al.*, 2002). The critical role of the UPS in prostate cancer is thus well recognized and may result from direct control of stability and function of androgen receptor and/or regulation of other cancer-related proteins such as oncoproteins and tumor suppressors. However, though very important for development of new therapeutic approaches, the mechanisms of this regulation, as well as the proteins involved, remain poorly understood.

2.4 NEDD8-PATHWAY

3.4.1 NEDD8 as an ubiquitin-like protein

Among ubiquitin-like modifiers NEDD8 is one of the best studied. NEDD8 is the closest to Ub in sequence and structure, but they also have a non-overlapping function. NEDD8 was mainly characterized in the context of its function in the regulation of the biggest class of E3 ubiquitin-ligases – CRLs (cullin-RING-ligases). However, new studies show that NEDD8 probably have other target proteins and functions, the most well-studied being the regulation of p53 protein (Harper *et al*., 2004; Enchev *et al*., 2014).

Like in the Ub-pathway, neddylation requires a cascade of reactions performed by E1, E2 and E3 enzymes. Neddylation can be reversed by NEDD8-specific proteases. The NEDD8-conjugating cascade starts from the NEDD8-activating enzyme (NAE). NAE is a heterodimer comprising NAE1 and UBA3 subunits. Activated NEDD8 is subsequently transferred to the E2-conjugating enzyme. In metazoans, two NEDD8-specific E2 conjugating enzymes have been described: UBE2M (also known as UBC12) and UBE2F (Huang *et al.*, 2009). Finally, E3 ligases transfer NEDD8 to one of the Lys or N-terminus of the target protein. NEDD8-E3-ligases, with one exception, belong to the RING (really interesting new gene) finger proteins.

The best characterized NEDD8-E3-ligases are RBX1 (RING-box protein 1, neddylates cullins 1-4 and 7) and RBX2 (RING-box protein 2, specific to cullin 5). Neddylation of cullins by RBX1/2 accompanied by DCUN1 proteins (defective in cullin neddylation protein 1-like proteins; there are 5 of them in human). Both RBX1 and RBX2 are part of the multi-subunit complexes Cullin-RING-E3-Ub-Ligases (CRLs), and neddylation of cullins leads to activation of CRLs. Other described NEDD8-E3-ligases from the RING family are MDM2 (which neddylates p53 and p73 and attenuates its transactivation function), c-CBL (which neddylates receptor tyrosine kinases, e.g. EGFR and TGFIIβ, and targets them to cell compartments), RNF111 (which neddylates histone H4 during DNA-damage response), and DIAP1 (which neddylates caspases and thus prevents apoptosis) (Harper, 2004; Watson *et al*., 2006; Oved *et al*., 2006; Yang *et al*., 2007; Broemer *et al*., 2010; Ma *et al*., 2013; Zuo *et al*., 2013). Recently, the HECT-domain family of E3 ligase, SMURF1, was shown to be auto-neddylated at multiple sites, which increases its activity (Enchev *et al*., 2014). A few deneddylases have been identified, including the CSN5, NEDP1, USP21, Ataxin-3, UCH-L1, and UCH-L3 (Watson *et al*., 2011). CSN5 and NEDP1 are selective to NEDD8, whereas the other

above mentioned NEDD8 ligases also cleave Ub. The principal cullin deneddylase is CSN5, which is active only being a part of 8-subunit COP9 signalosome complex (CSN). NEDP1 complements the activity of CSN and ensures maturation of the NEDD8 precursor (Enchev *et al.*, 2014).

Normally, both Ub and NEDD8-pathway enzymes are highly specific (Souphron *et al.*, 2008), but in conditions of increased ratio of NEDD8:Ub, ubiquitylating enzyme E1 UBA1 can activate NEDD8, and redirect it to Ub-conjugation pathway. Unfortunately, the biological role of this effect is unclear. One possibility is that formation of mixed Ub-NEDD8 chains mediates specific stress-response pathways (Leidecker *et al.*, 2012; Hjerpe *et al.*, 2012).

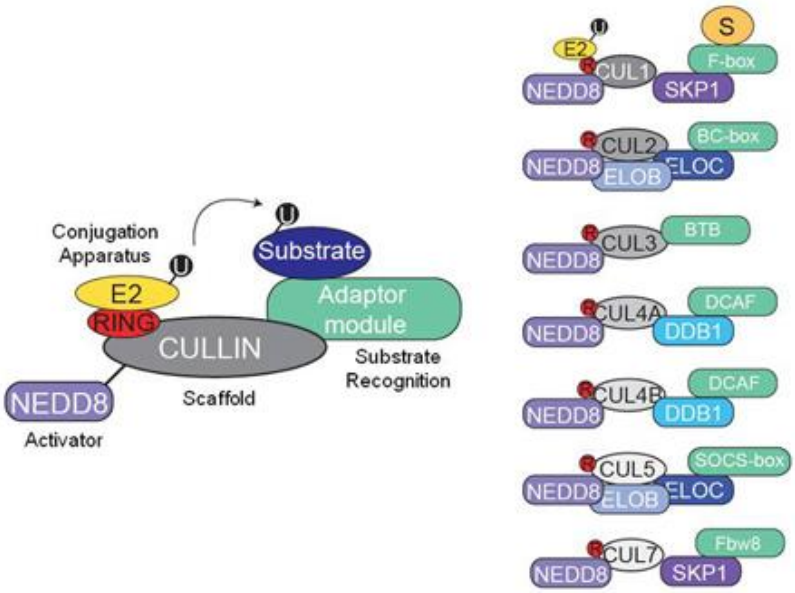

Figure 8. Architecture of Cullin-RING-ligases. http://biology.ucsd.edu/research/faculty/e1bennett

3.4.2 NEDD8 targets

The best-known function of neddylation is regulation of the activity of Cullin-RING ligases (CRLs), the biggest class of E3 ubiquitin ligases. CRLs are multisubunit complexes which consist of the cullin scaffold, a conjugating apparatus represented by E2-conjugase and RING-E3-ligases RBX1/2 and an adaptor module, which determines specificity to substrate protein (Figure 8). There are a few subclasses of CRLs, depending on the type of cullin and adaptor protein involved. In mammals, 7 cullins have been identified (1, 2, 3, 4A, 4B, 5 and 7), forming about 300 distinct CRL complexes. Two other proteins, CUL9 (also known as PARC) and APC2 (anaphase promoting complex

subunit 2), also have significant sequence homology to cullins over a ~180 a.a. region and bind RBX1 or a homologous small RING protein, APC11.

The major regulator of CRLs' function is neddylation. Modification of the cullin by NEDD8 causes change of its conformation, stimulating binding to Ub-loaded E2, bringing together E2 and substrate, and facilitates transfer of Ub from the E2 active site. Upon substrate exhaustion, deneddylation by CSN5 turns off CRL activity and allows changing of substrate specificity (Figure 9, C-E). Another key regulator of CRL is the protein CAND1. Binding of CAND1 is mutually exclusive with neddylation and the adaptor complex of proteins (Figure 9, A-C). CAND1 helps to change the adaptor unit and thus change substrate specificity (Merlet *et al.*, 2009; Duda *et al.*, 2011; Pierce *et al.*, 2013; Abidi & Xirodimas, 2015).

Other ubiquitin E3 ligases reported to be neddylated include VHL, parkin, BRCA1-associated protein 2 (BRAP2) and MDM2. These are all members of the RING domain family. Apart from E3 ligases, other proteins modified by NEDD8 include p53, NF-κB, L11, HIF1α, E2F1 and APP (Hjerpe *et al.*, 2012; Enchev *et al.*, 2014).

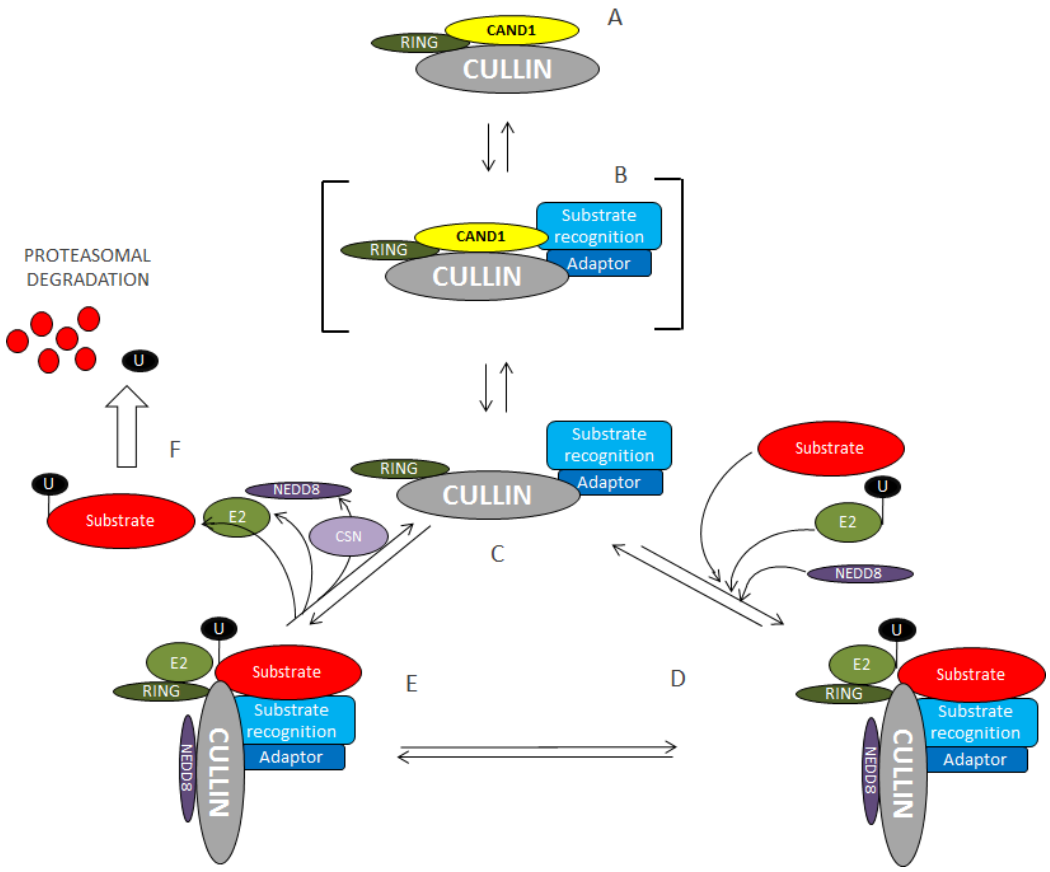

Figure 9. CRLs regulation. CAND1 works as an exchange factor for substrate-recognition unit (A-C), while neddylation stabilizes substrate- and E2- conjugated state of the complex (D-E). Ubiquitylated substrate can be degraded by proteasome. Figure demonstrates the mechanism described by Pierce *et al.*, 2013 and Merlet *et al.*, 2009.

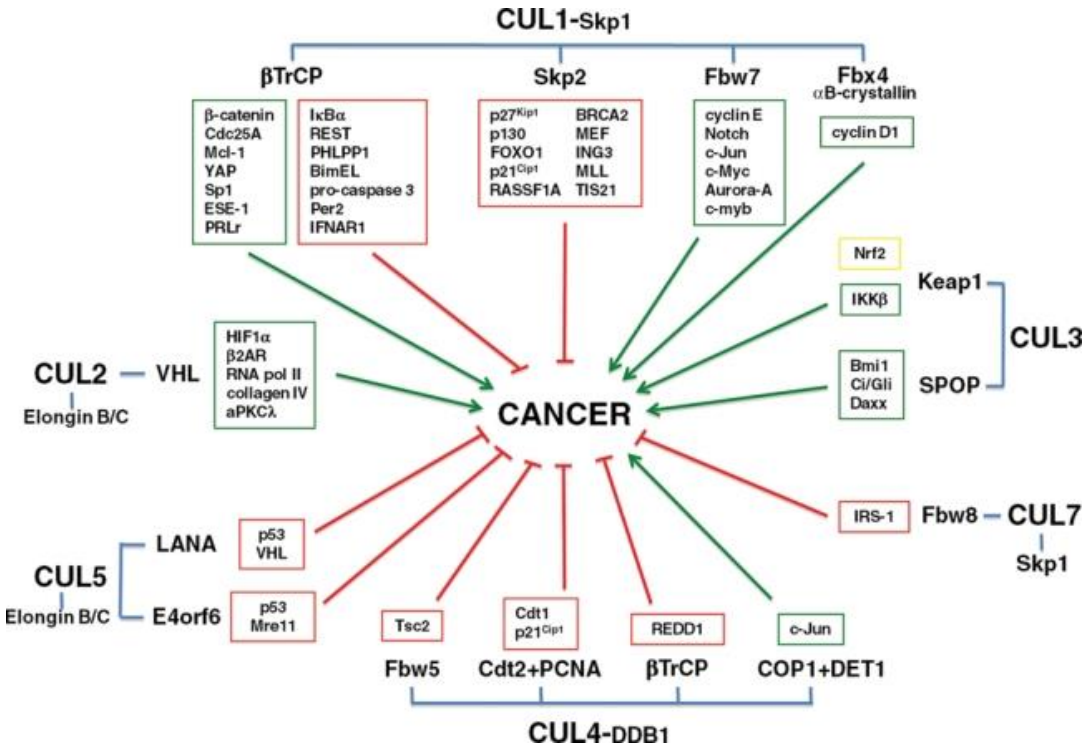

Figure 10. Involvement of CRLs and their substrates in promoting (green boxes/arrows) or inhibiting (red boxes/arrows) growth and survival of cancer cells, thus impacting oncogenesis. Figure from Lee J & Zhou, 2010.

3.4.3 Role of CRL/NEDD8 pathway in cancer

Proteins involved in the regulation of the CRL/NEDD8 pathway are not conventional oncoproteins because their effect depends on their targets. Nevertheless, there are well-established roles in tumor biology for some final effectors (Figure 10). Therefore, the CRL/NEDD8 pathway can function both in promotion and in suppression of cancer development (Lee J & Zhou, 2010). In addition, different sorts of NEDD8-pathway deregulations have been found in cancer. For example, overexpression of NAE and UBC12 and global hyper-neddylation are found in a variety of cancers, including lung adenocarcinomas and squamous-cell carcinomas (Chairatvit & Ngamkitidechaku, 2007; Li *et al*., 2014), while in prostate cancer the pathway is thought to be down-regulated (Meehan *et al*., 2002). Another CRL regulatory protein, DCUN1D1, is amplified in cancer, particularly in squamous cell carcinoma. Targeting the expression of DCUN1D1 by short hairpin RNA induces apoptosis, while another member of DCNL family, DCUN1D3, functions as a tumor suppressor by antagonizing the neddylation activity of DCUN1D1 (Sarkaria *et al*. 2006). NEDD8 was reported to cause an anti-proliferative effect through degradation of Estrogen Receptor-alpha (Fan, 2003). Neddylation of pVHL can also inhibit proliferation because it results in pVHL binding to

fibronectin and the assembly of extracellular fibronectin. The fibronectin matrix promotes differentiation and suppresses the proliferative and metastatic potentials of transformed cells in various model systems (Stickle *et al*., 2004). On the other hand, in its deneddylated form pVHL becomes a part of ECV complex (Elongin B/C-CUL2-VHL) and participates in the destruction of hypoxia-inducible factor which in turn plays an essential role in tumor angiogenesis (Russell & Ohh, 2008).

Collectively, these data demonstrate the important role of NEDD8-pathway in tumorigenesis and suggest that inhibition of neddylation may be a valid therapeutic approach for cancer treatment. The development of a potent small molecule inhibitor of NAE, MLN4924, was reported in 2009 by Millennium Pharmaceuticals. MLN4924 is structurally related to adenosine 5′-monophosphate (AMP), a product of the NAE reaction. MLN4924 forms covalent NEDD8-MLN4924 adduct within the active site of NAE. MLN4924 is a potent inhibitor of NAE (half-maximal inhibitory concentration IC50 = 4 nM), and does not affect related pathways (SUMO, Ub, etc.) or other ATP-dependent enzymes (Soucy *et al.*, 2009). Treatment of cells with MLN4924 resulted in a dose-dependent stabilization of known CRL substrates (Soucy *et al.*, 2009).

CHAPTER 3. RNA INTERFERENCE

In this project RNA interference (RNAi) was used to perform loss-of-function screening of the UPS components. The discovery of RNA interference made a revolution in the field of molecular biology and created a powerful tool for the modulation of gene expression. Compared to other methods, RNAi is easy to perform, cost-effective, specific to a selected gene and also low in toxicity. As a result, RNAi currently is the most used method for gene knockdown. After the development of this technology, genome-wide functional screenings became a standard research method, helping to identify the function of a gene, the involvement of a protein in a certain process, and, therefore also potential new drug targets. Most likely, RNAi will also be used in medicine to treat viral infections and cancer, even though there are still some difficulties related to its non-specific effects and its delivery system. RNAi and major aspects of its application for molecular biology research are discussed below.

3.1 DISCOVERY OF RNAi

The term RNAi describes the phenomenon when a double stranded RNA (dsRNA) initiates a cellular response, leading to sequence-dependent recognition of a target mRNA and thus causes modulation of its function (degradation of mRNA, temporary stimulation or inactivation). It has been known by many names, including co-suppression, post-transcriptional gene silencing (PTGS) and quelling. Only after the underlying mechanisms were understood well enough was it given with its current name “RNA-interference”, or RNAi.

The first piece of evidence comes from the 1970s with experiments showing that the introduction of oligonucleotides complementary to the target RNA causes the formation of RNA-RNA duplexes and interferes with the function of the target RNA. First this phenomenon was shown for the E. coli 16s rRNA where antisense RNAs inhibited translation. Later the same effect was shown for many other nucleotide sequences, and sometimes this interaction has regulatory, but not inhibitory effect. One such example is the regulation of the E. coli mobile genetic element Tn10. Hybridization of a small anti-sense transcript of Tn10 to its mRNA contributes to the regulation of Tn10 transposition. Finally, the same effect was shown for mRNAs, where the expression of sequences complementary to the herpes simplex virus I (HSV) thymidine kinase (TK)

diminishes activity of the enzyme fivefold (Izant & Weintraub, 1984). However, it has since been shown that not only can complementary (antisense) RNA cause such a silencing, but so can sense oligonucleotides, too.

In 1990 three reports described a similar phenomenon. To make petunia have brighter flowers, petunia genes responsible for flowers coloration (chalcone synthase *CHS* and dihydroflavonol-4-reductase *DFR*) were overexpressed in transgenic plants. Unexpectedly, ¼ to ½ of resultant petunias had completely white flowers or had uncolored patterns on the naturally-colored violet flowers. None of transgenic plants had flowers darker than the parental genotype. It was found that the level of the introduced mRNA was extremely low. Likewise, the level of mRNA of the corresponding endogenous gene was very low, too (Napoli *et al.*, 1990; van der Krol *et al.*, 1990). Similar results were reported for the tomato polygalacturonase gene. This phenomenon was named "co-suppression" (Smith *et al.*, 1990). In 1994 it was shown that, despite the strong decrease of *CHS* mRNA, the transcription of this gene was unchanged (de Lange *et al.*, 1994). This suggested that co-suppression was a posttranscriptional event. The next important step was made in 1997 by Metzlaff and colleagues, who showed that at least in some cases the introduced genes could cause formation of dsRNA, which induces silencing. For example, the petunia *CHS* mRNA forms dsRNA region at the 3'-end of transgenic mRNA.

Andrew Fire and Craig C. Mello brought all this evidence together and proved that double stranded RNAs are up to 100 times more efficient comparing to single-stranded antisense RNA (Fire *et al*., 1998). For this discovery they were awarded with the Nobel Prize in Physiology or Medicine in 2006. This work, performed on nematode *C. Elegans*, stimulated research in the field, leading to the discovery of RNAi mechanisms and key RNAi enzymes. It was shown also, that RNAi is evolutionarily conserved and is used by many eukaryotes, from protozoa to animals, for gene regulation and for protection from viruses. Recently RNAi has become widely used in molecular biology as a tool for analyzing gene function.

3.2 MECHANISM OF RNAi

As mentioned before, RNAi is initiated by the exogenous or endogenous dsRNA. For all vertebrates the efficiency of the interference correlates with the length of dsRNA: the longer dsRNA is, the greater the amount of siRNA produced and the greater number of target sites recognized on the mRNA molecule. The minimal size of dsRNA sufficient

for inducing interference is 19 bp. Most likely this limitation prevents degradation of the cell's own mRNA with short intramolecular self-complementary structures (Elbashir *et al.*, 2002). At the same time, in vertebrates, the large dsRNAs cause non-specific effects, such as the activation of the interferon response, which leads to suppression of protein synthesis and cell death. These non-specific responses can be avoided using small interfering RNAs (siRNAs) less the 30 bp long (Caplen *et al.*, 2001).

The first step in RNAi is the formation of short double stranded RNA fragments of 21-28 nt (depending on the species) with 2-nt overhangs at the 3' ends; the 3'-ends are finished an –OH group, and 5'-ends have a phosphate group (Tomari *et al.*, 2004; Lima *et al.*, 2009). These small dsRNAs are produced by the enzyme called Dicer, a type III RNase, which selectively binds to and cleaves dsRNA. The sequence of this protein is highly conserved through evolution (Chiu & Rana., 2002). Dicer contains the following domains (Figure 11): PAZ with a "platform", which recognizes 3'-overhangs on dsRNA; double RNase domains, which form intramolecular dimer with a functional RNase active site (Vermeulen *et al.*, 2005); dsRBD responsible for the recognition and binding to dsRNA (Ketting *et al.*, 2001). At the N-terminus, Dicer has a predicted helicase domain, but the helicase function has not yet been demonstrated. Instead, this domain has been shown to have some regulatory function – for example, it can function as an autoinhibitory module essential for Dicer processivity. The role of the DUF domain (Domain of Unknown Function) is still controversial, but it has been suggested that it can bind dsRNA and Dicer's co-enzymes (Dlakic, 2006; Ma *et al.*, 2008; Sawh & Duchaine, 2012).

The dsRNA produced by Dicer is transferred to an Ago protein, which uses one strand of this RNA as a template for recognition and cleavage of target RNAs. Ago is the major protein of RISC (RNA-induced silencing complex), a multisubunit enzyme responsible for RNA interference. The RNA strand used as a template for silencing is called the "guide chain", while the remaining "passenger strand" is eliminated. The choice of the chain and the loading of this chain onto Ago protein are performed by RISC-loading complex (RLC). RLC is formed by the binding of Dicer to a specific protein (TRBP in human and R2D2 in *D. Melanogaster*) with a few cofactors (Figure 12). The positioning of RNA in this complex seems to play a crucial role: the favorable position is when R2D2 is attached to the end with the higher melting temperature, while Dicer is still attached to the opposite end (Song *et al.*, 2004). After the attachment of Ago to this complex, the chain with lower melting temperature of 5'-end is then cleaved

between 9th and 10th nt from the 5′-end of the guide chain by one of the domains of Ago and eliminated from the complex; the second chain then becomes the guide (Leuschner *et al*., 2006).

The highest assortment of proteins involved in RNAi is found in plants. For example, *Arabidopsis thaliana* has 4 types of Dicer and 10 of Ago, each with its unique function. This diversity probably reflects the need of immobile organisms to struggle against biotic and abiotic stresses. Drosophila has 2 Dicers: one works with miRNAs and the second with siRNAs (described below). This is due to the fact that Drosophila actively use RNAi to regulate the activity of its own genes, but also to protect against viruses; thus, this separation of function could decrease the concurrence for the enzymes between these two processes. This hypothesis is consistent with the observation that Dicer and Ago have a very high rate of evolution which may reflect evolutionary pressure from viruses. For mammals, silencing of viral genes is not crucial because they developed a highly efficient protein-based immune system, and, for them, one type of Dicer is enough (Ghildiyal *et al.,* 2009).

The small RNAs that guide RISC have been given a variety of similar sounding names, including siRNA, miRNA, piRNA, rasiRNA, tasiRNA, tncRNA, hcRNA, and scnRNA. These molecules are virtually indistinguishable biochemically and functionally, and thus they are classified based on the biosynthetic pathway of the precursors or on the type of RISC in which the RNA is found. But all of them have the same function: to be a template for the recognition of target RNA transcripts for silencing (Pratt & MacRae, 2009). Nevertheless, there are two major classes of these regulatory RNAs: siRNAs (small interfering RNAs) of 21-23 nucleotides in length formed from longer dsRNA; and microRNAs (miRNAs) formed from intramolecular double-stranded structures (hairpins) of RNA precursors (Vilgelm *et al.*, 2006; Kim *et al*., 2009b).

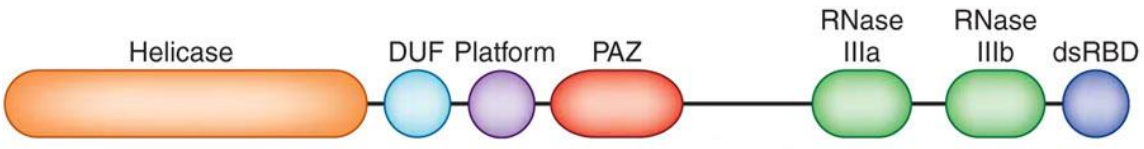

Figure 11. Domains of Dicer. Figure from Sawh & Duchaine, 2012

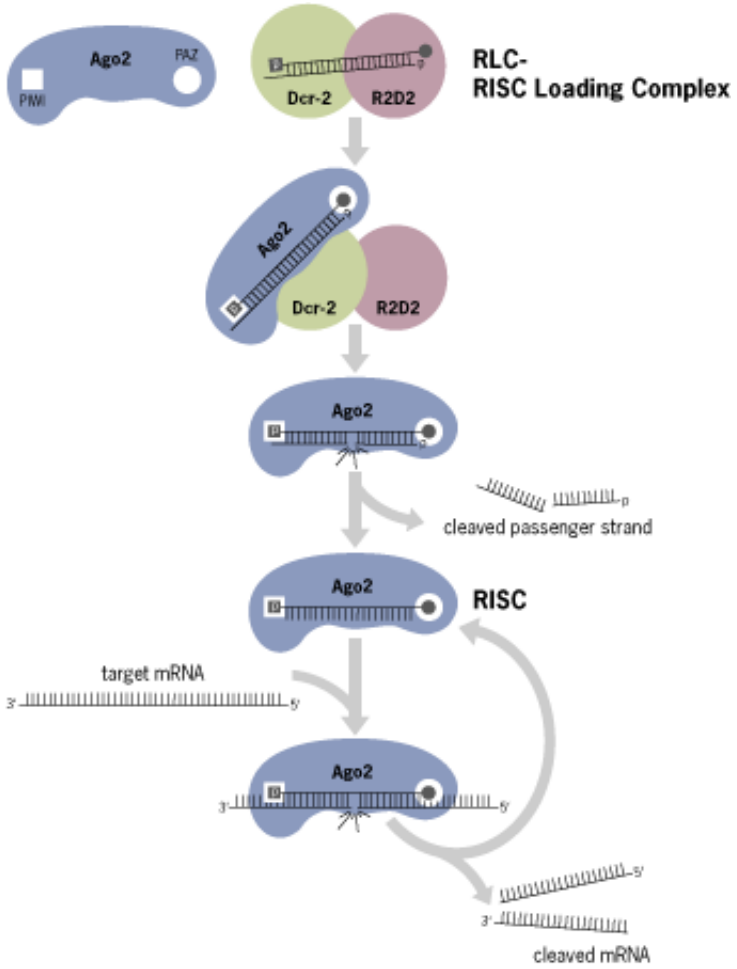

Figure 12. Formation of RISC-loading complex and destruction of the passenger chain. http://helicase.pbworks.com/w/page/17605619/Emily-Devol

miRNAs. miRNA were found to be involved in the regulation of gene expression in both plant and animal kingdoms. Genes of miRNA are often clustered into polycistronic units and thus transcribed together; nevertheless it has been shown that they also can have their own promoter. Moreover, they have been shown to be inserted into the introns or exons of coding and non-coding RNAs. Genes of miRNAs are usually transcribed by RNA-polymerase II (or, rarer, RNA-pol III) (Borchert *et al.*, 2006); the resulting transcripts have self-complementary regions forming "hairpin" structures (Figure 13). Those transcripts are cleaved (most likely, co-transcriptionally), by microprocessor complexes, into smaller fragments of pre-miRNA (Denli *et al.*, 2004). The microprocessor complex comprises two major proteins: Pasha (for *C. Elegans*; human analogue: DGCR8) which binds dsRNA, and Drosha which has RNase activity (Lee *et al.*, 2003). These pre-miRNAs are then transported to the cytoplasm by Exportin-5, where they are processed by Dicer (which cuts off the loop) and Ago (as described above). As a result, the mature RISC complex is formed (Khvorova *et al.*, 2003). The

next step depends on the level of homology between miRNAs and the target RNA. For most animals these sequences are not completely complementary, and they have been shown to bind 3'-UTR of target mRNA and inhibit its translation (Grosshans & Slack, 2002; Kim *et al.*, 2009b). Plant mRNAs more often have full complementarity to target RNAs and thus more often cause their degradation (Llave *et al.*, 2002).

siRNAs. This type of regulatory RNAs is most often formed from complementary transcripts encoded by transposable elements of the genome or from partially complementary transcripts of mRNA from different genes. These transcripts are also produced in the nuclei and then transported into the cytoplasm where they are processed by Dicer and Ago (Kim *et al.*, 2009b). The highest diversity of endogenous siRNA, and of proteins involved in their processing, is found in plants. The distinctive feature of plant siRNA is methylation of the 3'-end by the enzyme HEN1. In plants, production of siRNAs depends on the activity of RNA-dependent RNA-polymerase (RdRP).

The genomes of mammals and Drosophila do not encode RdRP, and the discovery of endogenous siRNA in these organisms was unexpected. The first discovered mammal siRNA was targeted against one of the transposable element of the genome – LINE1 (long interspersed nuclear element 1). LINE1 has promoters for the sense and antisense chains which produce complementary transcripts forming dsRNA. Soon afterward, endogenous siRNAs targeting transposons were also found in *C. Elegans* and *D. Melanogaster* (Ghildiyal *et al.*, 2009).

RNAi is also used by plants and fungi as a protective mechanism against viruses. Very often viruses, during their replication, go through a stage of dsRNA. These dsRNAs are then processed by cellular machinery and transformed into siRNAs that have complete complementarity with target RNAs, which usually result in their degradation (Haasnoot *et al.*, 2007).

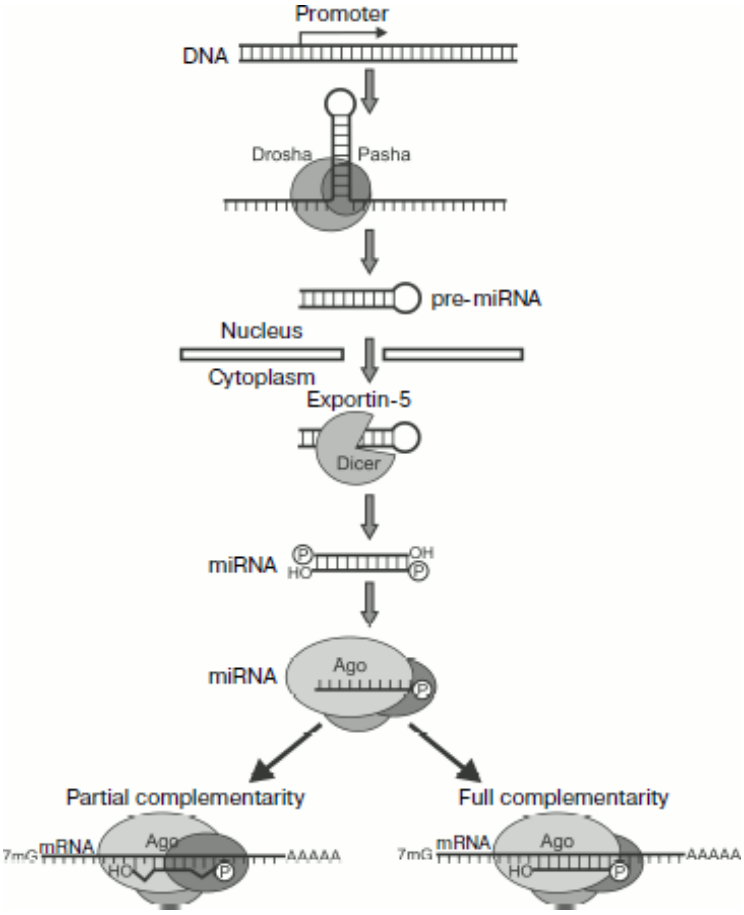

Figure 13. Biogenesis of miRNA. Figure from Vilgelm *et al*., 2006

3.3 RNAi AS A TECHNOLOGY

To induce RNAi in mammal cells synthetic siRNA are used, having a 19 bp dsRNA core with a 2 nt 3'-overhang (21 bp total). It is very important to design siRNA to be fully complementary to the targeted mRNA, because even 1 nt difference may significantly decrease or even abolish the activity of the siRNA. The second important factor to consider is the region of the target mRNA corresponding to the sequence of siRNA. The secondary structure of the mRNA or its attached regulatory proteins could decrease its availability for RISC, and thus significantly diminish the efficiency of RNAi. For this reason it is not recommended to target 5'-UTR or the first exon of mRNA, because most likely there will be some regulatory sequences and binding sites for proteins. Despite all these precautions, the design of siRNA goes through "trial-and-error" methods: usually 3-4 siRNA sequences, which are complementary to the different regions on the target RNA, are chosen and synthesized, and then the most efficient are experimentally selected (Kim, 2003; Vilgelm *et al*., 2006). There are many commercial

organizations who offer synthesis of custom siRNA sequences; very often they also provide programs for siRNA design.

Despite world-wide use of RNAi, there are still some limitations in this approach:

1) Stability. The effect of RNAi is based on the degradation of target mRNA, but protein is not affected by RNAi and is instead degraded by natural mechanisms. Time of the half-life for each protein is different, thus usually the effect of siRNA on phenotype can be detected after the first day, but in case of long-living proteins it develops later. A related problem is that the effect of RNAi is transient and lasts until siRNA is present in high enough concentrations: after 3-5 mitoses transfected siRNA usually loses its activity. To overcome these difficulties it is possible to make additional transfections or to introduce into the cells constructions which stably express the necessary siRNA. For stable transformation the siRNA is often expressed in the form of shRNAs (Figure 14), where sense and anti-sense chains are separated by a short (9 nt) spacer. During maturation this spacer loop is cleaved by Dicer as it occurs in the case of miRNA (Vilgelm *et al*., 2006).

2) Delivery. RNA has a negative charge due to the phosphate groups, which makes it difficult to enter the cell through the negatively-charged membrane. Currently, there are three major methods for siRNA delivery: electroporation, transfection, and stable transformation using DNA-incorporated vectors. Electroporation can be used in the case of difficult-to-transfect cells, such as primary and suspension cultures. This method was shown to be highly efficient, but harmful, causing up to 50% mortality in cell culture. Transfection using lipophilic molecules is currently the most used method for siRNA delivery. The most used particles for delivery are liposomes, but there are still considerable efforts to find better ways for siRNA delivery (Figure 15). For example, polymeric nanoparticles are promising delivery systems because they offer stability and controlled release, have the capacity to encapsulate large amounts of genetic material, allow for co-delivery, and can readily be surface-modified to enhance stability, transport properties, targeting, or uptake. Polymers that are biodegradable, biocompatible, and non-toxic make attractive candidates for constructing *in vivo* delivery vehicles. Chitosan, cyclodextrin, polyethyleneimine (PEI), poly(lactic-co-glycolic) acid (PLGA), dendrimers, and metallic core nanoparticles are becoming popular for delivery, although none of these materials possess all of the desirable properties (Vilgelm et al., 2006; Gavrilov & Saltzman; 2012). Moreover, self-assembling virus-like particles can be used to deliver siRNA into the cells (Kimchi-Sarfaty *et al*., 2005).

As it was said before, for stable inhibition of gene expressing shRNA is often used, which can be delivered in the form of plasmids or using virus-based systems (lentiviral, adenoviral, adeno-associated or synthetic viruses). These viral vectors have been engineered and optimized to facilitate the entry of siRNA into difficlt to transfect cells. (http://www.sabiosciences.com/pathwaymagazine/pathways9/sirna-delivery-methods-mammalian-cells.php)

3) Off-target effects. Highly-specific RNAi has been converted into a tool for molecular biology resulting in a method that has unexpectedly high level of off-target effects. siRNAs are designed to have full complementarity to the target and, thus, to have no off-target effects. Unfortunately, many studies have shown that siRNA can behave like miRNA and regulate expression of RNAs with partial complementarity, which leads to appearance of non-specific effects. Considering the amount of these non-target mRNA (several hundred), the side-effects can be very strong (Laganà *et al*., 2014). It appeared that the transcripts with sequences complementary to the seed region (nucleotide positions 2–8 from the 5′ end of siRNA guide strand), are usually sufficient to yield a significant repression of the target (Figure 16). The seed-dependent off-target effect can be eliminated by chemical modifications (Ui-Tei *et al*., 2012). Another approach to the off-targeting problem employs pools of siRNAs targeting a single gene in multiple sites. This approach may be more specific because such pools combine the effects of individual siRNAs on a specific target, while decreasing siRNA effective concentrations and, thus, potential off-target effects (Laganà *et al*., 2014).

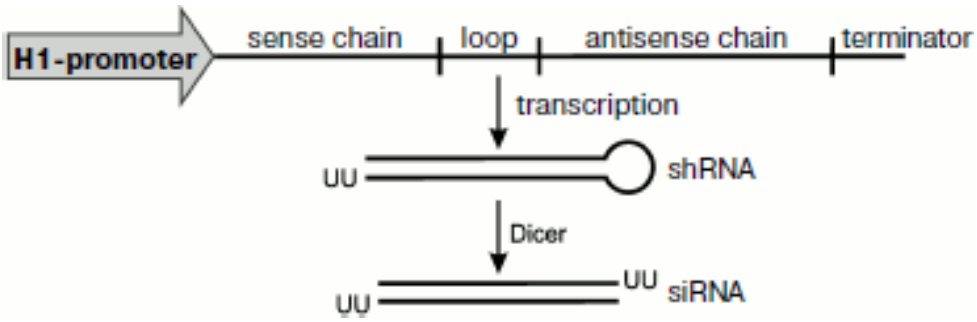

Figure 14. Expression of shRNA.

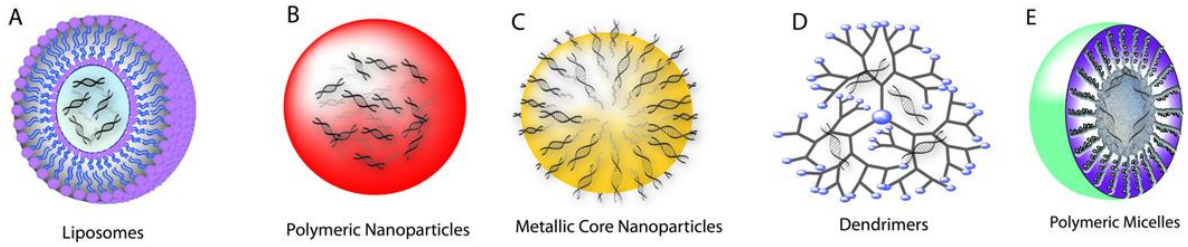

Figure 15. The examples of siRNA nanocarriers. Figure from Gavrilov & Saltzman, 2012

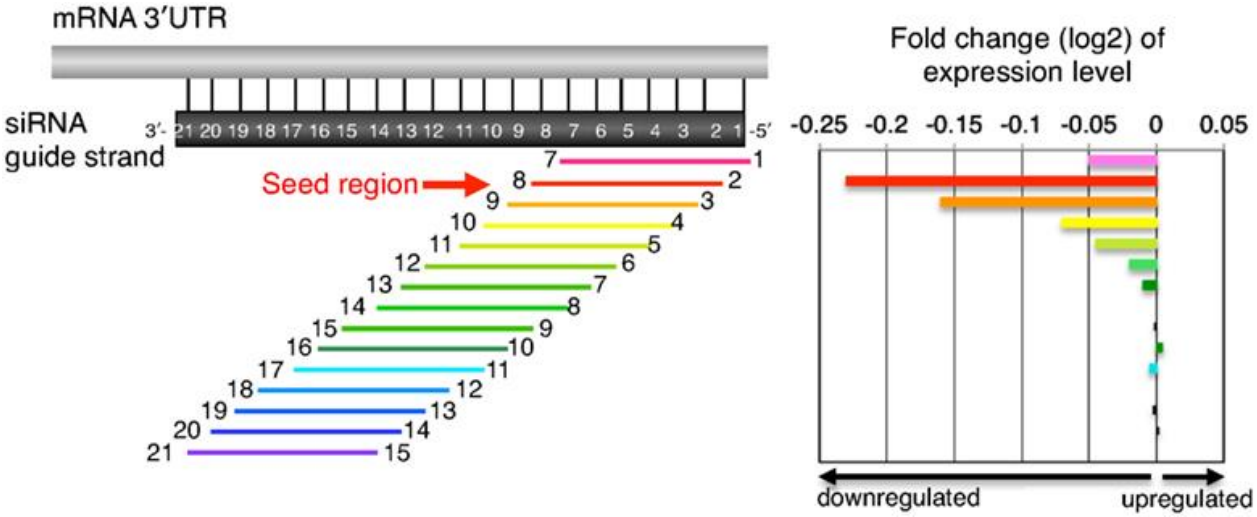

Figure 16. Schematic representation of downregulation of transcripts with seed-complementary sequences. In the left panel, transcripts possessing 3′UTR complementarity to a given 7-nt-long guide strand sequence were divided into 15 groups based on the position of the complementary sequence in the siRNA guide strand. Transcripts labeled with "1" and "7" at both ends possess complementarity to nucleotides 1–7 of the siRNA guide strand and vice versa. The horizontal arrow indicates a transcript group with seed complementarity. In the right panel, changes in gene expression levels are shown by log 2 of fold change ratio to mock transfection. Note that the groups of transcripts labeled with 2–8 are the most sensitive to the off-target effects, suggesting that guide strand nucleotides 2–8 serve as a "seed." Figure from Ui-Tei *et al*., 2012)

II. MATERIALS AND METHODS

CELL CULTURE

VCaP and DuCaP cells were cultured in DMEM (Gibco, 41966) containing 10% FBS (PAN Biotech, P30-3302) and 1% penicillin/streptomycin (Gibco, 15140). PC3 and LNCaP cells were cultured in RPMI1640 (Gibco, 61870) with the same supplements. RWPE1 were grown in a medium optimized for this cell line (Invitrogen, Keratinocyte Serum Free Medium K-SFM) supplemented with bovine pituitary extract (BPE, Invitrogen, K-SFM component), human recombinant epidermal growth factor (EGF) and L-glutamine (GIBCO, Kit Catalog Number 17005-075). The cells were then grown in the incubator at 37°C with 5% CO2. The RWPE1, PC3, LNCaP and VCaP cell lines were purchased from the American Type Culture Collection (ATCC). The VCaP cells were also kindly provided by Dr. Matthias Nees from the University of Turku. The DuCaP cell line was kindly provided by Prof. Jack Schalken from the Radboud University Nijmegen Medical Center, who originally received them from Kenneth J. Pienta, MD, Director of Research at The Brady Urological Institute Baltimore where this cell line was created. For different passages, the cells were washed twice with PBS (no calcium, no magnesium, Gibco, 14190) followed by the addition of trypsin-EDTA (Gibco, 25300) and incubation for 3-10 minutes depending on cell line. Subculture was done depending on the density of the cells. Usually for VCaP cells, subculture was done once per week, with dilution to 1/2; DuCaP was once per week, with dilution to 1/10; LNCaP, PC3 and RWPE1 were twice per week, with dilution to 1/5.

CHARCOAL/DEXTRAN STRIPPING OF SERUM

Charcoal/dextran stripping removes non-polar material such as lipophilic materials (virus, certain growth factors, hormones and cytokines) but has little effect on salts, glucose, amino acids, etc. Dextran coated charcoal was prepared by stirring 2.5% (w/v) Norit-A charcoal and dextran T-70 (0.25% w/v) into PBS and incubating for 18 hours at 4°C. The dextran-coated charcoal was pelleted by centrifugation at 1,000 g for 5 minutes. The supernatant was drained off and replaced with the same volume of Fetal Bovine Serum. The mixture was vortexed, to thoroughly mix the charcoal with the serum, and then incubated for 12 hours at 4°C. The resulting mixture was passed through a prefilter

and 0.45 micron filter before sterilizing through a 0.2 micron filter. The stripped serum was aliquoted by 50 ml and stored at -20°C.

DOUBLE THYMIDINE BLOCK

The VCaP cells were plated at 50% confluency in a tissue culture flask. The next day, after cells attachment, thymidine was added to a final concentration of 5 mM. Cells were incubated in tissue culture incubator for 48 hours (this period corresponds to one cell cycle of VCaPs). Next, the culture medium with thymidine was removed, the cells were washed once with fresh culture medium, and incubated in fresh DMEM for another 24 hours to allow cell cycling to restart. After that, thymidine was added for the second time to a final concentration of 5 mM. The cells were then incubated for another 48 hours in a tissue culture incubator. The cells were released from the block by washing with normal culture medium and the addition of fresh DMEM.

LENS-FREE CELL IMAGING

CYTONOTE – a Lens-Free Cell Imaging Device (iPRASENSE) is based on holographic imaging. Image acquisition using Cytonote doesn't require any labeling or synchronization of cells, and has a large field of view (~30 mm^2). This permits the monitoring of major morphological properties of cells, including cell adhesion, shape, velocity, and also some biological processes, such as cell division and apoptosis (Kesavan *et al*., 2014). For the acquisitions, the cells were plated on culture tissue plates in suspension with the testing drugs, and monitored during 3 days using the lens-free imaging system. Analysis was performed by Dr. Cedric Allier from CEA Grenoble according to the developed and described algorithm (Kesavan *et al*., 2014).

SPHEROID FORMATION ASSAY

To estimate the speed of formation of spheroids time-lapse video microscopy was used. Cells were suspended in the standard medium, were subject to treatments (where required) and distributed into ultra-low attachment U-bottom plates (Falcon, 353910) at concentration of 500 cells/well/100 µl. This resulted in formation of spheroids with avarage 400 µm length. For the assay, acquisitions were made every 60 minutes during 4 days. Typically, 10 spheroids per condition were monitored. For long-term experiments, spheroids were grown in the same ultra-low attachment U-bottom plates with a change of

culture medim once a week. Prior to the addition of fresh medium, the old culture medium were removed using a multichannel pipet.

SPHEROID SPREADING ASSAY

Prior to the assay, VCaP spheroids were pre-assembled in ultra-low attachment U-bottom plates (Falcon, 353910) as described above. Next, the old culture medium was removed using multichannel pipet and fresh charcoal-stripped culture medium with or without drugs was added into the well. The total volume of the medium along with the spheroid were transferred into flat-bottom cell culture plates (Falcon, 353072) using a multi-channel pipet. To estimate the speed of spheroids spreading time-lapse video microscopy was used. Acquisitions were made every hour during 3 days. The development of the images was done using a modified macro script (which was kindly created by Dr. Monika Dolega for this purpose). The macro is enclosed in the Supplementary Materials.

TEST FOR SENESCENCE

Analysis of senescence was performed by measuring of β-galactosidase activity according to the protocol described in Nature Protocols (Debacq-Chainiaux *et al*., 2009). The protocol was slightly modified when the test was performed with spheroids. This involved the suspension of VCaP cells being distributed in ultra-low attachment U-bottom plates (Falcon, 353910) in concentrations of 500 cells/well/100 µl and being incubated during 10 days. Typically, 30 spheroids per condition were used. Next, the spheroids were harvested, pelleted at 600 rpm for 5 min, resuspended in 150 µl of 1.5% low-melting agarose (Sigma, A9414) and distributed into Lab Tek chambers (Dominique Dutscher, 055082). After polymerization for about 30 minutes, the gels were washed twice with PBS, fixed with 2% formaldehyde and 0.2% glutaraldehyde in PBS during 7 minutes. This was folled by a double wash with PBS, and the addition of a staining solution (containing citric acid/Na phosphate buffer, 5 mM K4[Fe(CN)6] 3H2O, 5 mM K3[Fe(CN)6], 150 mM sodium chloride, 2 mM magnesium chloride and 1 mg/ml X-gal in distilled water). The spheroids were then incubated at 37°C during 5 hours. Then the gels were washed multiple times with PBS to remove the background yellow staining of agarose. As a final step, the gels were washed with methanol during 1 min and viewed by bright field microscopy.

RNA EXTRACTION/RT-PCR/PCR/qPCR

RNA was extracted with an RNeasy Mini Kit (QIAGEN, 74104). 1.5 µg RNA was reverse-transcribed in a total volume of 20 µl using a SuperScript® VILO cDNA Synthesis Kit (Life Technologies, 11754050) with random primers according to the manufacturer's protocol. Reverse transcription reactions were diluted to 200 µl of distilled water and further used in concentrations of 2.5 µl per reaction of quantitative PCR (qPCR).

qPCR was carried out with a Platinum Quantitative PCR SuperMIX-UDG Kit (Life Technologies, 11730-017) using a StepOnePlus Real-Time PCR system (Applied Biosystems, 4376600). All experiments were run in triplicates, and the results were normalized to 18S rRNA expression. Primer sequences are listed in Supplementary Table 5.

Standard PCR was done using Herculase II Fusion DNA Polymerase from Agilent Technologies (600677). Samples were purified using a MinElute PCR Purification Kit from Qiagen (28004) according to the manufacturer's protocol. Sequencing of PCR products was performed on the platform of Beckman Coulter Genomics.

siRNA TRANSFECTION

Cells were transfected with siRNA using Lipofectamine® RNAiMAX Transfection Reagent (Invitrogen, Ref. 13778) according to the manufacturer's protocol with minor modifications: RNAiMAX was taken 0.75 µl for 1 well of 96-well plate and 386-well plate.

Screening of the ubiquitin-proteasome system was performed using ON-TARGETplus® SMART pool® siRNA Library-Human Ubiquitin Conjugation Subset 1 from Dharmacon (Supplementary tables 1, 2, 4). Transfection of the SMART pool was done at a final concentration of 20 nM of siRNA. Individual siRNAs were added in concentrations of 10 nM.

As controls for transfection AllStars Negative Control siRNA (SI03650318, Qiagen) and AllStars Hs Cell Death siRNA Positive cell death phenotype control (SI04381048, Qiagen) were used. All controls were used in concentrations equal to the concentration of siRNA in the experiment. The siRNA against the ERG gene was prepared by Eurogentec. The sequences of siERG were taken from publication of Tan *et*

al., 2009: sense - 5'-CGACAUCCUUCUCUCACAUAU-3'; antisense - 5'-AUGUGAGAGAAGGAUGUCGUG -3'

siAndrogenReceptor (siAR) were obtained from Dharmacon; used as a mixture:

Duplex Catalog Number	Gene Symbol	GENE ID	Gene Accession	GI Number	Sequence
J-003400-05	AR	367	NM_001011645	58535454	GAGCGUGGACUUUCCGGAA
J-003400-06	AR	367	NM_001011645	58535454	UCAAGGAACUCGAUCGUAU
J-003400-07	AR	367	NM_001011645	58535454	CGAGAGAGCUGCAUCAGUU

WESTERN BLOT

All cellular proteins were extracted using RIPA lysis buffer (Sigma, R0278) with protease inhibitor cocktail tablets (Complete Mini from Roche Diagnostics, Cat. No. 11 836 153 001) and supplements:

Component	[C]	Application
RIPA	10 ml	base lysis buffer
Complete Mini pills	1 pill	inhibitor of proteases
OPA (ortho-phenanthroline)	10 mM	inhibitor of metalloproteases (de-neddylation, de-ubiquitylation)
NEM (N-Ethylmaleimide)	30 mM	inhibitor of cysteine proteases (de-ubiquitination, de-sumoylation)
$NaVO_4$ (sodium orthovanadate)	5 mM	inhibitor of phosphatases
NaF	5 mM	inhibitor of phosphatases

After quantification with a BCA protein assay kit (Pierce, 23225), an equal range of concentration (typically 2.5 ng of protein per sample) was run on a NuPAGE Novex Bis-Tris Gel (Life Technologies, NP0322BOX, EC60252BOX, NP0323BOX) in MES buffer and then transferred onto the nitrocellulose membrane (Amersham™ Protran®, GE Healthcare, 10600001). The membranes were blocked in 5% nonfat milk/TBST during 40 minutes at 37°C, incubated with primary antibodies (a list of antibodies is given in Supplementary Table 4) in 5% nonfat milk/TBST during 1 hour at RT or overnight at 4°C. This step was followed by incubation with secondary HRP-conjugated antibodies. Detection was performed with a chemiluminescent reagent depending on the concentration of the target protein (Plus-ECL, Perkin Elmer, NEL105001EA; ECL Prime, GE Healthcare, RPN2232; SuperSignal West Femto Substrate, Thermo Fisher Scientific, 34095).

IMMUNOFLUORESCENCE MICROSCOPY OF CELLS

Cells were grown on plasma-treated glass slides. The culture medium was removed and replaced by 4% paraformaldehyde (PFA) for 15 min at RT. Then PFA was replaced with 0.2% Tween for 5 min at RT. Treatment with Tween was followed by the addition of NH_4Cl 0,1M for 10 min at RT. Then the slides were washed briefly in PBS $+Ca^{2+}$ $+Mg^{2+}$ (PBS++, Sigma, P4417) and blocked with 3 % BSA in PBS++ which had been filtered through a 0.2 µm filter for 30 min. Primary antibodies were added in 1.5 % BSA (filtered) and left for 2 hours at RT. This was followed by 3 washes with PBS++, and then the slides were incubated with secondary antibodies and phalloidin in 1.5 % BSA (filtered) for 45 min at RT. This was followed by a 5 min wash in PBS++, then a 5 min wash in Hoechst, and then again 5 min with PBS++. Then, these glass slides were placed on standard microscope slides with mounting solution (DAKO, S302380) and dried for 24 hours. Finally, the slides were analyzed by Zeiss Axioimager Z1 Apotome from Zeiss.

IMMUNOFLUORESCENCE MICROSCOPY OF SPHEROIDS

Prior to the assay, VCaP spheroids were pre-assembled in ultra-low attachment U-bottom plates (Falcon, 353910) as described above (SPHEROID FORMATION ASSAY). Next, the spheroids were harvested, precipitated at 600 rpm for 5 min, and resuspended in fresh charcoal-stripped medium with or without treatments. Next, the spheroids were poured onto plasma-treated glass slides in 24-well plates (Falcon, 353047) and incubated during 5 days to allow attachment and spreading on the slide. The protocol of immunostaining here is identical to the above described protocol for the cells, but with longer times of incubation (see details below).

The culture medium was removed and replaced by 4 % paraformaldehyde (PFA) for 30 min at RT. Then PFA was replaced by 0.2 % Tween for 8 min at RT. Treatment with Tween were followed by the addition of NH_4Cl 0.1M for 30 min at RT. Then slides were washed twice in PBS $+Ca^{2+}$ $+Mg^{2+}$ (PBS++, Sigma, P4417) for 10 min and blocked with 3% BSA in PBS++ filtered through a 0.2µm filter for 2 hours at RT. The primary antibodies were added in 1.5% BSA (filtered) and left for overnight at 4°. After 4x wash with PBS++ for 15 min, the slides were incubated with secondary antibodies and phalloidin in 1.5 % BSA (filtered) for 1.5 hours at RT. This was followed by a 15 min wash in PBS++, then a 10 min wash in Hoechst, and then again 15 min with PBS++.

Then the slides were placed on the microscope slide with mounting solution (DAKO, S302380) and dried for 24 hours. Finally the slides were analyzed by Zeiss Axioimager Z1 Apotome from Zeiss.

ANALYSIS OF CELL CYCLE

The cell cycle was analyzed by the measurement of total DNA content using flow cytometry. Cells were grown in culture medium with or without drug treatment during 5 days. They were harvested with trypsin as described above, neutralized by culture medium and washed once in PBS. Then these cells were fixed with 70% fridge-cold ethanol for 30 minutes. Next, BSA was added to a final concentration of 0.5%. Then, the cells were spun at 3000 rpm for 7 minutes. The supernatant was discarded, while the cells were resuspended in 0.25 % BSA in PBS and spun again at 3000 rpm 7 minutes. The supernatant was once more discarded, and replaced by a 50 µg/ml 7-AAD (7-Aminoactinomycin D) solution in PBS. Then the cells were analyzed by BD™ LSR II flow cytometer from BD Biosciences.

PROLIFERATION ASSAY BY ATP CONTENT

Level of proliferation/viability of cells was analyzed by measuring ATP content using ViaLight™ Plus Cell Proliferation and Cytotoxicity BioAssay Kit from Lonza (LT07-121) according to the manufacturer's protocol. In short, cells were seeded in white plates with transparent bottom suitable for luminescence assays (Grenier, 655088). The treatments were performed on the next day after cell seeding. At indicated times, the lysis reagent was added to the cells directly into culture medium for 10 minutes, followed by addition of ATP monitoring reagent for 5 minutes. Luminescence was measured using GloMax®-Multi Detection System.

PROLIFERATION BY EdU INCORPORATION

The quantity of proliferating cells in the population was determined by measurement of DNA synthesis (by EdU incorporation) using Click-iT® EdU Alexa Fluor® 647 Flow Cytometry Assay Kit from Invitrogen (C-10419). This involved the cells being seeded in black plates with transparent bottoms suitable for fluorescent measurements (Fisher Scientific, 781091). The treatments were performed on the day after cell seeding. At indicated times, VCaP cells were treated with EdU for 5 hours and then fixed and stained according to the manufacturer's protocol. Finally, some Hoechst

reagent was added to the cells followed by incubation for 30 minutes. The labeled cells were covered with Glycerol and PBS++ solution (in a ratio 1:1) and stored at 4°C. Image acquisitions were performed using CellInsight™ NXT High Content Screening Platform from Thermo Scientific. The images were analyzed and quantified by the "Cell Health Profiling" program, installed within CellInsight™. The identification of cells (cell segmentation) is based on the detection of nuclei by the Hoechst channel. Next, the EdU signal was quantified for each nucleus. The results were presented as a percentage of cells having nuclear EdU staining.

APOPTOSIS BY ACTIVATION OF CASPASES

The increase in the amount of apoptotic cells was estimated using CellEvent™ Caspase-3/7 Green Detection Reagent from Invitrogen (C10423). This involved the cells being seeded in black plates with transparent bottoms suitable for fluorescent measurements (Fisher Scientific, 781091). The treatments were performed on the day after cell seeding. Some CellEvent reagent was added during the treatment according to the manufacturer's protocol. At the end of treatment, some Hoechst reagent was added to the cells before incubation for 30 minutes. The image acquisitions were performed using CellInsight™ NXT High Content Screening Platform from Thermo Scientific. The images were analyzed and quantified by "Cell Health Profiling" program, installed within CellInsight™. Segmentation is based on the detection of nuclei with the Hoechst channel. Using this segmentation, the CellEvent signal was then quantified in each nucleus. The apoptotic cells were determined by the increase of the signal from CellEvent reagent (see below, SCREEN QUANTIFICATION).

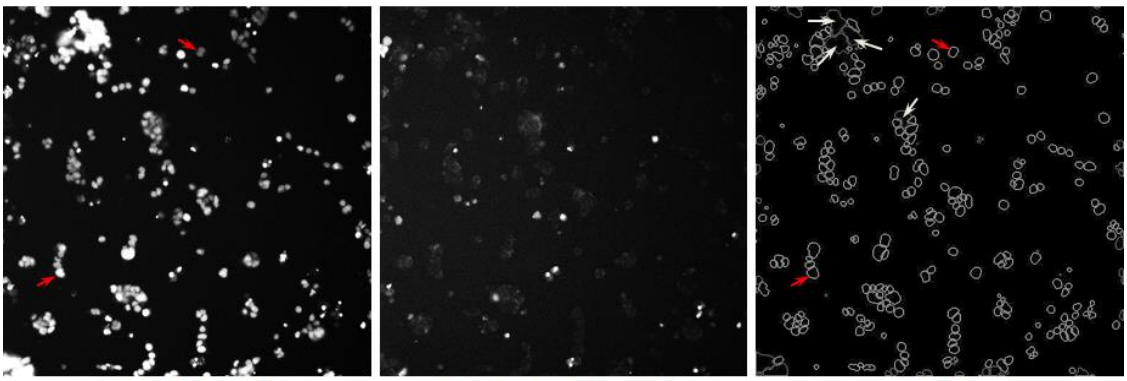

Figure 17. Segmentation of cells during CellEvent-based apoptosis assay on CellInsight. The software detects nuclei (Hoechst) (A) and fluorescent CellEvent reagent that accumulated in the nucleus upon cleavage by caspases 3/7 activity. In case of unclear segmentation, the software excludes some areas from analysis: light gray are included and dark gray (shown with white arrows) are excluded. In the case of VCaP cells, which are growing in groups, this algorithm is not optimal and may count 2 or 3 cells as 1 (red arrows).

SCREEN QUANTIFICATION

The percentage of apoptotic cells was calculated as described above (APOPTOSIS BY ACTIVATION OF CASPASES). For each gene the effect of four individual siRNAs targeting different exons was analyzed. The effect of each siRNA was measured in 4 well replicates split into two 384-microwell plates (2 replicates per plate). The fluorescent signals (Hoechst and CellEvent) were measured in 9 fields per well-replicate. Based on these signals, the "Cell Health Profiling" program performs cell segmentation and obtains information about each individual cell, including the intensity of the signal from the channel (Hoechst and CellEvent), the area of the nuclei and the total number of cells per field. Based on the CellEvent signal intensities from negative siAllStars and positive siCellDeath controls, the threshold that distinguishes alive cells from apoptotic was established. Based on this threshold, the median value of the percentage of dying cells was then calculated.

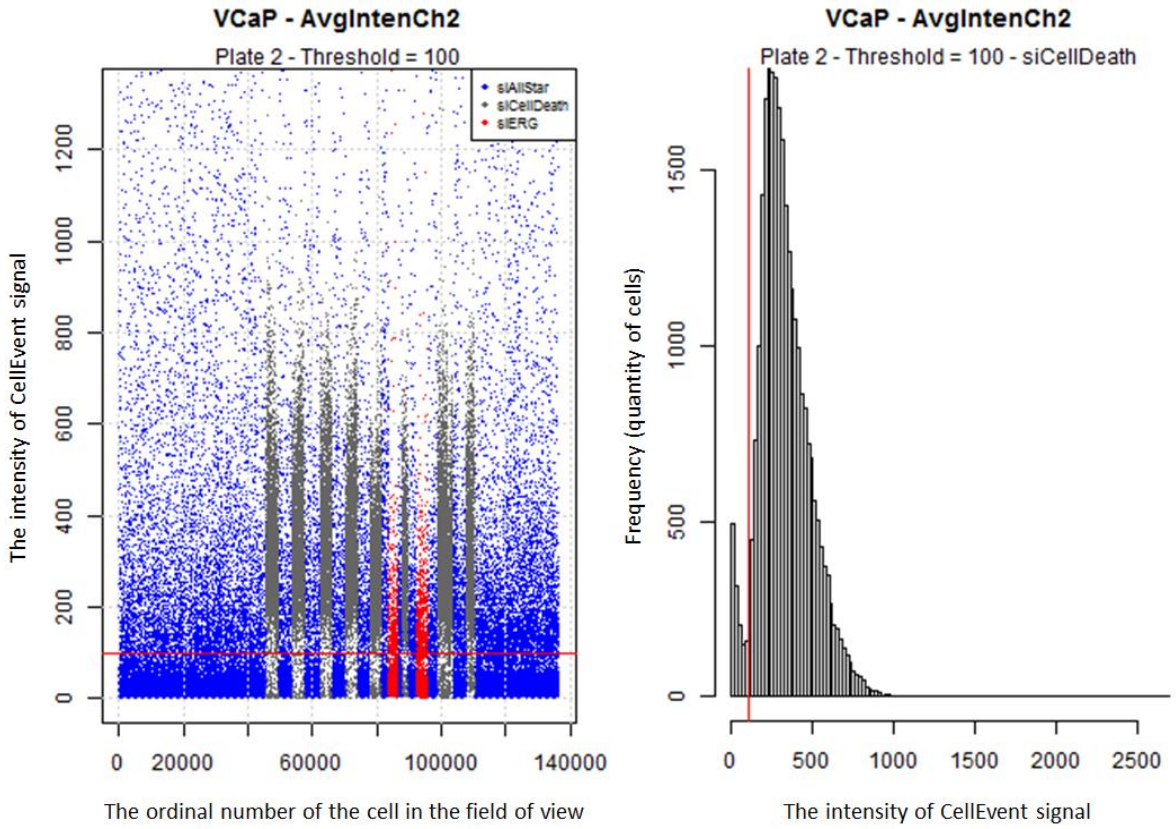

Figure 18. CellEvent values for cells treated with controls for plate 2 of VCaP screen. The scatter plot on the left shows that siCellDeath increased the population of CellEvent-positive apoptotic cells compared to the negative controls siAllStars and siERG. The histogram on the right shows the distribution of cells treated with siCellDeath. The population of apoptotic cells is clearly identified, allowing to set a CellEvent signal threshold at 100 (the cells having CellEvent signal intensity > 100, were considered apoptotic).

For the statistical analysis we used robust Z-score (RZ), which allows the data to be less dependent on "outliers". The Z-score is the distance from the mean of the whole plate normalized by its standard deviation. Its robust version, RZ, calculates as follow (Birmingham *et al*., 2009):

$$RZ_w = \frac{X_w - Md}{MAD*k}$$

where $\mathbf{RZ_w}$ is a robust Z-score for the well w, $\mathbf{X_w}$ is the value for the well (either percentage of dying cells or cell number); **Md** is a median value of the X_w for the whole plate, **MAD** is a median absolute deviation of X_w for the whole plate and **k** is the constant scale factor, which depends on the distribution, and is equal to 1.4826 in case of the Gaussian distribution.

RZ scores were then averaged between 4 repetitions for every siRNA to give a merged score (**muRZ**). To identify hits, we chose a threshold of RZ = 0.82. This threshold gives 5% hits (i.e. 5% False Positive) in the hypothetical case where all siRNAs are inactive (called null or H_0 hypothesis), the distribution of the values is Gaussian, and a pro-apoptotic effect of siRNA is the only possible outcome (one sided test). For a standard distribution, 95% of the values are below 1.64 but taking into account the 4 replicates, this threshold has to be divided by the square root of 4 leading to a value of 0.82.

III. RESULTS AND DISCUSSION

CHAPTER 1. UPS PROFILING IN PROSTATE CANCER

1.1 INTRODUCTION

The World Health Organization predicts that tumors may soon become the first leading cause of death, leaving behind cardiovascular diseases. At present, more than 5000 types of cancer are known, which are caused by structural-functional disorders of various genes. For the last decades our knowledge of the processes that govern carcinogenesis has been rapidly growing. Cancer development is a multistage process – it appears as a result of mutation of DNA in a single cell, which has managed to escape elimination and has thus subsequently proliferated. The offspring cells then evolve and accumulate new genetic alterations, depending on molecular context, lifestyle, treatment used, etc. Usually cancer evolution leads to the conservation of the most malignant clones, which are capable of avoiding apoptosis, proliferating infinitely, invading surrounding tissues, etc. (Hanahan & Weinberg, 2000; Boutros *et al*., 2015; Sidow & Spies, 2015). This phenomenon, known as "oncogene addiction", describes the dependency of cancer cells on the altered functioning of oncoproteins. Nevertheless, to date, only a few mutations are known to be generally implicated in cancer development, including p53, Rb, PTEN, BRCA, etc. At the same time, each cancer patient has a unique set of genetic rearrangements influencing the cancer phenotype (Greenman *et al*., 2007). Therefore, it is assumed that some mutations are causal, while the others are acquired during carcinogenesis. These latter, somatic mutations, influence the molecular context of cancer cells and affect their response to medication. As a result, cancer heterogeneity makes each tumor unique and prevents the development of effective anti-tumor drugs.

Cell constantly faces internal and external stresses, such as mistakes in DNA replication and DNA damage, misfolded proteins, toxic byproducts, new signals from the environment, etc. To maintain its integrity and homeostasis, the living cell has developed various stress-support systems. In a cancer cell, an altered genome redirects normal molecular pathways and brings about additional burdens for these systems, which makes them the cancer-specific Achilles' heel. This particularity of malignant cells is used in cancer treatment: radiotherapy and many chemotherapeutic agents target the increased sensitivity of malignant cells to DNA damage, while an inhibitor of the proteasome

Bortezomib (or Velcade from Millennium Pharmaceuticals) raises additional proteotoxic stress (Luo *et al.*, 2009). Recent data suggest that antioxidants promote cancer progression, and vise versa: increasing oxidative stress might suppress the development of metastasis in melanoma (Piskounova *et al.*, 2015). Such "non-oncogene addiction", which defines the dependency of tumor on the function of normal genes (Figure 19), represents a new attractive strategy for targeted anti-cancer therapy and is expected to be specifically toxic for cancer cells (Galluzzi *et al.*, 2013). In some cases, particular agents can display genotype-dependent toxicity. For example, it has been shown that inhibition of DNA-PKcs is synthetically lethal in cells with defective ATM. In conditions of genotoxic stress, suppression of DNA-PKcs leads to failure to repair DNA double-stranded breaks and to the activation of the apoptotic program (Riabinska *et al.*, 2013). Similar results were shown for the TMPRSS2:ERG protein, which affects normal Non-Homologous End Joining (NHEJ) machinery. Thus, further impairment of DNA repair pathway (e.g., inhibition of PARP protein) leads to strong radiosensitization of cells harboring this translocation (Chatterjee *et al.*, 2015).

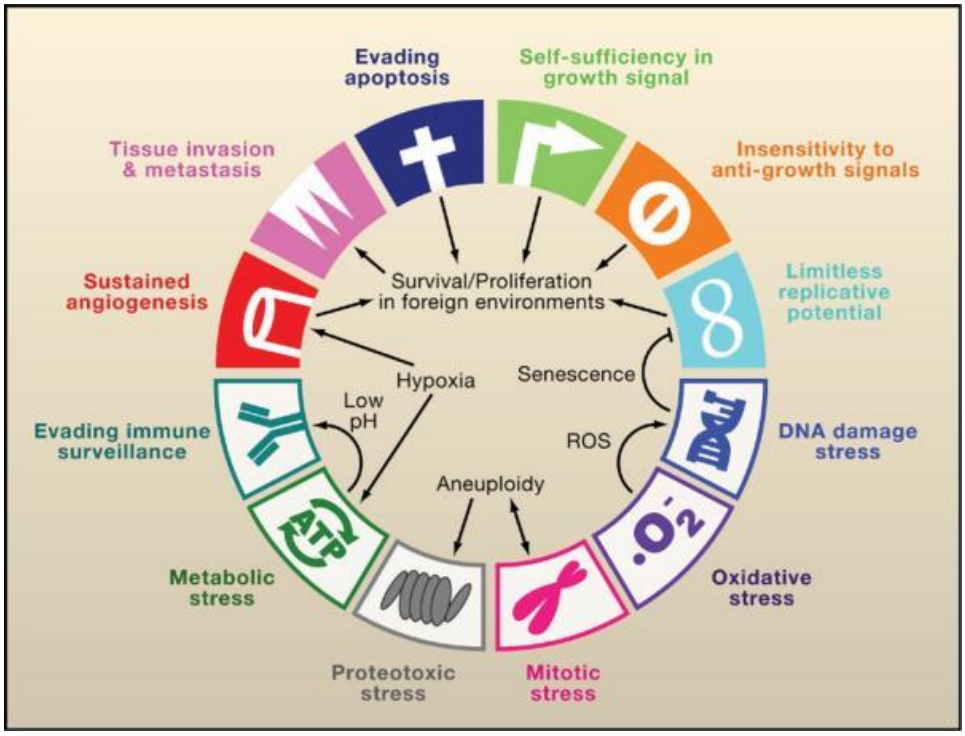

Figure 19. The Hallmarks of Cancer (Luo *et al.*, 2009). In 2000 Hanahan and Weinberg published an article in Cell where they describe distinctive features that cancer cells acquire during selection of the most malignant clones (six upper symbols). Later, in 2008, Kroemer and Pouyssegur propose an additional trait - avoidance of immune system. In 2009, Elledge and colleagues describe new features based on increased cellular stresses (metabolic, proteotoxic, mitotic, oxidative and DNA damage stress). These hallmarks are interdependent and promote the development of a tumor phenotype. Bringing additional instability to the stress-support system causes its failure and, as a result, tumor-specific lethality.

The ubiquitin-proteasome system (UPS) could be viewed as one such stress-support system. The UPS is a key mediator of molecular turnover in the majority of cellular functions, including cell cycle progression, DNA repair and receptor signaling. Mutations, genetic rearrangements and rewired molecular pathways result in an imbalance of protein levels, causing additional stress for the UPS. It is believed that further impairment of the UPS in cancer cells overloads the system, leading to its collapse and apoptosis. Indeed, proteasome inhibitors (such as Bortezomib and Carfilzomib) have been shown to be highly efficient in hematological malignancies. Unfortunately, because targeting the proteasome is a very general approach that influences the degradation of all proteins in a cell, these inhibitors often show a lot of negative side-effects. The aim was to benefit from the targeting of individual components of the UPS or ubiquitin-like modifiers (ULM) pathways, which could make therapy more selective toward tumor cells. Indeed, identification of the components of the UPS involved in oncogenesis and characterization of their drug susceptibility is of clinical importance as it may lead to the discovery of new therapeutic targets.

The aim of this project was to identify components of UPS/ULM involved in the functioning of prostate cancer cells and, in particular, PCa cells harboring the oncogenic translocation TMPRSS2:ERG. As a method the loss-of-function siRNA screen of the UPS was used. The effects of gene knockdowns were evaluated in five cell lines, representing models of non-cancerous cells (RWPE1), ERG-negative cancer cells (LNCaP, PC3) and ERG-positive cancer cells (VCaP, DuCaP) (Figure 20).

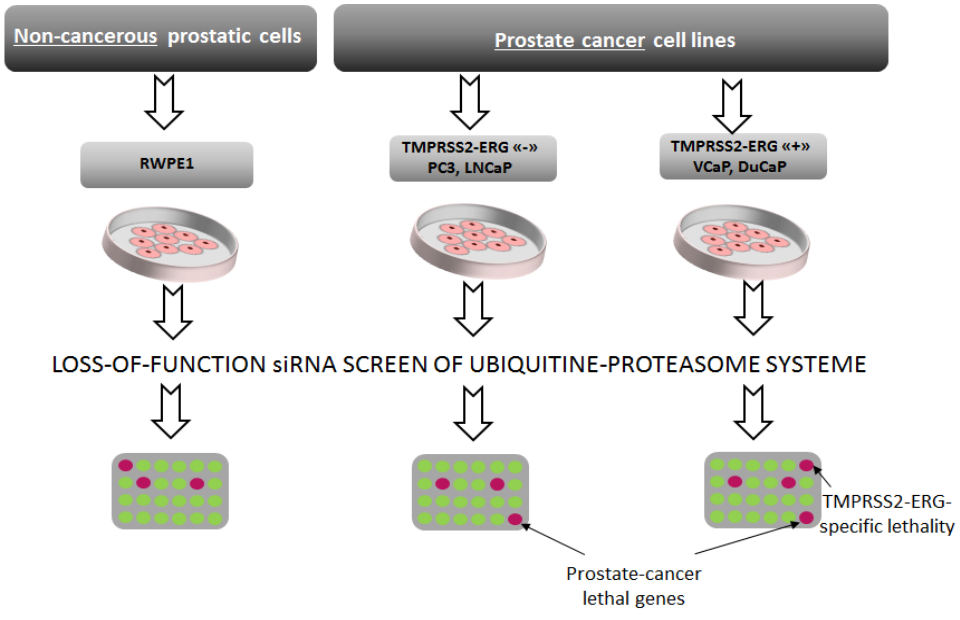

Figure 20. Diagram of the loss-of-function siRNA screen of UPS.

1.2 METHODOLOGY

In the course of this project, a novel systematic approach to the functional profiling of the UPS in prostate cancer was applied. This approach, named "cascade profiling", takes as its starting point the cascade organization of the UPS and uses its hierarchical mode of function which results in a rather compact and more targeted screen compared to genome-wide screens. Ubiquitin (and Ub-like proteins) are activated using one of the corresponding E1-activating enzymes. Then this moiety (Ub or ULM) is transferred to one of the E2-conjugating enzymes. Next, with the help of E3-ligase, it is attached directly to the target protein. At each enzymatic level, the number of individual components grows dramatically, which allows for an increase of specificity in a combinatorial way (Figure 21, A). Based on this cascade organization of the UPS, we were able to reduce the number of genes in the screen without loss of information: identification of E1 or E2 as a hit would facilitate identification of the E3s involved. To individually knockdown the UPS components siRNA technology was used.

ON-TARGETplus siRNA SMART-pool approach from Dharmacon was chosen. ON-TARGETplus technology reduces the off-target effects mediated by antisense seed-region interactions (the seed region is defined as nucleotide positions 2–8 from the 5′ end of siRNA antisense strand or miRNA loaded on Ago proteins that determine the selectivity of inhibition (Jackson *et al.*, 2006)). SMART-pool contains a mix of 4 individual siRNAs targeting the same gene, which was advantageous for two reasons: first it allows the decreasing of the concentration of individual siRNA that is reported to reduce off-target effects (Caffrey *et al.*, 2011), while keeping the concentration of the total siRNAs targeting the gene high enough to ensure efficient knockdown. Second, it allows for the decreasing of the number of samples, which is convenient for primary screens that aim to eliminate siRNAs having no effect. In the secondary validation screens individual siRNAs from the deconvoluted pools were used (Figure 21, B). Using several siRNAs targeting the same gene separately allowed for the confirmation of a phenotypic outcome (if several siRNA cause the same effect) or to reveal off-target effects (if only one siRNA induces a phenotype, while others have no effect). Pools were used at 20 nM total siRNA concentration to minimize off-target effects, while individual siRNAs were used at 10 nM concentration. A set of genes were screened using Dharmacon "Human siGENOME siRNA Library – Ubiquitin Conjugation Subset 1" complemented with siRNAs to target all known E1-E2 genes. The "Ubiquitin

Conjugation Subset 1" also contains siRNAs against some members of the E3-RING ligases, which were also included in the screen.

Because the aim was to identify genes which are synthetically lethal with TMPRSS2:ERG fusion, the primary screen was done with the ERG-dependent VCaP cell line (Figure 21, B). Based on three phenotypic parameters (induction of cell death, changes in cell count and ATP level reflecting cell viability/proliferation) 25 potential hits were selected out of 107 screened genes. Due to the abundance of the hits from the CRL/NEDD8 pathway in the primary screen, three more genes from this pathway were added in the secondary screen. The latter identified seven hits, four of which being components of CRL/NEDD8 pathway and 2 being potentially ERG-dependent. The detailed description of each step is presented below.

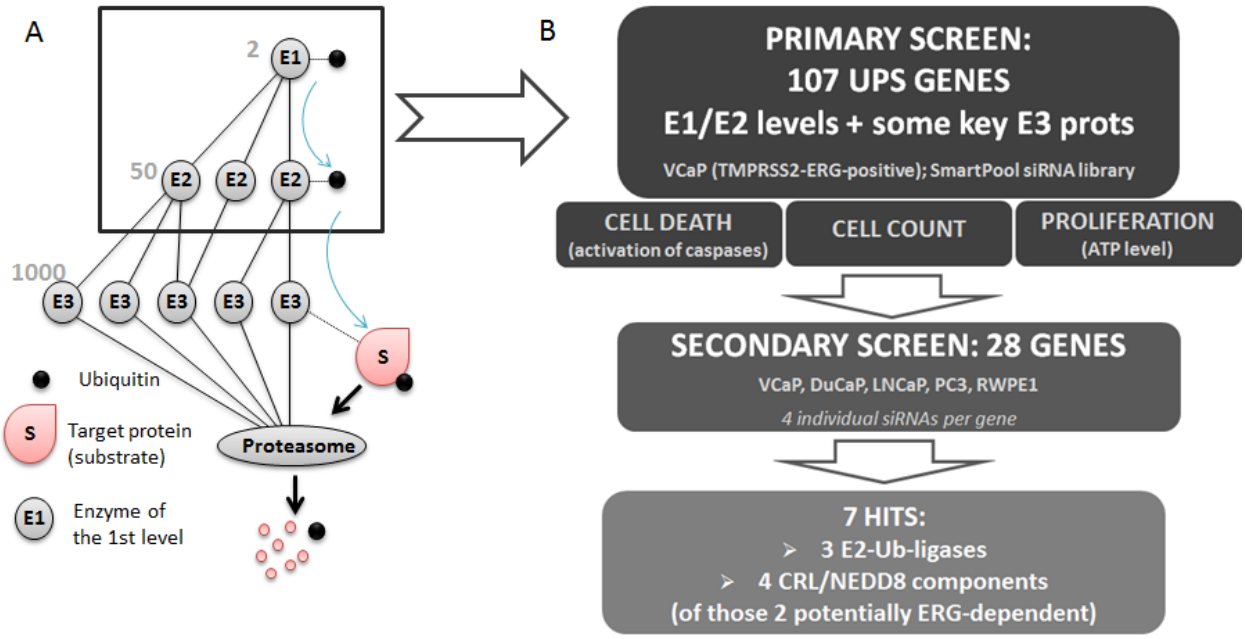

Figure 21. A. Hierarchical organization of UPS. Ubiquitin (or Ub-like protein) becomes activated by one of the corresponding E1-activating enzymes. This moiety is then transferred to one of the E2-conjugating enzymes, and then with the help of E3-ligase transferred directly to the target protein. The black square shows the enzymes taken into the primary screen. B. Diagram of the screens. The primary screen was done using the VCaP cell line which contains the TMPRSS2:ERG mutation. Based on 3 phenotypic parameters (cell death, cell count and cell viability/proliferation) 28 potential hits were selected out of 107 genes screened. The secondary screen was performed using five cell lines, 4 individual siRNA per gene from a deconvoluted pool. The secondary screen revealed seven hits, of those two are potentially ERG-dependent.

1.3 CANCER CELL LINES CHARACTERIZATION

The cell lines used in the screen (RWPE1, LNCaP, PC3, VCaP and DuCaP) represent different stages of cancer development (non-cancerous, cancerous and castration-resistant) and different cellular context (+/-/mut AR, +/-ERG) (Table 3). As a model for non-cancerous prostatic cells we used the RWPE1 line, established from the peripheral zone of a histologically normal adult human prostate, transfected with a single copy of the human papilloma virus 18. Among the PCa cell lines we selected two TMPRSS2:ERG-positive (VCaP and DuCaP) and two fusion-negative cell lines (PC3 and LNCaP). Despite the fact that the LNCaP cells do not possess oncogenic fusion TMPRSS:ERG, they harbor another translocation, activating the ETV1 gene from the same ETS-family of transcription factors (Tomlins *et al*., 2007a). The LNCaP, VCaP and DuCaP cell lines are AR signaling dependent, while PC3 is AR-independent. The VCaP and DuCaP cells have non-mutated AR (Sobel & Sadar, 2005), while the LNCaP cell line harbors a mutation in the ligand-binding domain of AR (T877A) in both alleles, which allows the receptor to be activated by progesterone, estrogen, adrenal androgens, and hydroxyflutamide in addition to androgens (Veldscholte *et al*., 1992).

The VCaP and DuCaP cell lines are derived from the same patient, but from different metastatic sites: VCaP were established from vertebral metastases and DuCaP – from the dura mater sites (Lee *et al*., 2001). Although these cell lines have the same origin, both of them also have distinctive genetic rearrangements (van Bokhoven *et al*., 2003a). Because both DuCaP cell line was established from mouse xenografts, DuCaP appears to have a contamination with mouse stromal cells, which could reach up to 50% in culture. Moreover, complete elimination of stromal cells is difficult in DuCaP cultures, because they seem to be required for the growth and adhesion of DuCaP cells (van Bokhoven *et al*., 2003b). Therefore, although we used the DuCaP cell line in our screen, the results obtained with this cell line should be considered carefully.

Table 3. Description of cell lines used in the screen.

Cell lines	TMPRSS2: ERG fusion	AR status	Metastatic site	Comments
RWPE1	-	+	-	Non-cancerous immortalized basalcells
VCaP	+++	+++	Vertebral	
LNCaP	-	+++ (T877A)	Lymph node	ETV1-activating fusion. AR is mutated in ligand binding domain
PC3	-	-	Vertebrae	
DuCaP	+	+	Dura mater	Derived from the same patient as VCaP cell line, but from another metastatic site. Highly contaminated with stromal cells

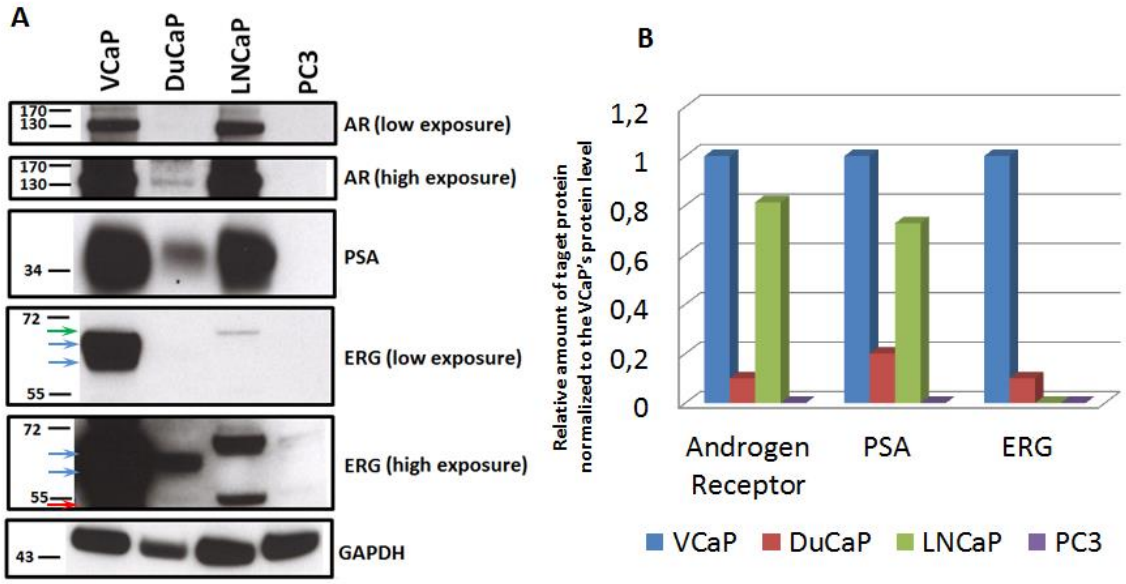

Figure 22. Presence of major prostate cancer markers in four PCa cell lines used in the screen. A. Total cell lysates of VCaP, DuCaP, LNCaP and PC3 cells were immunoblotted for major prostate cancer markers. The blots for AR and ERG presented in two levels of exposure because of differences in quantity of target protein. ERG (blue arrows) is found in VCaP cell lines (2 isoforms) and DuCaP (1 isoform). The red arrow shows a band that possibly corresponds to the Fli-1 gene product, since the antibodies we used were shown to cross-react with Fli-1, whose molecular weight is about 51 kDa. In LNCaP cells a band of higher molecular weight was observed (green arrow). B. Summary graph with quantification of Western Blot data.

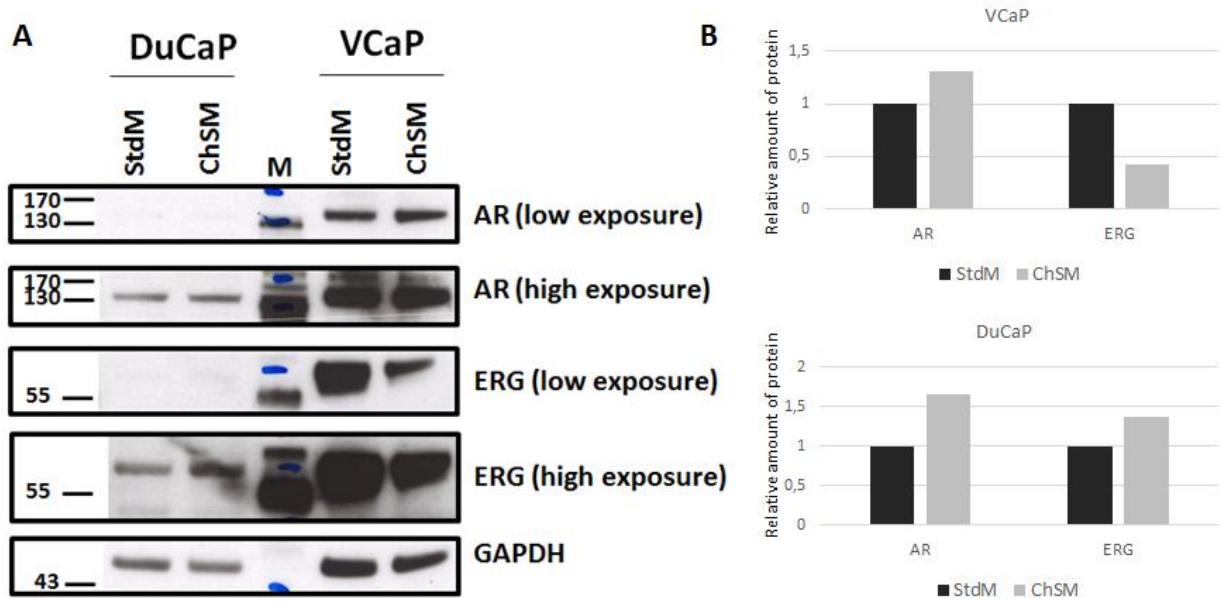

Figure 23. Difference in ERG and AR expression under hormone-depleted conditions. A. Cells were grown during 5 days on standard medium (StdM) or charcoal/dextran stripped medium (ChSM). Total cell lysates were immunoblotted for AR and ERG. The blots are presented in two types of exposures because of the differences in the concentrations of proteins in different cell lines. B. Summary graph with quantification of Bestern Blot data.

There are some discrepancies in the description of expression profiles of cell lines in the literature. Thus, even for such a well-known cell line as PC3, which is believed to be independent on the AR signaling and not expressing AR, there are reports describing the presence of AR mRNA and protein (Alimirah *et al*., 2006). Considering also possible stromal contamination of DuCaP cells, precautionary screening was done for major prostate cancer markers of the cell lines used. WB was used to detect the presence of AR, PSA and ERG proteins in the PCa cell lines (Figure 22). All cell lines, except PC3, expressed AR and PSA, but in DuCaP cells the level of these proteins was significantly lower. VCaP and DuCaP cells both expressed ERG fusion. In VCaP cells antibodies revealed two bands very close in molecular weight, which might represent two the isoforms described for VCaP cells: fusion of the first exon of TMPRSS2 gene with the forth exon of ERG (T1E4 isoform) with or without the 72 bp fragment of the eleventh exon (Wang *et al*., 2008). DuCaP cells possessed only a high molecular weight isoform at low concentrations.

To recapitulate the conditions of androgen-deprivation therapy a DMEM medium, supplemented with the charcoal/dextran stripped FBS (Charcoal-Stripped Medium, ChSM), was used. Charcoal/dextran stripping is frequently used for the depletion of serum from androgens, but this treatment also decreases the amount of other hormones and certain growth factors, such as estradiol, cortisol, corticosterone, the B vitamins, triiodothyronine (T3), thyroxine (T4) and prostaglandins (Carter, 1978). The depletion of androgens leads to a decrease in the expression of AR-responsive genes, such as PSA and TMPRSS2:ERG, which is shown using Western Blot (Figure 23). Interestingly, the amount of ERG protein in the DuCaP cell line does not change under hormone-depleted conditions (Figure 23). To examine possible differences in the effect of gene knockdown in conditions when ERG is depleted or expressed at usual level, this cell line was screened on both ChSM and Standard Medium (StdM, when normal, non-stripped, FBS is used).

1.4 PRIMARY SCREEN

The purpose of the primary screen was to identify putative gene-hits important for the viability of PCa cells. To estimate the effect of gene knockdown on cell viability three parameters were used: induction of apoptosis, proliferation and cell count. Induction of apoptosis was measured by activation of caspases (CellEvent Caspase-3/7 Green Detection Reagent, Life Technologies). The acquisitions were performed using CellInsight™ NXT High Content Screening Platform from Thermo Scientific. The images were analyzed and quantified by the "Cell Health Profiling" program, installed within the CellInsight™. Proliferation was estimated by the level of ATP (ViaLight™ Plus Cell Proliferation and Cytotoxicity BioAssay Kit, Lonza). Cell count was measured using images obtained in CellEvent experiments. Using several methods gave complementary information while permitting the choice of the most robust method for the secondary screen. The primary screen was done on ChSM with VCaP cells; the effects of siRNA knockdown were estimated on the fifth day after transfection. The results of the primary screen are presented on Figure 24, Figure 25 and Figure 26. Part **A** of each figure represents an ordered distributions of the values (from smallest to the biggest), while part **B** reprensents lists of "positive" and "negative" hits. The thresholds for each readout were chosen arbitrarily.

The dataset "Cell Death" (Figure 24) shows a very good distribution, which allows easy detection of hits. The plot has obvious "bends" in the upper and lower part of the graph, corresponding to about 20% outliers. The siRNAs found in the middle region had no apparent effect on cell viability. The negative control siAllStars is located in the center of the assumed "no effect" area, whereas the positive control siCellDeath had the highest level of dying cells (93%), which confirms the performance of the screen. The second highest value (75% of dying cells) was shown by siUBB, targeting ubiquitin itself. Knockdown of ubiquitin by siRNA is known to cause cell death (Oh *et al*., 2013) and is used as a part of siCellDeath from Qiagen (Hahn *et al*., 2013).

The results obtained from the measurement of proliferation also show a correct distribution. Control siRNAs are at the expected places (Figure 26). The data sets "Proliferation" and "Cell Death" show a quite good negative correlation (R= -0.714) (Figure 27), reflecting the expected antagonistic relationship between these phenotypes.

Both assays (Apoptosis and ViaLight) were most sensitive to the “toxic” siRNAs, which inhibit proliferation and induce apoptosis.

The “cell count” values show a much worse distribution, which complicates identification of the hits (Figure 25). Control siRNAs does not show the expected results: the effect of siCellDeath is very weak and siAS is shifted to the bottom of the graph. Moreover, its correlation with the other two datasets is the lowest. Of note, the parameters “Percentage of apoptotic cells” and “Cell Number” were obtained from the same experiment and thus supposed to be interdependent. However, the anti-correlation between these data sets is weak, with a correlation coefficient r = -0.299 (Figure 28). A possible explanation for this poor correlation is that the number of cells is a less repeatable parameter in general: it is difficult to put exactly the same amount of cells in the well and make them equally distributed within the well – there will always be fields with more and less cells. A second reason may be the low proliferation rate of VCaP cells: according to ATCC their doubling time is about 53 hours. Proliferation of VcaP cells in ChSM is even slower, which does not allow for detecting minor differences in the number of cells. Other sources of noise could be the way of cell segmentation during the data acquisitions, which is complicated by the properties of VCaP cells. The segmentation by the “Cell Health Profiling” program is based on the detection of nuclear staining (by Hoechst and CellEvent reagent), which is not often evident with VCaP cells growing in tight groups (**Error! Reference source not found.**). From all these considerations we conclude that the parameter “Cell Count” is not a good metric for VCaP cells.

A

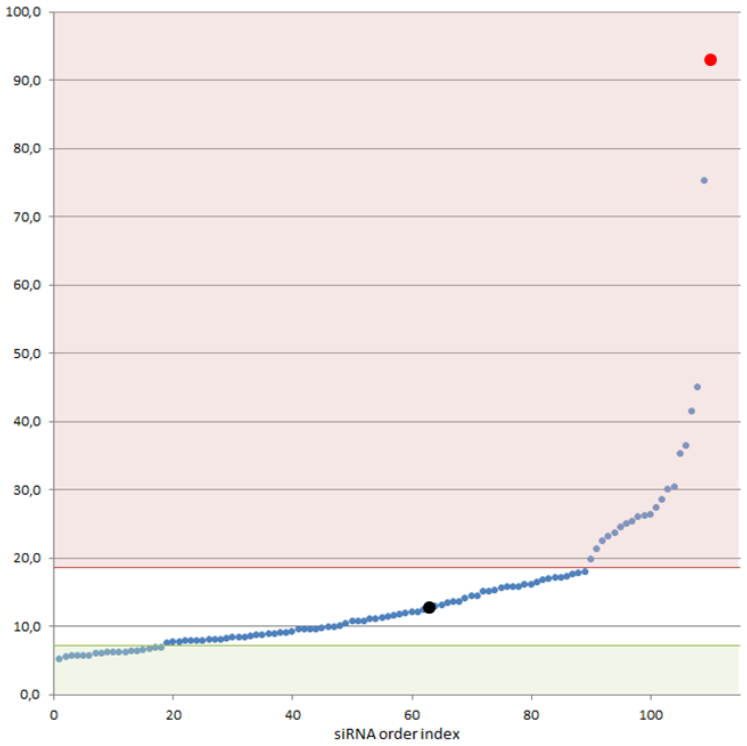

B

Index	siRNA	dead cells %
1	«+» control siCellDeath	92,9
2	UBB	75,3
3	UBE2U	45,0
4	HERC5	41,5
5	UBR4	36,5
6	CAND1	35,2
7	HERC2	30,4
8	UBR1	30,1
9	CACUL1	28,5
10	UBE2W	27,3
11	RNF25	26,4
12	VCP	26,2
13	UBR3	26,0
14	NEDD4	25,2
15	UBE2F	25,0
16	CUL2	24,5
17	UBR5	23,7
18	UBE2H	23,1
19	UBE2S	22,5
20	HECTD2	21,3
21	UBE2G1	19,7
48	«-» control siAllStar	12,7
93	USP9X	6,9
94	TRIP12	6,8
95	DCUN1D4	6,6
96	UFC1	6,5
97	HECTD3	6,4
98	UBE3A	6,3
99	UBE2E1	6,2
100	CAND2	6,2
101	UBE2M	6,2
102	UBA7	6,1
103	UBE2D1	6,0
104	CUL4A	5,9
105	USP2	5,7
106	UBE2G2	5,7
107	UBE2A	5,6
108	UBE2D3	5,6
109	UBR2	5,5
110	UBA1	5,2

Figure 24. Results of the primary screen with the VCaP cell line; readout - cell death. A – Ordered distributions of the data (from the smallest value to the biggest); B – the list of positive and negative hits. In black – negative control siAllStars, in red – positive control siCellDeath.

A

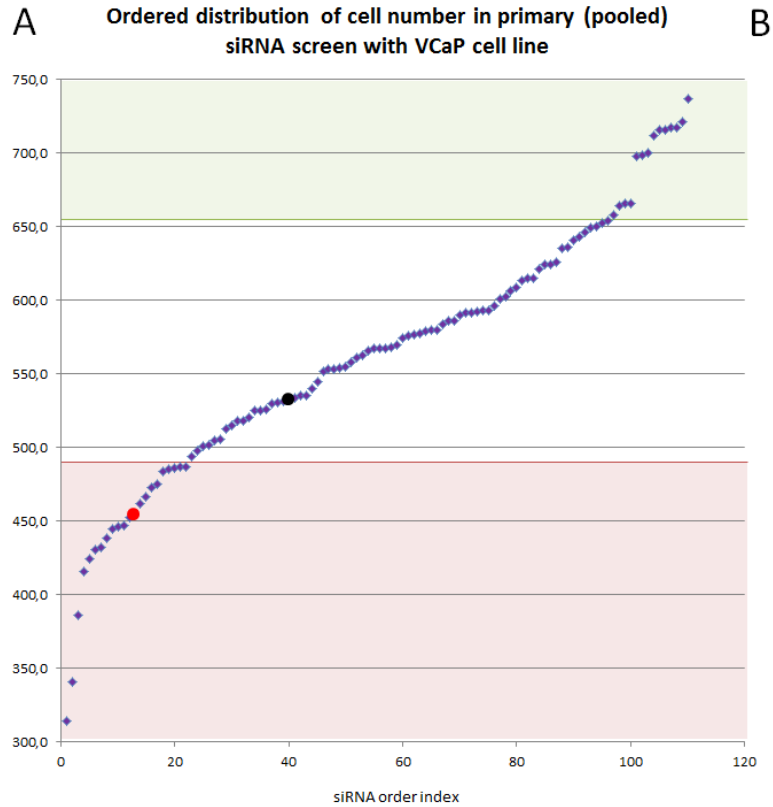

B

Index	siRNA	Cells per field
1	UBE2B	313,8
2	CACUL1	340,8
3	CUL2	385,8
4	UBE2U	416,0
5	TRIP12	424,0
6	CUL1	430,7
7	UBE2D1	432,0
8	UBE2F	438,5
9	UBR4	444,53
10	BIRC6	446,5
11	UBR5	446,8
12	UBE2N	452,2
13	«+» control siCellDeath	454,5
14	UBE2W	462,0
15	UBE2I	466,7
16	UBE2E3	472,7
17	NEDD4L	475,3
18	CUL5	483,7
19	UBA3	485,5
20	UBA6	485,7
40	«-» control siAllStar	533,7
97	UBE3C	658,2
98	DCUN1D5	664,3
99	CUL4B	665,5
100	DCUN1D3	666,2
101	UBE2Q1	698,2
102	UBE2QL1	698,7
103	CUL7	700,0
104	ATG7	712,2
105	UBE2J1	715,7
106	UBA2	716,0
107	UBE2Z	717,7
108	UBE2V2	717,8
109	UBE2D3	721,2
110	RWDD1	737,2

Figure 25. Results of primary screen with VCaP cell line; readout - cell number. A – Ordered distributions of the data (from the smallest value to the biggest); B – the list of positive and negative hits. In black – negative control siAllStars, in red – positive control siCellDeath.

A

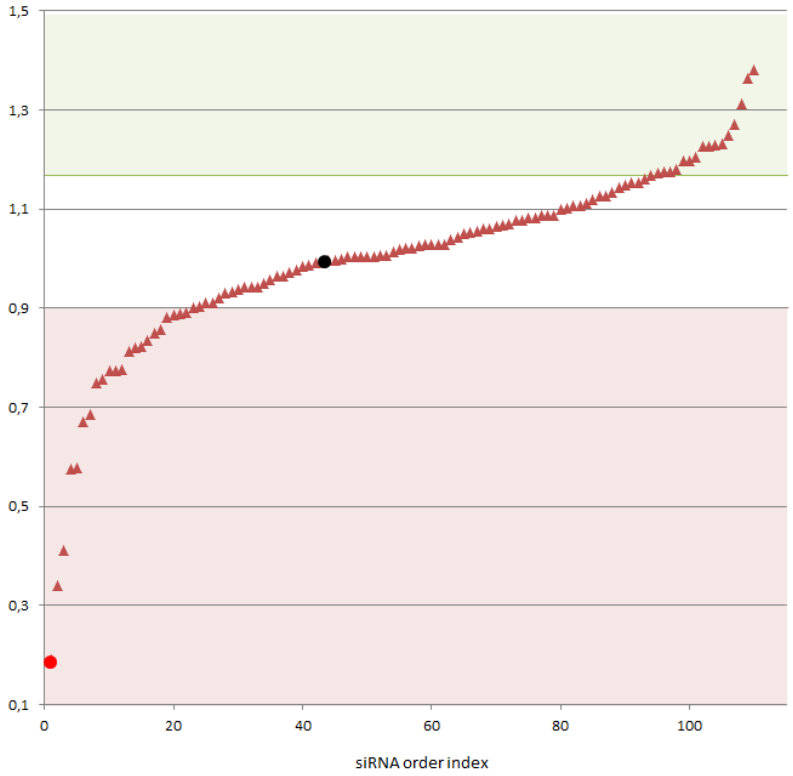

B

Index	siRNA	Proliferation, N
1	+» control siCellDeath	0,191768048
2	UBE2U	0,340725564
3	UBB	0,410244936
4	UBE2F	0,573752358
5	CAND1	0,576575101
6	UBA3	0,669861673
7	UBR4	0,684276054
8	KIAA0317	0,749014746
9	UBE2S	0,756090609
10	HUWE1	0,772750716
11	HERC5	0,773500448
12	ERG	0,776143455
13	UBR5	0,812703199
14	UBE2E3	0,820559833
15	SAE1	0,82327927
16	SMURF1	0,834906977
17	UBR1	0,848847473
18	UBE2G1	0,857380262
19	HECTD2	0,880758189
20	CUL2	0,886607055
21	UEVLD	0,888251741
22	HERC2	0,890862236
23	CACUL1	0,899664696
43	«-» control siAllStar	0,995287275
97	CUL3	1,175348471
98	RNF25	1,181142011
99	DCUN1D4	1,196678846
100	ARIH1	1,19681398
101	HERC1	1,203775838
102	UBE2Z	1,227014233
103	UBE2J1	1,227247814
104	UBE2E2	1,22856049
105	DCUN1D5	1,231392647
106	UBE2NL	1,247724711
107	DCUN1D3	1,26981908
108	CDC34	1,313110957
109	USP9X	1,364625151
110	UBE2D2	1,380614459

Figure 26. Results of primary screen with the VCaP cell line; readout - level of proliferation/ATP level. A – Ordered distributions of the data (from the smallest value to the biggest); B – the list of positive and negative hits. In black – negative control siAllStars, in red – positive control siCellDeath.

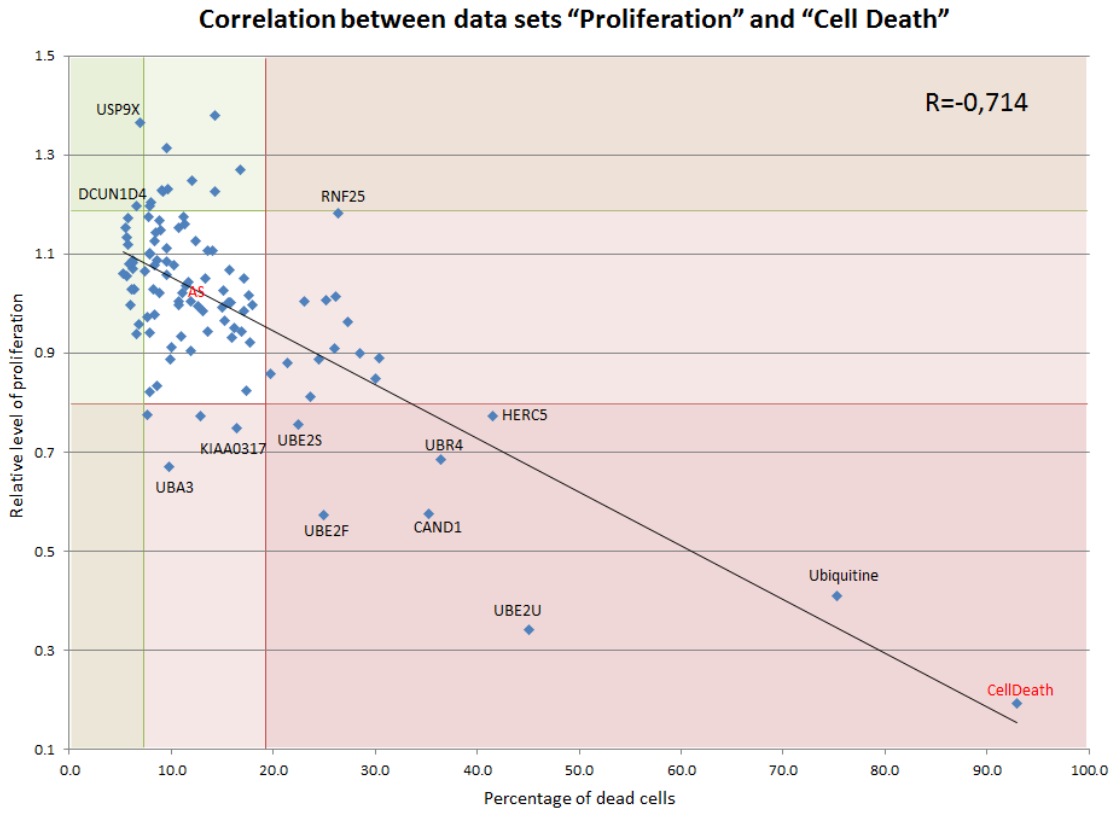

Figure 27. Correlation plot for data sets "Proliferation" (axis Y) and "Cell Death" (axis X).

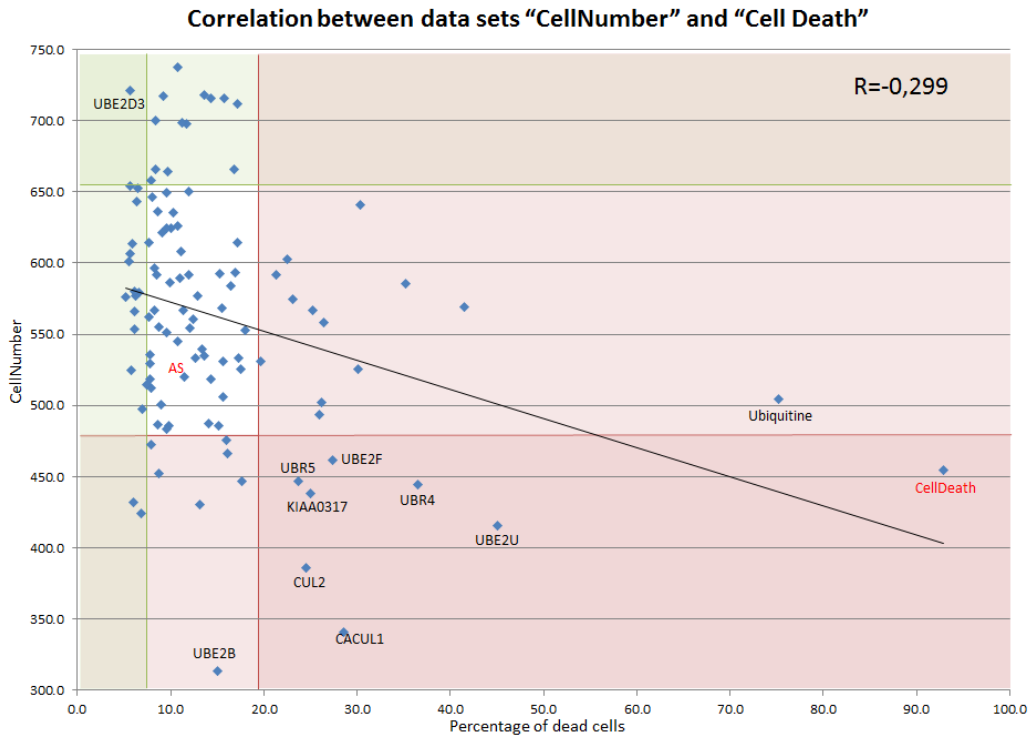

Figure 28. Correlation between data sets "Cell Number" (axis Y) and "Cell Death" (axis X).

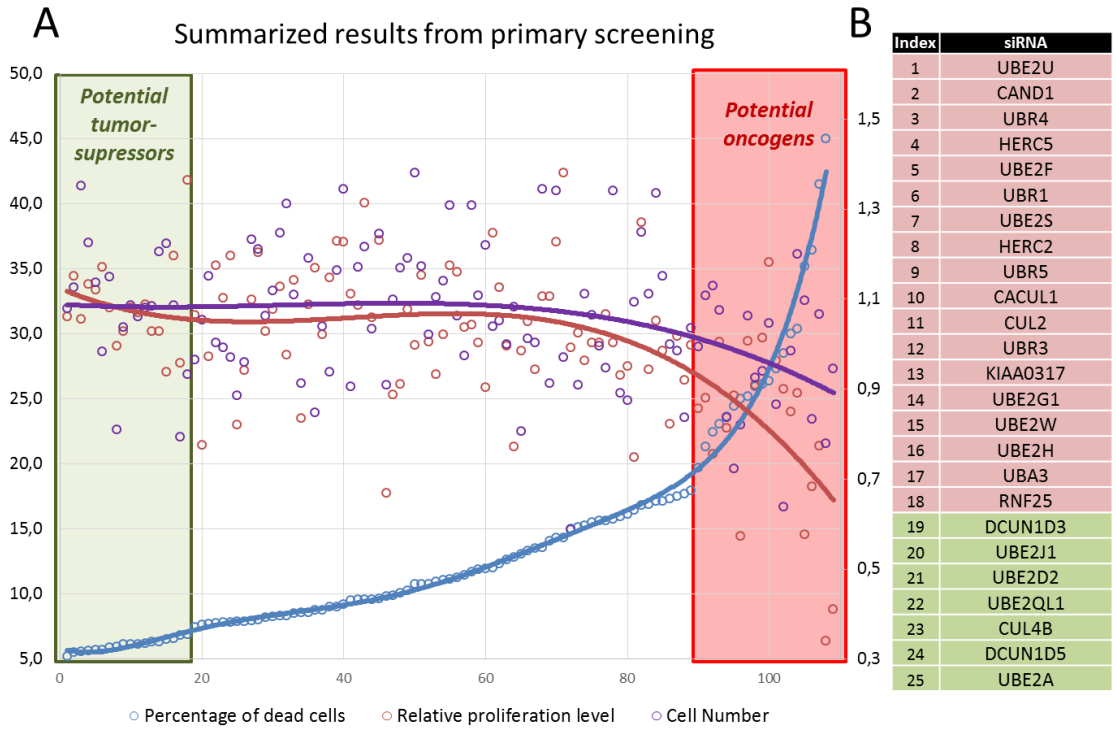

B

Index	siRNA
1	UBE2U
2	CAND1
3	UBR4
4	HERC5
5	UBE2F
6	UBR1
7	UBE2S
8	HERC2
9	UBR5
10	CACUL1
11	CUL2
12	UBR3
13	KIAA0317
14	UBE2G1
15	UBE2W
16	UBE2H
17	UBA3
18	RNF25
19	DCUN1D3
20	UBE2J1
21	UBE2D2
22	UBE2QL1
23	CUL4B
24	DCUN1D5
25	UBE2A

Figure 29. Summary of the primary screen. A**.** Data sets "Cell Death", "Proliferation" and "Cell Number" (blue, red and violet lines respectively) are summarized in one graph (without control siRNAs and siUbiquitin). Of interest are both potential proto-oncogenes (in the red square), whose suppression reduces viability of PCa cells, and potential onco-supressors (in the green square), whose knockdown increases proliferation and/or decreases apoptosis rate. B. Genes, selected for the secondary screen. In pink – potential proto-oncogenes; in green – potential onco-supressors. Genes are ordered by the strength of the effects (the strongest were UBE2U and UBE2A, the weakest were RNF25 and DCUN1D3).

During the primary screen two types of hits were identified (Figure 29): putative **proto-oncogenes** (genes, which knockdown decreases proliferation and induces apoptosis) and putative **tumor suppressors** (genes, which knockdown promotes proliferation and decreases spontaneous apoptosis). The terms proto-oncogenes and tumor suppressors are used to describe the observed short-term effects of knockdown. However, the long-term effects of the inhibition of these genes could be opposite: decrease in spontaneous apoptosis may be caused by induction of translesion synthesis, inhibition of DNA damage response (DDR) proteins, initiation of senescence, etc. These processes can lead to cell death through a different mechanism, and thus may not be beneficial to cancer cells. The strongest hits from both groups were selected for the secondary screen (Figure 29, B).

The 25 strongest hits obtained in the primary screen could be divided in 4 groups according to their functions (Figure 30):

1) **E2 Ub-conjugating enzymes** (UBE2A, UBE2D2, UBE2G1, UBE2H, UBE2J1, UBE2QL1, UBE2S, UBE2U, UBE2W).
2) **E3 Ub-ligases** (HERC2, HERC5, RNF25, KIAA0317).
3) **Members of CRL/NEDD8 pathway** (CACUL1, CAND1, CUL2, CUL4B, DCUN1D3, DCUN1D5, UBA3, UBE2F). The involvement of NEDD8-pathway in cancer progression is well-established, though there is much less information available on its role in PCa. One specific inhibitor of NEDD8-pathway, MLN4924, is currently in phase I of clinical trials. Of note, the screen revealed that the different members of NEDD8-pathway caused opposite effects: part of them could be referred to as proto-oncogenes, and others as potential onco-supressors (Figure 29).
4) **Members of N-end rule pathway** (UBR1, UBR3, UBR4 and UBR5). The N-end rule states that the N-terminal amino acid of a protein determines its half-life (chance of being degraded). Specific N-terminal protein residues, called N-degrons, are recognized by the recognition components N-recognins of UBR E3 ligases. Although UBR1-5 share the same mechanism of substrate recognition, these proteins perform independent functions.

Due to the enrichment of the hits from the CRL/NEDD8 pathway in the screen, to the secondary screen it was decided to add siRNA targeting other genes from this

pathway: RBX1 and RBX2 (E3 ligases of the pathway) and SPOP, a substrate receptor of CRL3 ligase, which is often mutated in prostate cancer, the event shown to be mutually exclusive with TMPRSS2:ERG mutation (Barbieri *et al*., 2012; Rubin, 2012). The final list of the 28 candidate genes selected for further validation is presented in Figure 30. The sequences of corresponding siRNAs are given in Supplementary Table 3.

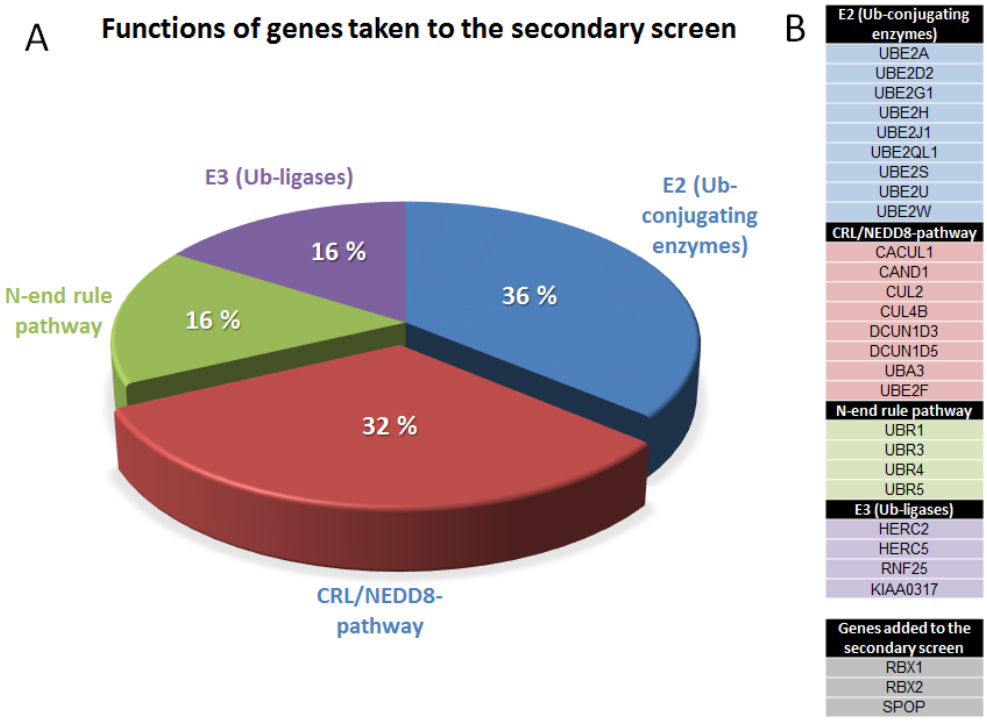

Figure 30. Classification of the hits from the primary screen. A. Classification of genes selected for secondary screen by their function. B. Final list the 28 candidate genes selected for further validation.

1.5 SECONDARY SCREEN

1.4.1 Technical notes

The goal of the secondary screens was preliminary confirmation of the hits. These screenings were performed with individual siRNAs from deconvoluted siRNA-pools. The complete list of siRNAs chosen for the validation is presented in Supplementary Table 3. The cell lines used in this screen were: transformed non-cancerous cells (RWPE1), ERG-negative cancer cells (LNCaP, PC3) and ERG-positive cells cancer (VCaP, DuCaP). Examination of cells with different status (+/-AR, +/- ERG, wt/mut p53, etc.) allowed for addressing the dependence of gene knockdown on cellular context. To diminish off-target effects, individual siRNAs were used at 10 nM concentration. The time of siRNA treatment was optimized for each cell line depending on the proliferation rate and sensitivity of the cell line to siRNA. Thus, the effect of gene knockdown was analyzed on the third day of siRNA treatment for the LNCaP, PC3 and RWPE1 cell lines, and on the fifth day for VCaP and DuCaP cells.

Because the most robust method to estimate the effect of siRNA on cell viability apparent from the primary screen was apoptosis assay for caspases activity (CellEvent reagent), this was used as a major parameter in the secondary screening. As a complementary method cell count was used. Although this parameter was not very reliable for the VCaP cell line, for the other cell lines the expected clear anti-correlation with apoptotic rate was observed and the controls were at the expected positions (Figure 31).

The same protocol of transfection for all cell lines was used, with 4 well replicates per siRNA separated into two plates. A hit was selected when muRZ, the average among replicates of the robust Z-score per siRNA was above 0.82 (see the section SCREEN QUANTIFICATION). Although this threshold is relatively low, it was considered reliable because 5 cell lines were screened and two siRNAs per gene with the same phenotype were required to select a gene hit. The scores for each siRNA and each cell lines for induction of apoptosis are presented in Supplementary Table 6. Positive scores signify increased value of the parameter, while negative scores indicate a decrease after siRNA transfection.

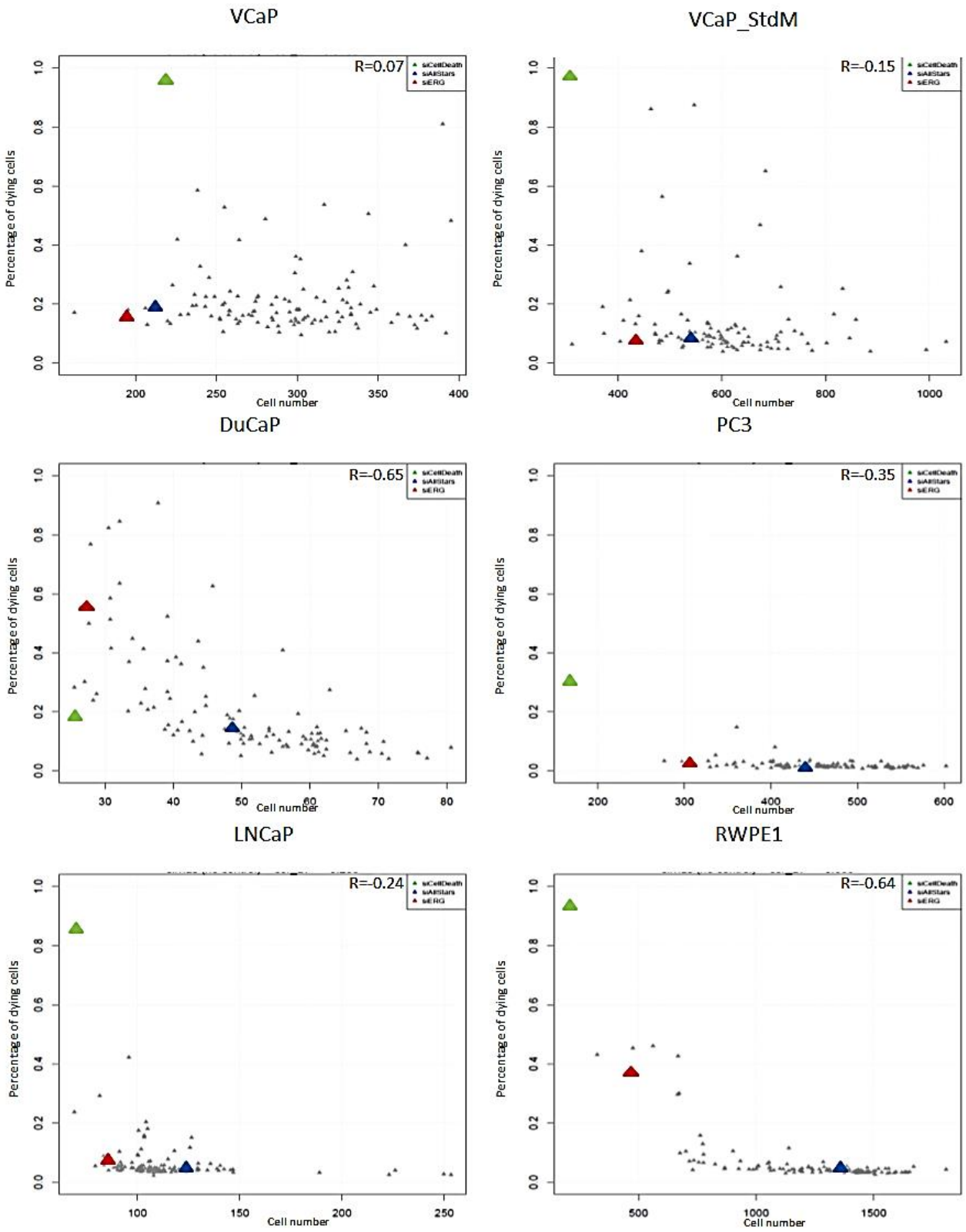

Figure 31. Correlation plots for parameters "Cell Death" and "Cell Number" for all the tested cell lines. Green triangle – siCellDeath, blue – negative control siAllStars, red – siERG. VCaP cells show poor anti-correlation and the control siAllStars is displaced from expected positions. Nevertheless, the other cell lines show much better correlation and controls are located at expected positions.

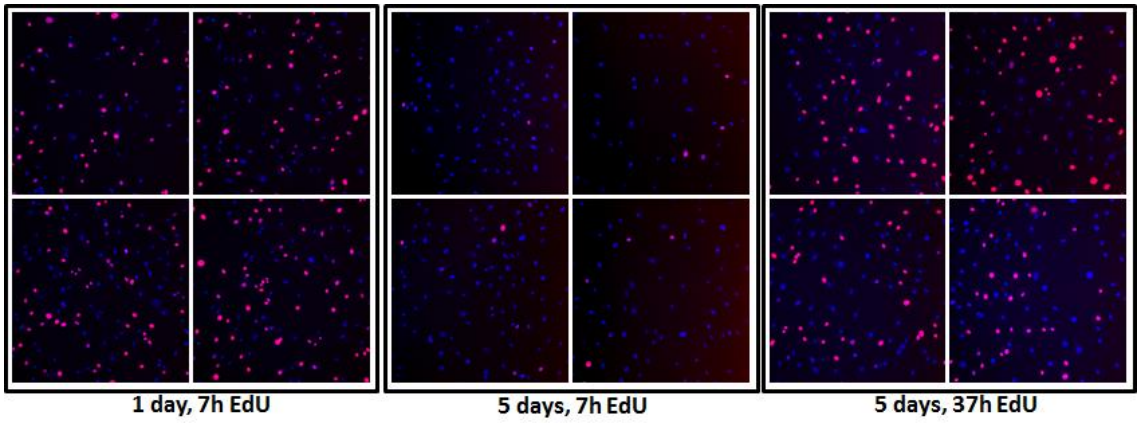

Figure 32. EdU pulse in DuCaP cells. Nuclear staining with Hoechst is shown in blue. EdU staining is shown in red. After 1 day of incubation there is about 40% proliferating cells in population. After 5 days of incubation the amount of proliferating cells (with the same time of EdU-pulse of 7 hours) decreases dramatically. After increasing the time of incubation of cells with EdU up to 37 hours we can visualize about 30% of cells incorporating EdU.

Performing the screen, some unexpected effects were observed on control siRNAs (Supplementary Table 6, Figure 31). In all tested cell lines, the negative control siAllStars did not cause apoptosis, which results in a very low muRZ-scores ranging from -0.03 up to 0.16 depending on cell line. The positive control siCellDeath caused massive apoptosis in the majority of cell lines resulting in muRZ-scores above 14. However, siCellDeath did not cause apoptosis in DuCaP cell line. siCellDeath target two genes: Ub and Polo-like kinase 1 (PLK1), which is responsible for progression through the cell cycle. Thus, an extremely low level of proliferation and slow metabolism could render cells insensitive to siCellDeath. To examine the proliferation level of the DuCaP cell line EdU incorporation pulse was performed. Indeed, despite the initial burst of proliferation, the growth rate of DuCaP cells decreased dramatically after a few days in culture (Figure 32, left and middle panel). Nevertheless, by increasing the time of EdU pulse up to 37 hours, it was possible to detect EdU incorporation (Figure 32, right panel). We believe that this extremely low proliferation rate was caused by contact inhibition. This could allow DuCaP cells to escape from proliferation-dependent apoptosis.

It was also observed that siRNA against ERG caused apoptosis in all tested cell lines except VCaP. Initially, this siRNA was taken as a second negative control, because it was shown to decrease proliferation of VCaP cells without induction of apoptosis (Tan *et al.*, 2009). Indeed, siERG caused a strong decrease in proliferation without causing apoptosis in VCaPs (Figure 24; Figure 26). Unexpectedly, other tested cell lines responded to siERG treatment by induction of apoptosis (Supplementary Table 6). At present, it is difficult to determine if this effect was specific or off-target. ERG protein

expression in prostate tissue is considered to be specific for TMPRSS2:ERG-positive samples. Nevertheless, the ERG gene is still present in all cell lines, and might be expressed at a very low level. Consistent with this assumption, it has been reported that ERG mRNA is expressed in normal prostatic cells and in TMPRSS2:ERG negative PCa samples and cell lines, including LNCaP used in the screen (Zammarchi *et al*., 2013). Thus, apoptosis caused by ERG inhibition in this present experiment could be explained by critical depletion of the protein resulting in the abortion of some vital function.

A very good reproducibility was observed of the screen between plate replicates with correlation coefficient above 0.9 for all cell lines (Figure 33, A-G). To compare the robustness of various cell lines in response to siRNA perturbations global Standard Deviation of the dataset (gSD) was used. This parameter reflects the number of hits and their strength for each cell line (Figure 33, H). Of note, because the primary screen was performed on VCaPs, the pre-selected hits were specific to this cell line. Nonetheless, according to gSD, the DuCaP cell line appeared to be the most sensitive to the perturbations induced by pre-selected siRNAs. The most robust cell line appeared to be PC3. Considering that even siCellDeath did not have a strong effect on PC3 (about 40 percent of dying cells in the population in comparison to 90-100 percent for other cell lines), it might suggest that the time of siRNA treatment (three days) was not optimal for this cell line. Increasing the incubation time might increase the sensitivity of PC3 cells to siRNA treatment.

To compare the effect of gene knockdown in conditions when ERG is depleted or expressed at normal level, VCaP cells were screened both in ChSM and in StdM. The correlation between the data obtained with VCaPs in these two conditions ($r = 0.83$) was higher than the correlation between VCaPs datasets and any other tested cell line (Figure 34, C). This suggests that the overall response of VCaP cells to siRNA knockdown was similar in ChSM and StdM (Figure 34, A). Among the strong hits ($muRZ > 2$) there were four specific to ChSM while the other four were observed only in StdM (Figure 34, B). However, because all these perceived hits were the only siRNA having an effect out of four siRNAs per gene, this most likely indicates off-target effects. Among weaker hits only siRNAs for cullin 2 (CUL2) and CAND1 showed differential behavior in ChSM and StdM. Moreover, siRNAs against CUL2 effectively caused cell death in another ERG-dependent cell line (DuCaP) and had a much weaker (or no) effect on other cell lines. Altogether, these data might suggest ERG-specificity of the CUL2 hit.

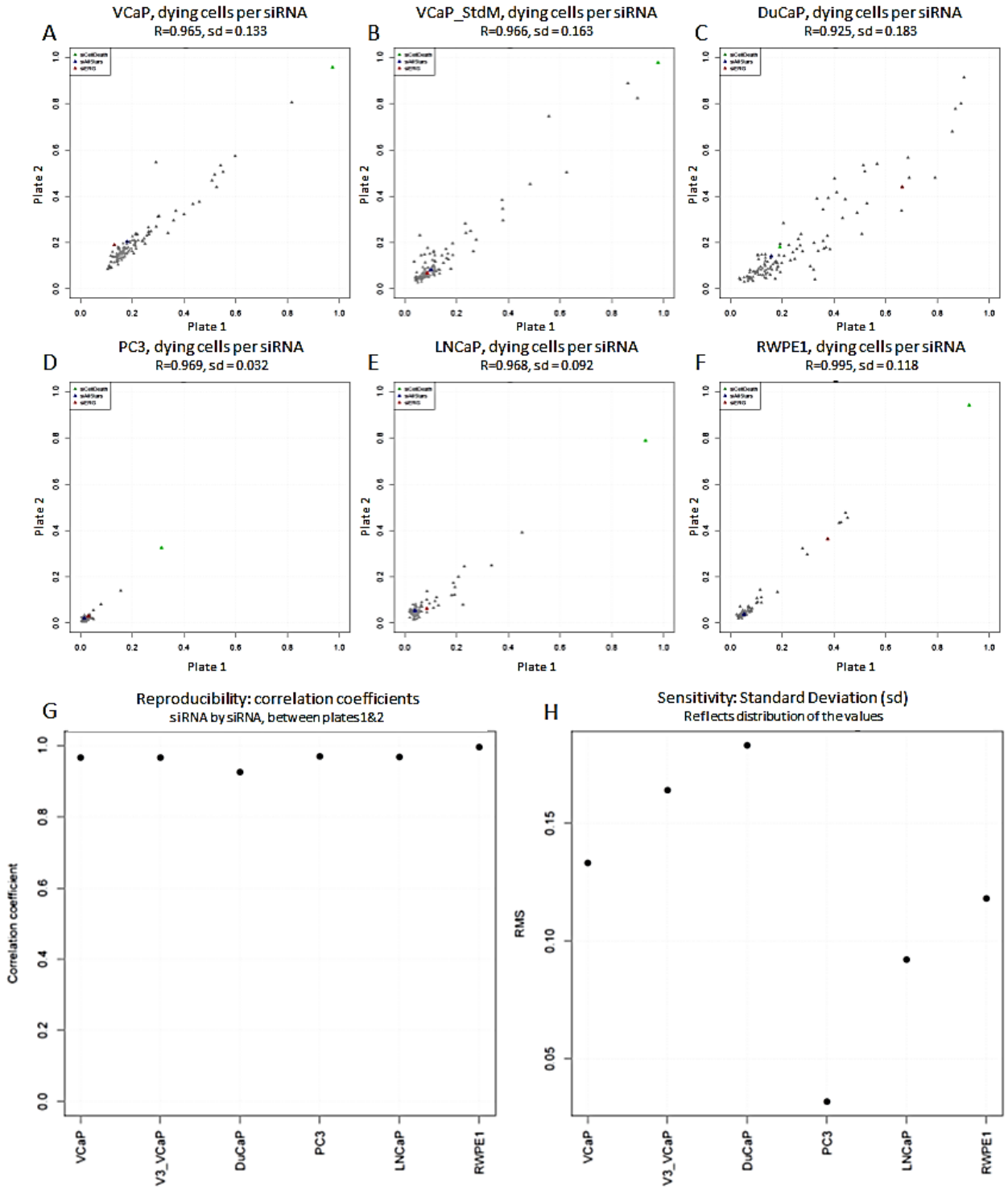

Figure 33. A-F. Reproducibility of "the percentage of dying cells per siRNA" parameter in two replicate plates for each cell line. G. Reproducibility (correlation coefficient between plates) is very high for all the cell lines (r > 0.9). H. Global Standard Deviation for each cell line reflects their robustness. The smaller the gSD – the more robust cell line is.

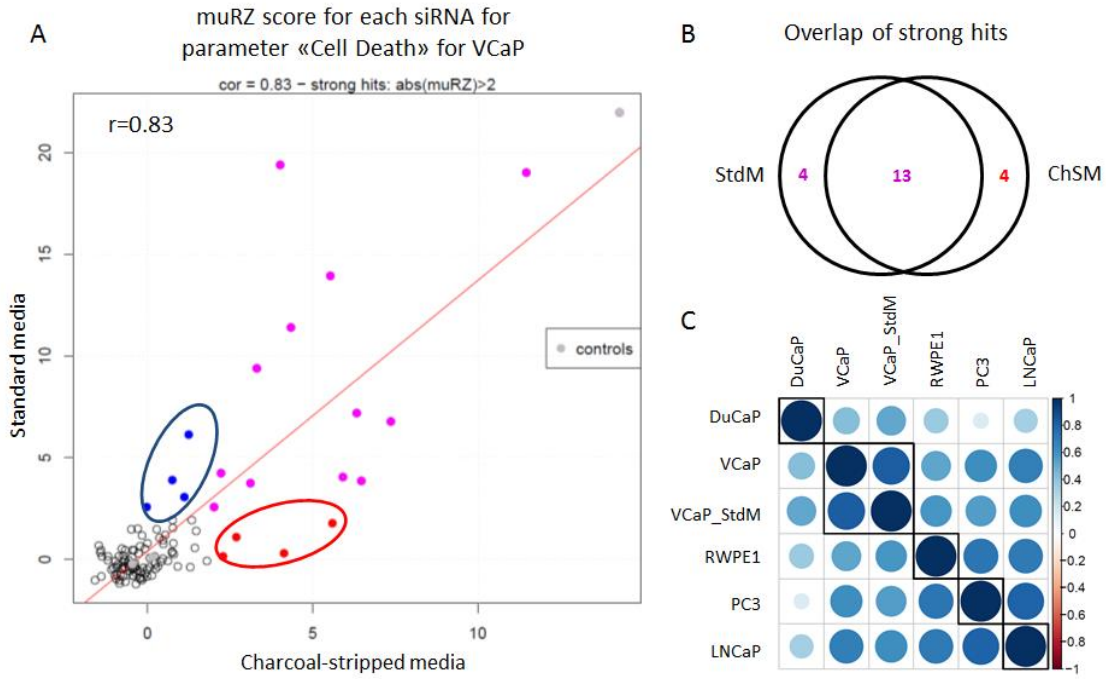

Figure 34. Comparison of hits for VCaP cell line on StdM and ChSM. A. Scores for each siRNA for the VCaP cell line in ChSM and StdM show strong positive correlation (r=0.83), which is close to the correlation coefficients observed between replicates for the same cell line. B. Venn diagram, showing overlap between strong hits (muRZ>2). There are 13 hits that are effective in both StdM and ChSM, and 8 siRNAs that are strong hits either in StdM or ChSM. C. Classification of cell lines based on correlation coefficient. VCaP on StdM and on ChSM have the highest correlation between each other than with other cell lines.

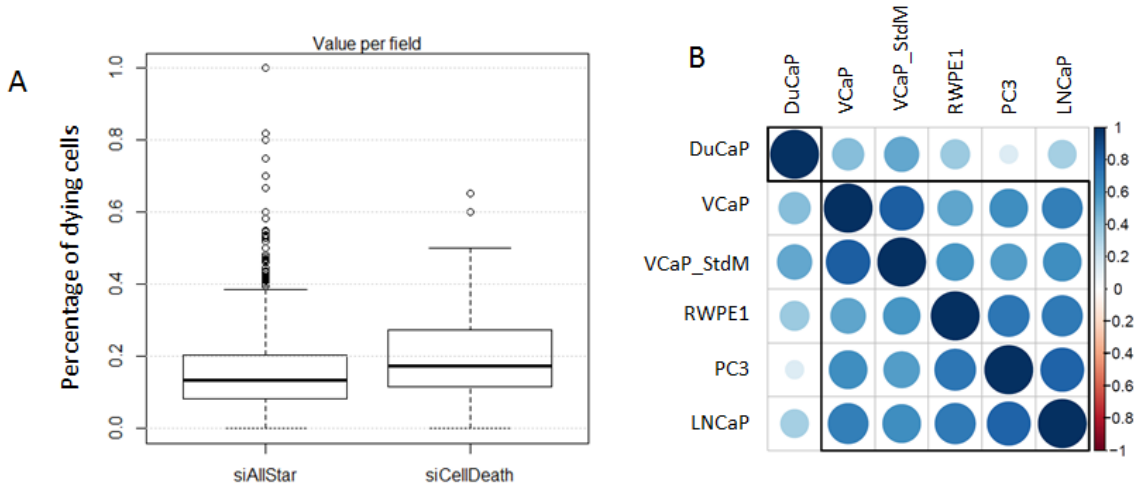

Figure 35. A. Relative level of apoptotic cells in a population of DuCaP cells when treated with control siRNAs: the negative control being siAllStars and positive control siCellDeath. B. Correlation plot showing that compared to other tested cell lines DuCaP is the most distinct in terms of apoptotic response after siRNA treatment.

The cell line DuCaP showed the most distinct behavior. First, siCellDeath did not induce apoptosis in this cell line (Figure 35, A). Second, the phenotypical outcome of the inhibition of the UPS genes in DuCaPs was the most different compared to other cell lines (Figure 35, B). Third, DuCaPs had significantly lower amounts of AR then other cell lines, and only one isoform of ERG was present at a significantly lower level compared to VCaPs (Figure 22). Moreover, despite DuCaP being considered to be androgen-responsive cell line, the amount of ERG protein did not change in ChSM compared to StdM (Figure 23). Considering also the reports about stromal contamination, it was conclude that the DuCaP cell line is not a reliable model of ERG-dependent PCa cells. Thus, VCaP cells were used as the major model of TMPRSS2:ERG-positive PCa, although data obtained with DuCaPs could give complementary information.

1.4.2 Description of hits

The results of the secondary screening are presented in Supplementary Table 6 (a table with muRZ-scores for each individual siRNA and every cell line) and Supplementary Table 7 (a table summarizing the screening). Hits selection were based on the following parameters:

1) How many siRNA per gene cause the same phenotype? If two or more siRNA had the same phenotype, this gene was considered a hit.

2) What is the relative strength of the hits? Are they similar in strength? If one siRNA causes a strong effect, while others are rather weak, this most likely signifies an off-target effect.

3) Does inhibition of the gene cause the same phenotype in all cell lines? Having the same effect for all tested cell lines would suggest that the function of gene is not dependent on cellular context and is of general importance for prostate cells.

Parameters 1 and 2 allow calculating mixt_muRZ, which represent relative probability of the hits for each cell lines. Graphical representations of mixt_muRZ for the VCaP cell line are presented in the Figure 36 (A and B). Based on the three parameters mentioned above we selected seven hits (Figure 36C). Of these seven, three are E2-Ub-ligases (UBE2U, UBE2H and UBE2A), while four are the members of CRL/NEDD8 pathway (CAND1, CUL4B, CUL2 and RBX1). Two hits are potentially ERG-dependent (CUL2 and RBX1), because they had an effect in ERG-positive cell lines only (VCaP, or

DuCaP, or both). Inhibition of genes had different effects, including apoptosis (for UBE2U, CAND1, CUL2, UBE2H) and survival (for UBE2A, CUL4B, RBX1). A detailed discussion of these hits is presented below.

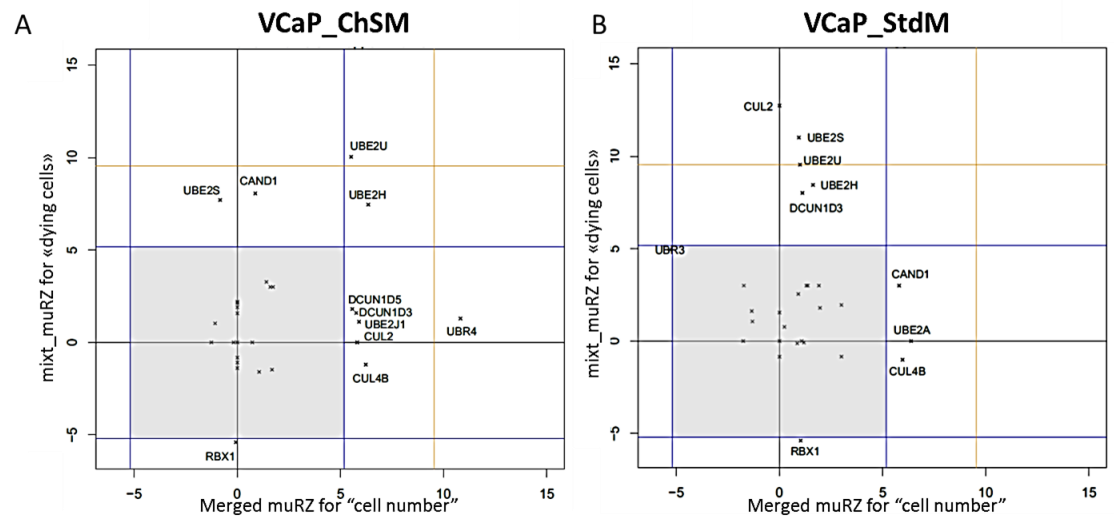

C

Gene	Overall	Consensus	VCaP	VCaP (StdM)	DuCaP	PC3	LnCaP	RWPE1	Comment
UBE2U	death	All	3 (but 09)	2	3	2	2	3	Extremely clear phenotype
CAND1	death	All	2 (to 3)	1	2	2	2	2 (but 12)	Extremely clear phenotype
UBE2H	death	Except PC3 and LNCaP	2 to 3	2	2	0 (but 07)	1 (but 08)	2	Potentially ERG-specific?
CUL4B	survival AND ↑ in cells	All except LNCaP	1 AND 2	2 (but 06) AND 2	0 AND 3 to 4	0 (but 07) AND 2	0 and 0	2 AND 1 to 2	weak but clear
UBE2A	survival AND ↑ in cells	All	0 to 2 AND 0	0 to 2 AND 2	1 AND 0	1 to 2 AND 1	2 to 4 AND 2	1 AND 0	weak but clear
RBX1	survival OR ↓ in cells	Only VCaP	2 to 3	2	1 (but 08) OR 0	0 (but 09) OR 1	0 OR 2 to 3	0 OR 3	Opposite phenotype for LNCaP and RWPE1
CUL2	death	VCaP & DuCap	0 to 1	3	2	1 (but 08 & 06)	1 (but 07)	1	No effect for VCaP in ChSM (ERG suppresed?)

Figure 36. General overview of the hits.
A and B: Mixt_muRZ scores for each gene based on the muRZ scores obtained from 4 siRNAs per gene. Genes beyond the blue line have 2 siRNAs being hits, beyond the orange line - 3 siRNAs. When on the line (e.g. UBE2U VCaP_StdM), it means just 2 siRNAs, but with high muRZ-score (above 3 here).
C: Table with summary information about hits (a full summary for each gene can be found in the Supplementary Table 7). Designations: numeric - number of hit siRNAs causing the same phenotype (apoptosis/increase in cells/etc.). 2 to 3: means 2 hits above the threshold, and 1 just below the threshold. 1 (but 07): 1 hit with the 'major' phenotype, but siRNA with catalogue number 07 has an opposite effect. In red - hits decreasing viability, in green - increasing viability. Column "Overall" describes the "major" phenotype caused by the gene inhibition: death – more apoptosis, survival – less apoptosis, ↓/↑ in cells – decrease or increase of cell number comparing to control.

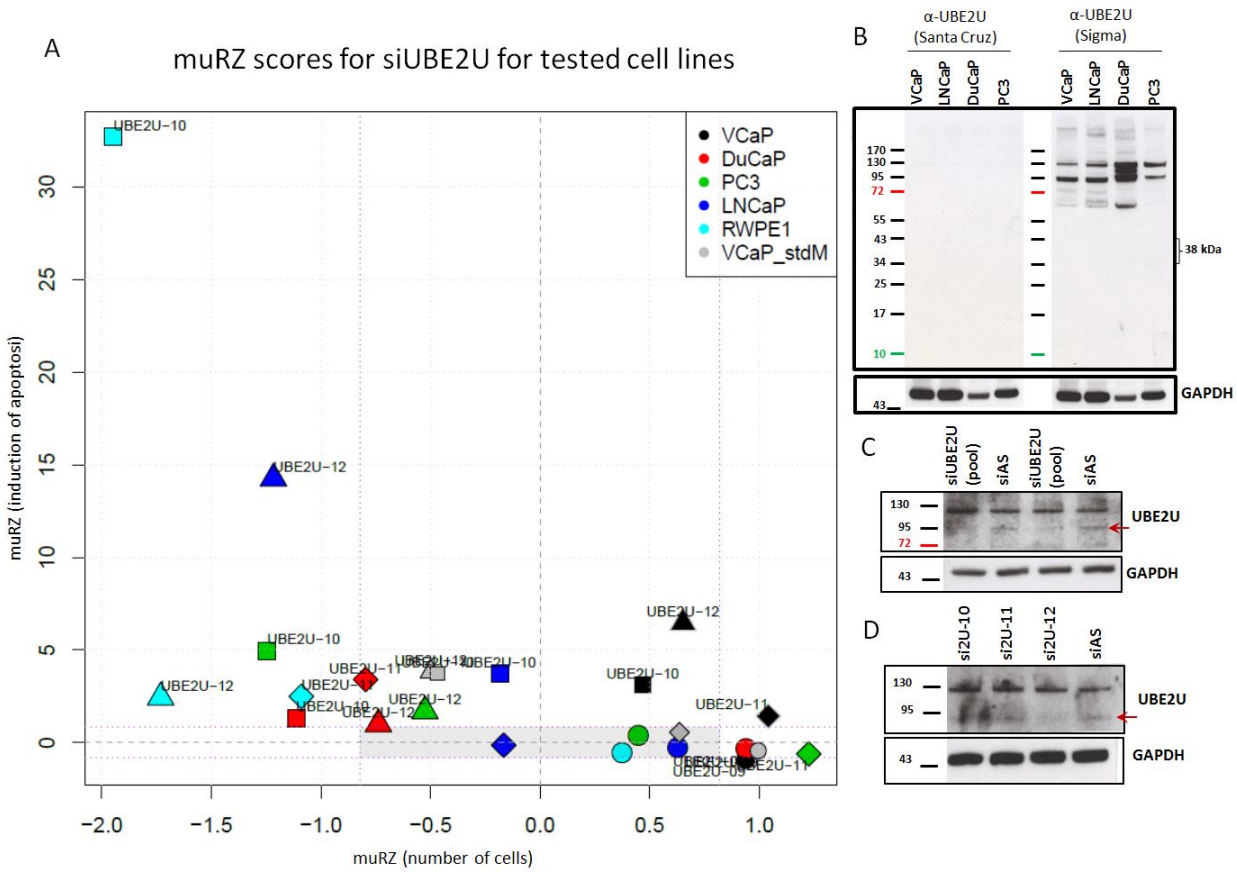

Figure 37. A. Graphical representation of siRNA action for the UBE2U gene. The graph represents the phenotypical changes (proportion of dying cells and changes in cell number) for each of 4 siRNAs and all the 5 cell lines tested (VCaP presented in 2 conditions: in ChSM, as all the other cell lines, and in StdM). muRZ is an averaged Robust Z-score from quadruplicates for each siRNA. The grey dotted lines indicate zero values for both axes. Pink dotted lines indicate threshold values: everything above or below these values (outside grey rectangle) is considered to be a hit.
B: The total cell lysates of VCaP, DuCaP, LNCaP and PC3 cells were immunoblotted with UBE2U antibodies from 2 manufacturers (Santa Cruz and Sigma). First the membrane was stained with antibodies from Santa Cruz, but since there was no signal, antibodies from Sigma were used on the same membrane; hence the loading control (GAPDH) is the same. Antibodies from Sigma also did not show any staining at the predicted MW of UBE2U (38 kDa), but it reveals bands of much higher MW (with 2 major bands at 95 kDa and 130 kDa).
C. VCaP cells which had been transfected with siUBE2U pool (total mix of 4 siRNAs) or with negative control siAS and immunoblotted against UBE2U (Sigma).
D. VCaP cells which had been transfected with 3 strongest siRNAs individually (si2U-12, si2U-10 and si2U-11 from strongest to the weaker) or with negative control siAS and immunoblotted against UBE2U (Sigma).

UBE2U

The strongest identified hit was UBE2U. Three of four tested siRNAs caused apoptosis in all cell lines with very high muRZ-scores (Supplementary Table 6 and Supplementary Table 7; Figure 37). There is almost no information about the function of this gene. UBE2U is mentioned only in genome-wide or E2-limited interactome screens (Markson *et al.*, 2009; van Wijk *et al.*, 2009; Rolland *et al.*, 2014, etc.). The UBE2U gene is only present in mammalian genomes and is mapped to the human Chromosome 1. There are about 30 predicted mRNA transcripts in the NCBI database, but only one of them has been confirmed so far (NM_152489.1) and it is used in all published reports

addressing the function of UBE2U. This isoform has 9 exons and is transcribed into a 226 a.a. protein (NCBI Reference Sequence: NP_689702.1). Because the protein has a characteristic E2-ubiquitin-conjugating fold with a preserved active site Cys, it could be a functional E2-Ub-conjugase. However, until now no ubiquitin (or ubiquitin-like) conjugation activity have been described in the literature. One of the reports has shown that UBE2U has no activity in an *in vitro* assay for the transfer of Ub from UBE1 or UBE6 (Jin *et al.*, 2007).

The data on UBE2U's interaction network vary a lot and are not conclusive. Van Wijk and colleagues using Y2H system and the E2 + E3 protein library have shown that UBE2U has the highest number of interactions with E3s (52 interactions) compared to other E2s. They have reported that UBE2U has a unique E3-interactome, and after removing UBE2U from the network only 20 of UBE2U's E3 partners remain connected to other E2s, whereas 32 E3s become unconnected (van Wijk *et al.,* 2009). This suggests a general role of UBE2U in ubiquitylation. Another team (Markson *et al*., 2009), also using the Y2H system, with E2-bait and genome-wide preys, has shown only 13 interaction with E3-ligases for this E2-conjugase. The most recent genome-wide study of its interactome (Rolland *et al*., 2014) shows only one E3-partner for UBE2U – TRIM32. Interaction partners reported in more than one paper are TRIM32 (Markson *et al.,* 2009; Rolland *et al*., 2014) and RNF144B (Markson *et al.,* 2009; van Wijk *et al*., 2009).

TRIM32 and RNF144B are poorly characterized proteins with unrelated functions. TRIM32 is a member of the TRIM E3-Ubiquitin ligases family of RING proteins with more than 70 members in the human genome. TRIM32 has been shown to play an important role in antiviral defense (Zhang *et al.,* 2012; Fu *et al*., 2015). One study showed that, upon induction by pro-inflammatory cytokines, TRIM32 is covalently modified by another Ub-like protein FAT10 (Aichem *et al*., 2012). TRIM32 was shown to negatively regulate p53 to promote tumorigenesis (Liu *et al*., 2014). RNF144B is an E3-Ubiquitin ligase with an important role in apoptosis. RNF144B is a transcriptional target of p53 and induces p53-dependent but caspase-independent apoptosis by ubiquitylation and degradation of p21 (Huang *et al*., 2006; Ng *et al*., 2003). RNF144B has also been shown to be a direct transcriptional target of ΔNp63 a (transcription factor that is critical for the development of stratified epithelia). At the same time RNF144B binds and mediates proteasomal degradation of ΔNp63α, generating an auto-regulatory

feedback loop. These findings substantiate RNF144B as a potentially critical component of epithelial homeostasis (Conforti *et al.*, 2013).

Considering that the expression of UBE2U mRNA has been shown to be restricted to the urogenital tract (to the testis by GTEx Analysis Release V4, Uhlen's Lab and Illumina Body Map, and to the prostate by the Cancer Genome Anatomy Project), and that there was a strong effect of UBE2U inhibition for all tested prostate cell lines, it was of interest to get more information on this protein and on its function in prostatic cells. First, the presence of the protein, in the current study's chosen cell lines, was examined (Figure 37, B). Two commercially available antibodies (from Santa Cruz and Sigma) were tested, but neither of them showed the presence of a protein of the predicted size (38 kDa). Finally, antibodies from Sigma, produced against a catalytic domain of UBE2U, did show protein staining at higher molecular weight with two major bands at 95 and 130 kDa. In order to check whether these bands are specific to UBE2U, VCaP cells were transfected with siUBE2U-pool (total mix of 4 siRNAs) or with the 3 strongest siRNAs separately (si2U-12, si2U-10 and si2U-11 from the strongest to the weakest) (Figure 37, C and D). After transfection, the 95-kDa band disappeared compared to the negative control siAllStars (siAS), and the strongest si2U-12 also had the strongest effect. Nevertheless, there was no success in obtaining a Western Blot of good quality for this protein due to the low level of expression and insufficient sensitivity of the method.

An attempt was made to detect the presence of UBE2U at mRNA level. Four pairs of primers were selected targeting different isoforms (pairs 1 and 2 – against described transcript NM_152489; pairs 3 and 4 – against predicted isoforms). Amplification was weak and not always equal (probably because of the low concentration of target mRNA), but using primer pair 3 (Supplementary Table 5) three major isoforms were obtained (Figure 38, A). Sequencing has shown that all these isoforms consist of the described exons of predicted UBE2U mRNA isoforms (Figure 38, B and C). However, the full transcripts were not identical to any described or predicted transcripts, and thus represent absolutely new isoforms. Unfortunately, none of the found isoforms contain exons with the sequence corresponding to the strongest siRNAs si2U-12, which is present in the majority of predicted isoforms from the NCBI database (Figure 39, A). Moreover, the proteins transcribed from the isoforms that had been amplified were truncated. The predicted protein sequences obtained by translation of identified UBE2U isoforms are shown below. Only the largest predicted protein still contains the active site, while the

medium and small constructs lack catalytic residues (Figure 39, B) and, therefore, also lack enzymatic activity.

The data from screening suggest an important role of UBE2U in the prostate. Unfortunately, at present it is not possible to tell if it is protein or RNA that is crucial for the survival of prostatic cells. By PCR the presence of several isoforms of UBE2U were demonstrated in the VCaP cell line, but considering the extremely low level of its expression and the absence of isoforms with exon bearing the sequence of the most potent siRNA, most likely there are many more isoforms present in the genome which could have different functions. The presence of a specific band of much higher MW than predicted (95 kDa instead of 38 kDa) in all tested prostatic cell lines supports this conclusion. To characterize the role of UBE2U in prostatic cell lines it is important to determine which isoforms are expressed and are crucial for the survival of these cells, and one of the possible ways is to use RACE amplification to identify all the possible isoforms.

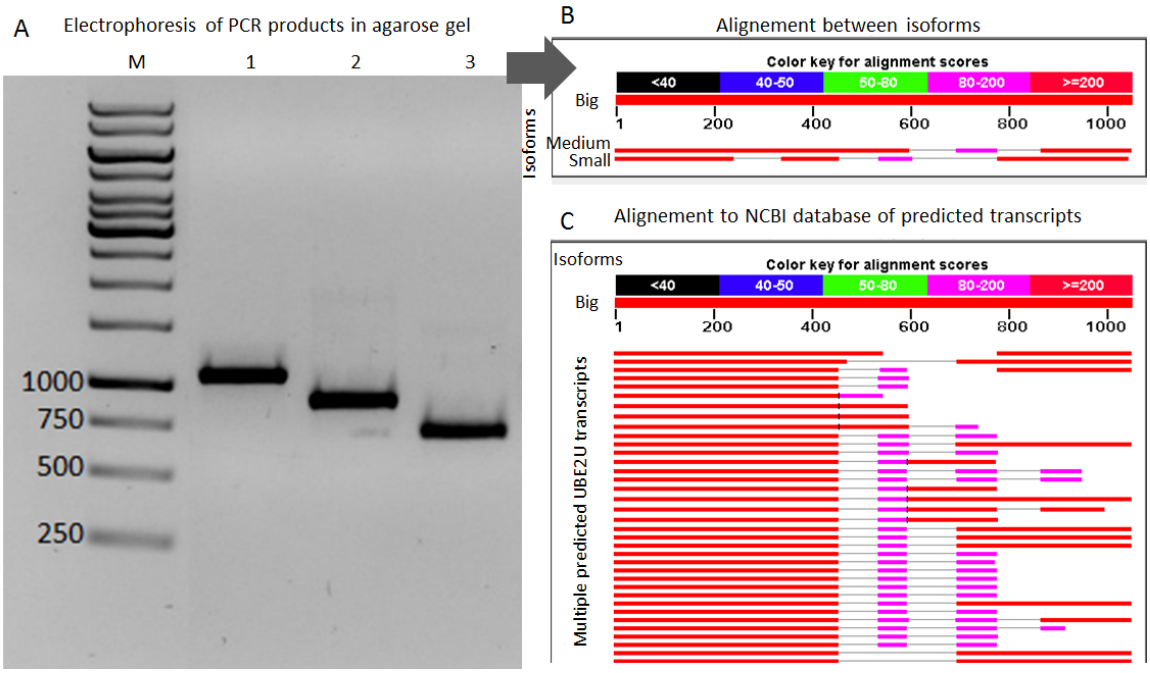

Figure 38. UBE2U mRNA amplification and sequencing. A. Representative electrophoresis of PCR products in agarose gel with 3 major isoforms (big, medium and small). B. Alignment of the sequences of obtained isoforms. C. Alignment of the big isoform to the NCBI database of transcripts.

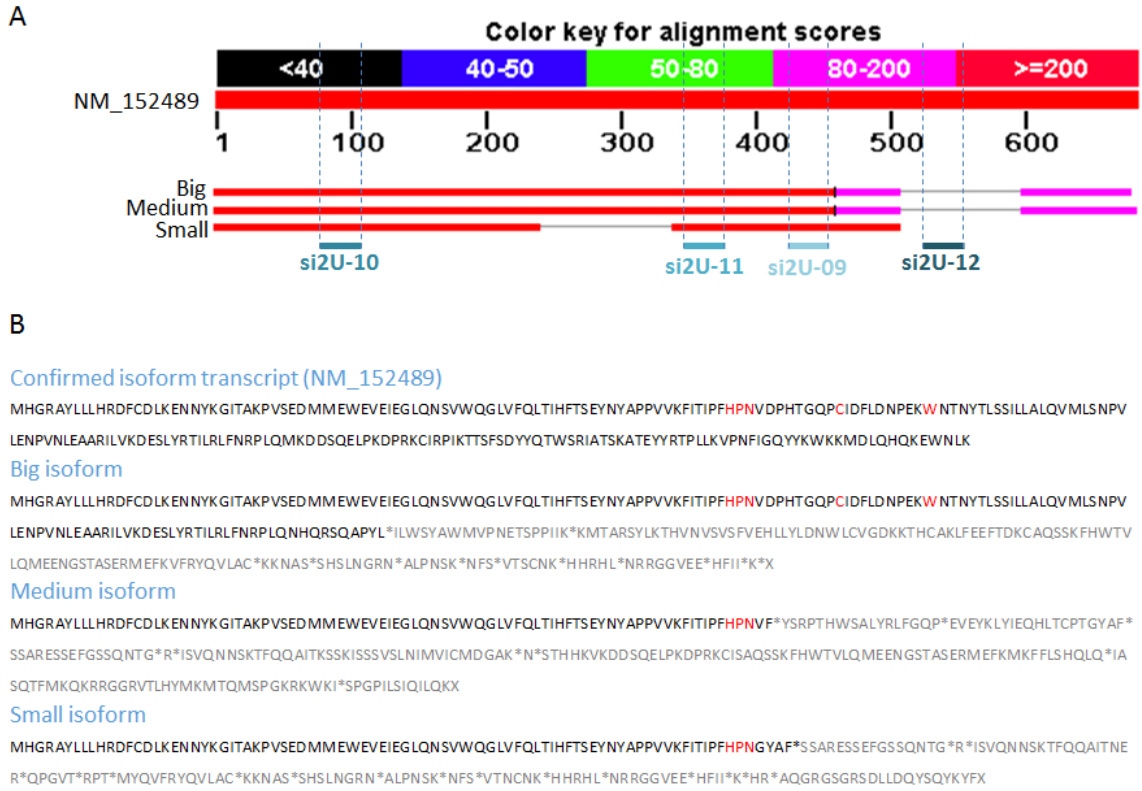

Figure 39. A. Location of siRNAs used in the screening on mRNAs of UBE2U. As a reference the confirmed isoform transcript NM_152489 is shown. The most potent si2U-12 does not target any of the amplified isoforms. B. Predicted translated proteins from isoforms detected in our research (big, medium and small isoforms) and from reference isoform NM_152489. In red the amino acids crucial for formation of active site of E2 enzymes are shown, including the active site cysteine (C), star – stop-codon, in grey – non-translated part of the protein. Only the reference isoform translates into a full-length protein. The big isoform is shortened, but nevertheless contains amino acids crucial for catalytic activity. Both the medium and the small isoform are predicted to be translated into short inactive proteins without catalytic activity.

UBE2H

Knockdown of UBE2H caused apoptosis in TMPRSS-ERG-positive cells VCaP and DuCaP, as well as in the non-cancer RWPE1 cell line, but had no effect on either PC3 (AR-independent) or LNCaP (ETV1-positive) (Supplementary Table 6 and Supplementary Table 7; Figure 40A). The efficacy of tested siUBE2H in the VCaP cell line was confirmed at protein level (Figure 40, B).

UBE2H is an E2-Ubiquitin conjugase overexpressed in many types of cancer, including cancer of the prostate, ovaries and breast (The Human Protein Atlas, Expression Atlas from EMBL). UBE2H plays an important role in several developmental pathways, including the negative regulation of skeletal myogenesis through ubiquitylation and the subsequent degradation of focal adhesion kinase (FAK) and insulin receptor substrate 1 (IRS-1) (Nguyen *et al.*, 2014; Yi *et al.*, 2013) and in the erythroid differentiation of hCD34(+) cells (Lausen *et al.*, 2010). UBE2H is also involved in spermatogenesis, where

it participates in ubiquitylation of H2A and H2B and thus is essential for chromosome remodeling, double strand break (DSB) repair and normal progression through meiosis (An *et al*., 2012). Furthermore, UBE2H participates in degradation of p53 protein (Doyle *et al*., 2010).

Among tested PCa cell lines, only the VCaPs expressed the UBE2H protein at a detectable level (Figure 40, C), which might suggest involvement in the ERG-dependent pathways. Nevertheless, considering that UBE2H is often overexpressed in cancers of reproductive system (prostate, ovarian and breast cancer) and is involved in cancer progression (by DNA remodeling and p53 degradation) it may be an interesting drug-target.

UBE2A

Knockdown of UBE2A decreased apoptosis and increased cell number in the VCaP, PC3 and LNCaP cell lines. A weaker prosurvival effect was also observed in DuCaP and RWPE1 cells (Supplementary Table 6 and Supplementary Table 7; Figure 41). Even though not many scores were beyond the threshold, it is clear that all of them are shifted to the right lower part of the graph. It should be noted, that due to the experimental setup the detection of apoptosis inhibition was more difficult compared to apoptosis induction, and thus requires stronger validation.

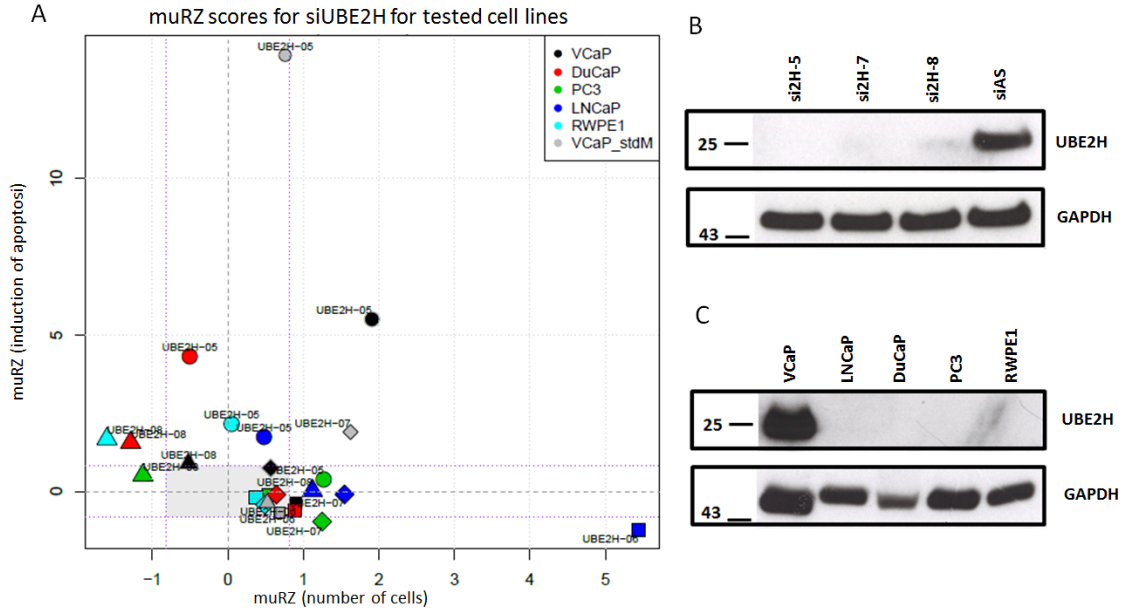

Figure 40. Graphical representation of siRNA action for the UBE2H gene. A. The graph represents the phenotypical changes (proportion of dying cells and changes in cell number) for each of 4 siRNAs and all 5 cell lines tested (VCaP presented in 2 conditions: in ChSM, like other cell lines, and in StdM). muRZ is an averaged Robust Z-score from quadruplicates for each siRNA. Grey dotted lines indicate zero values for both axis. Pink dotted lines indicate threshold values: everything above or below these values (outside of grey rectangle) is considered to be a hit. B. The effect of

si2H on expression of the protein. VCaP cells were transfected with the 3 strongest siRNAs individually (si2H-5, -7 and -8) or with the negative control siAS and immunoblotted against UBE2H. C. Expression of UBE2H in the tested cell lines. Only VCaP cells express UBE2H at a detectable level.

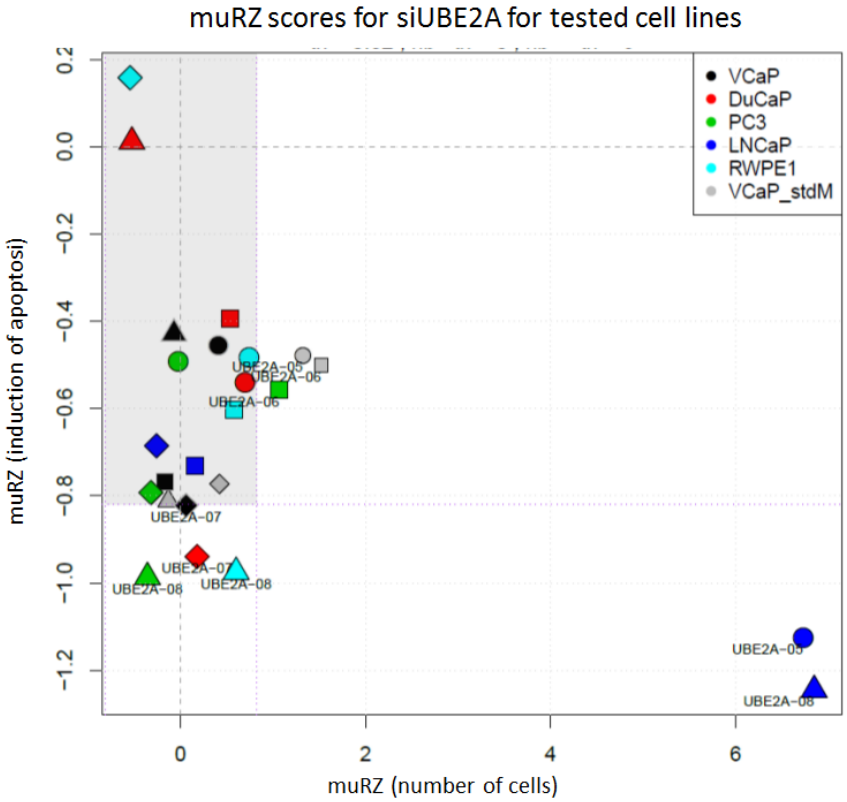

Figure 41. Graphical representation of siRNA action for the UBE2A gene. A. The graph represents the phenotypical changes (proportion of dying cells and changes in cell number) for each of 4 siRNAs and all the 5 cell lines tested (VCaP presented in 2 conditions: in ChSM, like the other cell lines, and in StdM). muRZ is an averaged Robust Z-score from quadruplicates for each siRNA. Grey dotted lines indicate zero values for both axis. Pink dotted lines indicate threshold values: everything above or below these values (outside of grey rectangle) is considered to be a hit.

UBE2A is an E2-Ubiquitin-conjugase homologous to yeast protein Rad6, which is a key player in DNA damage response. Monoubiquitylation of the proliferating cell nuclear antigen (PCNA) by Rad6 stimulates translesion (error-prone) DNA synthesis, while polyubiquitylation of the PCNA with the same enzyme activates the error-free repair pathway. Mutations in the catalytic site of Rad6 confer hypersensitivity to a variety of DNA damaging agents (Chen *et al.*, 2012b). The human genome encodes two homologues of Rad6 protein: UBE2A and UBE2B. They have 70 % of homology and often perform complementary, partially redundant functions (Xin *et al.*, 2000). For example, under exposure to ionizing radiation (IR), RNF168 attracts both UBE2A and UBE2B to the sites of DNA DSB, where they induce ubiquitylation of DNA-bound proteins and initiate DNA damage response. Depletion of either UBE2A or UBE2B individually does not affect DNA damage response, while the suppression of both

proteins at once abrogates DNA-damage-induced Chk1 activation, and affects G2/M cell cycle arrest (Liu *et al*., 2013). Similarly to yeasts, human UBE2A is required for mono- and poly-ubiquitylation of the PCNA, the key events of post-replication DNA repair. Depletion of UBE2A and 2B impairs homologues recombination (HR) following IR treatment and results in increased DNA damage (Liu *et al*., 2013, Chen *et al*., 2015).

UBE2A has also unique functions, distinct from UBE2B, in maintenance of cellular homeostasis. Similarly to Rad6, UBE2A may ubiquitylate histone H2B (Chen *et al*., 2012a; Kim *et al*., 2009a; Masuda *et al*., 2012). In the monoubiquitylated form H2B (H2Bub1) plays key roles in transcription, DDR and stem cell differentiation (Masuda *et al*., 2012; Sadeghi *et al*., 2014; Shchebet *et al*., 2012; Barkley *et al*., 2012; Cole *et al*., 2015). In many types of advanced cancers, including breast, colorectal, lung and parathyroid cancers, the level of H2Bub1 is downregulated (low to absent), which makes H2Bub1 and the enzymes affecting it level a promising therapeutic targets in cancer (Kim *et al*. 2009a; Cole *et al*., 2015). Indeed, the UBE2A gene was found to be recurrently mutated or inactivated in myeloproliferative diseases (de Miranda *et al*., 2014; Kunapuli *et al*., 2003).

According to the present study's results, the inhibition of UBE2A gene decreases the level of apoptotic cells and increases cell number. The basal level of apoptosis in the screens probably reflects spontaneous death induced by unbalanced proliferation and impaired DNA replication. Thus, inhibition of UBE2A protein may lead to the bypassing of apoptotic signaling by induction of error-prone DNA synthesis and/or insufficient activation of the p53 protein.

CAND1

The second strongest hit was CAND1. All 4 tested siRNAs (typically 2 siRNA per cell line) caused cell death in all tested cell lines with very high muRZ-scores (Supplementary Table 6 and Supplementary Table 7; Figure 42, A). The efficiency of tested siRNAs on the inhibition of CAND1 expression was confirmed at the protein level (Figure 42, B). The protein was detected in all cell lines at similar levels, with the exception of LNCaPs demonstrating significantly lower CAND1 expression (Figure 42, C).

CAND1 (cullin-associated and neddylation-dissociated 1) plays a critical role in the function of E3 CRL-ligases and thus in specific protein degradation. It is the only

known exchange factor allowing CRL complexes to change substrate specificity (for more details see chapter 2.4 NEDD8-pathway of the literature review). The data from the literature suggest an important role of CAND1 in cancer development, although the precise effect is not clear. Zhai and colleagues (2014) demonstrate downregulation of CAND1 protein in tumors compared to normal tissue. Nevertheless, non-biased screenings demonstrate both overexpression and downregulation of the protein during prostate cancer development (Expression Atlas from EMBL, Korzeniewski *et al*., 2012).

The direct effect of CAND1 knockdown on PCa cells was investigated in only one study, using LNCaP as a cell model. The authors described androgen-responsive miR-148a, which controls CAND1 expression (Murata *et al*., 2007). They showed that miR-148a inhibits CAND1 expression by binding to the 3′-UTR region of CAND1 mRNA, which promotes LNCaPs proliferation. Using siRNA against CAND1, they showed the same effect of promoting LNCaP cell proliferation compared to control siRNA. Nevertheless, inhibition of CAND1 expression and stimulation of proliferation could be independent events: miRNAs were shown to regulate hundreds of genes through partial complementarity in the seed region (Laganà *et al*., 2014). Moreover, the authors have tested the effect of a single siRNA against CAND1 with a single cell line. The off-target effects of siRNA are well known, and currently it is advised to use at least four siRNAs against different exons of the gene to confirm the phenotypical outcome. On the other hand, the mechanism of CAND1 regulation by miR-148a may be LNCaP-specific, as, according to the present study's data, CAND1 is strongly down-regulated in LNCaPs comparing to other cell lines (Figure 42, C).

In the present study, siRNAs targeting four different regions of CAND1 mRNA in five prostatic cell lines were used. Induced apoptosis in all four siRNAs was observed in all tested cell lines, including LNCaP. Interestingly, for the VCaP cell line the effect of siCAND1 is weaker in standard medium than in charcoal-dextran stripped medium (Supplementary Table 6 and Supplementary Table 7), this could suggest an AR-dependency of the CAND1 function.

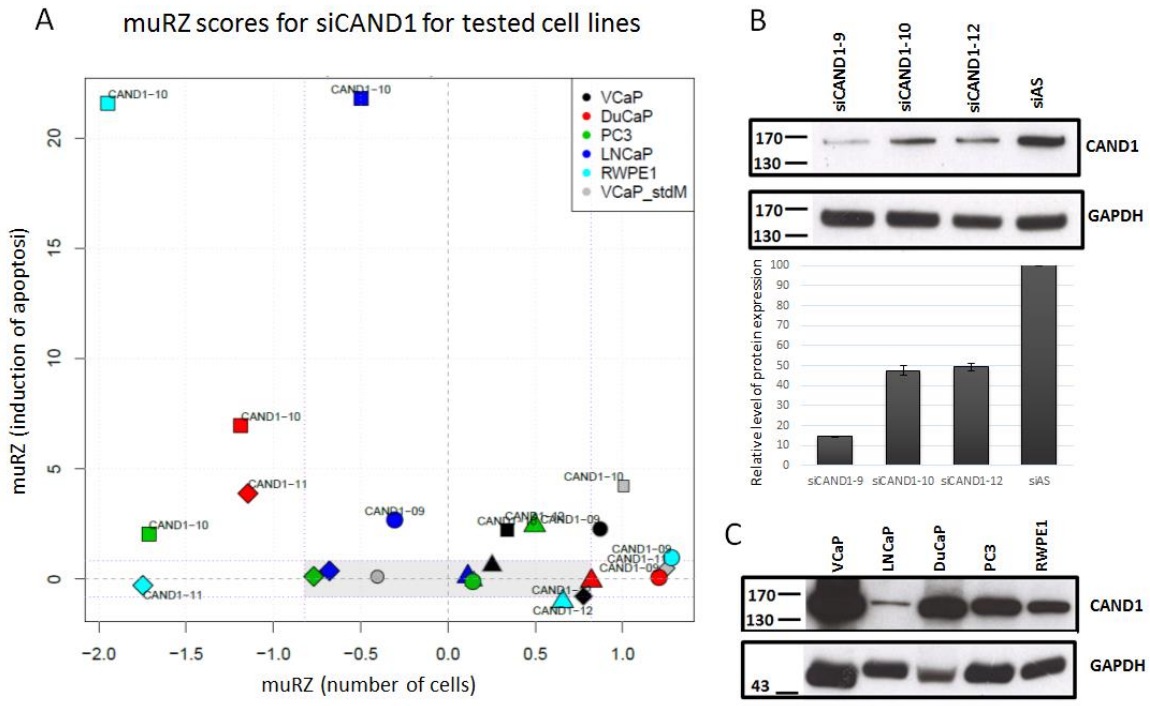

Figure 42. Graphical representation of siRNA action for the CAND1 gene. A. The graph represents the phenotypical changes (proportion of dying cells and changes in cell number) for each of 4 siRNAs and all the 5 cell lines tested (VCaP presented in 2 conditions: in ChSM, as all the other cell lines, and in StdM). muRZ is an averaged Robust Z-score from quadruplicates for each siRNA. Grey dotted lines indicate zero values for both axis. Pink dotted lines indicate threshold values: everything above or below these values (outside of the grey rectangle) is considered to be a hit. B. Effect of siCAND on the expression of the protein. VCaP cells were transfected with 3 strongest siRNAs individually (siCAND1-9, -10 and -12) or with negative control siAS and immunoblotted against CAND1. C. Expression of CAND1 protein in the tested cell lines.

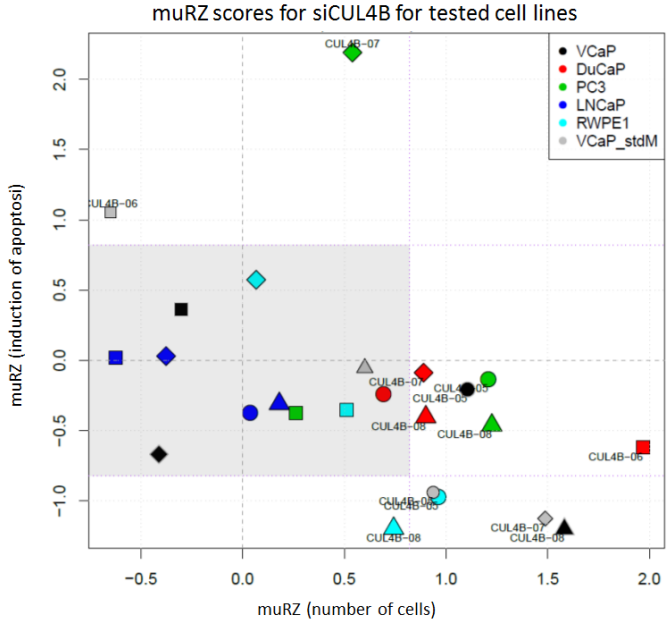

Figure 43. Graphical representation of siRNA action for CUL4B gene. A. The graph represents the phenotypical changes (proportion of dying cells and changes in cell number) for each of 4 siRNAs and all the 5 cell lines tested (VCaP presented in 2 conditions: in ChSM, like the other cell lines, and in StdM). muRZ is an averaged Robust Z-score from quadruplicates for each siRNA. Grey dotted lines indicate zero values for both axis. Pink dotted line indicates threshold values: everything above or below these values (outside of the grey rectangle) is considered to be a hit.

CUL4B

The knockdown of cullin 4B (CUL4B) decreased apoptosis and increased cell number in all tested cell lines except LNCaPs (Supplementary Table 6 and Supplementary Table 7; Figure 43).

CUL4B is a scaffold protein for E3-ubiquitin CRLs (Cullin-RING-Ligases) (more details about the structure and function of CRLs are given in the literature review, paragraph 3.4.2 NEDD8 TARGETS). Cullin 4-Ring E3 ligases (CRL4), assembled with CUL4B, DDB1 substrate adaptor and RBX1 as the core components, participate in a broad variety of physiologically and developmentally controlled processes such as cell cycle progression, replication, and DNA damage response. In mammals, there are two Cullin 4 members, CUL4A and CUL4B. CUL4A and CUL4B have many common substrates and are believed to be redundant for some functions (Sharifi *et al*., 2014).

CRL4 has emerged as a "master coordinator of cell cycle progression and genome stability" (Abbas & Dutta, 2011). CRL4 regulates cell cycle progression through the degradation of several factors upon entry into S phase, including replication licensing factor Cdt1, Cyclin E (responsible for G1 to S phase transition), cyclin-dependent kinase inhibitor p21 and transcriptional suppressor Set8. During DNA synthesis under normal conditions, CRL4 is required for translesion synthesis (TLS) via a mechanism that is dependent on PCNA monoubiquitylation by UBE2A (Havens & Walter, 2011). CRL4 also plays a key role in DNA-damage response by the activation of the error-free isoform of DNA-polymerase δ (Polδ) and the degradation of Cdt1, p21, and Set8 (Havens & Walter, 2011; Zhang *et al*., 2013). Depletion of CRL4 subunits induces replication stress and DNA damage, leading to cell cycle arrest in G2. This phenotype has been shown to depend, at least in part, on the DNA re-replication caused by failure to degrade replication origin licensing proteins (Sertic *et al*., 2013; Zou *et al*., 2009).

Although cullins 4A and 4B are thought to be functionally redundant, CUL4A does not substitute 4B in all functions. In response to DNA damage CRL4B was shown to ubiquitylate and degrade the HUWE1 protein (Yi *et al*., 2015), which is responsible for induction of apoptosis upon DNA damage. Unlike any other cullins, CUL4B contains a nuclear localization signal (NLS) and has been shown to colocalize with DNA-damage markers inside the nucleus (Guerrero-Santoro *et al*., 2008). Recent studies have established the role of CRL4s, especially of CRL4B, as important epigenetic regulators; CUL4B facilitates H3K9 tri-methylation and DNA methylation, two key epigenetic

modifications involved in gene silencing (Nakagawa & Xiong, 2011; Yang *et al*., 2015). Depletion of CUL4B resulted in loss of these markers, leading to de-repression of a number of genes, including the tumor suppressor IGFBP3 (Yang *et al*., 2015a; Hu *et al*., 2012).

In accordance with the experimental data, many recent works present CUL4B as an oncogene. Inhibition of CUL4B decreases proliferation and induces apoptosis in human osteosarcoma, glioma, cervical carcinoma and hepatocarcinoma cells (Chen *et al*., 2014; Yuan *et al*., 2015b; Dong *et al*., 2015; Yang *et al*., 2015). Moreover, in colon cancer CUL4B overexpression correlates with tumor invasion and metastases (Jiang *et al*., 2013). On the other hand, CUL4B has been shown to be strongly down-regulated or to have inactivating mutations in many cancer types (The Human Protein Atlas; de Miranda *et al*., 2014), which is not consistent with the oncoprotein role.

Collectively, all these data suggest that CUL4B plays an important role in chromatin remodeling and DNA-damage response. The present study's results, showing that a knockdown of CUL4B has a survival effect, could be explained by the induction of error-prone DNA synthesis and/or cell cycle arrest, which could decrease the level of spontaneous apoptosis, but may further lead to increased genetic instability, induction of senescence and apoptosis. These effects could be tracked with markers of senescence (beta-galactosidase activity, p21, Cdt1) and increased DNA-damage.

RBX1

Knockdown of the Ring-Box 1 (RBX1) gene decreased apoptosis and increased cell number in the ERG-positive cell line VCaP, and decreased proliferation in LNCaP, PC3 and RWPE1 (Supplementary Table 6 and Supplementary Table 7; Figure 44). The effect of RBX1 knockdown on another ERG-positive cell line (DuCaP) is not clear. However, considering the particularity of DuCaP cells (Figure 32, Figure 35), the effect of RBX1 inhibition may still be ERG-dependent.

RBX1 (also known as ROC1) is a RING E3-ligase, which is a part of the CRL complex (more details about the structure and function of CRLs are given in the literature review, paragraph 3.4.2 NEDD8 TARGETS). Both RBX1 and RBX2 are able to bind all the cullins. Nevertheless, under physiological conditions, RBX2 is selectively associated with CUL5, while RBX1 binds to the other members of the family (Wei & Sun, 2010; Kamura *et al*., 2004). Compared to RBX2, which is stress inducible, RBX1 is

constitutively expressed. Within the CRL complex RBX1 performs three important roles: 1) with the help of DCUN1D proteins, it transfers NEDD8 from E2 to cullin to activate a CRL; 2) it acts as a scaffold for the E2-conjugating enzyme; 3) it facilitates the transfer of Ub moiety from E2 to the substrate. RBX1 protein is expressed ubiquitously, but the level of RBX1 expression in malignant tissues seems to be dependent on cell type. For example, in ovarian, prostate and testes cancer RBX1 protein is often downregulated (Human Protein Atlas; Martinez *et al*., 2014), but it is often overexpressed in head and neck carcinoma, hepatocellular carcinomas, melanomas and gastric cancers (Human Protein Atlas; Yang *et al*., 2013; Nai &, Marques, 2011; Chen *et al*., 2015b).

Through promoting timely degradation of many key regulatory proteins as a part of E3 CRL ligases, RBX1 controls numerous cellular processes including DNA repair and cell cycle progression. There are many reported targets for RBX1, including Cdt1, IκBa, IKKβ, c-Jun, HIF-1α, histones H3 and H4, cyclin D1 and many others, including oncogenes and tumor suppressors. Thus, the effect of RBX1 gene inhibition relies on the stabilization of target proteins, and the resulting phenotypical outcome would vary depending on the cellular context. Thus, accumulation of Cdt1 and ORC1 proteins causes re-replication, genome instability and senescence, while stabilization of RhoB, p21 and p27 (CUL1) induces G2/M cell cycle arrest and apoptosis (Xu *et al*., 2015). These toxic effects have been shown for many cancer cell lines including glioblastoma, bladder and liver cancer, and non-small cell lung carcinoma (Jia *et al*., 2009; Yang *et al*., 2013; Wang *et al*., 2013). On the other hand, accumulation of Nrf2, which helps cells to maintain a favorable redox balance, or HIF1α, a master-gene in hypoxia, are beneficial for cancer progression (Park *et al*., 2010; Martinez *et al*., 2014; Martinez *et al*., 2015).

RBX1 neddylates, and thus activates, the majority of CRL complexes; respectively, RBX1 gene knockdown inhibits the CRL/NEDD8 pathway. The anti-cancer drug, MLN4924, has an effect similar to RBX1 inhibition: it prevents attachment of NEDD8 to the cullins (Lin *et al*., 2010). Indeed, in the present study, the effects of RBX1 inhibition resemble the effect of low-dose (<100 nM) MLN4924 treatment (CHAPTER 2), where VCaP cells undergo G0/G1 cell cycle arrest, thus decreasing spontaneous apoptosis, while other cell lines respond with a decrease of proliferation and induction of apoptosis. Thus, this study's data suggest that inhibition of cullin neddylation in PCa cell lines (by RBX1 gene knockdown and NAE inactivation by MLN4924) causes differential phenotypical outcomes in ERG-positive and negative cell lines.

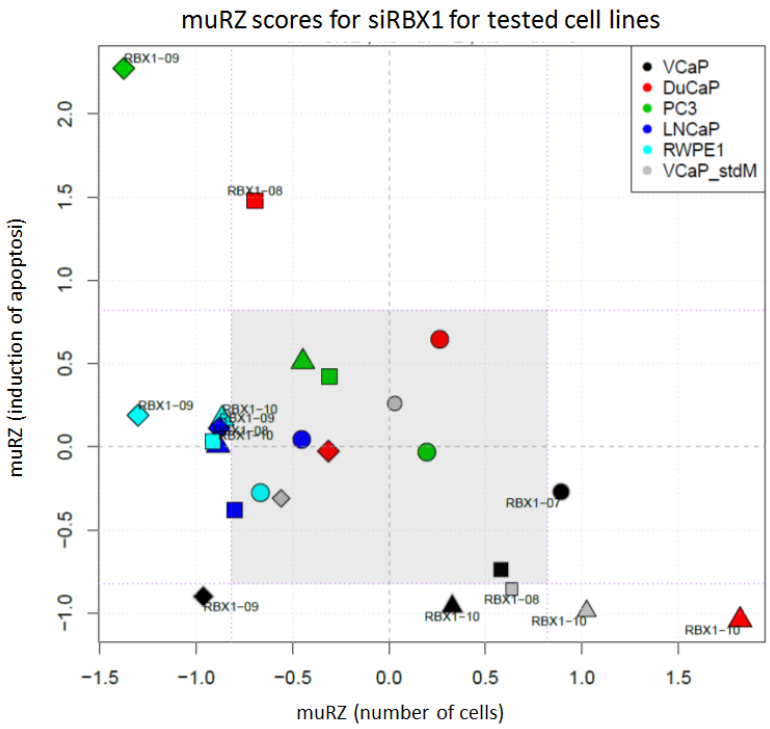

Figure 44. Graphical representation of siRNA action for RBX1 gene. A. The graph represents the phenotypical changes (proportion of dying cells and changes in cell number) for each of 4 the siRNAs and all 5 cell lines tested (VCaP presented in 2 conditions: in ChSM, like the other cell lines, and in StdM). muRZ is an averaged Robust Z-score from quadruplicates for each siRNA. Grey dotted lines indicate zero values for both axis. Pink dotted lines indicate threshold values: everything above or below these values (outside of the grey rectangle) is considered to be a hit.

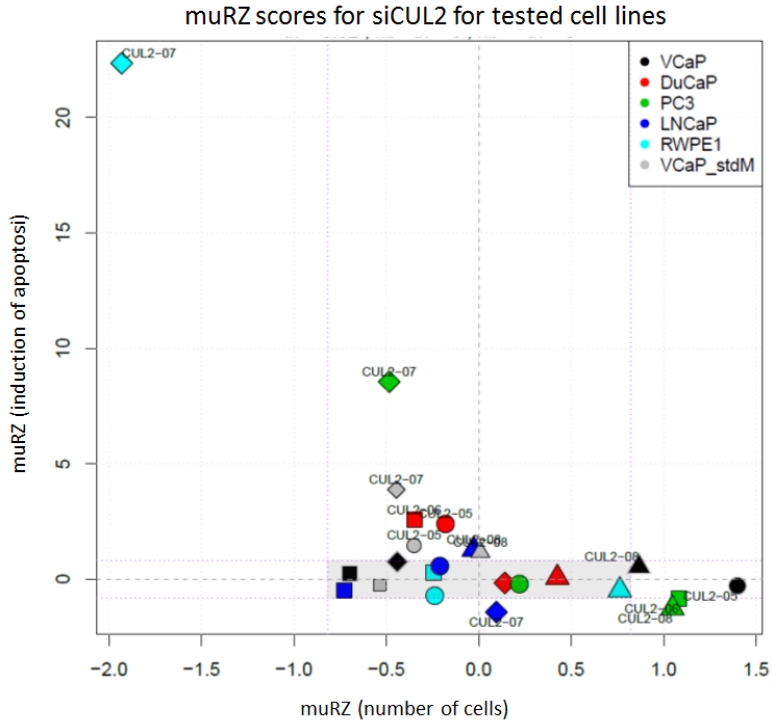

Figure 45. Graphical representation of siRNA action for CUL2 gene. A. The graph represents the phenotypical changes (proportion of dying cells and changes in cell number) for each of 4 siRNAs and all 5 cell lines tested (VCaP presented in 2 conditions: in ChSM, like the other cell lines, and in StdM). muRZ is an averaged Robust Z-score from quadruplicates for each siRNA. Grey dotted lines indicate zero values for both axis. Pink dotted lines indicate threshold values: everything above or below these values (outside of the grey rectangle) is considered to be a hit.

CUL2

Inhibition of CUL2 gene by siRNA induces apoptosis in the ERG-positive cell lines VCaP and DuCaP (Supplementary Table 6 and Supplementary Table 7; Figure 45). Therefore, it seems that this hit is possibly ERG-dependent.

Cullin 2 (CUL2) is a scaffold protein of the CRL2 complex (more details about the structure and function of CRLs are given in the literature review, paragraph 3.4.2 NEDD8 TARGETS). The effect of CUL2 inhibition is caused by the stabilization and accumulation of target proteins of the CRL2 E3-ligases. The majority of CRL2 substrates are oncogenes: HIF1α (Maeda *et al*., 2008; Okumura *et al*., 2012), NF-κB (Maine *et al*., 2007), RNA polymerase II subunit hsRPB7 (Brower *et al*., 2002), PKCλ (Okuda *et al*., 2001), topoisomerase IIα (Yun *et al*., 2009), β2AR (Xie *et al*., 2009). Nevertheless, some reports suggest that CUL2 function may favor cancer development. Upregulation of CUL2 was found in aggressive PCa and was linked to a poor prostate cancer outcome (Shipitsin *et al*., 2014). In esophageal cancer, CUL2 upregulation was shown to be a predictive factor for resistance to neoadjuvant chemotherapy; and vice versa – downregulation of CUL2 mRNA correlated with a favorable prognosis (Metzger *et al*., 2010). According to the Human protein Atlas, CUL2 is overexpressed in some types of cancer, including glioma, pancreatic and prostate cancer. On the other hand, downregulation of CUL2 was associated with a bad prognosis in oral squamous cell carcinoma (Diniz *et al*., 2015).

Altogether these data show the important role of CUL2 in carcinogenesis. The data of the present study suggest a potential ERG-dependence of the outcome of CUL2 knockdown in PCa cell lines, which requires further validation.

1.6 DISCUSSION

1.5.1 Screening parameters

The outcome of the inhibition of a gene depends on the cellular context and may vary strongly depending on the cell line. The use of multiple cell lines allows for the identification of hits which are generally important for the functioning of cells of a given cellular type (prostate), as well as hits specific to cell lines bearing certain a pheno-/geno-type, such as castration-resistance, specific mutations, etc. When comparing the effects of siRNAs in different cell lines the unique characteristics of each cell line should be taken into account, such as the level of proliferation, basal rate of apoptosis, transfection

efficiency, robustness in response to perturbations and many others. For these reasons, for each cell line it was important to make a primary optimization of the screening conditions by using control siRNAs. This helped to have similar and, thus, comparable responses to siRNA treatment. To adjust the efficiency of transfection, three-day siRNA treatments were used for fast proliferating cell lines (PC3, LNCaP and RWPE1) and five-day treatments for the slow proliferating ones (VCaP and DuCaP). Nevertheless, the treatment time was still not optimal for the PC3 cells and possibly should be increased to four or five days. To compare the results in different cell lines the same parameters was used (i.e. apoptosis and cell number), as well as the same layout of the plates, and statistical analysis. The particularity of DuCaP cells did not allow using this cell line as a proper model for an ERG-dependent PCa. The data obtained with DuCaPs was taken into account, but the results should be interpreted carefully.

An important part of the optimization process is the choice of siRNA concentration. In the screening low concentration of siRNA were used (20 nM in the primary screen and 10 nM in the secondary), despite that many reported screens use much higher (up to 100 nM) concentrations (Reynolds *et al*., 2004). Therefore, a complete knockdown of a gene might not have always been achieved, and there may have been more false-negative results. On the other hand, lower concentrations of siRNA decrease the amount of false-positive results and off-target effects. Usually, for optimized siRNAs, a concentration of a few nM (typically 1-2.5 nM) is sufficient to suppress the expression of a target protein. To achieve efficient knockdown it is better to use slightly higher concentration, but this may affect expression of many other, potentially hundreds, of genes (Caffrey *et al*., 2011; Laganà *et al*., 2014; Urbinati *et al*., 2015). Therefore, the choice was made to use lower concentration of siRNA for the present study, while paying attention to weak effects by decreasing the muRZ threshold.

Performing a relatively small siRNA screening (107 genes in the primary screen) has several advantages compared to genome-wide approach. It decreases cost, time and effort, while increasing control over the conditions, allowing a more detailed analysis with multiple cell lines to be carried out. Nevertheless, even in these conditions, it was difficult to analyze all the available information. The “Cell Health Profiling” software allows estimating many parameters: the total number of cells in the field, the percentage of apoptotic cells, the area of the nucleus, the total Hoechst in the nuclei that reflect DNA content, etc. However, after primary screening, the level of apoptosis was chosen as the

most reliable parameter, thus omitting some data. A lot of information is also found in cell line-specific effects. In the screen attention was focused on the genes important for the survival of all the prostate cancer cell lines and on the ERG-specific effects. Nevertheless, siRNAs for DCUN1D5, CACUL1 and UBE2S also had an impact on the viability of PCa cells, but it was more dependent on cellular context and thus requires further validation.

Among the parameters used in the analysis (induction of apoptosis, cell count and measurement of proliferation/ATP level), cell count proved to be the least reliable. The number of cells always slightly varies between wells. Moreover, with slow-proliferating cells (such as VCaPs) it was difficult to obtain a significant change in the number of cells in five-day experiments. A measurement of the level of apoptosis was the most reliable parameter. The "Cell Health Profiling" software is suitable for high-throughput screens in 384-well plates, which allows for a sufficient number of replicates to be made, and, with acquisition of 9 fields per well, the analysis of about 2 million cells per cell lines. It provides a reliable data distribution and allows for the detecting of weak effects. The parameter "apoptosis" was found to be highly reproducible between replicates and different experiments, even when distinct experimental design were used (e.g., during primary and secondary screens). A measurement of proliferation by the level of ATP can also be used, but optimization is needed, because this parameter is sensitive to the seeding density. Also this readout has a lower dynamic range thus allowing mainly the strongest effects to be seen only.

Finally, although both measurement of apoptosis and proliferation are easy-to-follow phenotypical parameters, they are too general which complicates the validation of the hits and the elucidation of the mechanism of their function. Cell growth and death could be affected by many factors, including the deregulation of the proteins governing cell cycle progression, DNA repair and replication, cytoskeleton assembly, metabolism and many others. It would be better to find more "targeted" parameters to follow, which would allow for the identification of the affected pathway and thus facilitate hit validation. Examples of such parameters are degradation of a specific protein, or activation/inhibition of specific pathways, where the role of the UPS has been suggested.

1.5.2 Hits and primary validation

The objective of the primary screening was to identify the UPS components crucial to the viability of prostate cancer cells and, in particular, PCa cells harboring the oncogenic translocation TMPRSS2:ERG. Seven genes were identified, of which two are potentially ERG-specific.

The most prominent hit is **UBE2U**. This uncharacterized protein, with an urogenital pattern of expression and a robust apoptotic effect of its knockdown in prostatic cells, could potentially be a perfect drug target for prostate cancer. Attempts in cloning and characterization of this protein suggest the existence of multiple mRNA splicing isoforms, with at least some of them truncated. This might suggest that these mRNA could have some specific functions. For example, UBE3A was shown to have multiple mRNA isoforms coding enzymatically inactive proteins. These mRNAs were shown to regulate miRNA governing neuronal development (Valluy *et al.*, 2015). To better understand the function of UBE2U, and its role in the prostate and PCa, it is important to characterize the existing isoforms and identify those involved in PCa cell viability.

The genes **UBE2H, UBE2A, CUL4B** have the established roles in chromatin remodeling and DNA-damage response. The data from the literature suggest their general role in cancer development, and therefore, these genes may not be PCa-specific. For these hits basic validation has been done using multiple siRNA targeting the same gene as well as confirmation of the efficiency of these siRNA by Western Blot.

Four (**CAND1, CUL4B, RBX1** and **CUL2**) of the seven identified hits belong to the **CRL/NEDD8-pathway**. Moreover, two of them (RBX1 and CUL2) are potentially ERG-specific. In order to elucidate the role of the CRL/NEDD8 pathway in prostate cancer MLN4924 was used, which is a potent inhibitor of neddylation, recently introduced in biomedical research (CHAPTERS 2 & 3).

CHAPTER 2. DISTINCT OUTCOMES OF CRL/NEDD8 PATHWAY INHIBITION IN CANCER CELLS

2.1 INTRODUCTION

The major goal of cancer therapy is to specifically suppress malignant neoplasm without detriment to normal cells. Recently, the ubiquitin-proteasome system (UPS) appeared as one of the principal cancer targets. Indeed, the inhibition of the major UPS component, the proteasome, has proven to be efficient against many types of cancer. Two proteasome inhibitors, Bortezomib and Carfilzomib, have been approved by FDA for the treatment of hematologic malignancies, while other related compounds, Ixazomib and Oprozomib, are in clinical trials. Among major difficulties in cancer treatment are extreme plasticity, evolvability, and heterogeneity of the disease. Thus, although Bortezomib (+/- Dexamethasone) has shown efficacy against multiple myeloma and, more recently, against mantle cell lymphoma, the treatment often leads to a relapsed, refractory disease. In some cases, this problem may be addressed by combining proteasome inhibitors with additional drugs such as Panobinostat and Thalidomide/Lenalidomide, which target other tumor-specific liabilities (http://www.themmrf.org/multiple-myeloma-knowledge-center/myeloma-drugs-guide/velcade/velcade-clinical-studies/). It is also noteworthy that in standard regimens, Bortezomib fails against solid tumors, while a dose increase results in peripheral neuropathy. Given that the proteasome plays an important role in normal cells, the observed neurotoxicity raises the question of the selectivity of proteasome inhibitors in cancer treatment.

Apart from the proteasome, other potential anti-cancer targets from the UPS comprise cullin-RING E3 ligases (CRLs). Deregulation of CRLs has been observed in many cancers and is linked to tumorigenesis (Lee J & Zhou, 2010; Chairatvit & Ngamkitidechaku, 2007; Li *et al*., 2014; Meehan *et al*., 2002). Notably, the inhibition of CRLs can stabilize a number of tumor suppressors without affecting global cellular catabolism, and, therefore, it seems to be a more specific anti-cancer approach compared to proteasome inhibition (Soucy *et al.*, 2009). CRLs are multi-protein complexes assembled (in mammals) on seven cullin scaffolds (cullins 1, 2, 3, 4a, 4b, 5, 7). Pro-degradative Ub-ligase activity of CRLs requires modification of the cullin subunit with a small Ub-like protein – NEDD8. Similar to ubiquitylation, the neddylation involves an

ordered transfer of NEDD8 by specific E1-activating enzymes (NAE/Uba3 heterodimer), E2-conjugating enzymes (UBE2F or UBE2M) and E3 ligases (RBX1 and RBX2 for CRLs, and others). Some of these enzymes are druggable and, therefore, provide a powerful way to block CRL function. Thus, a recently developed NAE inhibitor, MLN4924, efficiently abrogates cullin neddylation and suppresses the growth of various types of cancer cells *in vitro* and *in vivo* (Soucy *et al.*, 2009). MLN4924 is currently being evaluated in clinical trials for the treatment of both hematologic malignancies and solid tumors (https://clinicaltrials.gov).

Despite the growing evidence for non-cullin NEDD8 regulation (Hjerpe *et al.*, 2012; Enchev *et al.*, 2014), all proposed mechanisms of MLN4924 function/action implicate inhibition of CRLs. Depending on the cell type these include: (1) induction of DNA re-replication through the stabilization of chromatin licensing factor Cdt1 (2) cell cycle arrest through the upregulation of cell cycle regulators such as p21, p27, and Wee1; (3) inhibition of the NF-κB pathway in NF-κB-dependent cancer cells; (4) suppression of tumor angiogenesis as a result of cell cycle arrest and accumulation of RhoA GTPase (Enchev *et al.*, 2014; Yao *et al*., 2014) , etc. Surprisingly, only two outputs for these multitude of mechanisms have been documented, which recapitulate the therapeutic effect of MLN4924: cancer cell senescence and apoptosis. However, considering a complex network of CRL regulation in the cell, one would expect a much wider range of cellular responses to CRL inhibition. It seems possible that, by tracking only death outcomes, some cellular phenotypes could be overlooked. Indeed, despite the unique target (NAE, IC50 ~5 nM), the toxicity of MLN4924 (EC50) in various cell lines can vary by three orders of magnitude, suggesting that suppression of CRL does not necessary lead to cell death. Consistent with this conclusion, a recent study has shown that inhibition of $CRL1^{\beta Trcp}$ and $CRL2^{VHL}$ by MLN4924 can also induce autophagy that protects cancer cells from apoptosis (Zhao *et al*., 2012). Complementing MLN4924 treatment with an autophagy inhibitor markedly enhanced the drug efficacy. Therefore, analysis of all possible outcomes of MLN4924 action is of clinical importance for the evaluation of CRL/NEDD8 pathway as a therapeutic target and for optimization of treatment regimens.

Here the consequences of CRL/NEDD8 pathway inhibition in prostate cancer cells are investigated. Notably, this study shows that: (1) distinct cell lines have significantly different sensitivity to MLN4924; (2) knockdown of CRL components may have opposite effects on cell proliferation and survival; (3) a different degree of

CRL/NEDD8 pathway inhibition can result in a completely different cell fate. Specifically we found that in VCaP cancer cells, 95% suppression of NEDD8 conjugation activates androgen receptor (AR), resulting in reversible cell quiescence and protection from proliferation-dependent cell death. Also demonstrated is the fact that knocking down/suppressing supplementary targets such as CAND1 and AR can potentiate the toxic effect of MLN4924 on prostate cancer cells. All together, these results demonstrate plasticity of cancer cells and suggest ways for the optimal utilization of NAE inhibitors in prostate cancer treatment.

2.2 DIFFERENT SENSITIVITY OF PROSTATE CANCER CELL LINES TO MLN4924

Previous work has shown that MLN efficiently induced cell death in the LNCaP prostate cancer cell line (EC50=50 nM) (Soucy *et al*., 2009). To investigate whether MLN4924 is generally potent against other types of prostate cancer we compared its effect on LNCaP cells (AR+, androgen-dependent, p53-wt) with PC3 (AR-, androgen-independent, p53-null) cells, and DuCaP and VCaP cells (both of these AR+, androgen-sensitive, and contain the TMPRSS2:ERG mutation, p53-R248W). First we used ViaLight™ Plus Cell Proliferation chemiluminescent assay to measure cellular ATP level. Consistent with previous observations (Soucy *et al*., 2009), MLN4924 induced a marked decrease in total cellular ATP in LNCaP cells, suggesting efficient growth and metabolism inhibition in this cell line (Figure 46, A). Treatment of LNCaP cells with 500 nM MLN4924 for 3 days resulted in 95% cell mortality confirmed by phase-contrast microscopy (Figure 46, A, right panel). Though less sensitive, PC3 cells also showed a significant decline in ATP level (>60%) and cytotoxicity with 500 nM MLN4924. On the contrary, DuCaP and VCaP cells were largely resistant to up to 1 μM of MLN4924, showing little effect on ATP level and on the number of cells after 3 days of treatment (Figure 46, A). Most surprisingly, at the concentrations below 1 μM, MLN4924 induced an apparent increase of total ATP in DuCaP cells. Both VCaP and DuCaP cell lines were derived from the same patient and contain an amplified AR gene as well as TMPRSS2:ERG chromosomal translocation. This mutation, which is present in 50-70% of prostate cancers, fuses the TMPRSS2 promoter to the ERG gene resulting in androgen-dependent expression of the truncated ERG protein (Tomlins *et al.*, 2005). ERG is a transcription factor that tightly interacts with AR in reprogramming the fate of prostate

cancer cells (Yu *et al*., 2010). It seems, therefore, possible that this particular genetic context renders VCaP and DuCaP cells less dependent on the CRL/NEDD8 pathway.

Inhibition of the CRL/NEDD8 pathway was shown to induce senescence and apoptosis in cancer cells (Enchev *et al.*, 2014). To investigate whether the MLN4924-inflicted death of prostate cancer cells was due to the induction of apoptosis, we examined the activation of pro-apoptotic caspases 3&7 (Figure 46, B). Cells were incubated with CellEvent™ Caspase-3/7 fluorogenic substrate (CE) and analyzed by automated fluorescence microscopy. MLN4924 induced massive apoptosis in LNCaP cells, while PC3 cells were much less affected. Consistent with a MLN4924-resistant phenotype, at 3 days of treatment, VCaP and DuCaP cells showed negligible caspase 3/7 activity, even with 1 μM of MLN4924 (Figure 46, B, right panel).

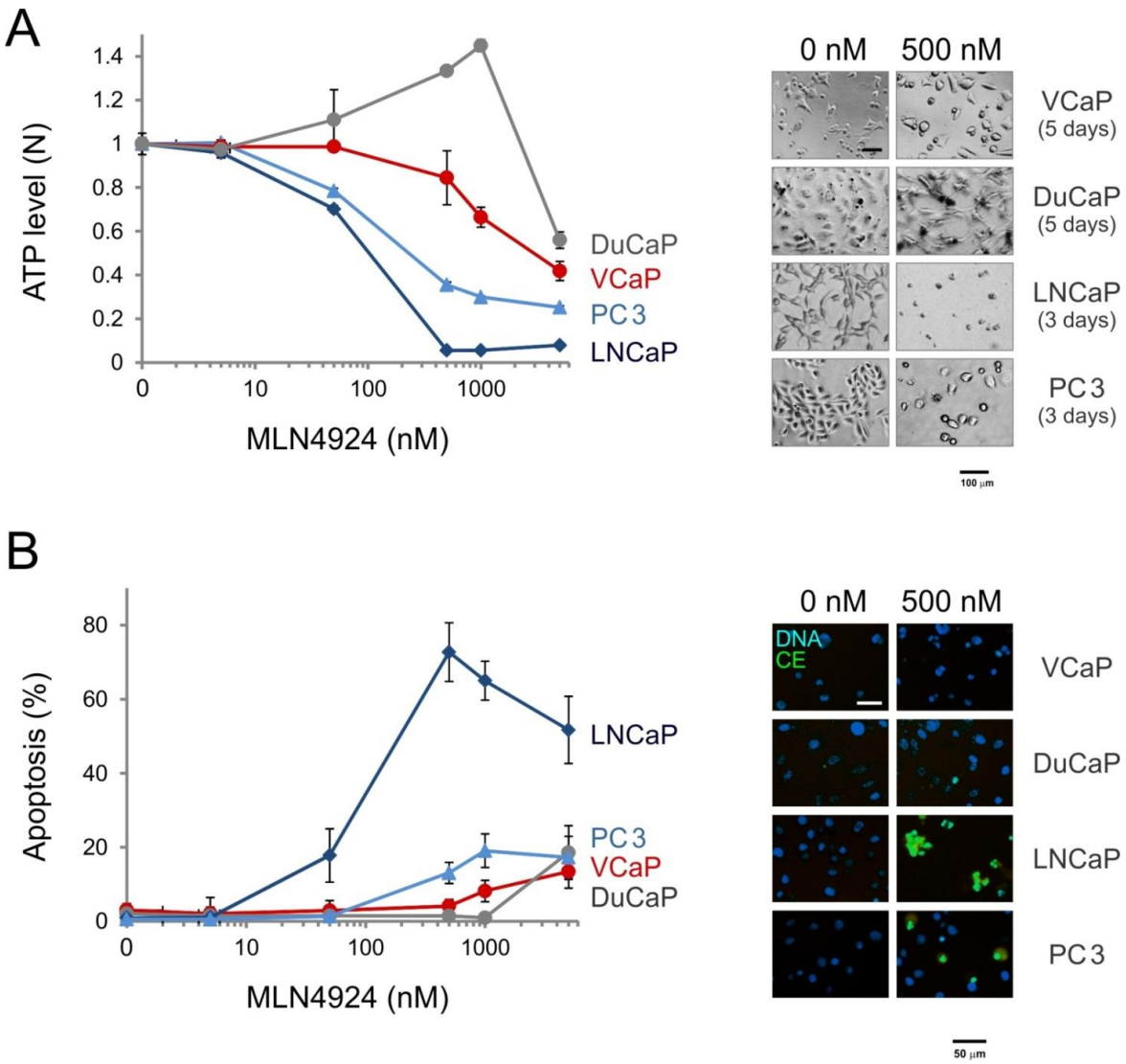

Figure 46. The effect of MLN4924 treatment on proliferation (A) and apoptosis (B) in PCa cell lines grown in ChSM. The images represent phase-contrast (A, right panel) or fluorescent acquisitions (B, right panel) of PCa cells treated

with vehicle (DMSO) or 500 nM MLN4924. On the fluorescent images the nuclei are shown in blue, while the caspase CellEvent substrate is in green.

Taken together, these results revealed significant difference in the sensitivity of prostate cancer cells toward NAE inhibition. This may reflect genetic and functional heterogeneity of these cells apparent from their different phenotypes, androgen dependences and proliferation indexes. Thus, VCaP and DuCaP cells have two to three times longer doubling time compared with LNCaP and PC3 cells (60-120h vs 30-35h). Because the toxic effect of MLN4924 on cancer cells was shown to be proliferation-dependent (Lin *et al*., 2010), this may be one of the reasons for their resistance to the drug. However, though a longer treatment of VCaP cells with MLN4924 increased the cytotoxicity, it was still much less pronounced then with LNCaP cells (see below, and Supplementary Figure 1). Furthermore, despite the different proliferation rates, a quite similar MLN4924-inhibition profile was observed in cells cultured on standard (Supplementary Figure 3) and androgen-deprived (Figure 46) medium, suggesting that cell cycle progression is not the only factor determining MLN4924 toxicity. The distinct sensitivity of prostate cancer cell lines toward NAE inhibition might also reflect their different p53 status, though, contrary to our results, MLN4924 has been shown to be generally more toxic to the cells with a mutant p53 (Lin *et al*., 2010).

2.3 MLN4924 EFFICIENTLY INHIBITS NEDD8 PATHWAY IN VCaP CELLS

Poor drug bioavailability and multidrug resistance are common causes of cancer cell resistance to a variety of drugs (Kuppens *et al*., 2005; Holohan *et al*., 2013). To investigate whether the resistance of TMPRSS2:ERG-positive prostate cancer cells toward MLN4924 treatment results from inefficient NAE inhibition, we examined the effect of this drug on protein neddylation in VCaP cells. Expressing major prostate epithelial markers, this cell line is a widely used cellular model for androgen-sensitive TMPRSS2:ERG-positive prostate tumors (van Bokhoven *et al*., 2003a). We found that the increasing concentration of MLN4924 induced a progressive decline in the amount of NEDD8 conjugates (Figure 47, A). Because no significant changes were observed with Ub and SUMO1 conjugates, the inhibition appeared to be NAE-specific (Supplementary Figure 5). Surprisingly, the efficacy and profile of the inhibition of the neddylation were quite similar to those previously reported for highly MLN4924-sensitive cell lines (Soucy *et al*., 2009; Brownell *et al*., 2010): with an abrupt decline in NAE- and Ube2M-NEDD8 conjugates at 10-25 nM of the drug (bands 4 and 6) and slightly shifted toward higher

~100 nM MLN4924 concentrations, a decrease in neddylated cullins (bands 2/3). Notably, the suppression of total NEDD8 conjugates attained ~ 90% at 50 nM MLN4924 and was almost complete at 100 nM (Figure 47, B). These findings were corroborated by immunofluorescence microscopy, where negligible anti-NEDD8 staining was observed already at 50 nM MLN4924 (Figure 47, C).

The results presented on Figure 46 and Figure 47 lead to the unexpected conclusion that the inhibition of the majority of cellular neddylation is not toxic for TMPRSS2:ERG-positive prostate cancer cells. Although surprising, the possible explanations for this finding could be that: (1) toxic effects are present but are not detected; (2) residual (~5%) neddylation is still sufficient to perform vital cellular functions; (3) the cells somehow adapt to low neddylation; (4) vital cellular functions do not depend on NEDD8 pathway in these cells.

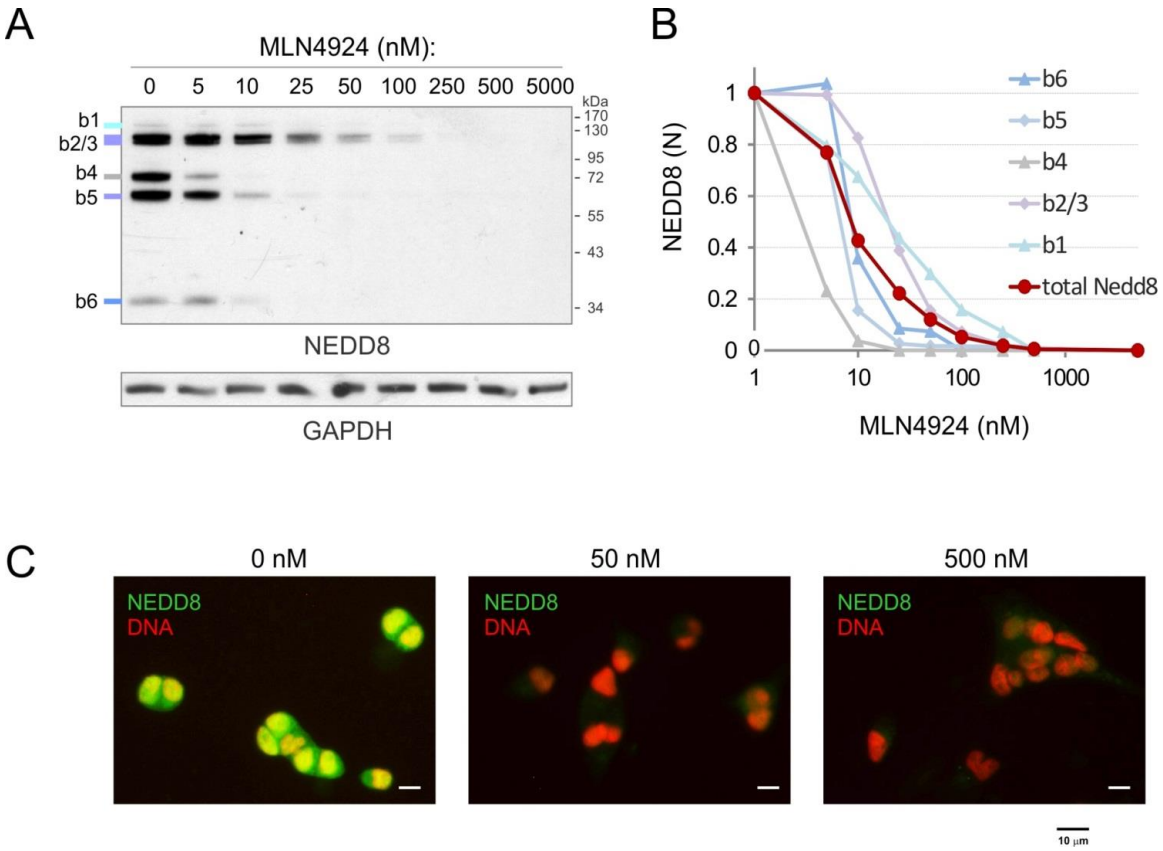

Figure 47. The effect of MLN4924 on neddylation in the VCaP cell line. A. Western Blot shows a dose-dependent decrease in neddylated proteins. Quantification of the WB (B) shows IC50 for total neddylation is about 10 nM, while IC50 for CRL is equal to 25 nM. At 50 nM residual neddylation is 10 % compared to control, while 500 nM causes complete blocking of neddylation. Immunostaining against NEDD8 (C) showed that neddylation is negligible for both 50 nM and 500 nM concentrations of MLN4924.

2.4 DIFFERENTIAL EFFECT OF NEDD8 PATHWAY INHIBITION ON CELL CYCLE PROGRESSION AND VIABILITY

Because VCaP are slow cycling cells (their doubling time is more than 53 hours according to ATCC), more prolonged incubation with MLN4924 might be required to see the cytotoxic effect of NAE inhibition. Indeed, extending the MLN4924 treatment to 5 days increased the percentage of apoptotic cells, albeit only for the drug concentrations above 500 nM (Supplementary Figure 1). Curiously, for lower drug doses we observed small, but repeatable decrease in caspase 3/7 activity compared to the control, thereby inferring a decreased rate of spontaneous apoptosis (Supplementary Figure 1).

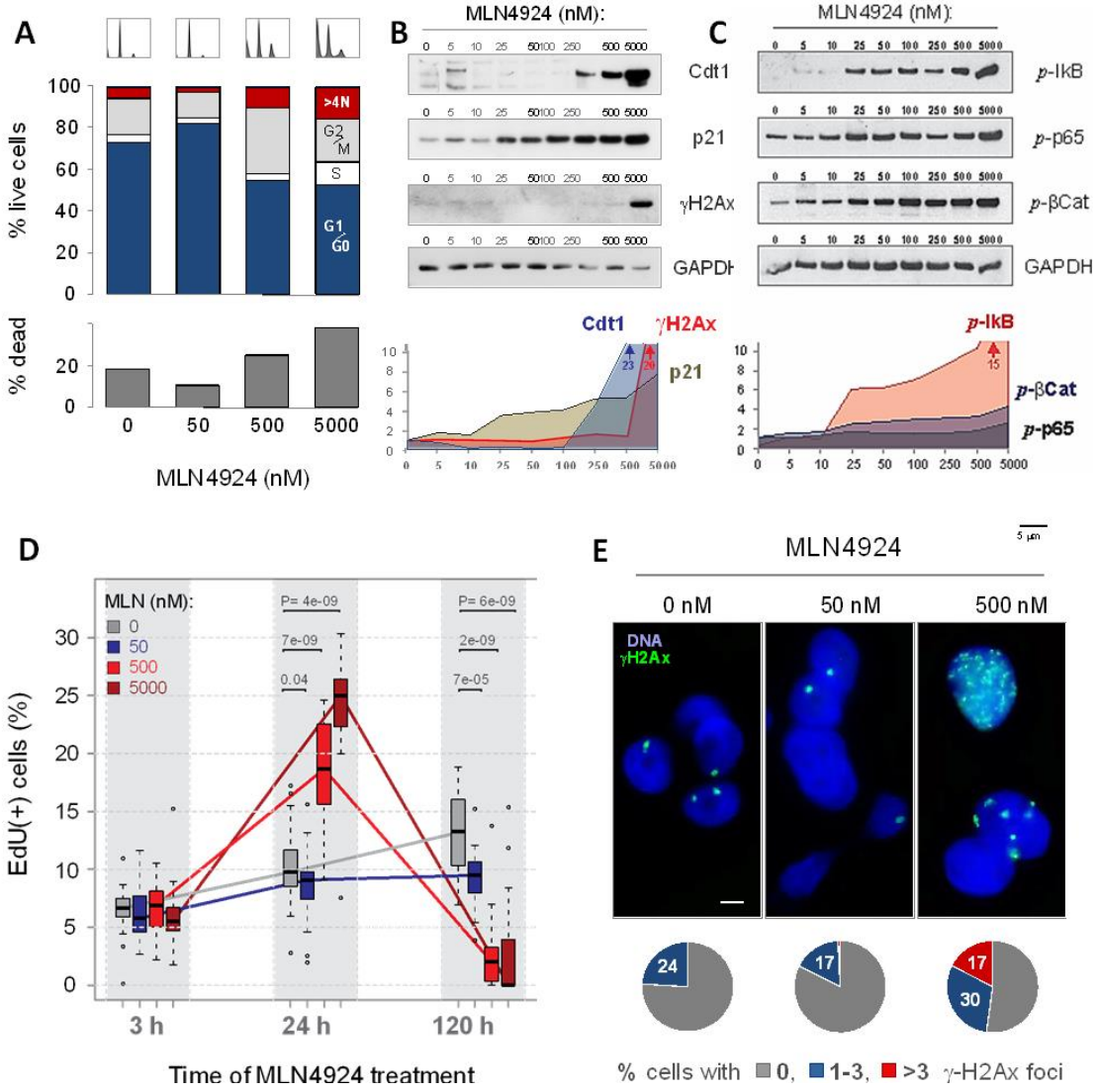

Figure 48. The effect of NEDD8 pathway inhibition using different concentration of MLN4924 on cell cycling and viability. A. Analysis of the cell cycle by flow cytometry using 7-AAD staining after 5 days of treatment on VCaP cells with MLN4924. B. Effect of MLN4924 on the NF-κB pathway (*phospho*-p65 and *phospho*-IκB) and *phospho*-β-catenin. C. Effect of MLN4924 on the markers of NF-κB pathway (Cdt1), senescence (p21) and DNA-damage (γH2AX). D. Effect on DNA synthesis after 3, 24 or 120 hours after treatment with MLN4924. E. Immunostaining for γH2AX-positive foci in the nuclei of VCaP cells. We analyzed 3 groups of cells, having 0, 1-3, or more than 3 foci per nuclei.

The cytotoxic effect of MLN4924 has been linked to the accumulation of a number of CRL substrates, e. g. Cdt1, p21, Wee1 (Lin *et al*., 2010; Jia *et al*., 2011; Wei *et al*., 2012). This can provoke DNA re-replication and/or cell cycle arrest. Notably, in some cell lines the growth arrest by MLN4924 does not necessary cause apoptosis (Jia *et al*., 2011). We, therefore, used flow cytometry to examine how NAE inhibition affects cell cycle in VCaP cells (Figure 48, A).

Consistent with the reduced rate of spontaneous death (Supplementary Figure 1), the treatment of cells with 50 nM MLN4924 decreased the percentage of sub-G1/G0 (dead) cells compared to control (Figure 48, A, bottom histogram). Unexpectedly, the cells accumulated in the G1/G0 phase, indicating a cell cycle arrest. Because VCaP cells express mutant p53-R248W, they are unable to induce G1 arrest (Sobel & Sadar, 2005; Willis *et al*., 2004) and therefore other mechanisms seem to be involved. Higher doses of MLN4924 increased the fraction of sub-G1/G0 dead cells, the cells in G2/M (500 nM of drug) and S (5 μM of drug) phases as well as a percentage of cells with high (>4N) DNA content. These data are in agreement with the proposed mechanism of MLN4924 action, which includes stabilization of replication licensing factor Cdt1 factor, of which accumulation leads to DNA re-replication, cell cycle arrest at G2/M, and apoptosis. Corroborating this conclusion, Western Blot analysis revealed an elevated level of cellular Cdt1 at higher MLN4924 concentrations (Figure 48, B).

To detect possible DNA re-replication, we measured cellular DNA synthesis following different times of NAE inhibition. The Click-iT EdU incorporation assay was used. Here, again, distinct responses to low and high doses of MLN4924 were observed both in androgen-deprived (Figure 48, D) and in standard medium (Supplementary Figure 2). Specifically, the treatment with 50 nM MLN4924 induced progressive inhibition of EdU incorporation from 90% of the control value at 24h to 65% at 120h. Meanwhile at 500 nM and 5 μM the effect of the drug was biphasic: at 24 hours the EdU signal rose to 200-250% of the control value, followed by complete cessation of DNA synthesis at 120h. This initial increase in EdU incorporation coincided with Cdt1 accumulation and might indicate DNA re-replication and/or repair processes induced by DNA damage. On the other hand, the DNA synthesis arrest probably reflects a shutdown of cell functions as the result of an inability to repair the inflicted damage.

To ascertain that MLN4924 can induce DNA damage we examined the status of Ser-140 phosphorylated histone H2AX (γH2AX), a marker of DNA double strand breaks.

Western Blot analysis revealed a massive accumulation of γH2AX in the cells treated with 5 μM MLN4924, while only a small increase in γH2AX signal was observed with 250-500 nM concentrations (Figure 48, B). This small increase in total γH2AX could indicate an onset of DNA damage provoked by intermediate MLN4924 doses. Indeed, an analysis of the cells treated with 500 nM MLN4924 by immunofluorescence microscopy revealed a marked increase in population of cells having multiple γH2AX foci, the presumed sites of DNA damage (Figure 48, E). Notably, at 50 nM, MLN4924 slightly reduced the incidence of γH2AX foci compared to the control, inferring that the G0/G1 cell cycle arrest and reduced rate of DNA synthesis imposed by this dose prevents spontaneous DNA breaks.

A similar dose-response to MLN4924 in γH2AX formation and caspase 3/7 activation pointed to DNA damage as a primary trigger of apoptosis. On the other hand, what caused a G0/G1 cell cycle arrest at MLN4924 concentrations below 100 nM was less clear. We observed a significant increase in cyclin-dependent kinase inhibitor p21, the substrates of multiple CRLs (Abbas & Dutta, 2011; Yu *et al*., 1998), already at 25 nM MLN4924 (Figure 48, C). This, by itself, may contribute to cell cycle arrest at G0/G1. Furthermore, at the same concentration, MLN4924 induced a marked buildup of phosphorylated IκB (p-IκB) protein; an inhibitor of NF-κB and a substrate of $CRL1^{\beta Trcp}$ (Figure 48, C). NF-κB, a key transcription factor in prostate carcinogenesis, is constitutively active in advanced tumors and in ETS-positive cancer cells (Lambert *et al*., 1997; Wang *et al*., 2011; Rayet & Gélinas, 1999). Because an inhibition of NF-κB signaling in VCaP cells was shown to suppress cell growth (Wang *et al*., 2011), this may be the mechanism/cause of G0/G1 cell cycle arrest by MLN4924. Consistent with this, the stabilization of IκB by MLN4924 was accompanied by an accumulation of cytoplasmic, but not nuclear, *phospho*-p65, an active subunit of NF-κB (Supplementary Figure 7). Finally, we observed that MLN4924 also stabilized phosphorylated β-catenin (p-b-Cat) (Figure 48, C). *Phospho*-β-Cat is a component of β-Cat/Wnt signaling, one of the major ERG-driven transformation pathways in TMPRSS2:ERG-positive prostate cancer cells (Gupta *et al*., 2010).

Collectively, our data suggest that, depending on the dose, MLN4924 can instigate two apparently distinct cell responses: (1) at concentration below 100 nM (~95% inhibition of cellular neddylation), the drug affects NF-κB and β-Cat/Wnt pathways, arrests cells in the G1/G0 phase and inhibits DNA synthesis, thus preventing spontaneous

DNA damage and apoptosis; (2) at concentration above 500 nM (complete neddylation inhibition) MLN4924 causes DNA damage, cell cycle arrest in G2/M and S phases, and apoptosis.

2.5 KNOCKDOWN OF CRL COMPONENTS CAN HAVE OPPOSITE EFFECT ON CELL PROLIFERATION AND SURVIVAL

Although surprising, the discontinuous effect of "almost complete" to "complete" NAE inhibition on cell fate was not totally unexpected. Cullins are major neddylation substrates. Various CRLs regulate thousands of diverse cellular factors that have distinct impacts on cell function (Lee J & Zhou, 2010). It is possible, therefore, that the inhibition of some CRLs by MLN4924 would promote cell death, while the inhibition of others would favor pro-survival processes. In this case the final outcome could be discontinuous depending on the role, weight, and degree of (susceptibility to) the inhibition of each component within the CRL network. To test this hypothesis we analyzed the effect of inhibition of CRL components on the viability of VCaP cells (data obtained during our primary screening) (Figure 49, A).

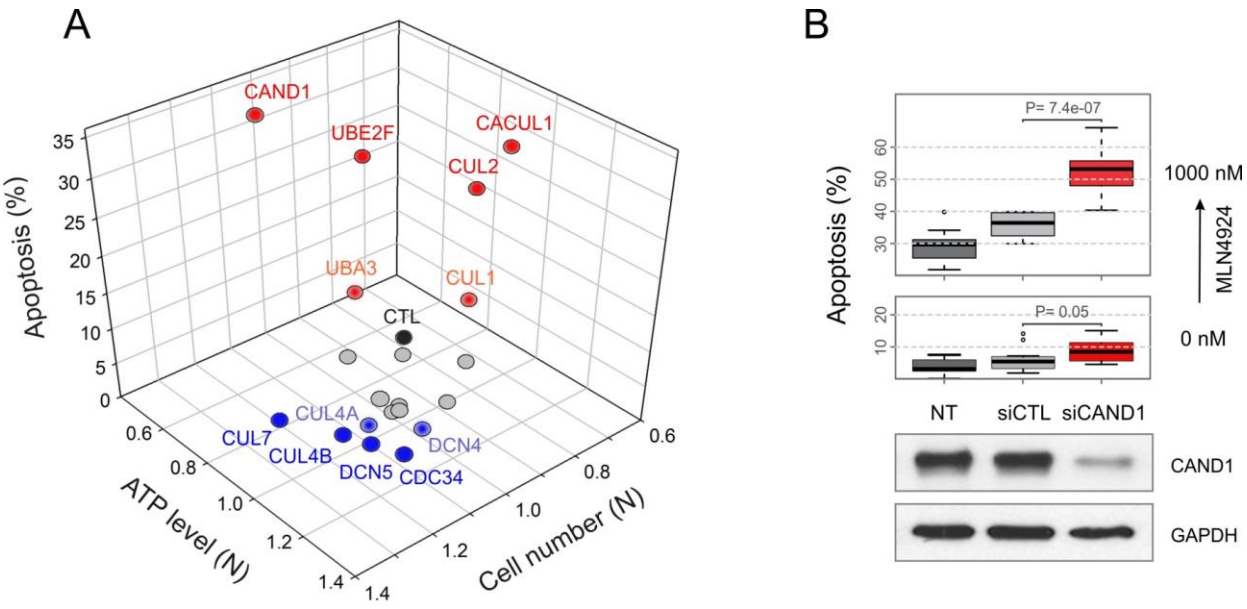

Figure 49. A. The effect of inhibition of CRL components on viability of VCaP cells. B. Inhibition of CAND1 protein using sub-optimal concentration of siRNA potentiates the toxic effect of MLN4924.

We found that, while knockdown of CUL1 and, particularly, CUL2 inhibited cell growth and induced apoptosis, knockdown of CUL7 and CUL4B had an apparent beneficial effect by increasing cell number or reducing the fraction of apoptotic cells. Some other components of CRL/NEDD8 pathway were also found on the opposite ends

of the distribution: CAND1, UBE2F, CACUL1 (pro-apoptotic siRNAs) and DCUN1D4/DCN4, DCUN1D5/DCN5 (growth promoting siRNAs). These results suggest that the inhibition of NEDD8-dependent activation of CRLs may have opposite outcomes depending on the balance within the CRL network.

Notably, CAND1, one of the key regulators of the CRL network balance, was the most prominent hit identified by this screening. CAND1 acts as a protein exchange factor catalyzing dynamic redistribution of substrate-receptors between CRLs. Knocking down CAND1 induced a significant apoptotic death suggesting it is a limiting component of the CRL network in VCaP cells (Figure 49, A). We reasoned, therefore, that, if the cytotoxicity of MLN4924 was mainly due to compromised CRL function, the inhibition of CAND1 would further potentiate the toxic effect. To examine this possibility we suppressed CAND1 with suboptimal concentration of siRNA (1 nM). Under these conditions, the extinction of CAND1 protein was not complete and only a limited cell mortality was observed (Figure 49, B). Yet, this amount of siCAND1 significantly increased the apoptosis induced by 500 nM MLN4924, pointing to the epistatic relationship between CAND1 and NAE in prostate cells (Figure 49, B).

Taking together these data (1) provide some explanation for the differential effect of MLN4924 on VCaP cells; (2) support the role of CRLs as a major effector of NAE inhibition; (3) suggest CAND1 as another potential therapeutic target for prostate cancer.

2.6 MLN4924 INDUCES REVERSIBLE GROWTH ARREST IN 3D PROSTATOSPHERE MODEL

The results shown above suggest that the apparent resistance of TMPRSS2:ERG-positive cancer cells toward MLN4924-induced apoptosis may come from cell cycle arrest at the G0/G1 phase. Considering a potential clinical application of MLN4924, the principal question is whether this arrest is irreversible (senescence) or reversible (quiescence). The latter may lead to tumor re-growth in the case of sub-optimal MLN4924 treatment. To address this question we investigated the outcome of NAE inhibition in tumor-relevant 3D prostatosphere model. VCaP spheroids were pre-formed in 96-well round bottom ultra-low attachment plates, subjected to long-term MLN4924 treatment, and analyzed by optical microscopy (Figure 50, A, B). Exponential spheroid growth was observed in control condition (Figure 50, A, B). Treatment of the spheroids with 50 nM MLN4924 blocked their growth for about 6 weeks without visible impact on

spheroid integrity (Figure 50, A, B). By contrast, applied at a 500 nM concentration, MLN4924 caused complete dissolution/dispersion of the prostatospheres within 2-3 weeks of treatment (Figure 50, A, B). These results corroborate our findings in 2D culture, where significant cell apoptosis was detected only at MLN4924 concentrations above 500 nM (Figure 46, B).

Confirming apoptotic cell death, the staining with CellEvent™ reagent revealed strong activation of Caspases-3/7 upon the treatment of the prostatospheres with 500 nM MLN4924 (Figure 50, C). Curiously, some caspase activity was also seen in the center of the spheroids grown under control conditions. This basal apoptosis may be caused by intensive cell proliferation that leads to a local exhaustion of nutrients within the core of a rapidly growing spheroid (Hamilton, 1998). On the other hand, consistent with growth arrest, only rare apoptotic events were detected in prostatospheres treated with 50 nM MLN4924 (Figure 50, C).

It has been shown that MLN4924 can trigger senescence in some cell types (Jia *et al*., 2011). To test whether MLN4924 treatment causes irreversible growth arrest in VCaP spheroids, we measured the activity of senescence-associated beta-galactosidase (SA-β-GAL) by using colorimetric X-GAL substrate. While the prostatospheres treated with 500 nM MLN4924 showed intensive X-GAL staining, negligible SA-β-GAL activity was detected in control and 50 nM MLN4924 conditions (Figure 50, C). This result implies that the cell growth arrest imposed by sub-total NAE inhibition in VCaP cells is not senescence and, therefore, may be reversible. In agreement with this conclusion, transferring the spheroids arrested for 40 days (with 50 nM MLN4924) into a drug-free medium resulted in spheroid re-growth similar to normal pace (Figure 50, A, B).

Summing up, the results suggest that 90-95% inhibition of cellular neddylation by MLN4924 induces quiescence in TMPRSS2:ERG-positive VCaP cells that may protect these cells from cycling-dependent apoptosis.

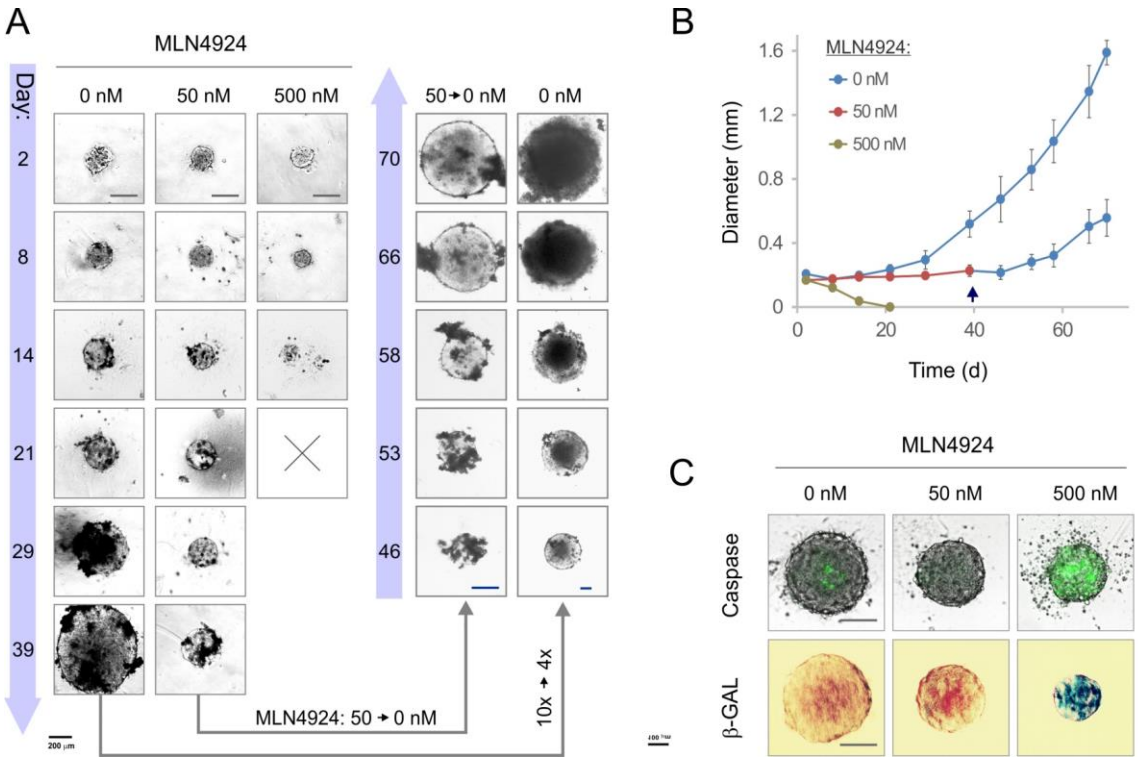

Figure 50. A. Differential effect of CRL/NEDD8 pathway inhibition on the viability of VCaP spheroids. A, B. MLN4924 caused reversible (at 50 nM) or irreversible (at 500 nM) inhibition of spheroids proliferation. C. MLN4924 induced accumulation of senescence (β-galactosidase) and apoptosis (caspases 3,7) markers only at 500 nM concentration

2.7 INHIBITION OF NAE ACTIVATES ANDROGEN RECEPTOR

For many types of cells the G0/G1 cell cycle arrest and exit into a quiescent state is an essential step in terminal differentiation. In normal prostate epithelium and low-grade primary cancer this process is driven by the androgen receptor (AR). Accumulation of various mutations during carcinogenesis results in AR reprogramming in favor of cell dedifferentiation and proliferation that often accompanies the resurgence of castration-resistant (androgen-refractory) prostate cancer (Yeh *et al*., 2009). In TMPRSS2:ERG-positive cancers, ERG oncogene plays a critical role in suppressing the AR activity leading to poorly differentiated, invasive tumor phenotypes (Yu *et al*., 2010).

Because the inhibition of cellular neddylation triggered quiescence in VCaP cells, we asked whether it involves a reactivation of the AR differentiation program. First, we analyzed the effect of MLN4924 on the protein level of AR, ERG and PSA, as AR-specific differentiation markers (Figure 51, A).

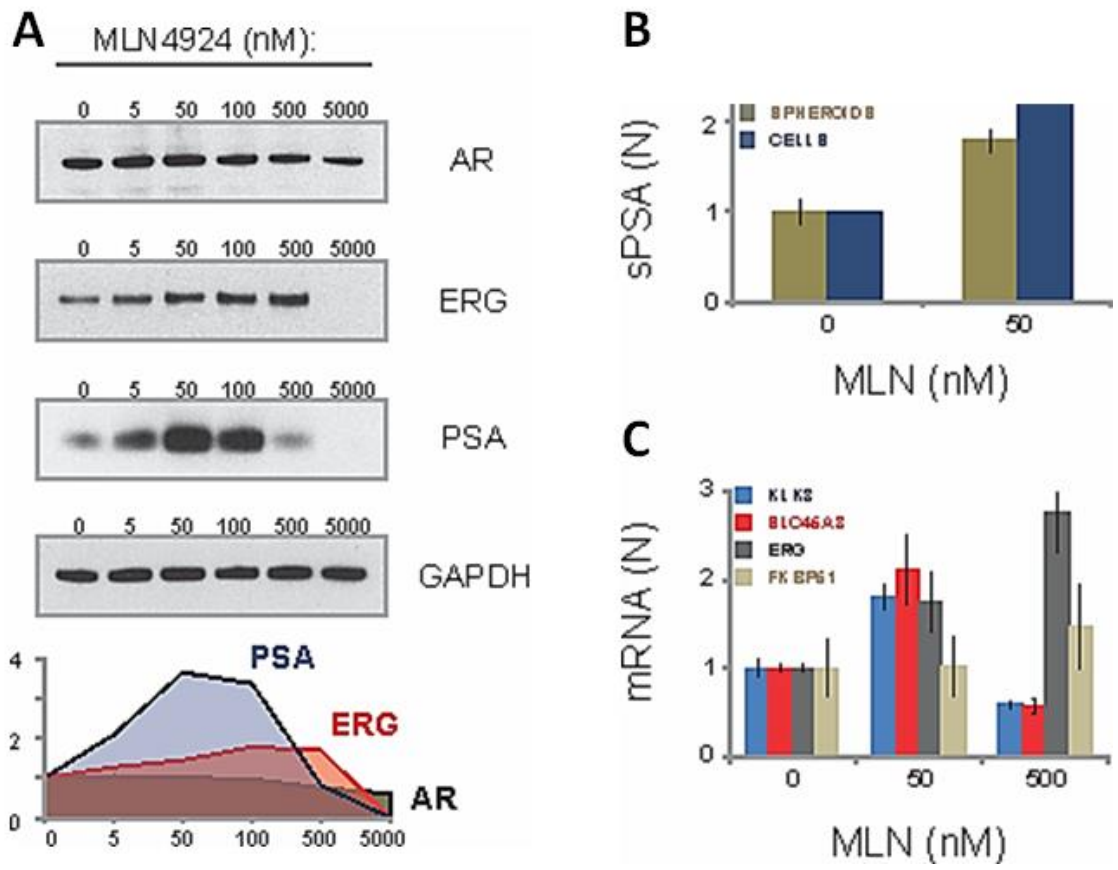

Figure 51. Effect of CRL/NEDD8 pathway inhibition on the AR transcription program in VCaP cells. A. Western Blot demonstrates the level of AR and AR-responsive proteins (PSA and ERG). B. Test ELISA showed that 50 nM concentration stimulates secretion of soluble PSA in 3D (spheroids) and 2D (cells) models. C. Examination of RNA level by qPCR showed that a 50 nM concentration of MLN4924 stimulated expression of AR-responsive genes PSA (KLK3), prostein (SLC45A3) and ERG. Treatment of VCaP cells with 500 nM MLN4924 caused a decrease in PSA and prostein expression, while expression of ERG was still strong. Another AR-responsive gene FKBP51 seemed to not be sensitive to MLN4924 treatment.

Treatment of the cells with up to 100 nM MLN4924 did not change the level of AR, while at higher doses the drug caused a slight decline in AR protein probably reflecting an onset of cytotoxicity. By contrast, the level of ERG protein rose progressively reaching the maximum at 100-500 nM of MLN4924 (Figure 51, A). This increase in ERG could result from the stimulation of AR-dependent transcription, or, alternatively, from the stabilization of the protein. The abrupt disappearance of ERG in cells treated with 5 μM MLN4924 (Figure 51, A) and our qPCR data (see below) strongly suggest transcriptional regulation. Most strikingly, when cells were treated with 50-100 nM of MLN4924, the level of PSA protein rose approximately fourfold, but dropped again when higher doses of the drug where used. A similar biphasic dose-response was observed for two others prostate differentiation markers, SLC45A3/prostein and FKBP51, whose expression is controlled by AR (Supplementary Figure 6). Notably, despite the

accumulation of ERG, the level of presumed ERG targets, FZD4 and LEF1, remained unchanged suggesting that the MLN4924 effect was AR-specific (Figure 61).

To confirm that the changes in differentiation markers observed by Western Blot were due to differential gene expression, we measured the level of the corresponding transcripts. The cells were treated with 0, 50 and 500 nM of MLN4924 and the expression of four AR target genes, TMPRSS2:ERG, KLK3 (PSA), SLC45A3 (prostein) and FKBP51, and then analyzed by quantitative RT-PCR (qPCR). We found that the inhibition of NAE with 50 nM of MLN4924 stimulates the expression of all tested AR target genes except FKBP51. In accordance with previous observations (Figure 51, A; Supplementary Figure 6), 500 nM MLN4924 inhibits transcription of PSA and SLC45A3, while transcription of ERG continues to increase (Figure 51, C).

Finally, we examined whether the spheroid growth arrest caused by 50 nM of MLN4924 (Figure 5) is accompanied by one of the prostatic differentiation features, the secretion of PSA. The spheroids were treated with 0 or 50 nM of MLN4924 for 5 days and the amount of PSA in the medium was measured by the standard ELISA kit. About a twofold increase in secreted PSA compared to the control value was observed (Figure 51, B).

Taking together these results demonstrate that at <100 nM-doses MLN4924 stimulates AR-dependent transcription leading to the expression of prostate differentiation markers. Thus, the activation of the differentiation program may be one of the reasons for cell quiescence caused by subtotal NAE inhibition.

2.8 OPPOSITE ROLES OF AR & ERG IN VCaP CELL RESPONSE TO NAE INHIBITION

It has been shown that in TMPRSS2:ERG-positive prostate cancer cells ERG binds to AR and the majority of AR target genes, disrupting androgen signaling. Our finding, that at <100 nM doses MLN4924 activates AR and the AR-dependent differentiation program, may imply that subtotal inhibition of neddylation somehow relieves AR from ERG suppression. This may switch the cellular program from a potentially detrimental ERG-dependent pro-proliferating regime to a pro-differentiated AR-dependent quiescent state, thus protecting cells from ERG- and re-replication-inflicted DNA damage in S-G2 phases.

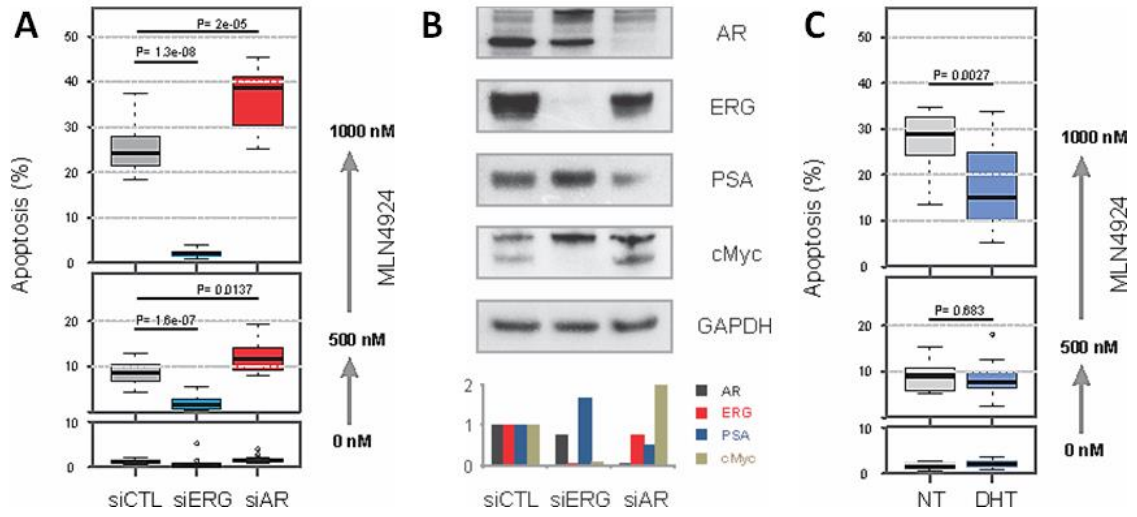

Figure 52. A. Knockdown of ERG using siRNA protects VCaP cells against MLN4924-induced cytotoxicity, while knockdown of AR sensitizes them. In accordance with these data, stimulation of the AR-program by DHT (C) has a protective effect upon MLN4924 treatment. B. Western Blot confirmed that using siRNA efficiently suppresses target proteins (AR and ERG) and alters the expression of markers corresponding to the AR program (PSA) or the ERG program (c-Myc).

This scenario suggests that in TMPRSS2:ERG-positive prostate cancer cells the cytotoxic effect of MLN4924 is suppressed by AR and potentiated by ERG. To test this hypothesis we examined the effect of AR- and ERG-knockdowns on MLN4924-induced apoptosis (Figure 52, A). We used specific siRNAs that potently downregulated the level of target proteins in VCaP cells (Figure 52, B). Knockdown of ERG strongly suppress the levels of ERG and c-Myc protein, the expression of which in VCaP cells was shown to be a part of the ERG-dependent transformation program (Sun *et al.*, 2008). This was accompanied by a visible increase in the amount of PSA protein consistent with the previously reported AR de-repression and activation (Yu *et al.*, 2010). Strikingly, siERG also strongly suppressed the apoptosis induced by MLN4924. It may be, at least in part, due to the activation/reprograming of AR by ERG knockdown. Indeed, stimulation of AR by DHT also had an anti-apoptotic effect, though much less pronounced compared to siERG (Figure 52, C). On the other hand, AR knockdown significantly increased the MLN4924 cytotoxicity within the whole range of drug concentrations (Figure 52, A).

These data support an antagonistic role of AR and ERG in response to MLN4924, though the mechanism of how CRL inhibition de-represses AR transcription is not clear. One possible link may be the NF-κB pathway, which is positively regulated by ETS transcription factors, and ERG in particular (Lambert *et al.*, 1997; Wang *et al.*, 2011; Rayet & Gélinas, 1999). Several previous reports demonstrated mutual transcriptional

repression between AR and NF-κB (Palvimo *et al*., 1996; Nelius *et al*., 2007; Han *et al*., 2014). We observed that the inhibition of NF-κB signaling occurred at low doses of MLN4924 and correlated with AR activation (Figure 48; Figure 51). It seems, therefore, possible that NF-κB plays the role of transcriptional switch between ERG-dependent proliferation and AR-dependent cell growth arrest.

Another important question is how the activation of AR is linked to G0/G1 cell cycle arrest and quiescence induced by MLN4924. Although we observed that AR stimulation by MLN4924 correlated with a buildup of cyclin-dependent kinase inhibitors p21Cip1 (Figure 48), this resulted, most probably, from direct inhibition of the degradation of these proteins by MLN4924 rather than from AR transcriptional activity. Indeed, at higher doses, MLN4924 produced an even more significant accumulation of p21Cip1 without inducing G0/G1 cell cycle arrest (Figure 48). This observation suggests that the induction of a differentiation-like quiescence state was not, or not only, due to the stabilization of p21Cip1. Recent reports from John T. Isaacs's laboratory documented that AR suppresses cell proliferation via AR/b-Cat/TCF-4 complex inhibition of c-MYC transcription (Antony *et al*., 2014). This mechanism could also explain our data showing that the knockdown of ERG, which stimulated AR and abolished c-Myc expression (Figure 52, B), protected cells from MLN4924-induced proliferation-dependent apoptosis (Figure 52, B). To determine whether NAE inhibition by MLN4924 affects c-Myc expression we performed a Western Blot. Indeed, five days of treatment with low doses of MLN4924 (10-50 nM) caused a significant decrease in c-Myc protein level, and an accumulation at higher doses (> 100 nM) (Supplementary Figure 4). This correlated with the profile of activation of the transcriptional program of AR (Figure 51; Supplementary Figure 6).

Taken together, these data demonstrate that the subtotal inhibition of the CRL/NAE pathway by MLN4924 triggers cell reprograming by turning off NF-κB signaling, stimulating AR, and suppressing c-Myc. As a result, the cells acquire a pro-differentiated quiescent phenotype and become resistant to proliferation-dependent DNA damage.

2.9 DISCUSSION

2.8.1 Causes of differential phenotypic outcome.

We observed differential sensitivity of PCa cells toward MLN4924 depending on ERG and proliferation status, where TMPRSS2:ERG-positive slow-proliferating cell lines (VCaP and DuCaP) were the most resistant. Moreover, in the VCaP cell line the inhibition of the CRL/NEDD8 pathway has a discontinuous effect with two major outcomes: quiescence and apoptosis/senescence.

Using the siRNA approach we have demonstrated that the knockdown of the principal CRL components, i.e. cullins and neddylation regulators, can have different outcomes. It should be noted that the organization of the CRL system is much more complex and comprises a combinatorial hierarchical assembly of adaptor proteins and substrate receptors. Thus, multiple CRL complexes can be assembled on the same cullin scaffold and play distinct and even opposite roles in cell fate. We did not address this complexity in our small siRNA screening. Nevertheless, our data demonstrate that, even on the primary level, knockdown of the basic CRL/NEDD8 components may have different outcomes. Therefore, the discontinuous cellular response to MLN4924 may, in principle, be explained by differential susceptibility of various CRLs to neddylation inhibition. Specifically, our results suggest that CRL-suppressors of pro-quiescent pathways are more sensitive to MLN4924 (inhibited at < 100 nM doses), whereas CRL-regulators of pro-apoptotic/senescence pathways are less susceptible to MLN4924 inhibition (> 250 nM). The latter suggests robust apoptosis suppression by CRL even at low level of neddylation, and may reflect the irreversible “last solution” role of this outcome.

Notably, our results imply a principal role of CAND1 protein for CRL functioning under suboptimal neddylation conditions. CAND1 is an exchange factor that catalyzes redistribution of CRL cofactors (Duda *et al.*, 2011). CAND1 binds non-neddylated cullin complexes which are produced by COP9 deneddylase. This binding stimulates the dynamics of the CRL adaptor proteins’ exchange and redistribution of CRL components for performing diverse cellular functions (Pierce *et al.*, 2013). Therefore, CAND1 may become particularly important when the dynamics of the CRL network is perturbed by MLN4924. There is also evidence that CAND1 can function as a chaperon by protecting non-neddylated cullins from the degradation by proteasome. Notably, this CAND1

function becomes apparent when the neddylation of cullins is suppressed (Kim *et al*., 2010). Therefore, the knockdown of CAND1 may also potentiate the inhibitory effect of MLN4924 by stimulating the degradation of cullins.

The role of CAND1 in carcinogenesis is largely unexplored. In pulmonary cancer, negative correlation between neddylated cullins and CAND1 has been observed, supporting the conclusion that CAND1 function is particularly important when neddylation is compromised (Salon *et al*., 2007). The data on the implications of CAND1 in prostate cancer are controversial. It has been reported that in LNCaP prostate cancer cells the expression of CAND1 is negatively regulated by androgen-stimulated Lin RNA. On the other hand, analysis of the limited cohort of PC specimens revealed an aberrant CAND1 status in cancer tissue with both over- and under-expression levels compared to normal prostate. Notably, interrogation of the Oncomine database revealed general up-regulation of CAND1 in prostate cancer with CAND1 found in the top 2% of upregulated genes in intraepithelial neoplasia and in the top 3-10% in prostate adenocarcinoma.

These data suggest that inhibition of the CAND1-cullin interaction may represent a new approach in the treatment of cancer pathology.

2.8.2 Direct effectors of CRL inhibition

MLN4924 was reported to be highly selective and to have only one target – E1 enzyme for NEDD8, NAE. Nevertheless, different doses of MLN4924 caused accumulation of different proteins. At low doses (25-100 nM) we observed accumulation of *phospho*-IκB, p21 and *phospho*-β-catenin, while higher doses (250 nM and higher) lead to an accumulation of Cdt1. This might suggest that different doses of MLN4924 could lead to the inhibition of different CRL complexes, which would lead to an accumulation of different targets and, thus, would lead to different phenotypes.

IκB, β-catenin and p21 are degraded by CUL1-based CRLs. An accumulation of p21 can induce G0/G1 cell cycle arrest. Moreover, MLN4924 induced an accumulation of the NF-κB inhibitory subunit *phospho*-IκB and blocked the translocation of the *phospho*-p65 subunit of NF-κB into the nucleus (Supplementary Figure 7). As discussed previously, the inhibition of NF-κB signaling in ERG-positive VCaP cells was shown to suppress cell growth (Wang *et al*., 2011) and might be another cause of G0/G1 cell cycle arrest by MLN4924. A similar mechanism of MLN4924 action has been described with NF-κB-dependent activated B cell-like diffuse large B cell lymphoma (ABC) DLBCL

(Milhollen *et al*., 2010). These cells show constitutive IκB kinase (IKK) activity, and rapid IκB degradation that distinguish them from other subtypes of DLBCL cells. Treatment of ABC-DLBCL cells with MLN4924 results in IκB stabilization, inhibition of NF-κB signaling, G1 cycle arrest and apoptosis. Accumulating data suggest that activation of the NF-κB pathway also plays a central role in prostate carcinogenesis and, particularly, in the acquisition of castration resistance. NF-κB signaling promotes survival of prostate cancer cells at low androgen level and switches the transcriptional program to an invasive, metastatic phenotype (Lindholm *et al*., 2000; Wang *et al*., 2011). There is also a significant correlation between the constitutively active NF-κB pathway and the upregulation of ETS transcription factors suggesting a causal link. Indeed, ERG and other ETS proteins increase the expression of a number of NF-κB-associated genes and promote NF-κB-transcriptional activity while cytokines can stimulate ETS expression via NF-κB (Wang *et al*., 2011). This provides a positive feedback loop leading to constitutive activation of ETS and NF-κB through the sustained inflammatory circuit. A recent study demonstrated that the NF-κB-dependent production of lymphotoxin by B lymphocytes from tumor inflammatory infiltrates is essential for the growth of cancer cell progenitors (Ammirante *et al*., 2010). Therefore, the ability of MLN4924 to inhibit NF-κB both in prostate and B cells may be particularly efficient in suppression of castration resistance. Generally, however, the inhibition of NF-κB in prostate cancer cells is not sufficient to induce apoptosis (Evans *et al*., 2015). Moreover our data suggest that G1 cell cycle arrest induced by MLN4924 in TMPRSS2:ERG-positive VCaP cells is reversible.

Higher doses of MLN4924 (>250 nM) causes accumulation of the replication licensing factor Cdt1 protein, which is recognized to be a substrate of CRL1 and CRL4. Inability to degrade Cdt1 induces re-replication, and further DNA damage (followed by an increase of H2AX-positive foci), cell cycle arrest in the G2/M phase, which is finally manifested by senescence and apoptosis. The mechanism of apoptosis is not clear. VCaP cells have a R248W mutation in the p53 gene which abolishes the ability of p53 to initiate apoptosis (Sobel & Sadar, 2005; Song *et al*., 2007). The putative effectors are p21 and c-Myc.

2.8.3 General outcomes: transcriptional reprogramming

In our study, the inhibition of the classical NF-κB pathway (< 100 nM MLN4924) correlates with an activation of the AR transcriptional program. AR activation results in

the expression of prostate differentiation markers (PSA, prostein, FKBP51); moreover, using 2D and 3D prostatosphere models, we showed an increased secretion of PSA. We also observed increased ERG expression, but the ERG-expression program seemed to be intact (judging by LEF1 and FZD protein levels). Altogether, these data suggest an activation of the differentiation program that might be a potential cause of observed cellular quiescence (G1 cell cycle arrest without apoptosis and senescence). The finding that the knockdown of AR sensitizes cells to low doses of MLN4924, while the activation of AR by DHT has a protective effect, supports this conclusion. Some possible mechanisms of AR activation:

1. Direct regulation of AR transcriptional activity by neddylation. Some evidence suggest that the intact NEDD8-pathway is essential for transcriptional activation of steroid receptors, but they have never show direct neddylation of these proteins (Fan *et al.*, 2002; Fan *et al.*, 2003). The direct neddylation of AR was reported in grant application (Don Chen, 2009), but the final results are still not published. Moreover, we did not detect neddylation of AR in VCaP cells (data not shown).

2. Activation of the AR-dependent program by accumulated *phospho*-β-catenin. Several studies suggest a complex interaction between AR and the Wnt/β-cat pathway. It has been shown that β-cat interacts with AR and potentiates AR signaling in prostate cells (Pawlowski *et al*., 2002; Truica *et al*., 2000), while AR represses the β-cat-induced transcriptional program (Chesire & Isaacs, 2002; Song *et al*., 2003). Thus, in VCaP cells an accumulation of β-cat without activation of the Wnt-dependent program could lead to the re-activation of AR transcription program.

3. Mutually exclusive activity of AR with NF-κB. Thus, the inhibition of NF-κB would de-represses AR activity. Previous reports on NF-κB-AR interaction were contradictory. Several reports demonstrated mutual transcriptional repression between AR and NF-κB (Palvimo *et al*., 1996; Nelius *et al*., 2007; Han *et al*., 2014), while others suggest the opposite correlation (Zhang *et al*., 2009; Chen & Sawyers, 2002). Our data supports mutual inhibition of AR and NF-κB. First, in VCaP cells, MLN4924 caused dose-dependent inhibition of NF-κB inhibition (stabilization of IκB) negatively correlated with AR activation (expression of differentiation markers). Second, the transcriptional program of ERG, the major driver of NF-κB activation in TMPRSS2:ERG-positive cells, was not stimulated despite a higher ERG protein level. Considering that in TMPRSS2:ERG-positive cells AR was shown to be suppressed due to NF-κB activation,

we conclude that AR re-activation may occur, at least partially, through NF-κB inhibition, though other CRL-NEDD8-dependent mechanisms may exist.

High doses of MLN4924 (250-500 nM) shut down transcription of AR targets except ERG. Of note, at 5 μM MLN4924 we observed a spectacular disappearance of ERG and PSA proteins but at this dose MLN4924 may cause a general, non-specific toxicity. Strikingly, MLN4924-induced apoptosis was almost completely ERG-dependent. Pro-proliferation-inducing activity of ERG (and other ETS proteins) in prostate cancer cells was shown to generate a relatively high level of spontaneous DNA damage (Swanson *et al*., 2011). Also, aberrant transcriptional activity of AR in cancer cells can also produce a significant rate of DNA damage (Shen MM & Abate-Shen C, 2010). Although the detailed mechanisms of inflicted DNA damage are not clear, this seems to be a general hallmark of carcinogenesis which aims for the suppression of DDR in favor of proliferation. Furthermore, with a compromised DDR, the high rate of replication-associated DNA lesions may lead to genomic instability, providing some evolutional advantage to cancer cells. More specifically, in ETS-positive cancers, ERG has been shown to directly suppress the expression of master checkpoint kinase Chk1 releasing the blocking of error-prone DNA replication. This leads to an ERG-dependent accumulation of spontaneous DNA damage in VCaP cells; this effect we also observed in our experiments. At the same time, ERG and other ETS factors cooperate with PARP1 and upregulate the NF-κB pathway, insuring cancer cell survival even at high level of DNA damage. We found that, in contrast to other AR-targets, high doses of MLN4924 (500 nM) significantly induced ERG both on transcription and protein synthesis levels. Thus, ERG-driven cell cycling in combination with re-replication imposed by Cdt1 may favor further accumulation of DNA damage, G2/M cell cycle arrest, and apoptosis. Notably, the protective effect of G1-arrest at this MLN4924 concentration is overwritten by the suppression of AR activity.

2.8.4 Cancer cell plasticity: implication for cancer treatment

Thie discontinuous response to the inhibition of the CRL/NEDD8 pathway is an example of cancer cell plasticity. TMPRSS2:ERG mutation, found in more than 50% of prostate cancers, seems to be a master-gene, switching the transcriptional program from differentiation to proliferation. ERG has been shown to activate NF-κB (Wang et al., 2011), leading to increased proliferation in prostate tumors; induce the Wnt/β-cat

pathway (Wang *et al*., 2011; Birdsey *et al*., 2015), leading to increased migration; induce c-Myc (Sun *et al*., 2008), stimulating metabolism; suppress AR-signaling (Yu et al., 2010), which could lead to an amplification of AR and the induction of an androgen-independent phenotype (Figure 53).

On the other hand, switching the transcriptional program from pro-proliferating (ERG:NF-κB:c-Myc:Wnt/β-cat branch) to quiescent/differentiated (AR/β-cat) could help PCa cells to adapt to diverse internal and external stimuli. Thus, cancer progression, proliferation, invasion, and functioning under androgen deprivation would select cells with an active ERG:NF-κB:c-Myc:Wnt/β-cat pathway, whereas, adverse environmental conditions, negative pressure on proliferation and functioning under higher androgen level would favor the activation of the AR-dependent differentiated pathway. Thus, quiescence observed under low doses of MLN4924 (< 100 nM) could be considered as an adaptive mechanism to avoid apoptosis. Damage induced by higher doses of MLN4924 (> 500 nM) is too strong and cannot be overcome.

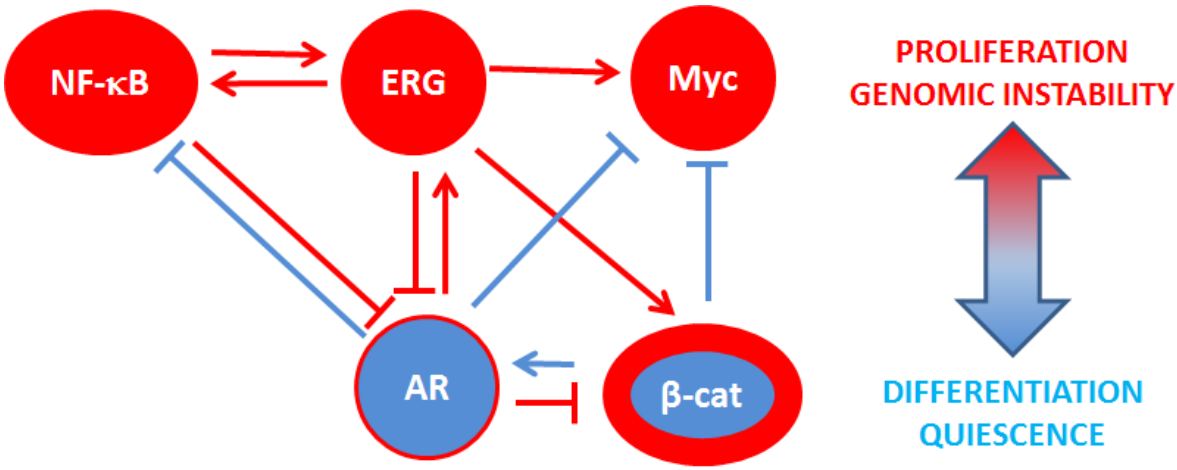

Figure 53. Known interactions between ERG, AR, NF-κB and β-catenin signaling.

CHAPTER 3. INHIBITION OF CRL/NEDD8 PATHWAY BY MLN4924 CHANGES VCaP MORPHOLOGY

3.1 INTRODUCTION AND PRELIMINARY OBSERVATIONS

Nowadays, genome-wide siRNA screening is a standard technique allowing the identification of protein functions. Cancer-related screening most often aims to identify new drug targets and thus look for proteins required for the survival of cancer cells. Often only a limited number of parameters, such as apoptosis, proliferation or DNA damage is analyzed. At the same time, some genes may be involved in diverse important biological processes, which are not vital and, therefore, not analyzed and, thus, omitted from the screenings. Therefore, paying attention to other phenotypes, distinct from cell death and proliferation, would help to obtain important information on cancer biology.

In our screening, we aimed to identify components of the UPS crucial for the viability of PCa cells. Among seven identified hits, four belong to the CRL/NEDD8-pathway; moreover, two of them are putatively ERG-dependent. In the screening and, further, using MLN4924 we showed that the inhibition of CRL/NEDD8 pathway in PCa has a complex outcome on viability and depends on cellular context. During the screening we noticed that MLN4924 also alters the morphology of VCaP cells, suggesting additional functions of the CRL/NEDD8-pathway. Thus, under normal conditions VCaP cells are rounded and weakly adherent, but increasing the density results in cells growing in colonies without visible borders between them (Figure 54, A). VCaP cells are nearly immobile, and do not move from the occupied positions after primary attachment to the substrate. Rarely, VCaP cells move to join bigger groups of cells that seem to favor their growth (Figure 54, B; supplementary video 1). This observation was corroborated by a wound-healing assay: VCaPs don't "heal wounds" after the scratch (Figure 54, C). Inhibition of the CRL/NEDD8 pathway caused a dose-dependent change in the morphology of VCaP cells (Figure 55, A). After 5 days of treatment with MLN4924, cells grown in 50 nM MLN4924 acquired a fibroblast-like morphology. An increase of MLN4924 concentration up to 500 nM caused an aggregation of the cells into clusters (Figure 55, A). To further investigate this morphological change we performed immunostaining with phalloidin (Figure 55, B). The obtained images demonstrated a fibroblast-like morphology of cells treated with 50 nM MLN4924, and tight groups at 500

nM. Moreover, we observed the appearance of stress-fibers and a clearly visible leading edge in the cells cultured in 500 nM MLN4924.

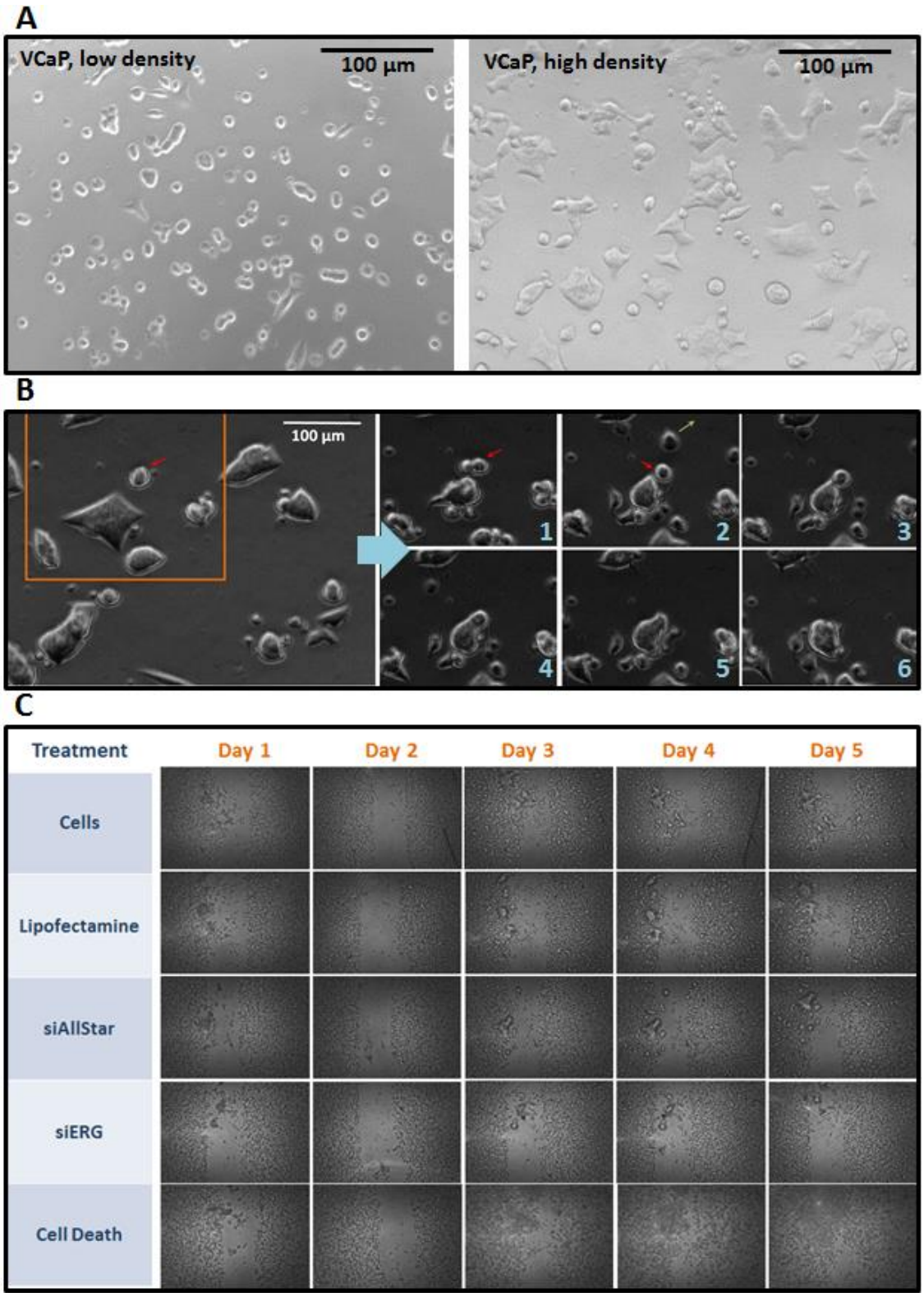

Figure 54. A. VCaP cells grown at low and high density. B. Exchange of cells between colonies (extract from supplementary video 1). Red arrows show the dividing cell. Two resulting cells have different fate – one of them joins the nearest colony, the other leaves the field of view. C. Wound healing assay on VCaP. After primary attachment VCaP cells do not fill the gap produced by scratching of the cell monolayer.

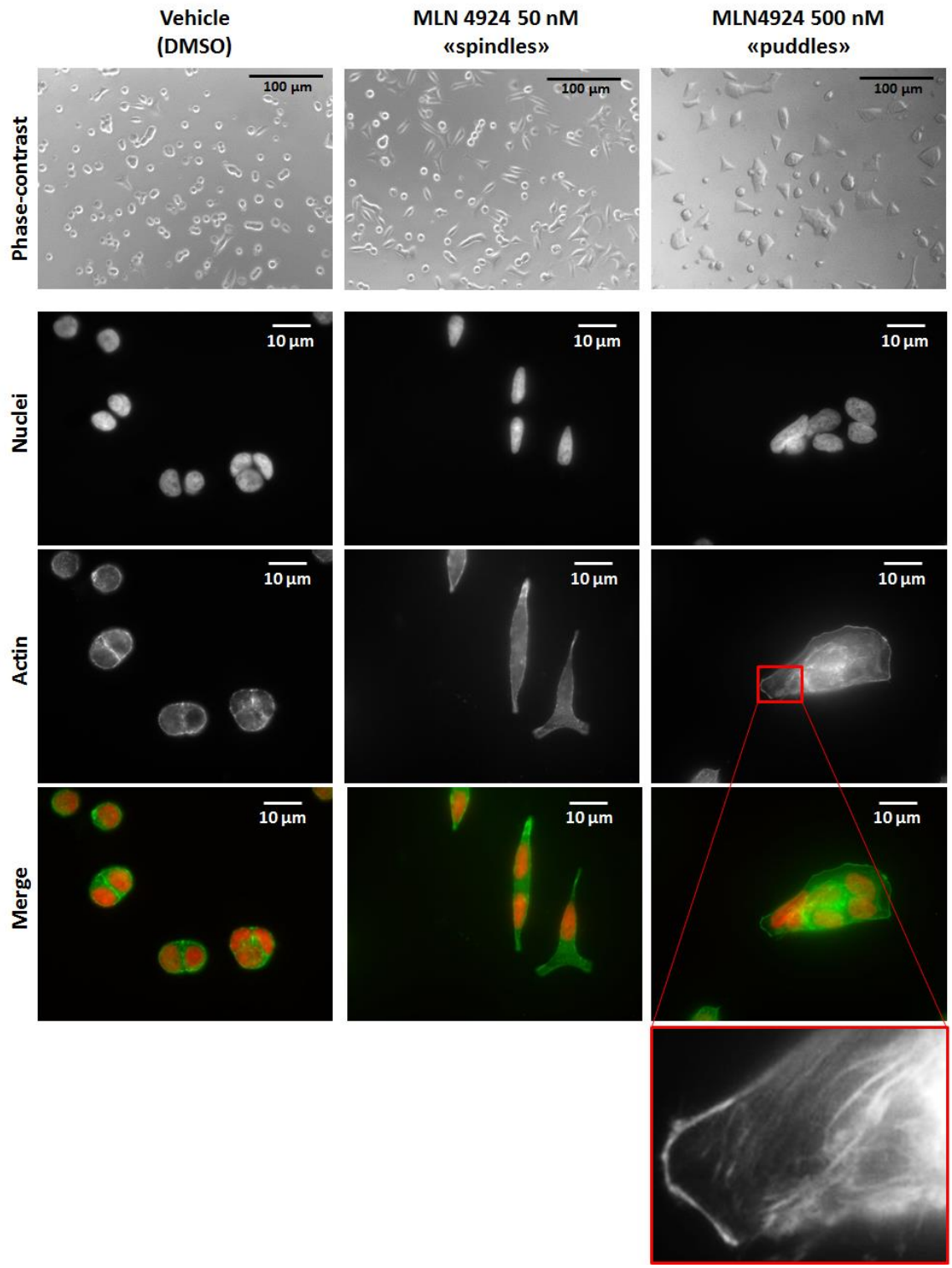

Figure 55. Dose-dependent effect of CRL/NEDD8 pathway inhibition on the VCaP cell line. Phase-contrast (A) and immunofluorescence (B) microscopy; images were obtained 5 days after treatment. Nuclei are shown in red, actin is shown in green. An addition of 50 nM MLN4924 leads to a strong increase of the number of fibroblast-like type of cells. An addition of 500 nM MLN4924 leads to aggregation of cells in clusters and the appearance of stress-fibers.

Altogether these observations suggest that neddylation might have additional functions in VCaP cells that might be important in cancer. We conducted a series of experiments to get more insights into the mechanism of this morphological change.

3.2 MORPHOLOGY CHANGE CORRELATES WITH INCREASED ADHESION OF VCaP CELLS

The fibroblast-like morphology and the appearance of stress-fibers are the signatures of many cellular processes, including cell adhesion and migration (Parsons *et al*., 2010; Vallenius *et al*., 2013). First, we examined the involvement of neddylation in cell adhesion. To follow cell-to-surface adhesion we used a CYTONOTE - Lens-Free Cell Imaging Device. CYTONOTE has a large field-of-view (29.4 mm^2) providing the possibility to follow several thousand cells at once. Analysis of the acquired images using a special algorithm allows for the retrieval of information about morphological properties of cells, such as cell adhesion, shape, size, velocity, etc. (Kesavan *et al*., 2014). The resulting scatterplots show the number of cells having a certain type of morphology (Figure 56). To perform lensless imaging we placed cell suspension with increasing concentrations of MLN4924 in cell culture treated plates. The acquisitions were performed every 20 minutes during 4 days. Low concentrations of MLN4924 (50 nM) lead to a dramatic increase in the number of adherent cells (60%) compared to the control (35%). There were also mostly elongated cells (high aspect ratio) with a relatively small cell surface. Higher concentrations of MLN4924 (500 nM) also increased the proportion of adherent cells (about 45%), but does not induce the "elongated" morphology. Instead, we observed an increase of the average cell surface, which probably reflects the formation of cell clusters. These results indicate that the inhibition of CRL/NEDD8 pathway increases adhesion of VCaP cells to the substrate.

To examine the effect of MLN4924 on cell-to-cell adhesion we performed a spheroid formation assay. To promote spheroids formation, we placed some cell suspension in low attachment U-bottom plates (~500 cells/well) in the presence of increasing concentrations of MLN4924. The spheroids assembly was monitored by videomicroscopy and the diameter of the spheroids was measured. Both tested concentration of MLN4924 (50 and 500 nM) decreased the characteristic time of spheroids formation by about 10 hours compared to the control (Figure 57). Thus, we conclude that MLN4924 increases the cell-to-cell adhesion of VCaP cells also.

In the Chapter 2 of Results and Discussion we showed that the inhibition of the NEDD8-pathway by MLN4924 leads to the re-activation of the AR program accompanied by an increase in ERG protein level. Both AR and ERG could stimulate migration and invasion of PCa cells (Wang *et al*., 2014; Wu *et al*., 2013; Tomlins *et al*., 2008; Zarif *et al*., 2015; Kim *et al*., 2015). We examined, therefore, whether the effects of MLN4924 on cell adhesion depends on ERG or AR. To this end the spheroid formation assay was performed after a 24-hour pre-treatment of cells with siRNA targeting ERG and AR (Figure 58). Both siRNAs abolished the stimulation of spheroids formation induced by MLN4924 at low concentration 50 nM, but not at higher concentration of the drug (500 nM).

Together, these data suggest that the inhibition of neddylation in VCaPs renders cells more adherent to the surrounding substrates. Stimulation of cell-to-cell interactions by MLN4924 is dependent on the intact AR and ERG transcriptional program at least at drug concentrations below 100 nM. On the other hand, the effect of higher doses of MLN4924 may also be affected by the onset of cytotoxicity.

3.3 STIMULATION OF SPHEROID SPREADING

A fibroblast-like phenotype and stress-fibers are both markers of migrating and invasive cells. Thus, we wanted to examine the effect of MLN4924 on cell invasion/migration properties. Different methods permit analysis of cell migration potential:

1) Measurement of average cell velocity. Our data obtained using lensless technology show that MLN4924 treatment did not change the speed of individual cells at all tested concentrations (Figure 56).

2) Cell spreading assays (Transwell migration assay, Platypus Migration Assay, Wound healing assay). No significant migration of VCaP cells was detected using these methods. Optimization of assay conditions, i.e. increase in seeding density, addition of chemoattractant in Transwell Migration Assay, etc., may be required to obtain measurable data.

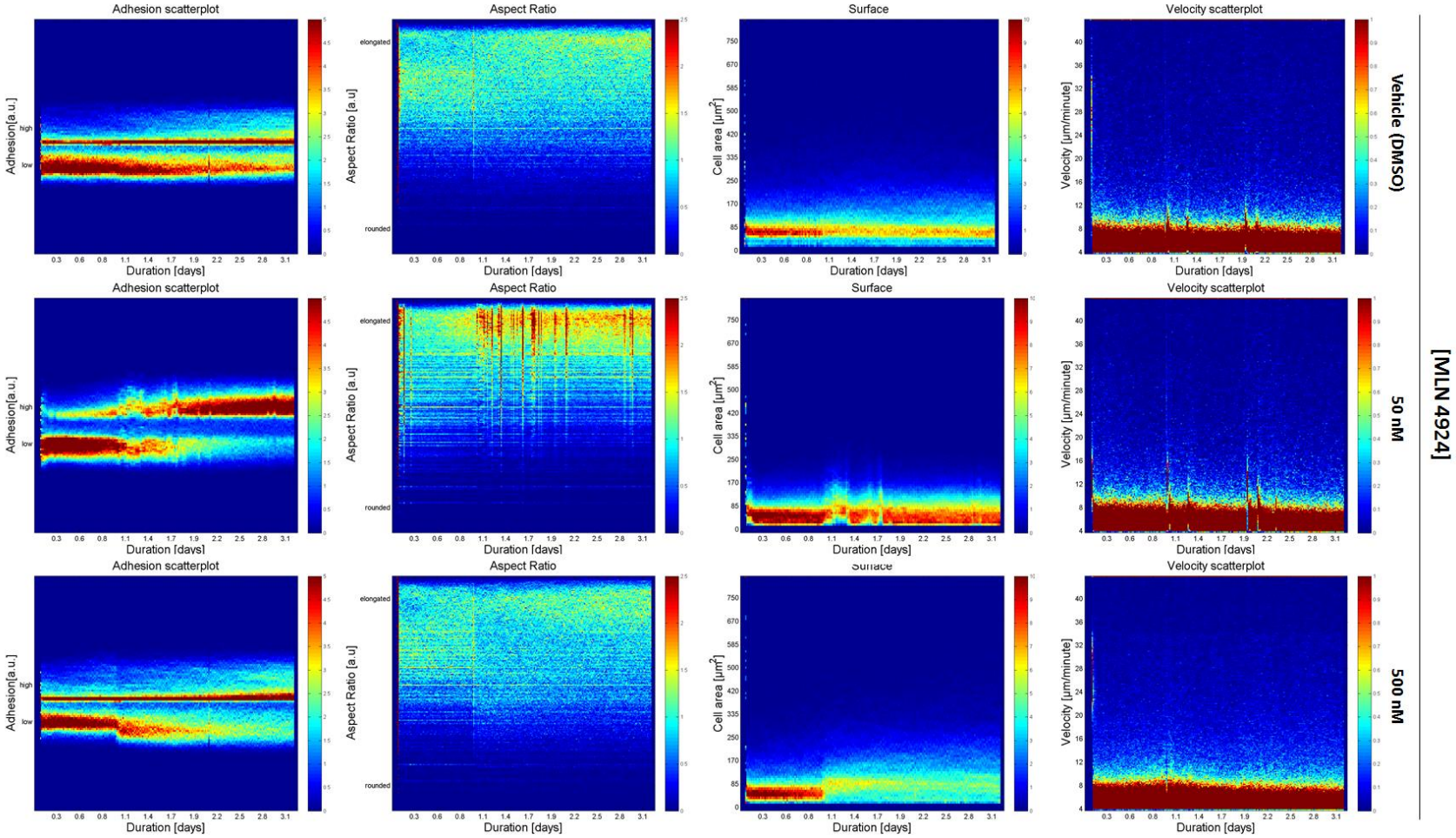

Figure 56. Characterization of changes in cellular morphology using lensless technology. Adhesion scatterplots reflect 2 different population of cells – with high and low adhesion to the substrate. Addition of 50 nM MLN4924 leads to a dramatic increase in the amount of cells with high adhesiveness (from 30 to 60 %). At 500 nM MLN4924 the proportion of weakly adhesive cells decreases significantly compared to the control. The Aspect Ratio scatterplot shows populations of cells having different morphology (from rounded to elongated). The addition of MLN4924 50 nM causes an increase in elongated population of cells. An increase in concentration to 500 nM abolishes this effect. Surface scatterplots show the size of the cells in the population. An addition of 500 nM MLN4924 causes an increase in the average size of the cells, which reflects the formation of clusters. The velocity scatterplots show the velocity of cells in the population. MLN4924 does not influence the velocity of the cells.

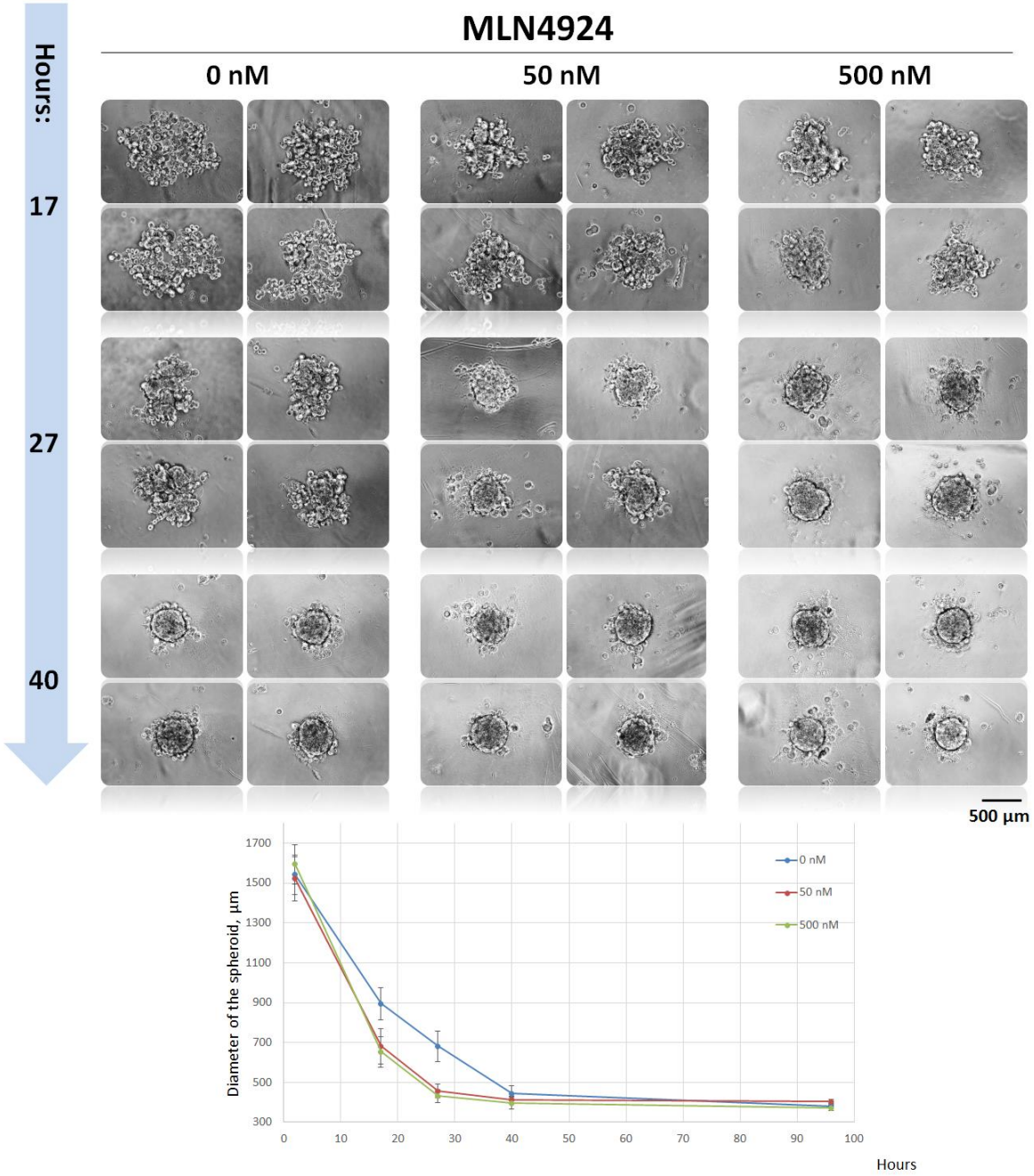

Figure 57. Spheroids formation assay. Cells were suspended in culture medium containing different concentrations of MLN4924 (0 nM with DMSO as a vehicle, 50 nM and 500 nM) and incubated in U-bottom ultra-low attachment plates to allow the formation of spheroids to occur. Cells were followed by videomicroscopy and the largest diameter of the spheroids was measured.

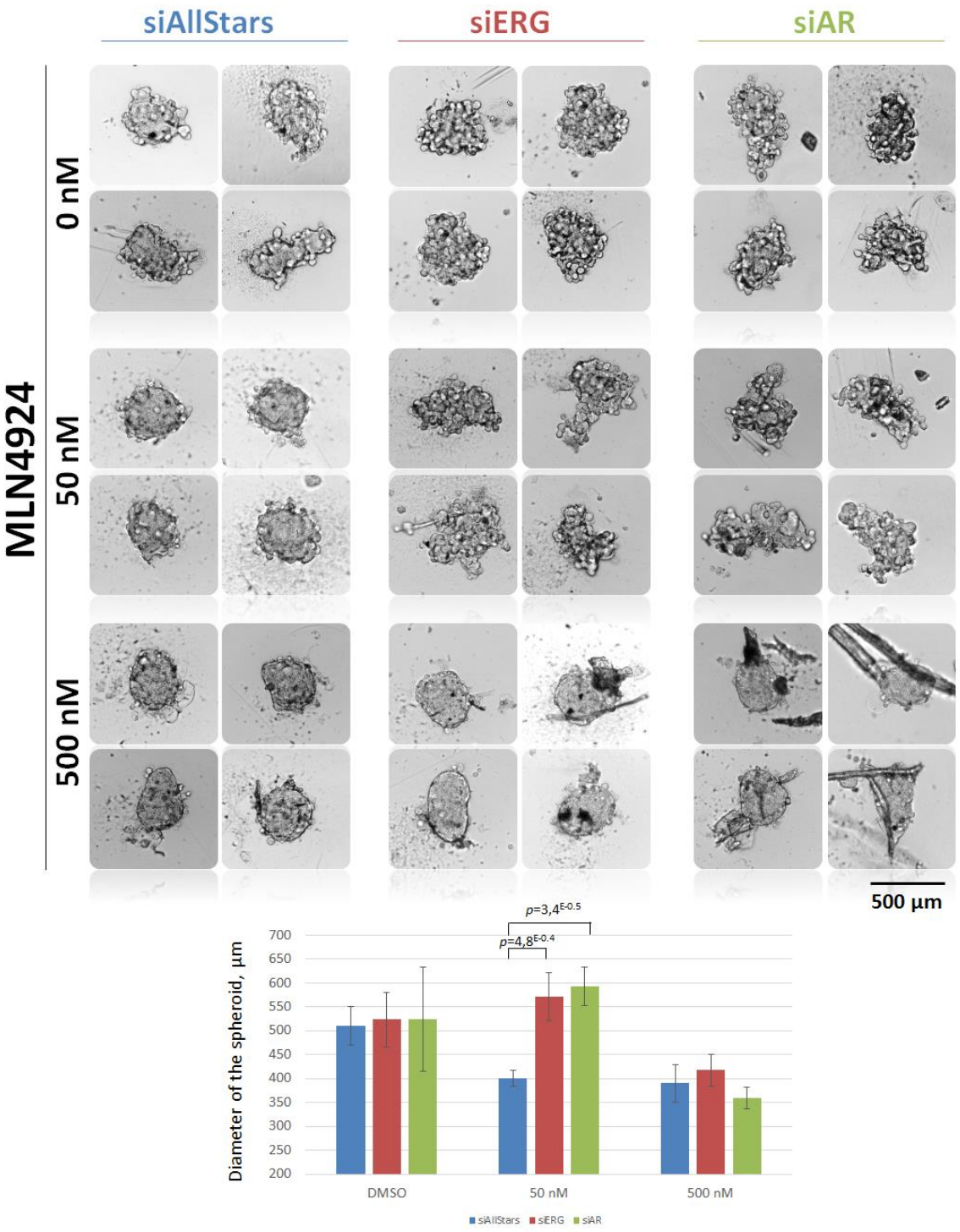

Figure 58. Spheroids formation assay. Suspensions of VCaP cells were distributed in U-bottom well plates together with one of the siRNAs (siAllStars negative control, siERG or siAR) for 24 hours. MLN4924 was added on the next day at indicated concentration (0 nM with DMSO as a vehicle, 50 nM, 500 nM). Cells were followed by videomicroscopy. The time point 30 hours after the addition of MLN4924 was shown. The tested siRNA targeting AR and ERG both abolished the effect of MLN4924 on spheroid formation at the low concentration of 50 nM, but did not change the effect of high-doses (500 nM) of MLN4924.

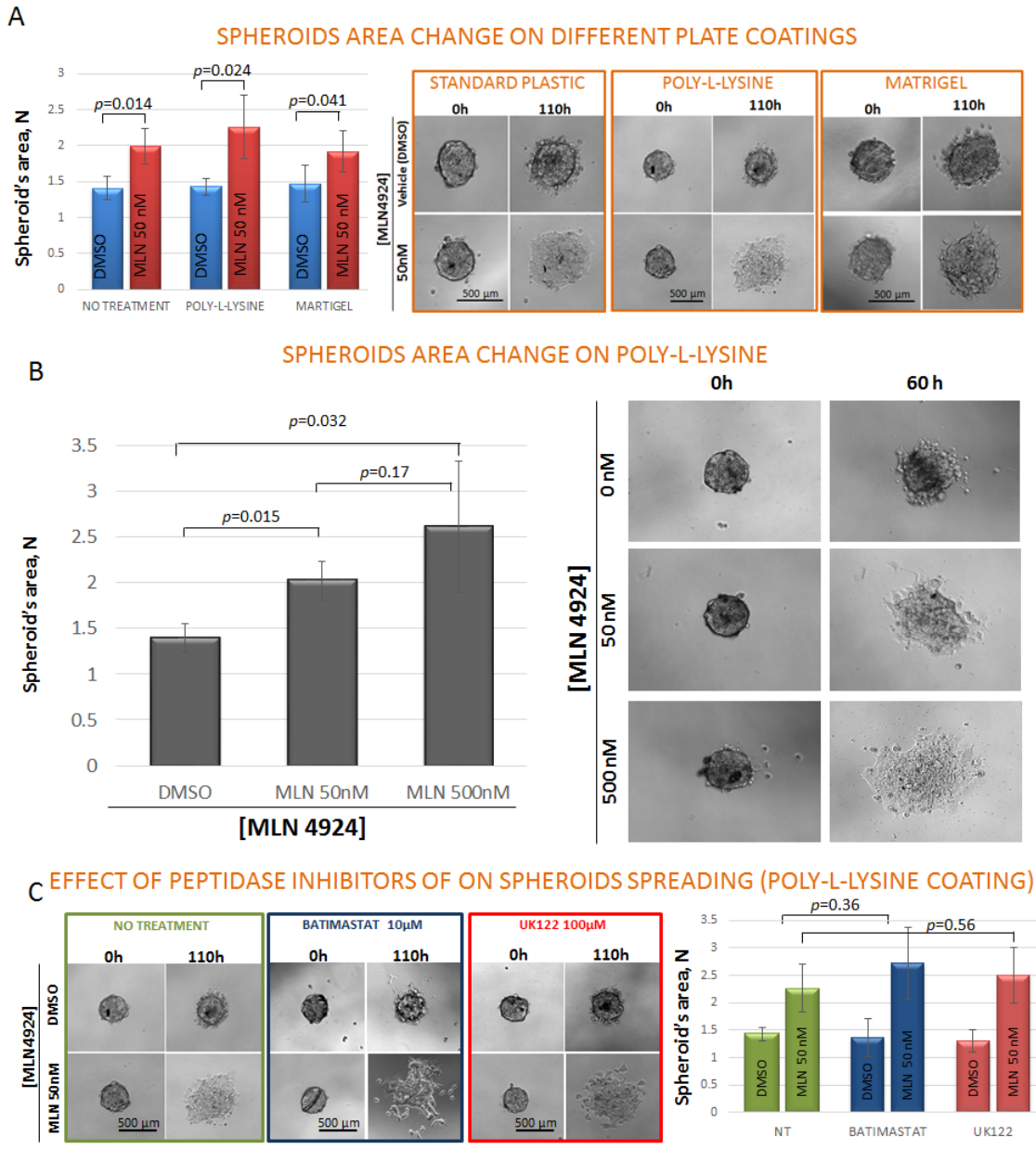

Figure 59. Spheroids Spreading Assay. A. Spreading on different coatings (no treatment, poly-L-lysine or Matrigel®) shows that MLN4924 increases the ability of spheroids to spread on a plane. B. An increase in the concentration of MLN4924 up to 500 nM potentiates spheroids spreading. C. MLN4924 stimulated spheroid spreading is not affected by MMP inhibitor Batimastat or PLAU inhibitor UK122.

3) Spheroid-based tests for spreading and invasion. Spheroids are organ-like cellular aggregates characterized by primitive hierarchy of cell-to-cell interactions and formation of an extra-cellular matrix (ECM). Compared to a 2D culture, spheroids better recapitulate the real situation in tumors. To study the effect of MLN4924 we performed a Spheroids Spreading Assay, which measures the disassembly of spheroids on a plane and its transformation into a 2D-layer (Xu *et al*., 2003; Burleson *et al*., 2006; Indovina *et al*., 2008). We tested different plate coatings: cell-culture untreated plates, plates coated with poly-L-lysine or with Matrigel®, which recapitulate the composition of the extra-cellular matrix (Figure 59, A). With all types of coating, 50 nM MLN4924 increased the spreading of VCaP spheroids. We performed all subsequent experiments in poly-L-lysine-coated plates, since it was the most efficient substrate inducing spheroid spreading. Using increasing concentrations of the drug, we observed that at any tested concentration, MLN4924 stimulates spreading of VCaP spheroids (Figure 59, A, Supplementary videos 2-4). Notably, the accelerated spreading was not a result of proliferation within the spheroids (we show in Chapter II that MLN4924 decreases the proliferation compared to the control).

We have shown that the inhibition of the NEDD8-pathway by MLN4924 leads to an increase in the amount of ERG protein (Figure 51, A). ERG was reported to increase the invasion potential of prostate cancer cells (Wang *et al*., 2014; Wu *et al*., 2013; Tian *et al*., 2014; Leshem *et al*., 2011; Tomlins *et al*., 2008). Moreover, ERG has been shown to enhance the expression of matrix metalloproteases (MMP3, MMP9, ADAM19) and serine-type endopeptidase PLAU (Plasminogen Activator, Urokinase) (Tomlins *et al*., 2008; Tian *et al*., 2014). Tomlins and his colleagues have demonstrated that the increase in invasion potential by ERG protein depended mainly on the activity of PLAU and could be abolished using PLAU inhibitors (Tomlins *et al*., 2008). We hypothesized that the activation of ERG could lead to the induction of MMPs and PLAU, thus facilitating disaggregation of ECM and accelerating the spreading of the spheroids. We examined the effect of pan-MMP inhibitor (Batimastat) and PLAU inhibitor (UK122) on spheroid spreading. Data presented in Figure 59C show that none of the tested inhibitors could reduce spheroids disaggregation and spreading. Therefore, we conclude that stimulation of spheroid spreading by MLN4924 does not depend on the increased activity of MMPs or PLAU. This is in accordance with our previous findings that, despite that the relative amount of ERG protein increases after the addition of MLN4924, the ERG-driven

transcription program seems to not be activated (as judged by the levels of Lef1 and FZD4 proteins).

We also investigated changes in the invasive potential of VCaP cells caused by the inhibition of the CRL/NEDD8 pathway. We decided to use VCaP spheroids pre-formed in low-attachment U-bottom plates. Pre-formed spheroids can grow in a 3D matrix, but do not invade into the Matrigel (Figure 60, A) and other tested 3D matrixes (Cultrex® and PuraMatrix®). Furthermore, MLN4924 (50 or 500 nM) did not stimulate the invasion of VCaP spheroids into Matrigel (Figure 60, B). Nevertheless, these results might also be explained by the particular properties of VCaP cells. It has been shown that individual VCaP cells do not form 3D-structures in Matrigel (Härmä *et al*., 2010). In this matrix VCaP cells remain single and might undergo terminal differentiation or senescence. VCaP growth was not, however, restricted in collagen type I gels (Härmä *et al*., 2010). Thus, it is possible that Matrigel is not a suitable matrix for invasion assays with VCaP spheroids.

The obtained results suggest that MLN4924 does not stimulate the migration of individual cells. However, MLN4924 does stimulate the disassembly and spreading of spheroids on the plane, which is not dependent on the activation of MMP or PLAU. The effect of CRL/NEDD8 pathway inhibition on invasion requires further investigation.

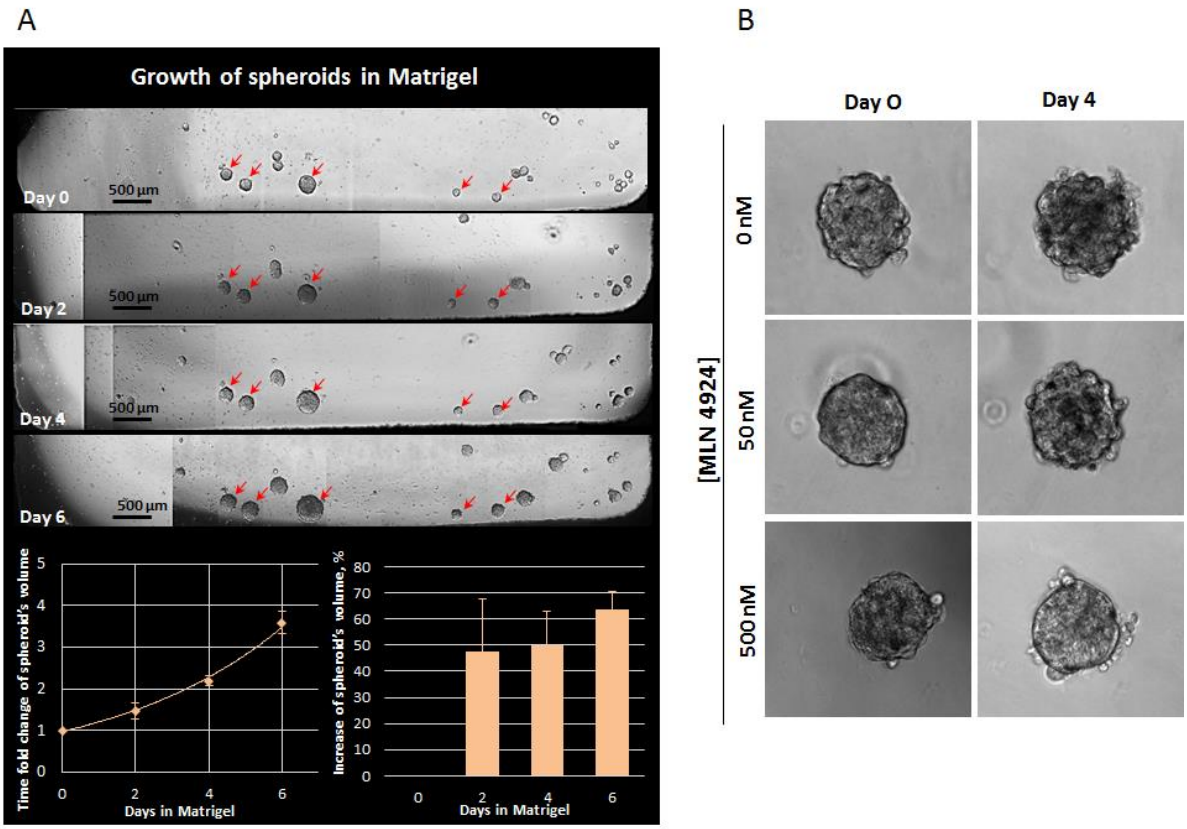

Figure 60. A. Growth of the pre-formed spheroids in Matrigel. Spheroids increase their volume for about 50% every two days. During the time of the observation (6 days) spheroids did not invade into the Matrigel ECM. B. Growth of the pre-formed spheroids in Matrigel in presence of MLN4924. During the time of the observation (4 days) none of the conditions induced invasion into the Matrigel.

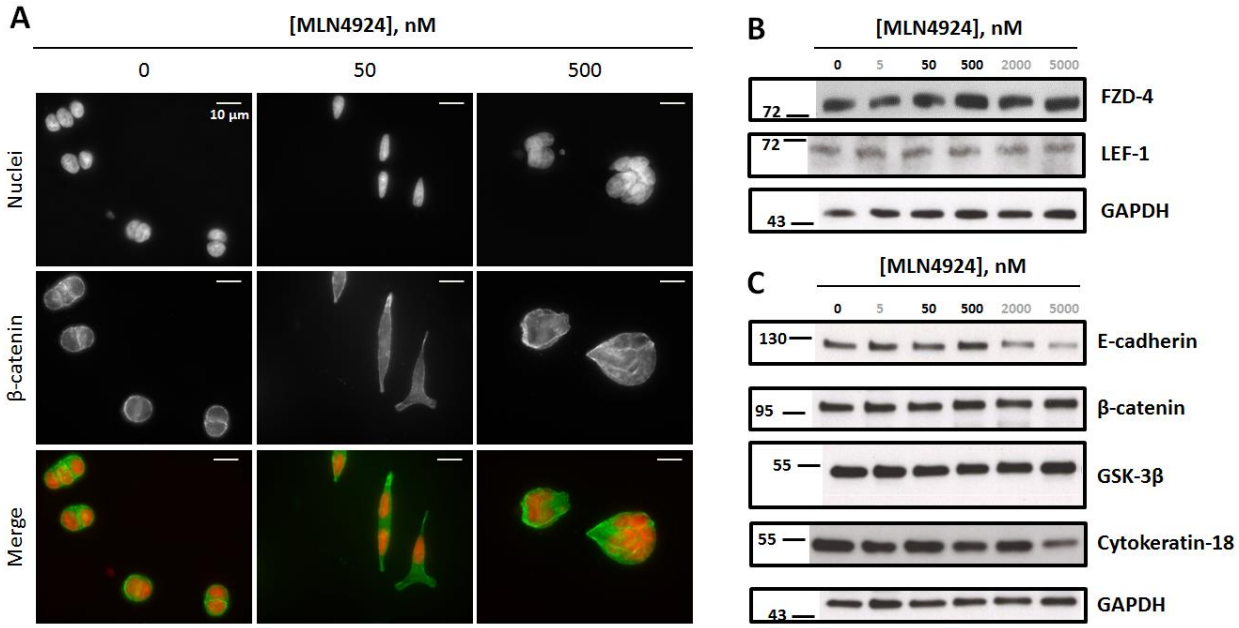

Figure 61. Expression of EMT markers. Localization of total β-catenin remains plasma membrane/cytoplasmic in presence of MLN4924 (A). The amount of LEF-1 and FZD-4 proteins does not change in the presence of MLN4924, suggesting no activation of the Wnt-pathway (B). The level of other principal EMT markers (E-cadherin, β-catenin, GSK-3β and cytokeratin-18) also does not change upon the inhibition of the CRL/NEDD8 pathway by MLN4924 (C).

3.4 MLN4924 DOES NOT INDUCE EMT

Change of cellular phenotype from epithelial to fibroblast-like is widely described for cancer cells by the term of Epithelial-to-Mesenchymal Transition (EMT), which is a hallmark of cancer invasion and metastasis. EMT has some well-established markers, including a loss of E-cadherin and some cytokeratins, a decrease in GSK3β expression, and a translocation of β-catenin into the nucleus upon the activation of Wnt-pathway (Thiery *et al*., 2002). Moreover, ERG was shown to induce EMT (Wang *et al*., 2014; Wu *et al*., 2013; Tian *et al*., 2014; Leshem *et al*., 2011; Tomlins *et al*., 2008) by the activation of FZD4/Lef1/Wnt-signaling (Gupta *et al*., 2010; Wu *et al*., 2013) and the up-regulation of the EMT transcription factors ZEB1 and ZEB2 leading to the suppression of E-cadherin expression (Leshem *et al*., 2011). In order to examine the possible induction of the EMT program on CRL/NEDD8 pathway inhibition we analyzed the expression of major EMT markers. The data presented in Figure 61 show that the expression of these markers is not affected by MLN4924. We showed the accumulation of *phospho*-β-catenin (Figure 48, C). However, using antibodies against total β-catenin, we did not detect its translocation to the nucleus, suggesting an inactive Wnt-pathway. These data suggest that mechanisms other than EMT are responsible for the change of the cellular phenotype induced by MLN4924.

3.5 EFFECT ON CELL JUNCTION PROTEINS

The increased cell adhesion might reflect changes in the composition of membrane proteins. There are five major classes of protein complexes involved in cell adhesion (Figure 62): tight junction, adherens junction, desmosomes, gap junction and focal adhesions (Kawauchi, 2012). We, therefore, analyzed the effect of inhibition of the CRL/NEDD8 pathway on some of these proteins.

Type	Where	What for	Proteins
Tight junction	Epithelium, including prostatic gland	Fuses cells together **to make a barrier,** enables selective transport of substances	Occludin, claudin, ZO-1,2,3
Adherens Junction	Many types, including epithelial and fibroblasts	Formation and maintenance of **physical association of cells** in a calcium-dependent manner	Cadherins, a/b/y-catenin, vinculin
Desmosomes	Tissues subjected to severe mechanical stress (heart, skin, bladder, intestine)	**Keep cells from slipping/sliding** out of the position (relatively to each other and to the basal membrane)	Desmogleins and desmocollins, intermediate filaments
Gap junction	Everywhere	**Communication** between the cells	Connexins
Focal Adhesions	Migrating cells	**Receive signals from ECM**. The dynamic assembly/disassembly of FA plays a central role in cell migration.	FAK, Integrins, vinculin, tallin, paxillin

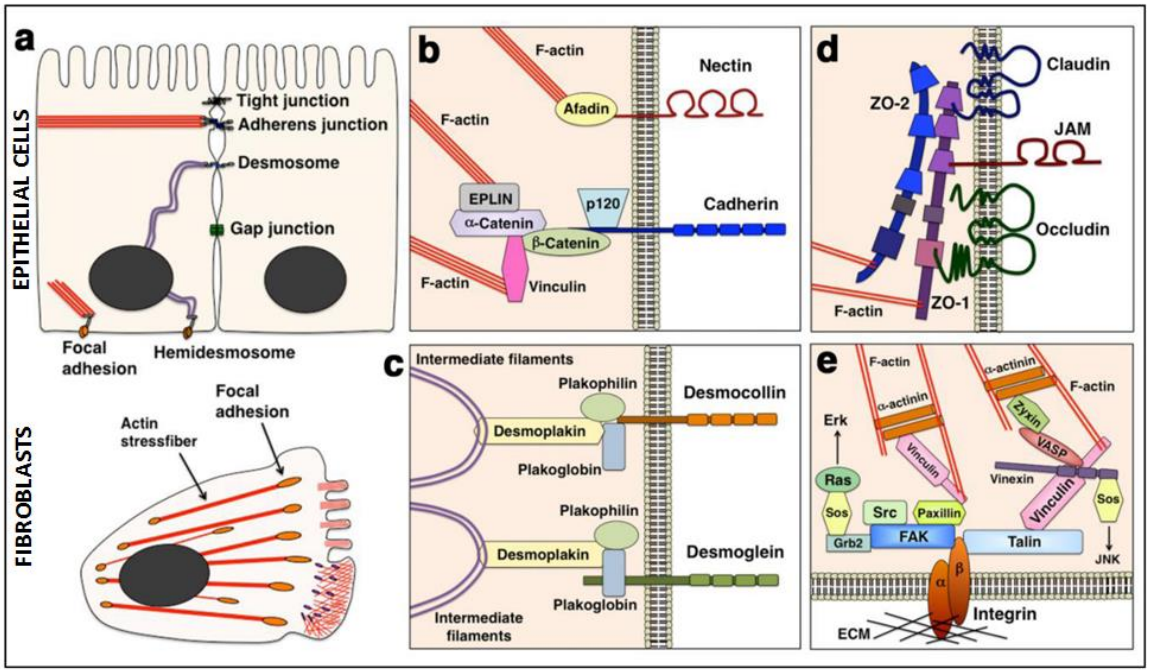

Figure 62. This table summarizes the major types of cellular contacts. The picture demonstrate the molecular structures of cell-cell and cell-ECM junctions. (a) Epithelial cells contain both cell-cell junctions (Tight junctions, Adherens junctions, Desmosomes and Gap junctions) and cell-ECM junctions (Focal adhesions and Hemidesmosomes). While fibroblasts are also able to form cadherin-based cell-cell junctions, the majority of adhesion in fibroblasts is still integrin-based focal adhesions. Red bars: actin filaments, Purple lines: intermediate filaments, Orange dots in the lower panel: focal adhesions, Purple dots in the lower panel: focal complex (immature focal adhesion); (b–e) Molecular components of adherens junctions (b), desmosomes (c), tight junctions (d) and focal adhesions (e). (Kawauchi, 2012)

3.5.1 Tight junction

The tight junction (TJ) is found in the apical region around the cell's circumference. Compared to other adhesion complexes, TJs form the closest contact between the adjacent cells. This brings the cells together to make a barrier with controllable transport of the substances around it. Another important function of TJs is the maintenance of the apical-basolateral polarity of epithelial cells. The transmembrane component of TJs is represented by occludin, claudin and JAM proteins. The intracellular scaffold consist of ZO1/2/3 proteins, coupled to actin filaments.

To estimate the effect of CRL/NEDD8 pathway inhibition on TJs proteins, we analyzed the expression of ZO-1 and occludin. We incubated VCaP cells and spheroids with increasing concentrations of MLN4924 and analyzed them using immunofluorescence microscopy (Figure 63, A-E). We did not observe significant change in the expression of the ZO-1 protein (Figure 63, D-E). However, the protein level of occludin increased dramatically after 5 days of incubation with 500 nM MLN4924 (Figure 63, A-B). In parallel, Western Blot demonstrated a dose dependent accumulation of occludin, starting at 25 nM MLN4924 and reaching a maximum (tenfold compared to the control) at 500 nM (Figure 63, F). According to the current data, the increased level of occludin might explain both the increased cell-to-cell adhesion and spheroid spreading (Du *et al*., 2010; Fletcher *et al*., 2012). Specifically, occludin was shown to participate in collective migration (Safferling *et al*., 2013; Karagiannis *et al*., 2014), modeled by the spheroid spreading assay.

Immunofluorescence microscopy revealed that occludin accumulates not only on the plasma membrane, but also in the granules within the cytoplasm (Figure 63, C). Occludin has been shown to be internalized through endocytosis and degraded in the lysosomes (Fletcher *et al*., 2014) in a ubiquitin-dependent manner (Murakami *et al*., 2009). We suggest that MLN4924 impedes the degradation of occludin in the lysosomes. This would lead to the accumulation of occludin in the late endosomes or lysosomes (seen as granules in cytoplasm) and on the plasma membrane after recycling.

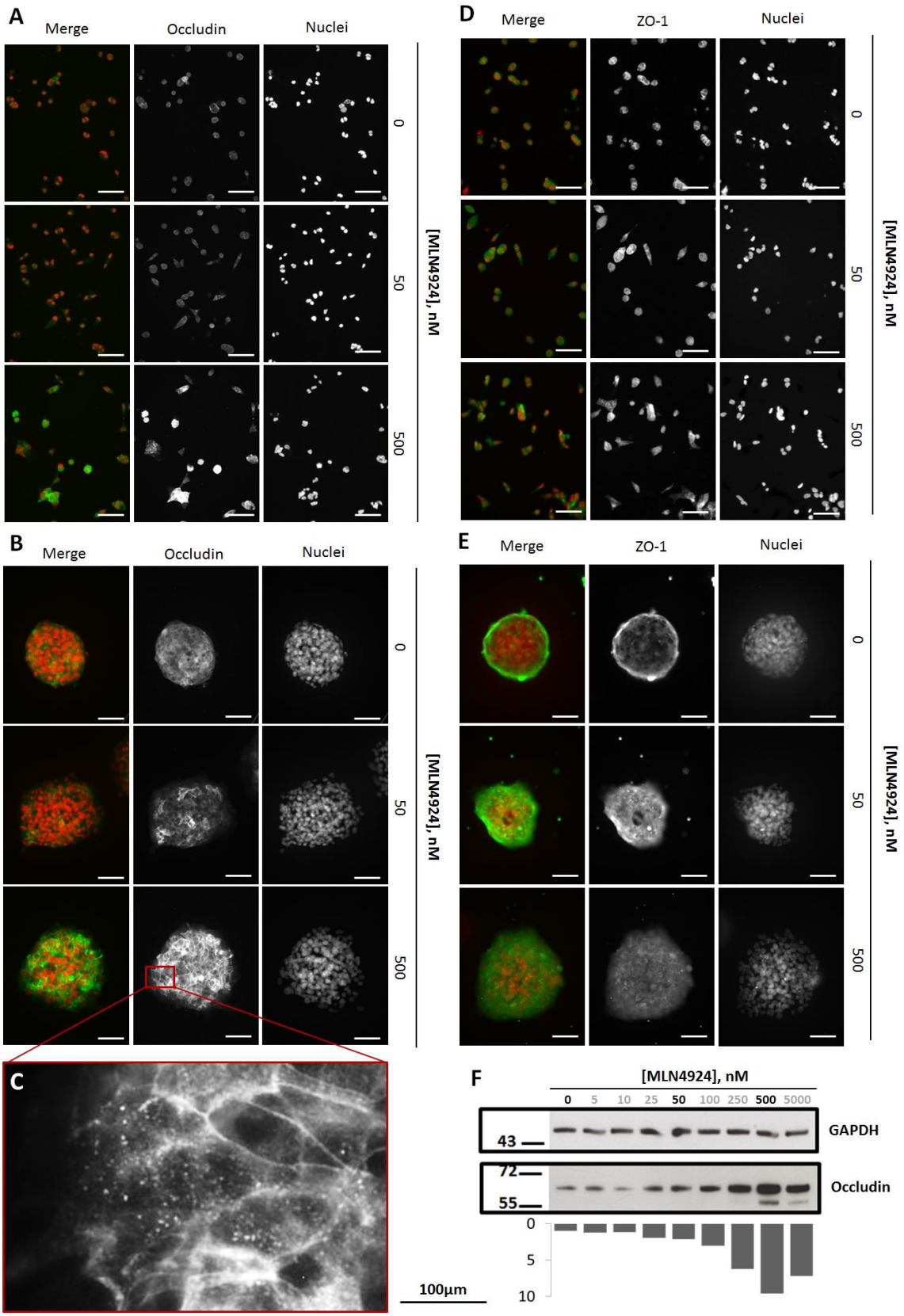

Figure 63. MLN4924-induced changes in tight junction proteins. Immunostaining of cells and spheroids for occludin (A, B, C) and ZO-1 (D, E). Western Blot (F) shows a dose-dependent increase in occludin in presence of MLN4924.

However, the CRL/NEDD8 pathway has not been reported to regulate occludin degradation (Traweger *et al*., 2002; Raikwar *et al*., 2010). Thus, to define the mechanism of the MLN4924-dependent accumulation of occluding, further investigation is needed. This may reveal the cause of this accumulation (due to an increased transcription or an attenuated degradation) and the mechanism (reinforced recycling, inability to degrade, etc.), as well as which role in these is processes played by the NEDD8-pathway.

3.5.2 Adherens junction

Adherens junctions (AJs) maintain the physical association between the cells, regulate cell shape and translate actomyosin-generated forces throughout the tissue. AJs are present in many types of tissue, where they have different localization. In epithelium, adherens junction form a belt in a juxtaluminal zone of the cells below the tight junction, while in fibroblast cells, AJs are spotty and discontinuous (Meng & Takeichi, 2009). Classical cadherins are the major transmembrane proteins of the AJs. Epithelial cells typically express E-cadherin, whereas mesenchymal cells express various cadherins, including N-cadherin, R-cadherin and cadherin-11. The intracellular scaffold consists of the catenin family of proteins and vinculin, attached to the actin filaments (Hartsock & Nelson, 2008).

To analyze the possible influence of the CRL/NEDD8 pathway inhibition on the proteins forming AJs we examined the expression of β-catenin, E-cadherin and N-cadherin using immunofluorescence microscopy and Western Blot. We found that the amount and localization (cytoplasmic) of total β-catenin did not change (Figure 61, C; Figure 64, A). Treatment of VCaP cells with MLN4924 did not affect the total level of cellular E-cadherin (Figure 61, C; Figure 64, B), but it did induce its cleavage (Figure 64, E). Because the antibody we used recognizes the intracellular C-terminal part of E-cadherin, the cleaved 38 kDa-fragment corresponds to the intracellular plus transmembrane domain of E-cadherin (David & Rajasekaran, 2012). This type of E-cadherin cleavage has been shown to be performed by multiple extracellular proteases, including MMPs, A-disintegrin-and-metalloproteinases (ADAMs), plasmin, and kallikrein 7. This cleavage has been shown to weaken cellular contacts and promote cell migration (Solanas *et al*., 2011; David & Rajasekaran, 2012; Grieve & Rabouille, 2014). Nevertheless, the effect of MLN4924 on cell phenotype was not abolished by MMPs or uPA inhibitors (Figure 59, C). This might suggest that either accelerated spheroid

spreading was not dependent on the cleavage of E-cadherin, or that other enzymes are involved in E-cadherin cleavage upon inhibition of the CRL/NEDD8-pathway.

Interestingly, we also observed that MLN4924 treatment causes translocation of N-cadherin from the plasma membrane to the peri-nuclear area (at 50 nM), and then to the nucleus (at 500 nM) (Figure 64, C, D). One major function of N-cadherin is the establishment of the AJ, which is a dynamic structure. N-cadherin is delivered to the plasma membrane, and then either internalized, degraded in the lysosomes, or recycled (Kowalczyk & Nanes, 2012). Thus, the observed effects of N-cadherin re-localization might be explained by impaired trafficking of N-cadherin inside the cell. A similar effect was reported for the insecticide DDT (1,1,1-trichloro-2,2-bis(p-chlorophenyl)ethane), which disrupts cellular contacts by causing re-localization of N-cadherin, ZO-1 and gap junction proteins from the membrane into the vacuoles (Fiorini *et al*., 2008). On the other hand, there are also several reports on the specific role of N-cadherin within the nucleus. N-cadherin was found in the nuclei of honey bee gonads (Florecki & Hartfelder, 2012) as well as the neuronal crest cell, where it serves as a transcription factor and antagonizes the Wnt/β-catenin program (Shoval *et al*., 2007). Moreover, there are some reports showing a correlation between cytoplasmic/nuclear localization of N-cadherin and poor cancer prognosis (Luo *et al*., 2012; Pawar *et al*., 2013). These data might suggest a specific role of the CRL/NEDD8 pathway inhibition in the regulation of N-cadherin localization.

3.5.3 Focal adhesion

Focal adhesions (FAs) are responsible for the establishment of the contact with ECM, mechanosensing and signaling. FAs play a crucial role in migration: new FAs are assembled at the leading edge of migrating cells. In resting cells, FAs serve as fixation points and help maintain cell shape. Extracellular component of FAs consist of α/β integrin heterodimer, which binds to the extracellular matrix. The intracellular element of FAs are comprised of multiple proteins. The core proteins are focal adhesion kinase (FAK), tallin, vinculin and paxillin. The macromolecular complex of FA is anchored on the actin cytoskeleton. To analyze the effect of CRL/NEDD8 pathway inhibition on the proteins forming FAs we examined the expression of paxillin and FAK by WB and immunofluorescence microscopy.

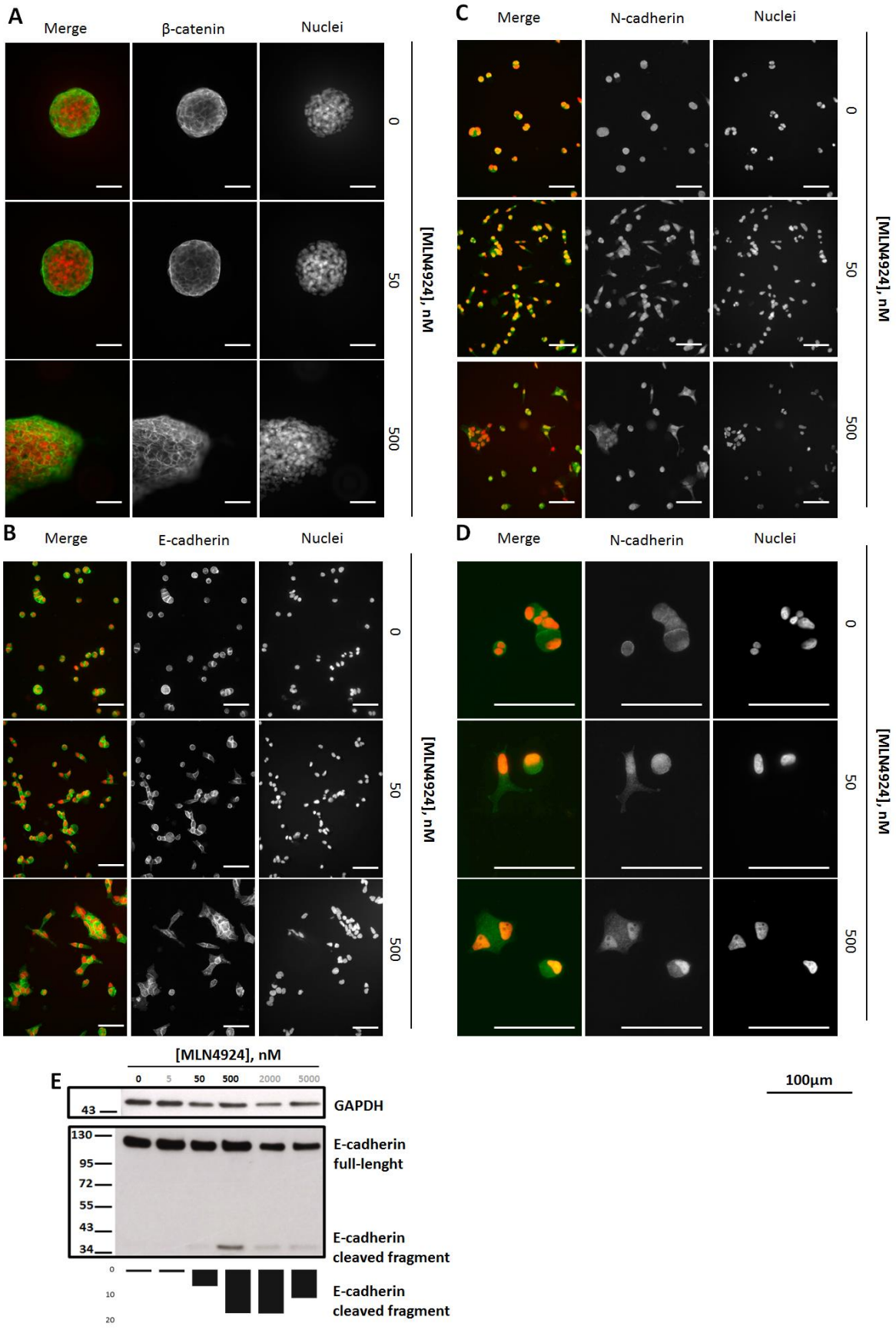

Figure 64. MLN4924-induced changes in adherens junction proteins. Immunostaining of cells and spheroids for β-catenin (A), E-cadherin (B) and N-cadherin (C, D). Western Blot shows cleavage of E-cadherin in the presence of MLN4924 (E).

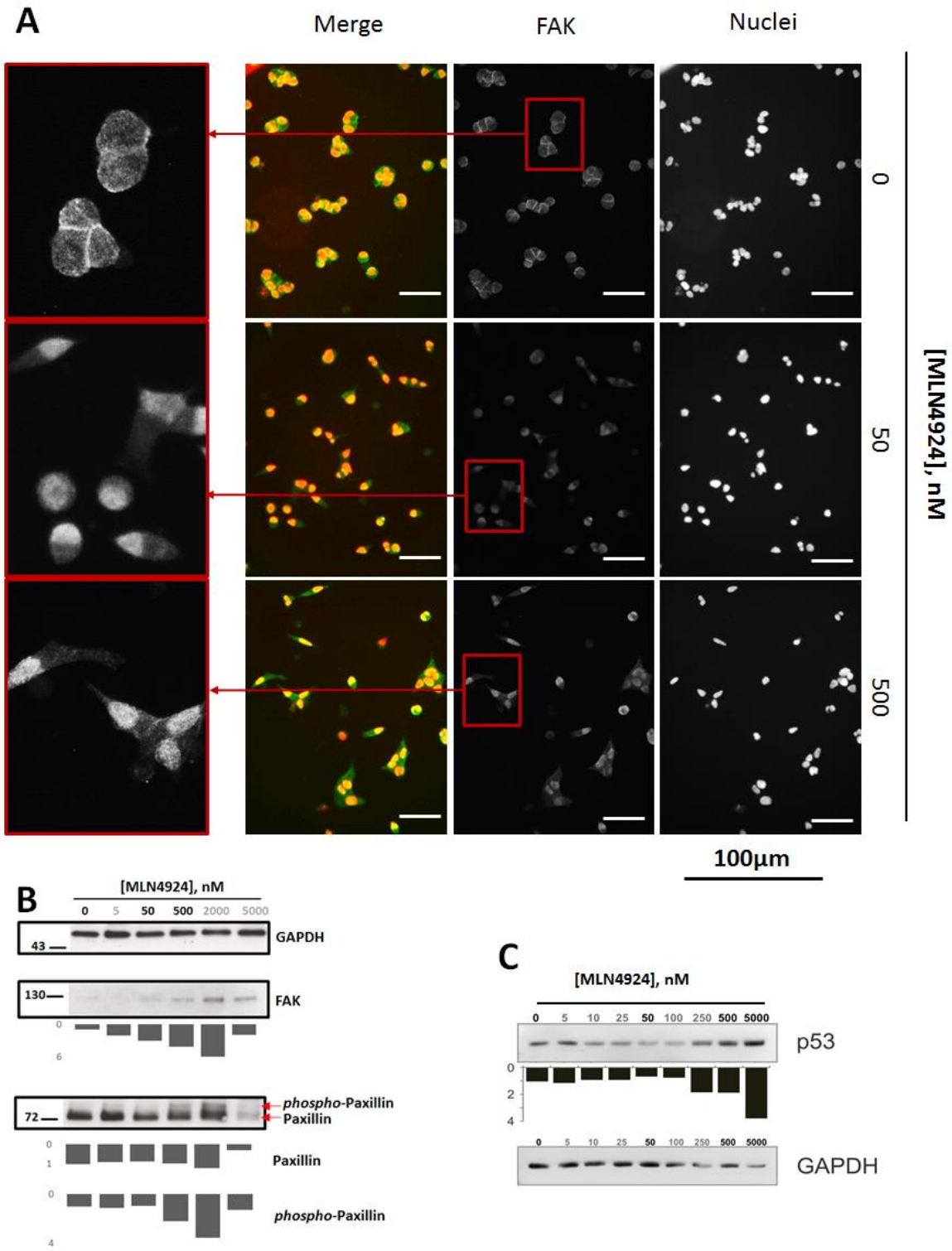

Figure 65. MLN4924-induced changes in focal adhesions proteins. Immunostaining of VCaP cells for FAK (A) shows a delocalization of FAK. Western Blot shows an accumulation of both total FAK and *phospho*-paxillin (B). The translocation of FAK to the nucleus correlates with a decrease of p53 protein level (C).

We found that while the amount of total paxillin did not visibly change, the level of phosphorylated paxillin increased significantly (Figure 65, B). Paxillin has been shown to be degraded by the UPS (Didier *et al*., 2003; Iioka *et al*., 2007), and at least in some cases this degradation is regulated by phosphorylation (Abou Zeid *et al*., 2006). However, the role of CRL/NEDD8 pathway in this process has never been shown.

In parallel we observed that MLN4924 increased the level of FAK in an adose-dependent manner. Moreover, immunofluorescence microscopy showed a translocation of FAK from the membrane to the perinuclear space and to the nuclei (Figure 65). FAK has multiple functions in FAs. It serves as a scaffold protein for the assembly of FA complexes, while, as a kinase, it translates signals from ECM into the cell by the activation of multiple pathways, including MAPK, PI3-K/Akt and Rho GTPases. FAK is often overexpressed in cancer, where it exerts pro-proliferative and anti-apoptotic effects (Kamarajan & Kapila, 2007; Tai *et al*., 2015). Nuclear localization was first shown for SUMOylated FAK (Golubovskaya *et al.*, 2005; Stewart *et al*., 2002), but the biological role of this translocation was not described. Recently, several articles reported novel, kinase- and SUMOylation-independent mechanism for nuclear FAK. Thus, nuclear FAK was shown to exert anti-inflammatory role (Lim *et al*., 2012) and to be a scaffold for MDM2-mediated degradation of p53 (Golubovskaya *et al*., 2008; Lim *et al*., 2008). Indeed, treatment of VCaP cells with 50-100 nM MLN4924 induced weak (2-fold), but a reproducible decrease in the amount of p53 protein in VCaP cells (Figure 65, C). Of note, VCaP cells bear a mutation in p53 R248W that abolishes the tumor-suppression activities of p53 (Sobel & Sadar, 2005; Song *et al*., 2007). Nevertheless, we don't have solid evidence that FAK re-location to the nucleus and decrease in p53 quantity are interdependent events. Moreover, at 500 nM, MLN4924 induced an increase in p53 protein, though the nuclear localization of FAK was even more pronounced.

3.6 DISCUSSION

This part of thesis documents that the inhibition of the CRL/NEDD8 pathway by MLN4924 induced morphological changes in VCaP cells, manifested by an increased cell-substrate and cell-to-cell adhesion and accelerated spreading of VCaP spheroids. Although we did not find induction of EMT markers, we demonstrated multiple dose-dependent changes in the expression and localization of proteins forming cellular contacts. These included: extracellular E-cadherin cleavage; accumulation of occludin on

the plasma membrane and into the intracellular granules; translocation of N-cadherin to the nuclei/perinuclear area; and accumulation of FAK and its translocation to nuclei/perinuclear area. Of course, each of these events may have an independent cause and function as discussed above. However, taken together these effects suggest that the inhibition of the CRL/NEDD8 pathway does result in some general alterations in the trafficking and degradation of membrane proteins. MLN4924 might affect trafficking through inhibition of CRLs or directly through inhibition of the neddylation of membrane receptors.

Ubiquitylation of membrane proteins is a well-acknowledged sorting signal for both lysosomal and proteasome-dependent degradation (Piper & Katzmann, 2007). However, only limited data are available on the participation of CRLs in this type of ubiquitylation; in mammals CRL ligases regulate trafficking of growth hormone receptor (van Kerkhof *et al*., 2011), influenza A virus and epidermal growth factor receptor (Huotari *et al*., 2012).

A growing body of knowledge demonstrates the important role of the CRL/NEDD8 pathway in the regulation of protein sorting. Recently, Cullin 3 has appeared as an important factor in protein trafficking. Cullin 3-based RING-ligases (CRL3) has been shown to control the formation of cytoskeleton tubules, allowing trafficking of vesicles from the Golgi to the plasma membrane (Yuan *et al*., 2014). Moreover, ubiquitylation of SEC31 by CRL3 regulates the size of the vesicles formed in the endoplasmic reticulum, which allows for the sorting of the molecules by size, which, in turn, is important for the transport of macromolecules such as collagen (Jin *et al*., 2012). Thus, the inhibition of CRL3 functions could lead to the incorrect trafficking and attenuated degradation of plasma receptors. Moreover, direct neddylation regulates trafficking and/or degradation of transmembrane proteins TGF-β type II receptor (TβRII) (Zuo *et al*., 2013), chemokine receptor CXCR5 (Renaudin *et al.*, 2014) and EGFR (Oved *et al*., 2006). Together these data suggest a general role of the CRL/NEDD8 pathway in the regulation of sorting and degradation of membrane proteins.

Further investigation is needed to elucidate the role of the NEDD8-pathway in the trafficking of membrane-bound proteins. We are planning to perform a proteomics of the plasma membrane and intracellular proteins in VCaP cells. This would make it possible to establish how general the effects of NEDD8-pathway inhibition on vesicle trafficking are, and which molecular pathways are involved.

IV. CONCLUSIONS

In this work we describe a systematic approach for the screening of the UPS, based on its cascade organization. We evaluated the effect of knockdowns of individual UPS components on the viability of PCa cell lines with a major focus on TMPRSS:ERG-positive cells, as a model for the prevalent phenotype of prostate cancer. Seven genes are identified as being involved in the functioning of tested PCa cell lines (UBE2U, CAND1, UBE2H, UBE2A, CUL4B, CUL2, RBX1), while two of them are putatively TMPRSS2:ERG-dependent (CUL2, RBX1). Importantly, the majority of identified hits belong to the CRL/NEDD8 pathway. The identified UPS components are crucial for PCa cell functioning and their investigation could provide some keys for a better understanding of cancer biology. We selected the most prominent hits, the CRL/NEDD8 pathway and the UBE2U enzyme, for further validation.

UBE2U was the strongest hit identified in siRNA screening. During characterization of the enzyme, we found that, in VCaP cells, UBE2U is present in multiple isoforms. Some of these isoforms are predicted to be enzymatically inactive. Moreover, in contrast to existing data, we demonstrate the presence of an UBE2U isoform of significantly higher molecular weight (95 kDa compared to 38 kDa). Thus, we first provide evidence for UBE2U involvement in prostate carcinogenesis. Although further investigation is required, our study is the first step the characterization of UBE2U as a potential drug-target.

Enrichment of the components of the CRL/NEDD8 pathway (CAND1, CUL4B, CUL2, RBX1) in the hits suggested a general importance of neddylation in PCa biology. Moreover, the potential ERG-dependency of CUL2 and RBX1 hits could indicate a specific role of neddylation in TMPRSS2:ERG-positive cells. Indeed, our investigation using the neddylation-specific inhibitor, MLN4924, has demonstrated that inhibition of the CRL/NEDD8 pathway in prostate cancer cells has a complex outcome that strongly depends on the cellular context. MLN4924 induced apoptosis in all tested cell lines, though TMPRSS2:ERG positive cell lines were significantly more resistant. We demonstrate that the resistance of VCaP cells toward NAE inhibition is the result of cell plasticity ensured by a sophisticated interaction network ERG:NF-κB:c-Myc:Wnt/β-

cat:AR. It has been shown that in TMPRSS2:ERG-positive PCa cells AR is suppressed by ERG (Yu *et al*., 2010). We found that in conditions of incomplete (90-95%) inhibition of neddylation, VCaP cells undergo transcriptional reprogramming leading to cell quiescence and inhibition of proliferation-dependent apoptosis. This was achieved by re-activation of the AR transcriptional program and induction of a differentiation-like state. These results suggest that targeting AR could potentiate the efficacy of MLN4924-based therapy in TMPRSS2:ERG-positive PCa cells. Indeed, knockdown of AR significantly increased apoptotic response to MLN4924. By contrast, knockdown of ERG completely abolished MLN4924-induced cytotoxicity. Higher doses of MLN4924 caused complete inhibition of CRLs and induced an accumulation of replication licensing factor Cdt1, leading to re-replication, DNA-damage and subsequent senescence and/or apoptosis.

Our siRNA screens have shown that the knockdown of different cullins in VCaP cells had opposite effects. We thus hypothesized, that the complex outcome of MLN4924 treatment that we observed in VCaP cells can be explained, at least partially, by the different sensitivity of cullins toward MLN4924. Indeed, using Western Blot we have shown that the accumulation of CRL substrates had two characteristic onsets: 25 nM (b-catenin, IKK and p21, being the substrates of CRL1) and 250 nM (Cdt1, being the substrate of CRL4). We thus conclude that the effect of MLN4924 might depend on the subset of CRLs inhibited at a given dose of the drug.

Our siRNA screening revealed the crucial role of CAND1 in PCa cells. Moreover, we have also shown that when neddylation is compromised, CAND1 exchange factor plays a critical role to ensure CRLs functioning. Indeed, knockdown of CAND1 increased the susceptibility of VCaP cells to MLN4924 treatment. These data suggest that CAND1 is a potential drug target.

Our conclusion is that the CRL/NEDD8 pathway regulates the cancer transcriptional network and determines cancer cells plasticity. This knowledge makes it possible to find better treatments for TMPRSS2:ERG-positive cancers using potential complementary drugs that target AR and CAND1.

Multiple studies of MLN4924 have shown that it efficiently induces senescence and/or apoptosis in many cancer cell lines, including PCa. Furthermore, MLN4924 is currently being evaluated in clinical trials for the treatment of hematological malignancies and solid tumors. Nevertheless, our data suggest that the effect of MLN4924 on prostate

cancer cell lines harbouring TMPRSS2:ERG translocation is mixed. Low-dose treatment with MLN4924 induces protective reversible quiescence in cancer cells. Taking into account a frequent problem of drug bioavailability, it raises concern about possible undertreatment in MLN4924 therapy. Of note, higher doses of MLN4924 were reported to produce side-effects and are generally toxic. In conclusion, our data question the suitability of MLN4924 for treatment of TMPRSS2:ERG-positive prostate cancers.

Apart from the above described effects on the viability, we have observed that MLN4924 changed membrane properties of VCaP cells and rendered them more adherent in cell-substrate and cell-to-cell interactions. While we did not find changes in the expression of several EMT markers, we demonstrated dose-dependent changes in the expression and re-localization of several membrane-associated proteins, including occludin, N-cadherin and FAK. We thus conclude that the CRL/NEDD8 pathway might be involved in the sorting/trafficking of membrane proteins. This part of the work requires further investigation, as understanding of the underlying mechanisms might uncover new a role of the CRL/NEDD8 pathway having general importance for cell biology. Our data reveal a potentially globally new role of the CRL/NEDD8 pathway in the regulation of intracellular trafficking, composition of plasma membrane and cell adhesion.

Final conclusions:

1) We have performed a comprehensive screening of the E1-E2 UPS components to identify the genes essential for PCa viability.
2) Our work has revealed new potential drug targets for PCa treatment (UBE2U, CAND1)
3) We have demonstrated the role of the CRL/NEDD8 pathway in the regulation of cancer cell plasticity and morphology.

V. SUPPLEMENTARY DATA

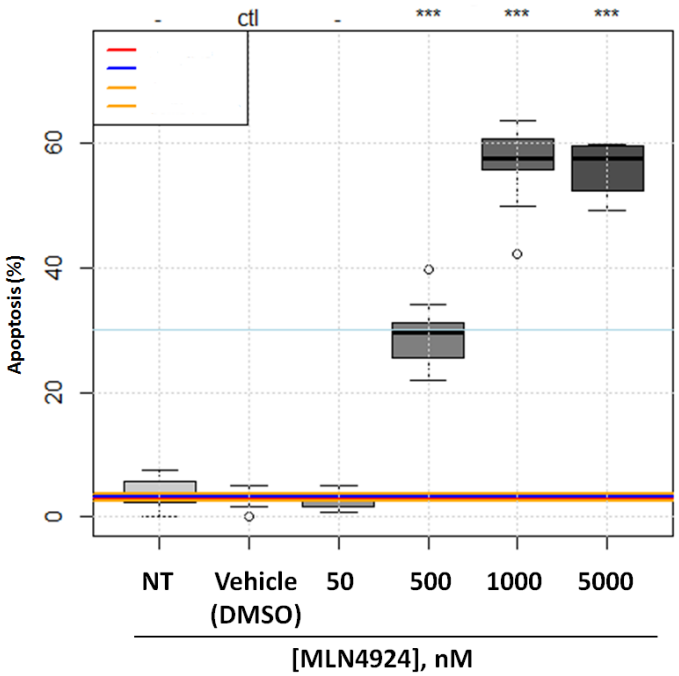

Supplementary Figure 1. The effect of MLN4924 treatment on apoptosis in VCaP cells grown in ChSM (5 days of treatment).

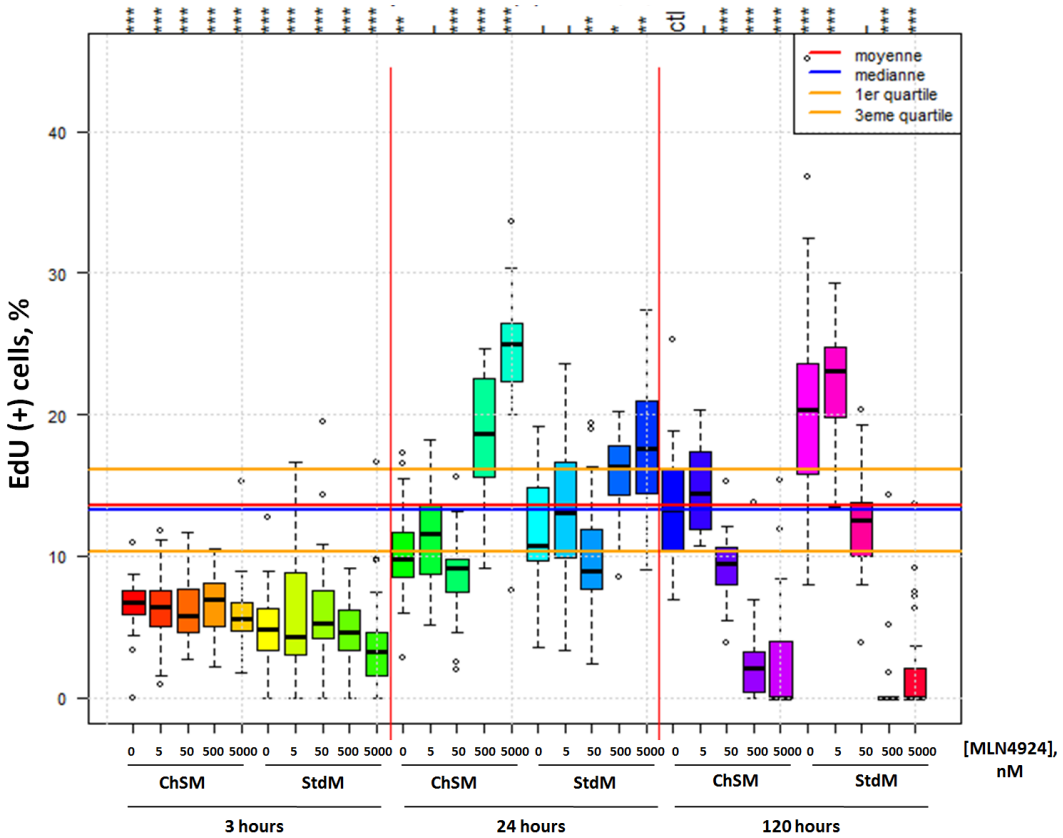

Supplementary Figure 2. Effect on DNA synthesis 3, 24 or 120 hours after treatment with MLN4924 in Standard (StdM) and Charcoal Stripped Medium (ChSM).

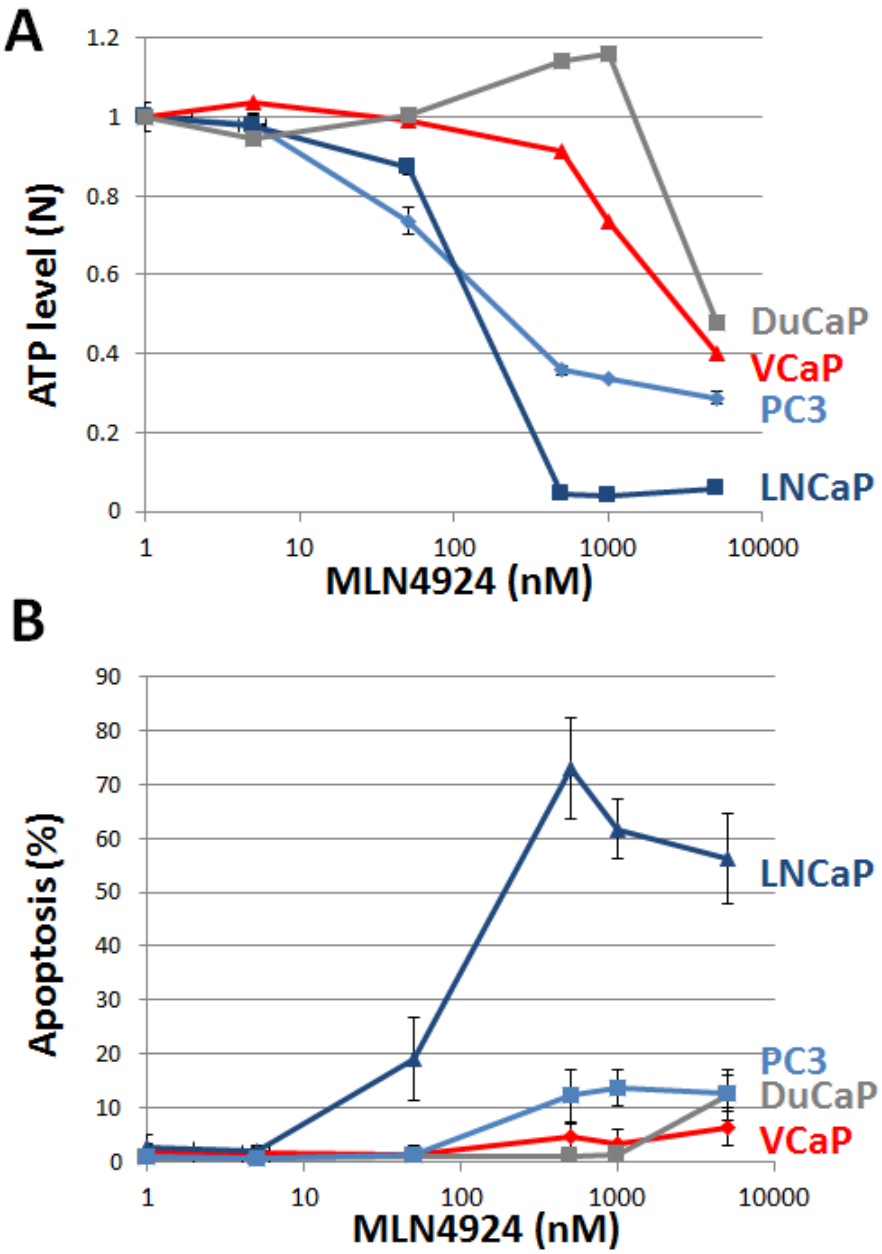

Supplementary Figure 3. The effect of MLN4924 treatment on proliferation (A) and apoptosis (B) of PCa cell lines grown in StdM (3 days of treatment).

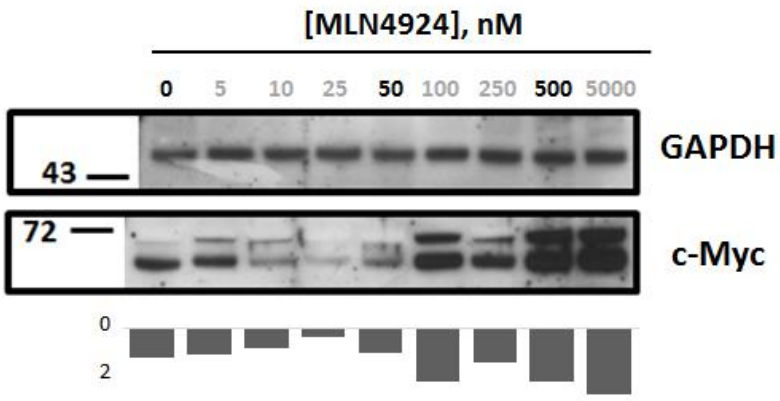

Supplementary Figure 4. Effect of MLN4924 on the expression of c-Myc proto-oncogene.

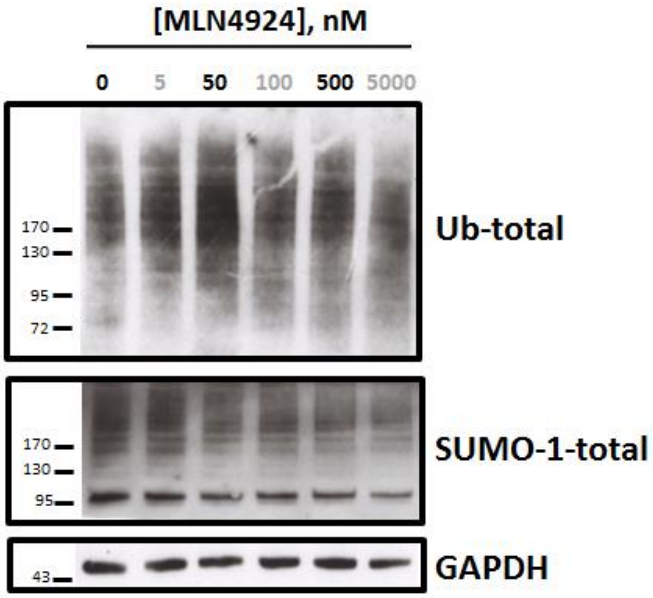

Supplementary Figure 5. Effect of MLN4924 on ubiquitylation and SUMOylation. Cells were treated with increased concentrations of MLN4924, lysed and immunoblotted with antibodies against total ubiquitin or SUMO-1.

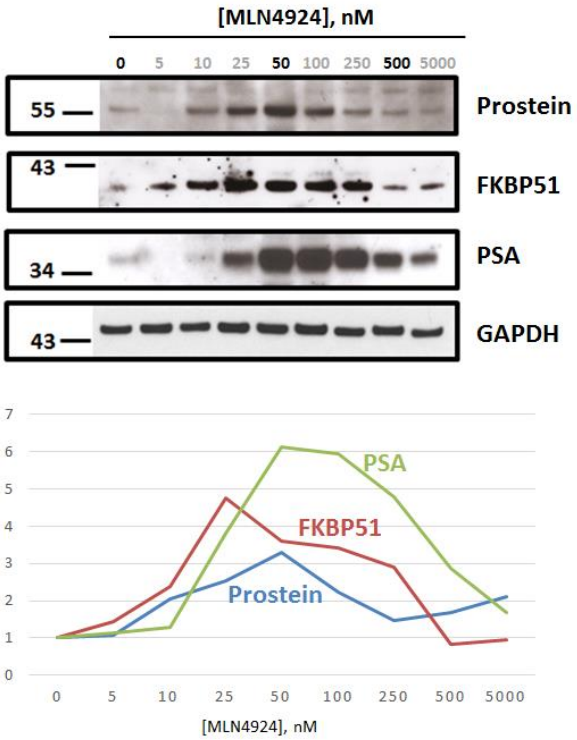

Supplementary Figure 6. Western Blot, demonstrating expression of AR-responsive genes prostein, FKBP51 and PSA at different concentrations of MLN4924. All the tested genes show biphasic behavior: protein level increases at low concentrations of MLN4924 (25-250 nM) and decreases at higher doses (> 500 nM).

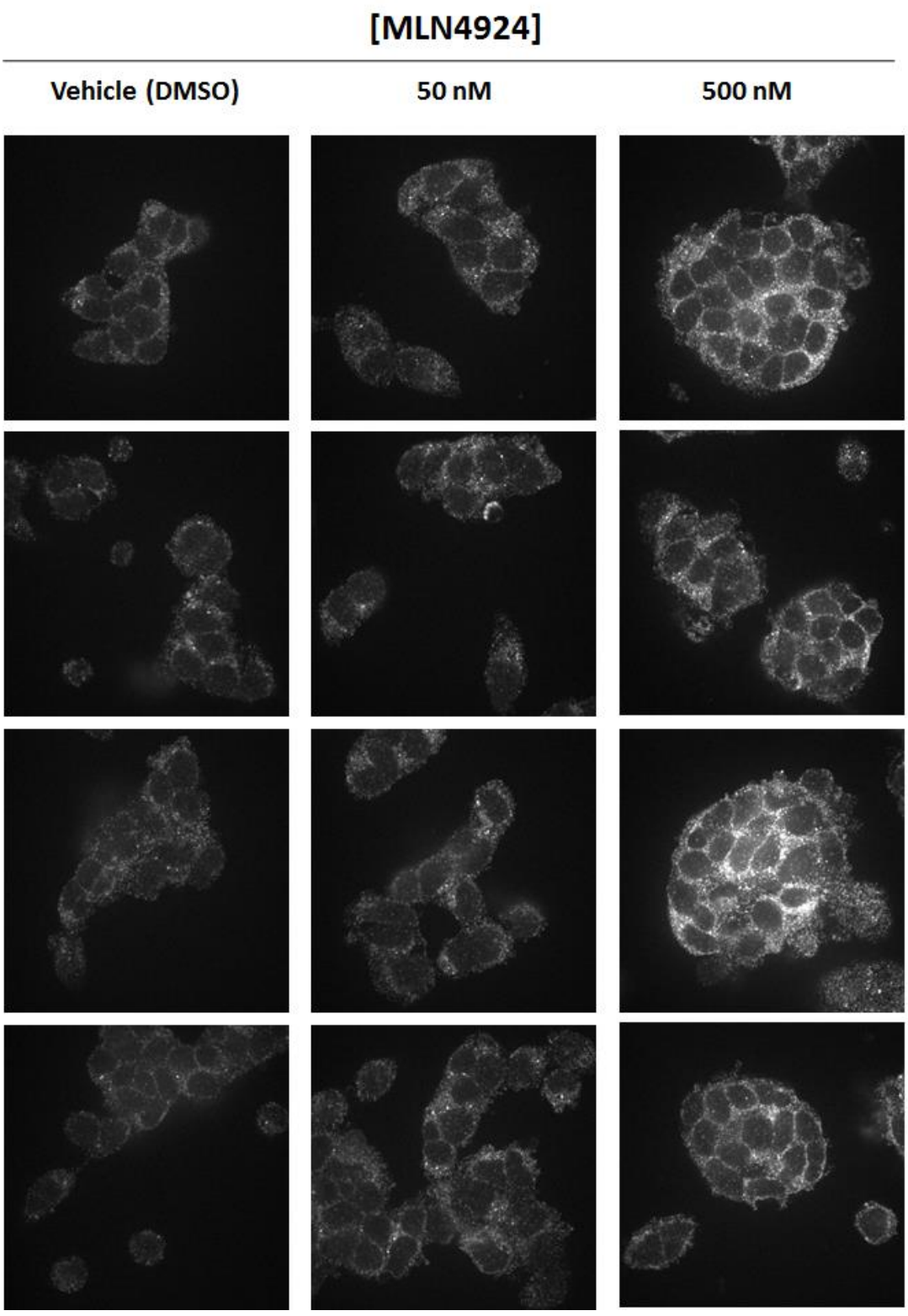

Supplementary Figure 7. Immunofluorescence microscopy for *phospho*-p65 component of NF-κB. Images demonstrate accumulation of *phospho*-p65. However, it remains cytoplasmic and does not enter the nuclei.

Supplementary Table 1. Dharmacon ON-TARGETplus® SMART pool® siRNA Library-Human Ubiquitin Conjugation Subset 1

Gene Symbol	Pool Catalog Number	Duplex Catalog Number	GENEID	Gene Accession	GINumber	Sequence
UBE2C	L-004693-00	J-004693-06	11065	NM_181803	32967290	GAACCCAACAUUGAUAGUC
UBE2C	L-004693-00	J-004693-07	11065	NM_181803	32967290	UAAAUUAAGCCUCGGUUGA
UBE2C	L-004693-00	J-004693-08	11065	NM_181803	32967290	GUAUAGGACUCUUUAUCUU
UBE2C	L-004693-00	J-004693-09	11065	NM_181803	32967290	GCAAGAAACCUACUCAAAG
SMURF1	L-007191-00	J-007191-09	57154	NM_181349	31317289	GCACUAUGAUCUAUAUGUU
SMURF1	L-007191-00	J-007191-10	57154	NM_181349	31317289	GGAGGAGACCUGCGGGUUU
SMURF1	L-007191-00	J-007191-11	57154	NM_181349	31317289	GAUCGACAUUCCACCAUAU
SMURF1	L-007191-00	J-007191-12	57154	NM_181349	31317289	AAGAAUACGUCCGGUUGUA
UBR5	L-007189-00	J-007189-06	51366	NM_015902	41352716	GCACUUAUAUACUGGAUUA
UBR5	L-007189-00	J-007189-07	51366	NM_015902	41352716	GAUUGUAGGUUACUUAGAA
UBR5	L-007189-00	J-007189-08	51366	NM_015902	41352716	GAUCAAUCCUAACUGAAUU
UBR5	L-007189-00	J-007189-09	51366	NM_015902	41352716	GGUCGAAGAUGUGCUACUA
UBE2K	L-009431-00	J-009431-05	3093	NM_005339	21536483	GAAUCAAGCGGGAGUUCAA
UBE2K	L-009431-00	J-009431-06	3093	NM_005339	21536483	CCUAAGGUCCGGUUUAUCA
UBE2K	L-009431-00	J-009431-07	3093	NM_005339	21536483	CCAGAAACAUACCCAUUUA
UBE2K	L-009431-00	J-009431-08	3093	NM_005339	21536483	GCAAAUCAGUACAAACAAA
HECTD1	L-007188-00	J-007188-06	25831	NM_015382	32698701	GUUAAUAGCUGUACUAGAA
HECTD1	L-007188-00	J-007188-07	25831	NM_015382	32698701	GCUCAUAGCUGCAUAUAAG
HECTD1	L-007188-00	J-007188-08	25831	NM_015382	32698701	CAUAGAGGAUUUAGGUUUA
HECTD1	L-007188-00	J-007188-09	25831	NM_015382	32698701	GAAAGGGACAUGCAACUAA
UBE2T	L-004898-00	J-004898-05	29089	NM_014176	7661807	CCUGCGAGCUCAAAUAUUA
UBE2T	L-004898-00	J-004898-06	29089	NM_014176	7661807	GAAGGCCAGUCAGCUAGUA
UBE2T	L-004898-00	J-004898-07	29089	NM_014176	7661807	GGAAGGAUUUGUCUGGAUG
UBE2T	L-004898-00	J-004898-08	29089	NM_014176	7661807	GUACACAACUCAACACAGA
CDC34	L-003230-00	J-003230-13	997	NM_004359	16357476	GCUCAGACCUCUUCUACGA
CDC34	L-003230-00	J-003230-14	997	NM_004359	16357476	GGACCAUUCUCCUGAGUGU
CDC34	L-003230-00	J-003230-15	997	NM_004359	16357476	CCUGACACCACCAGAAUAA
CDC34	L-003230-00	J-003230-16	997	NM_004359	16357476	GAUCGGGAGUACACAGACA
HECTD4	L-018270-01	J-018270-09	283450	NM_173813	31341139	GCAGAUGCUCUUCGCAAUA
HECTD4	L-018270-01	J-018270-10	283450	NM_173813	31341139	UGAAGAUUGUUGUACGAGA
HECTD4	L-018270-01	J-018270-11	283450	NM_173813	31341139	ACUGAAAGGAAUCGAGACA
HECTD4	L-018270-01	J-018270-12	283450	NM_173813	31341139	AAUGAGAAGUGGCCGUGAA
DCUN1D1	L-019139-00	J-019139-05	54165	NM_020640	36030882	GGAUAAAGUUCGUCAGUUU
DCUN1D1	L-019139-00	J-019139-06	54165	NM_020640	36030882	GCAUUAGUGUGUUGAUUAU

DCUN1D1	L-019139-00	J-019139-07	54165	NM_020640	36030882	CCAGGACGAUUUAAGGAUU
DCUN1D1	L-019139-00	J-019139-08	54165	NM_020640	36030882	GAACUUAGUGCUUAAUGGA
CUL2	L-007277-00	J-007277-05	8453	NM_003591	19482173	GGAAGUGCAUGGUAAAUUU
CUL2	L-007277-00	J-007277-06	8453	NM_003591	19482173	CAUCCAAGUUCAUAUACUA
CUL2	L-007277-00	J-007277-07	8453	NM_003591	19482173	GCAGAAAGACACACCACAA
CUL2	L-007277-00	J-007277-08	8453	NM_003591	19482173	UGGUUUACCUCAUAUGAUU
HERC3	L-007179-00	J-007179-06	8916	NM_014606	7657151	GAACUCAACUAGGGUGUUA
HERC3	L-007179-00	J-007179-07	8916	NM_014606	7657151	GCUGAUGGGUAGUGAAGUA
HERC3	L-007179-00	J-007179-08	8916	NM_014606	7657151	GCAAAGUACUAGAUAACUG
HERC3	L-007179-00	J-007179-09	8916	NM_014606	7657151	GGUGUGUGGUGGCAAAGUA
UBE2W	L-009643-00	J-009643-07	55284	NM_001001482	47933382	GGAAAUGAGUAGUGAUAUG
UBE2W	L-009643-00	J-009643-08	55284	NM_001001482	47933382	ACAUAGGCCUACAGAAUUA
UBE2W	L-009643-00	J-009643-09	55284	NM_001001482	47933382	GUAAUGCAUUGUUGAAAGA
UBE2W	L-009643-00	J-009643-10	55284	NM_001001482	47933382	GAGGAGGUACUGUGUGUUA
UBE2V2	L-008823-00	J-008823-05	7336	NM_003350	12025664	GUUAAAGUUCCUCGUAAUU
UBE2V2	L-008823-00	J-008823-06	7336	NM_003350	12025664	CAAGAGCUAAGACGUCUAA
UBE2V2	L-008823-00	J-008823-07	7336	NM_003350	12025664	CACCAAGGACAAAUUAUGA
UBE2V2	L-008823-00	J-008823-08	7336	NM_003350	12025664	GAGCAUACCAGUGUUAGCA
DCUN1D5	L-014842-01	J-014842-09	84259	NM_032299	34147410	CAAUCAAAGUAUCGUGUUA
DCUN1D5	L-014842-01	J-014842-10	84259	NM_032299	34147410	GUUGAAUGAUAUUUCGUCA
DCUN1D5	L-014842-01	J-014842-11	84259	NM_032299	34147410	CCGUCAGACAUCAUAGCAA
DCUN1D5	L-014842-01	J-014842-12	84259	NM_032299	34147410	UGAUGGGCAUUGAGCCACA
HERC2	L-007180-00	J-007180-09	8924	NM_004667	67190865	GCACAGAGUAUCACAGGUA
HERC2	L-007180-00	J-007180-10	8924	NM_004667	67190865	CGAUGAAGGUUUGGUAUUU
HERC2	L-007180-00	J-007180-11	8924	NM_004667	67190865	GAUAAUACGACACAGCUAA
HERC2	L-007180-00	J-007180-12	8924	NM_004667	67190865	GCAGAUGUGUGCUAAGAUG
UBE2N	L-003920-00	J-003920-06	7334	NM_003348	37577134	AACCAGGUCUUUAGAAUAU
UBE2N	L-003920-00	J-003920-07	7334	NM_003348	37577134	UGACUGACAUGUAGGACUU
UBE2N	L-003920-00	J-003920-08	7334	NM_003348	37577134	AGUAUCAAGUCCUCAGUUA
UBE2N	L-003920-00	J-003920-09	7334	NM_003348	37577134	GAUGAUCAUUGGUGUCUUG
UBE2Z	L-008596-00	J-008596-05	65264	NM_023079	20149671	GGGAAAGUCUGCUUGAGUA
UBE2Z	L-008596-00	J-008596-06	65264	NM_023079	20149671	CCUCAGUGCUCAUCUCUAU
UBE2Z	L-008596-00	J-008596-07	65264	NM_023079	20149671	GCACGAGACCAUCAGAGUU
UBE2Z	L-008596-00	J-008596-08	65264	NM_023079	20149671	UAAGAUUCAUGCAUUGAUC
UBE2L3	L-010384-00	J-010384-06	7332	NM_003347	38157977	GGGCUGACCUAGCUGAAGA
UBE2L3	L-010384-00	J-010384-07	7332	NM_003347	38157977	GUAAGAAUGCUGAAGAGUU
UBE2L3	L-010384-	J-010384-	7332	NM_003347	38157977	ACAAAGAUCUAUCACCCAA

	00	08				
UBE2L3	L-010384-00	J-010384-09	7332	NM_003347	38157977	CCACCGAAGAUCACAUUUA
HERC5	L-005174-00	J-005174-06	51191	NM_016323	7705930	GGAAGUAGCAUAACUGUCA
HERC5	L-005174-00	J-005174-07	51191	NM_016323	7705930	GAACCAGGAUAUAACAGUU
HERC5	L-005174-00	J-005174-08	51191	NM_016323	7705930	UAAGAGCACUGACAUGUUU
HERC5	L-005174-00	J-005174-09	51191	NM_016323	7705930	GACUUUCCCUGUUCAAUUG
UBE2NL	L-031625-00	J-031625-05	389898	NM_001012989	61175264	GGUCAUUGCUGGGGAAUCA
UBE2NL	L-031625-00	J-031625-06	389898	NM_001012989	61175264	AAACGUGAACUAUUACUUG
UBE2NL	L-031625-00	J-031625-07	389898	NM_001012989	61175264	GAUCCAAUCAUUAAGUGUG
UBE2NL	L-031625-00	J-031625-08	389898	NM_001012989	61175264	AAUAUGCUCUCUAUCCAAG
DCUN1D3	L-018390-00	J-018390-05	123879	NM_173475	27735046	AAGGAUCUCUACCGGUUUA
DCUN1D3	L-018390-00	J-018390-06	123879	NM_173475	27735046	ACGGUUCCCUAGCCUCUUA
DCUN1D3	L-018390-00	J-018390-07	123879	NM_173475	27735046	CCAGAACAAUCCUCCGGUA
DCUN1D3	L-018390-00	J-018390-08	123879	NM_173475	27735046	GUAAGAAUCCCUCAUCGAC
BIRC6	L-013857-00	J-013857-05	57448	NM_016252	61744455	ACAAGCACCUCUCGCAUUA
BIRC6	L-013857-00	J-013857-06	57448	NM_016252	61744455	GGUCAAAGAUCACUUAGUA
BIRC6	L-013857-00	J-013857-07	57448	NM_016252	61744455	GCAACGAUGUGCCAUGUUA
BIRC6	L-013857-00	J-013857-08	57448	NM_016252	61744455	CAAUAGAUCUGACUGUUAA
UBE2J2	L-008614-00	J-008614-05	118424	NM_194457	37577129	GUAUAGAGACGUCGGACUU
UBE2J2	L-008614-00	J-008614-06	118424	NM_194457	37577129	GUGCAGAGUUUAGCAUUUA
UBE2J2	L-008614-00	J-008614-07	118424	NM_194457	37577129	GCACAAGACGAACUCAGUA
UBE2J2	L-008614-00	J-008614-08	118424	NM_194457	37577129	CCCAGUAUCUAUAUGAUCA
HECW1	L-007186-00	J-007186-05	23072	NM_015052	51702517	CUAAAUGACUGGCGGAAUA
HECW1	L-007186-00	J-007186-06	23072	NM_015052	51702517	GAUGAGGUCUUGUCCGAAA
HECW1	L-007186-00	J-007186-07	23072	NM_015052	51702517	GAUGCCAGCUCGUACUUUG
HECW1	L-007186-00	J-007186-08	23072	NM_015052	51702517	CAGCUGCAAUUCCGAUUUG
UBA7	L-019759-00	J-019759-05	7318	NM_003335	38045947	CAUCUUUGCUAGUAAUCUA
UBA7	L-019759-00	J-019759-06	7318	NM_003335	38045947	CGAAUUGUGGGCCAGAUUA
UBA7	L-019759-00	J-019759-07	7318	NM_003335	38045947	AUAGAGCGCUCCAAUCUCA
UBA7	L-019759-00	J-019759-08	7318	NM_003335	38045947	GCAUGGAGUUUGCUUUCUG
UBA1	L-004509-00	J-004509-05	7317	NM_153280	23510339	GCGUGGAGAUCGCUAAGAA
UBA1	L-004509-00	J-004509-06	7317	NM_153280	23510339	CCUUAUACCUUUAGCAUCU
UBA1	L-004509-00	J-004509-07	7317	NM_153280	23510339	CCACAUAUCCGGGUGACAA
UBA1	L-004509-00	J-004509-08	7317	NM_153280	23510339	GAAGUCAAAUCUGAAUCGA
HERC1	L-007181-00	J-007181-06	8925	NM_003922	62422572	GCACCGACCUUAUUGUGUA
HERC1	L-007181-00	J-007181-07	8925	NM_003922	62422572	UAGAUUAGCUUCUGAGUUG
HERC1	L-007181-00	J-007181-08	8925	NM_003922	62422572	CCACAGGUCCUAUUACUAA

HERC1	L-007181-00	J-007181-09	8925	NM_003922	62422572	GAACAAAGGAACCACUUGA
HACE1	L-007193-00	J-007193-05	57531	NM_020771	34222116	GAACAACUUUUCAGCCUAA
HACE1	L-007193-00	J-007193-06	57531	NM_020771	34222116	GAAUGAAGACCUCCGAGAA
HACE1	L-007193-00	J-007193-07	57531	NM_020771	34222116	GCACAGAUCCUACUAUUAC
HACE1	L-007193-00	J-007193-08	57531	NM_020771	34222116	GAAUUGAUAUGGGCUACAA
CUL7	L-017673-00	J-017673-05	9820	NM_014780	41872645	GAUCUUGGGCUUUGAGGAA
CUL7	L-017673-00	J-017673-06	9820	NM_014780	41872645	CUAGUGAGGACUCGAGUUA
CUL7	L-017673-00	J-017673-07	9820	NM_014780	41872645	GAACCUAGAUGGGGAGAUU
CUL7	L-017673-00	J-017673-08	9820	NM_014780	41872645	GACGUGAAGUCCCUCAUUC
UBE2S	L-009707-00	J-009707-05	27338	NM_014501	7657045	ACAAGGAGGUGACGACACU
UBE2S	L-009707-00	J-009707-06	27338	NM_014501	7657045	GGAGGUCUGUUCCGCAUGA
UBE2S	L-009707-00	J-009707-07	27338	NM_014501	7657045	GCAUCAAGGUCUUUCCCAA
UBE2S	L-009707-00	J-009707-08	27338	NM_014501	7657045	CCAAGAAGCAUGCUGGCGA
CUL3	L-010224-00	J-010224-06	8452	NM_003590	45827792	GAAGGAAUGUUUAGGGAUA
CUL3	L-010224-00	J-010224-07	8452	NM_003590	45827792	GAGAUCAAGUUGUACGUUA
CUL3	L-010224-00	J-010224-08	8452	NM_003590	45827792	GAAAGUAGACGACGACAGA
CUL3	L-010224-00	J-010224-09	8452	NM_003590	45827792	GCACAUGAAGACUAUAGUA
ITCH	L-007196-00	J-007196-07	83737	NM_031483	27477108	GUUGGGAACUGCUGCAUUA
ITCH	L-007196-00	J-007196-08	83737	NM_031483	27477108	CAACAUGGGACGUAUUUAU
ITCH	L-007196-00	J-007196-09	83737	NM_031483	27477108	GAAAUUAAGAGUCAUGAUC
ITCH	L-007196-00	J-007196-10	83737	NM_031483	27477108	CGAAGACGUUUGUGGGUGA
HUWE1	L-007185-00	J-007185-07	10075	NM_031407	61676187	GCUUUGGGCUGGCCUAAUA
HUWE1	L-007185-00	J-007185-08	10075	NM_031407	61676187	GCAGUUGGCGGCUUUCUUA
HUWE1	L-007185-00	J-007185-09	10075	NM_031407	61676187	GAGCCCAGAUGACUAAGUA
HUWE1	L-007185-00	J-007185-10	10075	NM_031407	61676187	UAACAUCAAUUGUCCACUU
CAND2	L-023448-01	J-023448-09	23066	XM_944849	88968671	ACGAGGACAGCGAGCGCAA
CAND2	L-023448-01	J-023448-10	23066	XM_944849	88968671	GCACCCUGAUCCAAUGUUU
CAND2	L-023448-01	J-023448-11	23066	XM_944849	88968671	AGAACGGUGAGGUGCAGAA
CAND2	L-023448-01	J-023448-12	23066	XM_944849	88968671	UGUCGGAGUUGCAGAAGGA
UBE2D3	L-008478-00	J-008478-09	7323	NM_181893	33149323	CCACAAUUAUGGGACCUAA
UBE2D3	L-008478-00	J-008478-10	7323	NM_181893	33149323	GCCAUGUGAUGCUACCUUA
UBE2D3	L-008478-00	J-008478-11	7323	NM_181893	33149323	UCACAGUGGUCGCCUGCUU
UBE2D3	L-008478-00	J-008478-12	7323	NM_181893	33149323	GAUGAGUGAUCAACUAAUA
NEDD4	L-007178-00	J-007178-06	4734	NM_006154	38257154	GGAGGGAACAUACAAAGUA
NEDD4	L-007178-00	J-007178-07	4734	NM_006154	38257154	GAUCACAAUUCCAGAACGA
NEDD4	L-007178-00	J-007178-08	4734	NM_006154	38257154	GAACUAGAGCUUCUUAUGU
NEDD4	L-007178-	J-007178-	4734	NM_006154	38257154	CCAAUGAUCUAGGGCCUUU

	00	09				
UBA5	L-006405-00	J-006405-05	79876	NM_024818	163659923	GUAUUGAGCUGGUAUCUGA
UBA5	L-006405-00	J-006405-06	79876	NM_024818	163659923	GAAGCUCGAAUGACAAUAA
UBA5	L-006405-00	J-006405-07	79876	NM_024818	163659923	CAAGAUGUGGCAUUGGUAA
UBA5	L-006405-00	J-006405-08	79876	NM_024818	163659923	CGUGUUAAAGUUUCUGUUA
UBE2M	L-004348-00	J-004348-05	9040	NM_003969	37577133	GAAAUAGGGUUGGCGCAUA
UBE2M	L-004348-00	J-004348-06	9040	NM_003969	37577133	AAGCCAGUCCUUACGAUAA
UBE2M	L-004348-00	J-004348-07	9040	NM_003969	37577133	UUAAGGUGGGCCAGGGUUA
UBE2M	L-004348-00	J-004348-08	9040	NM_003969	37577133	GAUGAGGGCUUCUACAAGA
UEVLD	L-008494-02	J-008494-09	55293	NM_018314	23943813	GCAAAUCGAGUGAUCGGAA
UEVLD	L-008494-02	J-008494-10	55293	NM_018314	23943813	AUGGGUUAUUGGCGAGCAA
UEVLD	L-008494-02	J-008494-11	55293	NM_018314	23943813	AGGUGGAGAACUCGGUAUU
UEVLD	L-008494-02	J-008494-12	55293	NM_018314	23943813	GUACAAGUUCAGGGACCUA
UBE2F	L-009081-01	J-009081-09	140739	NM_080678	18087856	CAAGUAAACUGAAGCGUGA
UBE2F	L-009081-01	J-009081-10	140739	NM_080678	18087856	AUGACUACAUCAAACGUUA
UBE2F	L-009081-01	J-009081-11	140739	NM_080678	18087856	CAAUAAGAUACCCGCUACA
UBE2F	L-009081-01	J-009081-12	140739	NM_080678	18087856	CUGAAGUUCCCGAUGCGUA
DCUN1D2	L-020261-01	J-020261-09	55208	NM_001014283	62122951	GGGAGAGGAUCUUGUCGUA
DCUN1D2	L-020261-01	J-020261-10	55208	NM_001014283	62122951	GCCAGCAAUUCACGAUUUA
DCUN1D2	L-020261-01	J-020261-11	55208	NM_001014283	62122951	ACAGGGAGUCCAUGCGGAA
DCUN1D2	L-020261-01	J-020261-12	55208	NM_001014283	62122951	CAUCAUAGCUUUUGCGUUA
CUL1	L-004086-00	J-004086-06	8454	NM_003592	32307160	CAACGAAGAGUUCAGGUUU
CUL1	L-004086-00	J-004086-07	8454	NM_003592	32307160	CGAGGAAGACCGCAAACUA
CUL1	L-004086-00	J-004086-08	8454	NM_003592	32307160	AGACAGUGCUUGAUGUUCA
CUL1	L-004086-00	J-004086-09	8454	NM_003592	32307160	CAUAGAAGACAAAGACGUA
UBE3B	L-007197-00	J-007197-06	89910	NM_183415	35493951	CGAAUGCACACUCAAAUAA
UBE3B	L-007197-00	J-007197-07	89910	NM_183415	35493951	CAGAUGGGUUCGUGAGUUU
UBE3B	L-007197-00	J-007197-08	89910	NM_183415	35493951	GAGCAUGGUUCAUCGAUAG
UBE3B	L-007197-00	J-007197-09	89910	NM_183415	35493951	UGACAUGCUUCGUAAAUUC
UBE2A	L-009424-00	J-009424-05	7319	NM_181762	32967275	CUAUGCAGAUGGUAGUAUA
UBE2A	L-009424-00	J-009424-06	7319	NM_181762	32967275	GCGUGUUUCUGCAAUAGUA
UBE2A	L-009424-00	J-009424-07	7319	NM_181762	32967275	GGACAUACUUCAGAACCGU
UBE2A	L-009424-00	J-009424-08	7319	NM_181762	32967275	GAACAAACGGGAAUAUGAA
UBE2E2	L-031782-00	J-031782-05	7325	NM_152653	22749326	GCUGCUAAAUUGUCAACUA
UBE2E2	L-031782-00	J-031782-06	7325	NM_152653	22749326	UCACCAGACUAUCCGUUUA
UBE2E2	L-031782-00	J-031782-07	7325	NM_152653	22749326	GCACAAAGAGUUGAUGACA
UBE2E2	L-031782-00	J-031782-08	7325	NM_152653	22749326	GAGCAGAGCAUGACCGGAU

HECTD3	L-027468-00	J-027468-09	79654	NM_024602	50843830	CAACUAGUCUGGUGCGAUA
HECTD3	L-027468-00	J-027468-10	79654	NM_024602	50843830	CAGCACGGAUCUACAUCUA
HECTD3	L-027468-00	J-027468-11	79654	NM_024602	50843830	GGACCGUUCUCGUUUCAUC
HECTD3	L-027468-00	J-027468-12	79654	NM_024602	50843830	UCAAGAUCCUCGAUAGUGU
UBE2I	L-004910-00	J-004910-05	7329	NM_194260	35493995	GGGAAGGAGGCUUGUUUAA
UBE2I	L-004910-00	J-004910-06	7329	NM_194260	35493995	GAAGUUUGCGCCCUCAUAA
UBE2I	L-004910-00	J-004910-07	7329	NM_194260	35493995	GGCCAGCCAUCACAAUCAA
UBE2I	L-004910-00	J-004910-08	7329	NM_194260	35493995	GAACCACCAUUAUUUCACC
UBE2Q2	L-008326-01	J-008326-09	92912	NM_173469	29789400	GUACCGAAGAUGUUAGUUA
UBE2Q2	L-008326-01	J-008326-10	92912	NM_173469	29789400	GUAAAGUUCCUUAAGCCUA
UBE2Q2	L-008326-01	J-008326-11	92912	NM_173469	29789400	AGGUUUAAUCGAUGUUCAA
UBE2Q2	L-008326-01	J-008326-12	92912	NM_173469	29789400	CUACAUUGUGUGUGUUUAA
HERC6	L-005175-00	J-005175-07	55008	NM_001013000	61563737	GAAGAGAGGUCCACAACUU
HERC6	L-005175-00	J-005175-08	55008	NM_001013000	61563737	AAGAAUUGAUGGCCUAGUU
HERC6	L-005175-00	J-005175-09	55008	NM_001013000	61563737	GAAUCUAGGUGUGGUUUAU
HERC6	L-005175-00	J-005175-10	55008	NM_001013000	61563737	CAGAACCAAUUCAGGCAUU
WWP1	L-004251-00	J-004251-07	11059	NM_007013	33946331	GGUCUGAUACUAGUAAUAA
WWP1	L-004251-00	J-004251-08	11059	NM_007013	33946331	GAACGCGGCUUUAGGUGGA
WWP1	L-004251-00	J-004251-09	11059	NM_007013	33946331	GAAAAGCAACGAUAGAUUU
WWP1	L-004251-00	J-004251-10	11059	NM_007013	33946331	CCAGAUGGAUUGAAGAGUU
UBE2O	L-008979-00	J-008979-05	63893	NM_022066	33636749	GACUUUAGGUUCCGUACAA
UBE2O	L-008979-00	J-008979-06	63893	NM_022066	33636749	GUUGUAGAGUUGAAAGUUA
UBE2O	L-008979-00	J-008979-07	63893	NM_022066	33636749	CGACUCGGGUCUCUUCUUC
UBE2O	L-008979-00	J-008979-08	63893	NM_022066	33636749	GAACCAUACUACAACGAAG
UBE2V1	L-010064-00	J-010064-06	7335	NM_001032288	73765545	UGAAUGGAGUAAAUAGUUC
UBE2V1	L-010064-00	J-010064-07	7335	NM_001032288	73765545	GCCGAAGCAUAGAUUGUAA
UBE2V1	L-010064-00	J-010064-08	7335	NM_001032288	73765545	CACAUGAUCCCUCUGAAUU
UBE2V1	L-010064-00	J-010064-09	7335	NM_001032288	73765545	CAGGACCACUAAAUGCUGA
UBE2R2	L-009700-00	J-009700-07	54926	NM_017811	58530887	CCACAACCCUGGCGGAAUA
UBE2R2	L-009700-00	J-009700-08	54926	NM_017811	58530887	UCUGAAAGGUGGAAUCCUA
UBE2R2	L-009700-00	J-009700-09	54926	NM_017811	58530887	GCUCAGAUUUGCUUUACGA
UBE2R2	L-009700-00	J-009700-10	54926	NM_017811	58530887	CAAUGUCGAUGCUUCAGUU
AKTIP	L-008768-02	J-008768-11	64400	NM_022476	61743931	AGUAAUAUUCAUACGGCAU
AKTIP	L-008768-02	J-008768-12	64400	NM_022476	61743931	AGAAAACAGUGGCGACUUA
AKTIP	L-008768-02	J-008768-13	64400	NM_022476	61743931	AGGCGGAACCAUAAUCAUA
AKTIP	L-008768-02	J-008768-14	64400	NM_022476	61743931	GUGCACUGCUCGUUUGUUU
UBE2E1	L-008850-	J-008850-	7324	NM_182666	33359690	GAGAUACGCUACAUAAAUU

	00	06				
UBE2E1	L-008850-00	J-008850-07	7324	NM_182666	33359690	GCGAUAACAUCUAUGAAUG
UBE2E1	L-008850-00	J-008850-08	7324	NM_182666	33359690	GAGAGUAAAGUCAGCAUGA
UBE2E1	L-008850-00	J-008850-09	7324	NM_182666	33359690	GAACAUGACAGAAUGGCCA
UBE3C	L-007183-00	J-007183-05	9690	NM_014671	7661855	GGUCAAAGACAAUCAUCAA
UBE3C	L-007183-00	J-007183-06	9690	NM_014671	7661855	UUACAGCAUUUCAGAGUAU
UBE3C	L-007183-00	J-007183-07	9690	NM_014671	7661855	GGAGUUGUAUCCCGCAUUU
UBE3C	L-007183-00	J-007183-08	9690	NM_014671	7661855	UCUAAUAUCUUCCAUGUCA
TSG101	L-003549-00	J-003549-06	7251	NM_006292	18765712	CCGUUUAGAUCAAGAAGUA
TSG101	L-003549-00	J-003549-07	7251	NM_006292	18765712	CUCCAUACCCAUCCGGAUA
TSG101	L-003549-00	J-003549-08	7251	NM_006292	18765712	CCACAACAAGUUCUCAGUA
TSG101	L-003549-00	J-003549-09	7251	NM_006292	18765712	CCAAAUACUUCCUACAUGC
UBE2G2	L-009095-00	J-009095-06	7327	NM_003343	33359699	CCACUUGAUUACCCGUUAA
UBE2G2	L-009095-00	J-009095-07	7327	NM_003343	33359699	GCGAUGACCGGGAGCAGUU
UBE2G2	L-009095-00	J-009095-08	7327	NM_003343	33359699	GAGCUAACGUGGAUGCGUC
UBE2G2	L-009095-00	J-009095-09	7327	NM_003343	33359699	GAUGGGAGAGUCUGCAUUU
SMURF2	L-007194-00	J-007194-05	64750	NM_022739	56550041	GUUAAUGACUGGAAGGUAA
SMURF2	L-007194-00	J-007194-06	64750	NM_022739	56550041	AGAAUACGCUUGAUCCAAA
SMURF2	L-007194-00	J-007194-07	64750	NM_022739	56550041	CCACUUUGUUGGACGAAUA
SMURF2	L-007194-00	J-007194-08	64750	NM_022739	56550041	GCAAAAGUAUCCCUGUUAA
NEDD4L	L-007187-00	J-007187-06	23327	NM_015277	21361471	AAGGGAAUAUAUCGACUUA
NEDD4L	L-007187-00	J-007187-07	23327	NM_015277	21361471	GAAUAUCGCUGGAGACUCU
NEDD4L	L-007187-00	J-007187-08	23327	NM_015277	21361471	GAUCAUAACACAAAGACUA
NEDD4L	L-007187-00	J-007187-09	23327	NM_015277	21361471	GUACAUAUGCGGUCAAAGA
UBA3	L-005249-00	J-005249-05	9039	NM_198197	38045945	CAAUAGUGCUUCUCUGCAA
UBA3	L-005249-00	J-005249-06	9039	NM_198197	38045945	UACAGGAGGUUUUGGAUUA
UBA3	L-005249-00	J-005249-07	9039	NM_198197	38045945	GAUAAAUGGCAUGCUGAUA
UBA3	L-005249-00	J-005249-08	9039	NM_198197	38045945	CAAUCUAAAUAGGCAGUUU
UBE2E3	L-008845-00	J-008845-05	10477	NM_182678	33359693	GAGAUCAACUAUACUUGGU
UBE2E3	L-008845-00	J-008845-06	10477	NM_182678	33359693	GCAGAACACGACAGGAUAG
UBE2E3	L-008845-00	J-008845-07	10477	NM_182678	33359693	ACACCAAACUCUCUAGCAA
UBE2E3	L-008845-00	J-008845-08	10477	NM_182678	33359693	GGACAUCCUUAAAGACAAC
UBE2D1	L-009387-00	J-009387-06	7321	NM_003338	33149307	GCACAAAUCUAUAAAUCAG
UBE2D1	L-009387-00	J-009387-07	7321	NM_003338	33149307	GAAAGAAUUGAGUGAUCUA
UBE2D1	L-009387-00	J-009387-08	7321	NM_003338	33149307	CAUAAACAGUAAUGGAAGU
UBE2D1	L-009387-00	J-009387-09	7321	NM_003338	33149307	CAUAUGUUCUCUACUUUGU
UBE3A	L-005137-00	J-005137-05	7337	NM_130838	19718761	CCAGAUUGCUCUCUAAUGA

UBE3A	L-005137-00	J-005137-06	7337	NM_130838	19718761	GGAUAUUGAUGCCAUUAGA
UBE3A	L-005137-00	J-005137-07	7337	NM_130838	19718761	GUCGAAAUCUAGUGAAUGA
UBE3A	L-005137-00	J-005137-08	7337	NM_130838	19718761	GCAGUUGUAUGUGGAAUUU
TRIP12	L-007182-00	J-007182-06	9320	NM_004238	10863902	GAACACAGAUGGUGCGAUA
TRIP12	L-007182-00	J-007182-07	9320	NM_004238	10863902	GACAAAGACUCAUACAAUA
TRIP12	L-007182-00	J-007182-08	9320	NM_004238	10863902	GCUCAUAUCGCAAAGGUUA
TRIP12	L-007182-00	J-007182-09	9320	NM_004238	10863902	GGUAGUGACUCCACCCAUU
HECTD2	L-007198-00	J-007198-05	143279	NM_173497	27735098	CAAUUUGCCUUGAUGUUAG
HECTD2	L-007198-00	J-007198-06	143279	NM_173497	27735098	GGGAUUAAUGCUAAAUUUG
HECTD2	L-007198-00	J-007198-07	143279	NM_173497	27735098	CUGUUAGCCCGAAGAAAGA
HECTD2	L-007198-00	J-007198-08	143279	NM_173497	27735098	AAACAGAAGUUCACCUGCA
CUL4A	L-012610-00	J-012610-05	8451	NM_003589	57165422	GCACAGAUCCUUCCGUUUA
CUL4A	L-012610-00	J-012610-06	8451	NM_003589	57165422	GAACAGCGAUCGUAAUCAA
CUL4A	L-012610-00	J-012610-07	8451	NM_003589	57165422	GCAUGUGGAUUCAAAGUUA
CUL4A	L-012610-00	J-012610-08	8451	NM_003589	57165422	GCGAGUACAUCAAGACUUU
HERC4	L-021426-00	J-021426-05	26091	NM_001017972	63025217	GGUCCGAGAUGUAGGAUGU
HERC4	L-021426-00	J-021426-06	26091	NM_001017972	63025217	UGUCAGAUAUCCAGAUUGU
HERC4	L-021426-00	J-021426-07	26091	NM_001017972	63025217	GGAAGUAUUUCACGAAUUA
HERC4	L-021426-00	J-021426-08	26091	NM_001017972	63025217	GCAGAACAUCCUACGAUAA
HECW2	L-007192-00	J-007192-05	57520	NM_020760	55741472	GUGGGUACCUCCAGUUUAA
HECW2	L-007192-00	J-007192-06	57520	NM_020760	55741472	GAUAACUGAACGAGAAUUA
HECW2	L-007192-00	J-007192-07	57520	NM_020760	55741472	UUACUUAGAUGCUAUCGAA
HECW2	L-007192-00	J-007192-08	57520	NM_020760	55741472	UCACCGUGCUGCAUUCUAA
UBE2B	L-009930-00	J-009930-05	7320	NM_003337	32967281	GGAAUGCAGUUAUAUUUGG
UBE2B	L-009930-00	J-009930-06	7320	NM_003337	32967281	GAACCGAAUCCUAACAGUC
UBE2B	L-009930-00	J-009930-07	7320	NM_003337	32967281	GAGUUUCGGCCAUUGUUGA
UBE2B	L-009930-00	J-009930-08	7320	NM_003337	32967281	UAGAUAUCCUUCAGAAUCG
UBE2U	L-008998-01	J-008998-09	148581	NM_152489	22749026	CCUAAAGACCCACGUAAAU
UBE2U	L-008998-01	J-008998-10	148581	NM_152489	22749026	GGGUAUCACUGCUAAGCCU
UBE2U	L-008998-01	J-008998-11	148581	NM_152489	22749026	GCUUUCUAAUCCAGUGCUA
UBE2U	L-008998-01	J-008998-12	148581	NM_152489	22749026	ACAGAAUACUACAGAACUC
CAND1	L-015562-01	J-015562-09	55832	NM_018448	21361793	GACUUUAGGUUUAUGGCUA
CAND1	L-015562-01	J-015562-10	55832	NM_018448	21361793	CGUGCAACAUGUACAACUA
CAND1	L-015562-01	J-015562-11	55832	NM_018448	21361793	CAACAAGAACCUACAUACA
CAND1	L-015562-01	J-015562-12	55832	NM_018448	21361793	CAUAACAAGCCAUCAUUAA
KIAA0317	L-007184-00	J-007184-06	9870	NM_014821	42734314	GCGCAAGGCUGGGCGUUAU
KIAA0317	L-007184-	J-007184-	9870	NM_014821	42734314	CGAAGAAGGUGUACUGCUA

	00	07				
KIAA0317	L-007184-00	J-007184-08	9870	NM_014821	42734314	GCAUUUACUUUGAGGCUUA
KIAA0317	L-007184-00	J-007184-09	9870	NM_014821	42734314	GGGAAUGGUUUGAGCUAAU
UBE2D4	L-009435-00	J-009435-06	51619	NM_015983	19549332	GGAAUUAACCGACUUGCAG
UBE2D4	L-009435-00	J-009435-07	51619	NM_015983	19549332	GCAAGAGAGUGGACACAAA
UBE2D4	L-009435-00	J-009435-08	51619	NM_015983	19549332	GAAUGACAGUCCUUACCAA
UBE2D4	L-009435-00	J-009435-09	51619	NM_015983	19549332	ACCCUAAUAUCAACAGCAA
DCUN1D4	L-014118-01	J-014118-09	23142	NM_015115	32698693	GGUGACAUGUGAUCGUUUA
DCUN1D4	L-014118-01	J-014118-10	23142	NM_015115	32698693	GUGCAAUGUCCUAGAGUUU
DCUN1D4	L-014118-01	J-014118-11	23142	NM_015115	32698693	GAAUAUAGGUACCAAUGAA
DCUN1D4	L-014118-01	J-014118-12	23142	NM_015115	32698693	CCAACUAUCUGGUGCUAUU
CUL4B	L-017965-00	J-017965-05	8450	NM_003588	28372492	UAAAUAACCUCCUUGAUGA
CUL4B	L-017965-00	J-017965-06	8450	NM_003588	28372492	CAGAAGUCAUUAAUUGCUA
CUL4B	L-017965-00	J-017965-07	8450	NM_003588	28372492	CGGAAAGAGUGCAUCUGUA
CUL4B	L-017965-00	J-017965-08	8450	NM_003588	28372492	GCUAUUGGCCGACAUAUGU
UBE2L6	L-008569-00	J-008569-05	9246	NM_004223	38157980	GCUGGUGAAUAGACCGAAU
UBE2L6	L-008569-00	J-008569-06	9246	NM_004223	38157980	GGACGAGAACGGACAGAUU
UBE2L6	L-008569-00	J-008569-07	9246	NM_004223	38157980	UCAGAAAGAAUGCCGAAGA
UBE2L6	L-008569-00	J-008569-08	9246	NM_004223	38157980	UGAUCAAAUUCACAACCAA
UBE2J1	L-007266-00	J-007266-05	51465	NM_016021	37577121	GCUCUUAUAUUCCGACGAA
UBE2J1	L-007266-00	J-007266-06	51465	NM_016021	37577121	GAGUAUAAGGACAGCAUUA
UBE2J1	L-007266-00	J-007266-07	51465	NM_016021	37577121	GAUGUCCUGUUGCCUUUAA
UBE2J1	L-007266-00	J-007266-08	51465	NM_016021	37577121	GCCAUAGGUUCUCUAGAUU
UBE2QL1	L-024273-01	J-024273-09	134111	XM_940609	88987241	GCAAAUGCCGUUCGGAUUA
UBE2QL1	L-024273-01	J-024273-10	134111	XM_940609	88987241	CCACUUAGAUAUCGACUCA
UBE2QL1	L-024273-01	J-024273-11	134111	XM_940609	88987241	GAGUCAUAAUAGUCGUGAA
UBE2QL1	L-024273-01	J-024273-12	134111	XM_940609	88987241	GACUAAAGAUUGUCAACGA
UBE2Q1	L-008631-00	J-008631-06	55585	NM_017582	38045949	GAGGCAAGAUUACUUAAAU
UBE2Q1	L-008631-00	J-008631-07	55585	NM_017582	38045949	GGACAGCGCUUUGCACAAC
UBE2Q1	L-008631-00	J-008631-08	55585	NM_017582	38045949	CGACCUGUGUAAACUCUAU
UBE2Q1	L-008631-00	J-008631-09	55585	NM_017582	38045949	GGAGCCGACUUCAUUCUAC
UBE2G1	L-010154-00	J-010154-06	7326	NM_182682	75992938	GAUGGGAAGUCCUUAUUAU
UBE2G1	L-010154-00	J-010154-07	7326	NM_182682	75992938	GCUAGUAACUUCACUUAUU
UBE2G1	L-010154-00	J-010154-08	7326	NM_182682	75992938	GUAUAGAUCCCGUCACUAA
UBE2G1	L-010154-00	J-010154-09	7326	NM_182682	75992938	UAUAGAAACUCGUAAGUGU
UBE2H	L-009134-00	J-009134-05	7328	NM_182697	33356153	GAGUGGACCUACCUGAUAA
UBE2H	L-009134-00	J-009134-06	7328	NM_182697	33356153	GAUAUGGAGUUGUAGUAGA

UBE2H	L-009134-00	J-009134-07	7328	NM_182697	33356153	GGCGGAGUAUGGAAAGUUA
UBE2H	L-009134-00	J-009134-08	7328	NM_182697	33356153	UCAAGCUCAUCGAGAGUAA
CUL5	L-019553-00	J-019553-05	8065	NM_003478	67514034	GACACGACGUCUUAUAUUA
CUL5	L-019553-00	J-019553-06	8065	NM_003478	67514034	GCAAAUAGAGUGGCUAAUA
CUL5	L-019553-00	J-019553-07	8065	NM_003478	67514034	UAAACAAGCUUGCUAGAAU
CUL5	L-019553-00	J-019553-08	8065	NM_003478	67514034	CGUCUAAUCUGUUAAAGAA
ARIH1	L-019984-00	J-019984-05	25820	NM_005744	9966762	CGAGAUAUUUCCCAAGAUU
ARIH1	L-019984-00	J-019984-06	25820	NM_005744	9966762	GGAUAUGCCUUGUCAGAUC
ARIH1	L-019984-00	J-019984-07	25820	NM_005744	9966762	GAGAGUCGACGAAGGGUUU
ARIH1	L-019984-00	J-019984-08	25820	NM_005744	9966762	CCAAAUGCCAUGUCACAAU
UBA6	L-006403-01	J-006403-09	55236	NM_018227	40255038	GUGUAGAAUUAGCAAGAUU
UBA6	L-006403-01	J-006403-10	55236	NM_018227	40255038	GCAUAGCUGUCCAAGUUAA
UBA6	L-006403-01	J-006403-11	55236	NM_018227	40255038	CAGUGUUGUAGGAGCAAUA
UBA6	L-006403-01	J-006403-12	55236	NM_018227	40255038	GGAAUUUGGUCAAGGUUAU
UBE2D2	L-010383-00	J-010383-06	7322	NM_003339	33188457	UCUGUUCUCUGUUGUGUGA
UBE2D2	L-010383-00	J-010383-07	7322	NM_003339	33188457	CAAAUGACAGUCCCUAUCA
UBE2D2	L-010383-00	J-010383-08	7322	NM_003339	33188457	GUAUGUGGUUUCUCAGUUA
UBE2D2	L-010383-00	J-010383-09	7322	NM_003339	33188457	UCCAGGAACUUGAUUGUUA
CACUL1	L-016305-01	J-016305-09	143384	NM_153810	54262140	AGGCGAUGAUGGACGACCA
CACUL1	L-016305-01	J-016305-10	143384	NM_153810	54262140	GGAUAUUGGGAGCAAGUAA
CACUL1	L-016305-01	J-016305-11	143384	NM_153810	54262140	GGGUACAGAUAGUGAAUGU
CACUL1	L-016305-01	J-016305-12	143384	NM_153810	54262140	GCAUUAGAAAGUCUUGUUA

Supplementary Table 2. Custom genes for primary screen to complete selected set of enzymes.

Gene Symbol	Pool Catalog Number	Duplex Catalog Number	GENE ID	Gene Accession	GI Number	Sequence
SAE1	L-006402-01	J-006402-09	10055	NM_005500	4885584	GCACAGUAUGACCGGCAGA
SAE1	L-006402-01	J-006402-10	10055	NM_005500	4885584	GGGUCUGUUGGCCGAAAUA
SAE1	L-006402-01	J-006402-11	10055	NM_005500	4885584	UGAAGUCAUUGGCCCGAUA
SAE1	L-006402-01	J-006402-12	10055	NM_005500	4885584	GUUCUUGAGUUUUCGUUUA
UBA2	L-005248-01	J-005248-09	10054	NM_005499	50592990	GUGCAAAGAGGUCACGUAU
UBA2	L-005248-01	J-005248-10	10054	NM_005499	50592990	GGACAAACUAUGGCGGAAA
UBA2	L-005248-01	J-005248-11	10054	NM_005499	50592990	CAUAACCAGUCAUGAGAUA
UBA2	L-005248-01	J-005248-12	10054	NM_005499	50592990	GCUAGAACUGUUAGACACA
NAE1	L-006401-00	J-006401-05	8883	NM_001018160	66363687	GAUGAUCGCUGCAUAAAUA
NAE1	L-006401-00	J-006401-06	8883	NM_001018160	66363687	GCACAGUGGUAUAGUGAAA
NAE1	L-006401-00	J-006401-07	8883	NM_001018160	66363687	GAUUUUAGCUCGUGCCUUA
NAE1	L-006401-00	J-006401-08	8883	NM_001018160	66363687	GUUACGGGCUGUUGAUAGA
ATG7	L-020112-00	J-020112-05	10533	NM_006395	5453667	CCAACACACUCGAGUCUUU
ATG7	L-020112-00	J-020112-06	10533	NM_006395	5453667	GAUCUAAAUCUCAAACUGA
ATG7	L-020112-00	J-020112-07	10533	NM_006395	5453667	GCCCACAGAUGGAGUAGCA
ATG7	L-020112-00	J-020112-08	10533	NM_006395	5453667	GCCAGAGGAUUCAACAUGA
UFC1	L-020623-01	J-020623-09	51506	NM_016406	7705480	CCUUUGAUAGGCUACGAUA
UFC1	L-020623-01	J-020623-10	51506	NM_016406	7705480	AAAUAUGCCUGACGGAUCA
UFC1	L-020623-01	J-020623-11	51506	NM_016406	7705480	AAUAUGAGUUUGACAUCGA
UFC1	L-020623-01	J-020623-12	51506	NM_016406	7705480	AGUUGUGGGUGCAGCGACU
ATG10	L-019426-01	J-019426-09	83734	NM_031482	33589825	CGUCUCAGGAUGAACGAAA
ATG10	L-019426-01	J-019426-10	83734	NM_031482	33589825	AGGAAUUGCGGCACGAAGA
ATG10	L-019426-01	J-019426-11	83734	NM_031482	33589825	GGAGGAGGCUUUCGAGCUA
ATG10	L-019426-01	J-019426-12	83734	NM_031482	33589825	CCAACGUUAUUGUGCAGAA
ATG3	L-015375-00	J-015375-05	64422	NM_022488	34147490	GAGAGUGGAUUGUUGGAAA
ATG3	L-015375-00	J-015375-06	64422	NM_022488	34147490	GCGGAUGGGUAGAUACAUA
ATG3	L-015375-00	J-015375-07	64422	NM_022488	34147490	GAGCAACGGCAGCCUUUAA
ATG3	L-015375-00	J-015375-08	64422	NM_022488	34147490	ACAAGACACUUCACAAUGU
RNF25	L-007047-00	J-007047-05	64320	NM_022453	34878786	GGUCAAAUCAGCAAAGGUU
RNF25	L-007047-00	J-007047-06	64320	NM_022453	34878786	AGGCUGAGCGAAACCGAUA
RNF25	L-007047-00	J-007047-07	64320	NM_022453	34878786	UGAGUCAGCUGUAGAUGUC
RNF25	L-007047-00	J-007047-08	64320	NM_022453	34878786	GACCAGGAUUCACAGUAUG
RWDD1	L-020946-02	J-020946-18	51389	NM_015952	55953122	GGCUAUGCUCAGAGGGUUA
RWDD1	L-020946-02	J-020946-19	51389	NM_015952	55953122	UGAAGAUGAUCCAGACUAU
RWDD1	L-020946-02	J-020946-20	51389	NM_015952	55953122	GCAGAACUCUUGGAAAUUA
RWDD1	L-020946-02	J-020946-21	51389	NM_015952	55953122	UCUAGUGACAGCUGUGCAA
UBR4	L-014021-01	J-014021-09	23352	NM_020765	82659108	GGGAACACCCUGACGUAAA
UBR4	L-014021-01	J-014021-10	23352	NM_020765	82659108	UCAUGAAGCCUGUUCGAAA
UBR4	L-014021-01	J-014021-11	23352	NM_020765	82659108	CUACGAAGCUGCCGACAAA
UBR4	L-014021-01	J-014021-12	23352	NM_020765	82659108	UGAACAAAUUUGCCGAUAA
UBR3	L-016653-00	J-016653-05	130507	NM_172070	40255162	AGAAAAGUCUUACGAAGUA
UBR3	L-016653-00	J-016653-06	130507	NM_172070	40255162	AGGCAAACCUCUCUACAUU

UBR3	L-016653-00	J-016653-07	130507	NM_172070	40255162	GAGAAAGCUCACCCAGUUA
UBR3	L-016653-00	J-016653-08	130507	NM_172070	40255162	AGAUCGACCUACUGGAUUA
UBR2	L-006954-00	J-006954-05	23304	NM_015255	27597060	CAACAGAGAUUACGCUUAC
UBR2	L-006954-00	J-006954-06	23304	NM_015255	27597060	GCGUAGGUCUGUUCGAUAU
UBR2	L-006954-00	J-006954-07	23304	NM_015255	27597060	GCUUAGUGAUUCCAAAUUA
UBR2	L-006954-00	J-006954-08	23304	NM_015255	27597060	UCAGAGAUCAACUGUAUUA
UBR1	L-010691-00	J-010691-06	197131	NM_174916	83656781	GGAAAUCAGCGCGGAGUUA
UBR1	L-010691-00	J-010691-07	197131	NM_174916	83656781	GUACAAUCGUGUGGACAUA
UBR1	L-010691-00	J-010691-08	197131	NM_174916	83656781	GCGAAGAAAUGGACUGUCU
UBR1	L-010691-00	J-010691-09	197131	NM_174916	83656781	GAUCAGCAAACCCACAAUA
UBR7	L-016489-01	J-016489-09	55148	NM_175748	28411949	AUGAUGGAUUGGUGCGGAA
UBR7	L-016489-01	J-016489-10	55148	NM_175748	28411949	GAAAGGAUGAUGUCCGGGA
UBR7	L-016489-01	J-016489-11	55148	NM_175748	28411949	UGGCGUAGCAAGUUGUGUA
UBR7	L-016489-01	J-016489-12	55148	NM_175748	28411949	UGAAUAGAGUCCAGCAAGU
USP2	L-006069-00	J-006069-11	9099	NM_171997	28565284	ACACCAACCAUGCUGUUUA
USP2	L-006069-00	J-006069-12	9099	NM_171997	28565284	GCGCUUUGUUGGCUAUAAU
USP2	L-006069-00	J-006069-13	9099	NM_171997	28565284	GUGUACAGAUUGUGGUUAC
USP2	L-006069-00	J-006069-14	9099	NM_171997	28565284	GACCUAAGUCCAACCCUGA
USP9X	L-006099-00	J-006099-06	8239	NM_021906	74315357	AGAAAUCGCUGGUAUAAAU
USP9X	L-006099-00	J-006099-07	8239	NM_021906	74315357	ACACGAUGCUUUAGAAUUU
USP9X	L-006099-00	J-006099-08	8239	NM_021906	74315357	GUACGACGAUGUAUUCUCA
USP9X	L-006099-00	J-006099-09	8239	NM_021906	74315357	GAAAUAACUUCCUACCGAA
VCP	L-008727-00	J-008727-09	7415	NM_007126	7669552	GCAUGUGGGUGCUGACUUA
VCP	L-008727-00	J-008727-10	7415	NM_007126	7669552	CAAAUUGGCUGGUGAGUCU
VCP	L-008727-00	J-008727-11	7415	NM_007126	7669552	CCUGAUUGCUCGAGCUGUA
VCP	L-008727-00	J-008727-12	7415	NM_007126	7669552	GUAAUCUCUUCGAGGUAUA
SENP1	L-006357-00	J-006357-05	29843	NM_014554	45505133	GCAUUUCGCCUGACCAUUA
SENP1	L-006357-00	J-006357-06	29843	NM_014554	45505133	GGAAGUGACUGUGGGAUGU
SENP1	L-006357-00	J-006357-07	29843	NM_014554	45505133	CAAGAAGUGCAGCUUAUAA
SENP1	L-006357-00	J-006357-08	29843	NM_014554	45505133	GCAGUGAAACGUUGGACAA
UBB	L-013382-00	J-013382-05	7314	NM_018955	22538474	GCUGUUAAUUCUUCAGUCA
UBB	L-013382-00	J-013382-06	7314	NM_018955	22538474	GUAUGCAGAUCUUCGUGAA
UBB	L-013382-00	J-013382-07	7314	NM_018955	22538474	UCGAAAAUGUGAAGGCCAA
UBB	L-013382-00	J-013382-08	7314	NM_018955	22538474	CACCUGGUCCUGCGUCUGA
SUMO1	L-016005-00	J-016005-07	7341	NM_001005781	54792064	GUGCAUAUAUGAUACAGUU
SUMO1	L-016005-00	J-016005-08	7341	NM_001005781	54792064	GCACUGAAAGUUACUGAAG
SUMO1	L-016005-00	J-016005-09	7341	NM_001005781	54792064	CAUAAAUACUGGAAAUUGC
SUMO1	L-016005-00	J-016005-10	7341	NM_001005781	54792064	AAUACUCAGUGUUCUGUUU

Supplementary Table 3. Genes selected for the secondary screen.

Gene Symbol	Pool Catalog Number	Duplex Catalog Number	Gene Symbol	GENE ID	Gene Accession	GI Number	Sequence
AREL1	J-007184-09	J-007184-09	AREL1	9870	NM_014821	42734314	GGGAAUGGUUUGAGCUAAU
AREL1	J-007184-06	J-007184-06	AREL1	9870	NM_014821	42734314	GCGCAAGGCUGGGCGUUAU
AREL1	J-007184-07	J-007184-07	AREL1	9870	NM_014821	42734314	CGAAGAAGGUGUACUGCUA
AREL1	J-007184-08	J-007184-08	AREL1	9870	NM_014821	42734314	GCAUUUACUUUGAGGCUUA
CACUL1	J-016305-11	J-016305-11	CACUL1	143384	NM_153810	54262140	GGGUACAGAUAGUGAAUGU
CACUL1	J-016305-12	J-016305-12	CACUL1	143384	NM_153810	54262140	GCAUUAGAAAGUCUUGUUA
CACUL1	J-016305-09	J-016305-09	CACUL1	143384	NM_153810	54262140	AGGCGAUGAUGGACGACCA
CACUL1	J-016305-10	J-016305-10	CACUL1	143384	NM_153810	54262140	GGAUAUUGGGAGCAAGUAA
CAND1	J-015562-12	J-015562-12	CAND1	55832	NM_018448	21361793	CAUAACAAGCCAUCAUUAA
CAND1	J-015562-10	J-015562-10	CAND1	55832	NM_018448	21361793	CGUGCAACAUGUACAACUA
CAND1	J-015562-11	J-015562-11	CAND1	55832	NM_018448	21361793	CAACAAGAACCUACAUACA
CAND1	J-015562-09	J-015562-09	CAND1	55832	NM_018448	21361793	GACUUUAGGUUUAUGGCUA
CUL2	J-007277-06	J-007277-06	CUL2	8453	NM_003591	19482173	CAUCCAAGUUCAUAUACUA
CUL2	J-007277-05	J-007277-05	CUL2	8453	NM_003591	19482173	GGAAGUGCAUGGUAAAUUU
CUL2	J-007277-08	J-007277-08	CUL2	8453	NM_003591	19482173	UGGUUUACCUCAUAUGAUU
CUL2	J-007277-07	J-007277-07	CUL2	8453	NM_003591	19482173	GCAGAAAGACACACCACAA
CUL4B	J-017965-06	J-017965-06	CUL4B	8450	NM_003588	28372492	CAGAAGUCAUUAAUUGCUA
CUL4B	J-017965-08	J-017965-08	CUL4B	8450	NM_003588	28372492	GCUAUUGGCCGACAUAUGU
CUL4B	J-017965-05	J-017965-05	CUL4B	8450	NM_003588	28372492	UAAAUAACCUCCUUGAUGA
CUL4B	J-017965-07	J-017965-07	CUL4B	8450	NM_003588	28372492	CGGAAAGAGUGCAUCUGUA
DCUN1D3	J-018390-05	J-018390-05	DCUN1D3	123879	NM_173475	27735046	AAGGAUCUCUACCGGUUUA
DCUN1D3	J-018390-06	J-018390-06	DCUN1D3	123879	NM_173475	27735046	ACGGUUCCCUAGCCUCUUA
DCUN1D3	J-018390-07	J-018390-07	DCUN1D3	123879	NM_173475	27735046	CCAGAACAAUCCUCCGGUA
DCUN1D3	J-018390-08	J-018390-08	DCUN1D3	123879	NM_173475	27735046	GUAAGAAUCCCUCAUCGAC
DCUN1D5	J-014842-09	J-014842-09	DCUN1D5	84259	NM_032299	34147410	CAAUCAAAGUAUCGUGUUA
DCUN1D5	J-014842-10	J-014842-10	DCUN1D5	84259	NM_032299	34147410	GUUGAAUGAUAUUUCGUCA
DCUN1D5	J-014842-12	J-014842-12	DCUN1D5	84259	NM_032299	34147410	UGAUGGGCAUUGAGCCACA
DCUN1D5	J-014842-11	J-014842-11	DCUN1D5	84259	NM_032299	34147410	CCGUCAGACAUCAUAGCAA
HERC2	J-007180-12	J-007180-12	HERC2	8924	NM_004667	67190865	GCAGAUGUGUGCUAAGAUG
HERC2	J-007180-10	J-007180-10	HERC2	8924	NM_004667	67190865	CGAUGAAGGUUUGGUAUUU
HERC2	J-007180-09	J-007180-09	HERC2	8924	NM_004667	67190865	GCACAGAGUAUCACAGGUA
HERC2	J-007180-11	J-007180-11	HERC2	8924	NM_004667	67190865	GAUAAUACGACACAGCUAA
HERC5	J-005174-06	J-005174-06	HERC5	51191	NM_016323	7705930	GGAAGUAGCAUAACUGUCA
HERC5	J-005174-07	J-005174-07	HERC5	51191	NM_016323	7705930	GAACCAGGAUAUAACAGUU
HERC5	J-005174-08	J-005174-08	HERC5	51191	NM_016323	7705930	UAAGAGCACUGACAUGUUU
HERC5	J-005174-09	J-005174-09	HERC5	51191	NM_016323	7705930	GACUUUCCCUGUUCAAUUG
RBX1	J-004087-07	J-004087-07	RBX1	9978	NM_014248	22091459	GAAGCGCUUUGAAGUGAAA
RBX1	J-004087-08	J-004087-08	RBX1	9978	NM_014248	22091459	GGGAUAUUGUGGUUGAUAA
RBX1	J-004087-09	J-004087-09	RBX1	9978	NM_014248	22091459	GGAACCACAUUAUGGAUCU
RBX1	J-004087-10	J-004087-10	RBX1	9978	NM_014248	22091459	CAUAGAAUGUCAAGCUAAC
RNF25	J-007047-05	J-007047-05	RNF25	64320	NM_022453	34878786	GGUCAAAUCAGCAAAGGUU
RNF25	J-007047-06	J-007047-06	RNF25	64320	NM_022453	34878786	AGGCUGAGCGAAACCGAUA

RNF25	J-007047-07	J-007047-07	RNF25	64320	NM_022453	34878786	UGAGUCAGCUGUAGAUGUC
RNF25	J-007047-08	J-007047-08	RNF25	64320	NM_022453	34878786	GACCAGGAUUCACAGUAUG
SAG	J-011105-08	J-011105-08	SAG	6295	NM_000541	10880124	GCAAGAGAGCCUGCUUAAA
SAG	J-011105-06	J-011105-06	SAG	6295	NM_000541	10880124	GUUCUCUACUCGAGUGAUU
SAG	J-011105-07	J-011105-07	SAG	6295	NM_000541	10880124	GAACCGAACCAUGUUAUCU
SAG	J-011105-05	J-011105-05	SAG	6295	NM_000541	10880124	AAAGUUAUCAGGAUGCAAA
SPOP	J-017919-10	J-017919-10	SPOP	8405	NM_001007228	56117829	CAACUAUCAUGCUUCGGAU
SPOP	J-017919-09	J-017919-09	SPOP	8405	NM_001007228	56117829	GGUAAAGGUUCCUGAGUGC
SPOP	J-017919-08	J-017919-08	SPOP	8405	NM_001007228	56117829	GAGAGUCAACGGGCAUAUA
SPOP	J-017919-11	J-017919-11	SPOP	8405	NM_001007228	56117829	AAAUGGUGUUUGCGAGUAA
UBA3	J-005249-08	J-005249-08	UBA3	9039	NM_198197	38045945	CAAUCUAAAUAGGCAGUUU
UBA3	J-005249-05	J-005249-05	UBA3	9039	NM_198197	38045945	CAAUAGUGCUUCUCUGCAA
UBA3	J-005249-07	J-005249-07	UBA3	9039	NM_198197	38045945	GAUAAAUGGCAUGCUGAUA
UBA3	J-005249-06	J-005249-06	UBA3	9039	NM_198197	38045945	UACAGGAGGUUUUGGAUUA
UBE2A	J-009424-07	J-009424-07	UBE2A	7319	NM_181762	32967275	GGACAUACUUCAGAACCGU
UBE2A	J-009424-05	J-009424-05	UBE2A	7319	NM_181762	32967275	CUAUGCAGAUGGUAGUAUA
UBE2A	J-009424-08	J-009424-08	UBE2A	7319	NM_181762	32967275	GAACAAACGGGAAUAUGAA
UBE2A	J-009424-06	J-009424-06	UBE2A	7319	NM_181762	32967275	GCGUGUUUCUGCAAUAGUA
UBE2D2	J-010383-09	J-010383-09	UBE2D2	7322	NM_003339	33188457	UCCAGGAACUUGAUUGUUA
UBE2D2	J-010383-06	J-010383-06	UBE2D2	7322	NM_003339	33188457	UCUGUUCUCUGUUGUGUGA
UBE2D2	J-010383-08	J-010383-08	UBE2D2	7322	NM_003339	33188457	GUAUGUGGUUUCUCAGUUA
UBE2D2	J-010383-07	J-010383-07	UBE2D2	7322	NM_003339	33188457	CAAAUGACAGUCCCUAUCA
UBE2F	J-009081-09	J-009081-09	UBE2F	140739	NM_080678	18087856	CAAGUAAACUGAAGCGUGA
UBE2F	J-009081-11	J-009081-11	UBE2F	140739	NM_080678	18087856	CAAUAAGAUACCCGCUACA
UBE2F	J-009081-10	J-009081-10	UBE2F	140739	NM_080678	18087856	AUGACUACAUCAAACGUUA
UBE2F	J-009081-12	J-009081-12	UBE2F	140739	NM_080678	18087856	CUGAAGUUCCCGAUGCGUA
UBE2G1	J-010154-08	J-010154-08	UBE2G1	7326	NM_182682	75992938	GUAUAGAUCCCGUCACUAA
UBE2G1	J-010154-09	J-010154-09	UBE2G1	7326	NM_182682	75992938	UAUAGAAACUCGUAAGUGU
UBE2G1	J-010154-07	J-010154-07	UBE2G1	7326	NM_182682	75992938	GCUAGUAACUUCACUUAUU
UBE2G1	J-010154-06	J-010154-06	UBE2G1	7326	NM_182682	75992938	GAUGGGAAGUCCUUAUUAU
UBE2H	J-009134-05	J-009134-05	UBE2H	7328	NM_182697	33356153	GAGUGGACCUACCUGAUAA
UBE2H	J-009134-08	J-009134-08	UBE2H	7328	NM_182697	33356153	UCAAGCUCAUCGAGAGUAA
UBE2H	J-009134-06	J-009134-06	UBE2H	7328	NM_182697	33356153	GAUAUGGAGUUGUAGUAGA
UBE2H	J-009134-07	J-009134-07	UBE2H	7328	NM_182697	33356153	GGCGGAGUAUGGAAAGUUA
UBE2J1	J-007266-08	J-007266-08	UBE2J1	51465	NM_016021	37577121	GCCAUAGGUUCUCUAGAUU
UBE2J1	J-007266-06	J-007266-06	UBE2J1	51465	NM_016021	37577121	GAGUAUAAGGACAGCAUUA
UBE2J1	J-007266-07	J-007266-07	UBE2J1	51465	NM_016021	37577121	GAUGUCCUGUUGCCUUUAA
UBE2J1	J-007266-05	J-007266-05	UBE2J1	51465	NM_016021	37577121	GCUCUUAUAUUCCGACGAA
UBE2QL1	J-024273-12	J-024273-12	UBE2QL1	134111	XM_940609	88987241	GACUAAAGAUUGUCAACGA
UBE2QL1	J-024273-09	J-024273-09	UBE2QL1	134111	XM_940609	88987241	GCAAAUGCCGUUCGGAUUA
UBE2QL1	J-024273-10	J-024273-10	UBE2QL1	134111	XM_940609	88987241	CCACUUAGAUAUCGACUCA
UBE2QL1	J-024273-11	J-024273-11	UBE2QL1	134111	XM_940609	88987241	GAGUCAUAAUAGUCGUGAA
UBE2S	J-009707-06	J-009707-06	UBE2S	27338	NM_014501	7657045	GGAGGUCUGUUCCGCAUGA
UBE2S	J-009707-07	J-009707-07	UBE2S	27338	NM_014501	7657045	GCAUCAAGGUCUUUCCCAA
UBE2S	J-009707-05	J-009707-05	UBE2S	27338	NM_014501	7657045	ACAAGGAGGUGACGACACU
UBE2S	J-009707-08	J-009707-08	UBE2S	27338	NM_014501	7657045	CCAAGAAGCAUGCUGGCGA
UBE2U	J-008998-11	J-008998-11	UBE2U	148581	NM_152489	22749026	GCUUUCUAAUCCAGUGCUA

UBE2U	J-008998-09	J-008998-09	UBE2U	148581	NM_152489	22749026	CCUAAAGACCCACGUAAAU
UBE2U	J-008998-10	J-008998-10	UBE2U	148581	NM_152489	22749026	GGGUAUCACUGCUAAGCCU
UBE2U	J-008998-12	J-008998-12	UBE2U	148581	NM_152489	22749026	ACAGAAUACUACAGAACUC
UBE2W	J-009643-08	J-009643-08	UBE2W	55284	NM_001001482	47933382	ACAUAGGCCUACAGAAUUA
UBE2W	J-009643-07	J-009643-07	UBE2W	55284	NM_001001482	47933382	GGAAAUGAGUAGUGAUAUG
UBE2W	J-009643-10	J-009643-10	UBE2W	55284	NM_001001482	47933382	GAGGAGGUACUGUGUGUUA
UBE2W	J-009643-09	J-009643-09	UBE2W	55284	NM_001001482	47933382	GUAAUGCAUUGUUGAAAGA
UBR1	J-010691-06	J-010691-06	UBR1	197131	NM_174916	83656781	GGAAAUCAGCGCGGAGUUA
UBR1	J-010691-09	J-010691-09	UBR1	197131	NM_174916	83656781	GAUCAGCAAACCCACAAUA
UBR1	J-010691-07	J-010691-07	UBR1	197131	NM_174916	83656781	GUACAAUCGUGUGGACAUA
UBR1	J-010691-08	J-010691-08	UBR1	197131	NM_174916	83656781	GCGAAGAAAUGGACUGUCU
UBR3	J-016653-08	J-016653-08	UBR3	130507	NM_172070	40255162	AGAUCGACCUACUGGAUUA
UBR3	J-016653-07	J-016653-07	UBR3	130507	NM_172070	40255162	GAGAAAGCUCACCCAGUUA
UBR3	J-016653-06	J-016653-06	UBR3	130507	NM_172070	40255162	AGGCAAACCUCUCUACAUU
UBR3	J-016653-05	J-016653-05	UBR3	130507	NM_172070	40255162	AGAAAAGUCUUACGAAGUA
UBR4	J-014021-12	J-014021-12	UBR4	23352	NM_020765	82659108	UGAACAAAUUUGCCGAUAA
UBR4	J-014021-09	J-014021-09	UBR4	23352	NM_020765	82659108	GGGAACACCCUGACGUAAA
UBR4	J-014021-11	J-014021-11	UBR4	23352	NM_020765	82659108	CUACGAAGCUGCCGACAAA
UBR4	J-014021-10	J-014021-10	UBR4	23352	NM_020765	82659108	UCAUGAAGCCUGUUCGAAA
UBR5	J-007189-09	J-007189-09	UBR5	51366	NM_015902	41352716	GGUCGAAGAUGUGCUACUA
UBR5	J-007189-06	J-007189-06	UBR5	51366	NM_015902	41352716	GCACUUAUAUACUGGAUUA
UBR5	J-007189-07	J-007189-07	UBR5	51366	NM_015902	41352716	GAUUGUAGGUUACUUAGAA
UBR5	J-007189-08	J-007189-08	UBR5	51366	NM_015902	41352716	GAUCAAUCCUAACUGAAUU

Supplementary Table 4. List of antibodies.

Protein	Manufacturer	Reference	Application
Androgen Receptor	ThermoScientific	MA5-13426	WB
β-catenin (Ser33/37/Thr41-phospho)	Cell Signaling	9561	WB
β-catenin (total)	Transduc lab	610468	WB/IF
c-Myc	Santa Cruz	(1.N.2): sc-70469	WB
CACUL1 (C10orf46)	ABGENT	AP4997b-ev	WB
CAND1	Abnova	H00055832	WB
Cdt1	Abcam	ab70829	WB
Cytokeratin 18	Dako	M 7010	WB
E-Cadherin	BD Transduc lab	610181	WB/IF
ERG	Abcam	[EPR3864] (ab92513)	WB
ERG	Santa Cruz	(C-17): X sc-354 X	IP
FAK	Transduc lab	F15020	WB/IF
FKBP51	Santa Cruz	(H100) : sc-13983	WB
Frizzled-4	Santa Cruz	(C-18): sc-66450	WB
GAPDH	Santa Cruz	sc-25778	WB
GSK3-beta	Cell Signaling	9315	WB
γH2AX (Ser139)	Millipore	16-202A	WB/IF
phospho-IκB (Ser32)	Cell Signaling	2859	WB
Integrin beta 1	Abcam	ab30394	WB/IF
LEF1	Millipore	17-604	WB
N-Cadherin	BD Transduc lab	610921	WB/IF
NEDD8	Abcam	ab81264	WB/IF
phospho-NF-κB (Ser536)	Cell Signalling	3033	WB/IF
Occludin	In Vitrogen	33-1500	WB/IF
P21	Santa Cruz	(C-19): sc-397	WB
P27	Cell Signalling	3686	WB
P53	Santa Cruz	(FL-393 G): sc-6243-G	WB
Paxillin	Transduc lab	13520	WB
Prostein	Santa Cruz	(A-5) : sc-393069	WB
PSA	DAKO	A0562	WB
SUMO-1	Santa Cruz	(FL-101): sc-9060	WB
UBE2A	GeneTex	GTX114186	WB
UBE2H	Santa Cruz	(18-Z): sc-100620	WB
UBE2S	ABGENT	AP20071b-ev	WB
UBE2U	Sigma	HPA021660	WB/IF
UBE2U	Santa Cruz	sc-104725	WB
Ubiquitin	Santa Cruz	(P4D1): sc-8017	WB
ZO-1	Invitrogen	617300	WB/IF

Supplementary Table 5. List of primers.

Gene	Direction	Sequence (5' → 3')
PSA	Forward	GATGAAACAGGCTGTGCCG
	Reverse	CCTCACAGCTGCCCACTGCA
TMPRSS2:ERG	Forward	GAGCGCCGCCTGGAG
	Reverse	TAGGCACACTCAAACAACGACTG
18S	Forward	CGATGCGCCGGCGTTATT
	Reverse	CCTGGTGGTGCCCTTCCGT
Prostein	Forward	CGCCATCTCCCTGGTCTTC
	Reverse	CAGTGTCCCCTCGGTATTTG
FKBP1	Forward	AAAAGGCCAAGGAGCACAAC
	Reverse	TTGAGGAGGGGCCGAGTTC
UBE2U-1	Forward	CAGATGAGGAAGTGCCCAAGT
	Reverse	GCTCTTCCCCTATGCTGCT
UBE2U-2	Forward	CCTGAGGCATTTGGGGACAA
	Reverse	GAAGCTCATGCTCTTCCCCT
UBE2U-3*	Forward	CCTGAGGCATTTGGGGACAA
	Reverse	CCAAAATTGCTCCACAACGCT
UBE2U-4	Forward	CAGATGAGGAAGTGCCCAAGT
	Reverse	TCCAAAATTGCTCCACAACGC

Supplementary Table 6. Scores muRZ for Apoptosis and Cell Number, obtained during secondary screens. In red – scores above the threshold muRZ > 0,82, decreasing viability (increasing apoptosis or decreasing cell number). In gold - strongest scores RZ>1,5, decreasing viability (increasing apoptosis or decreasing cell number). In green –scores above the threshold muRZ > 0,82, increasing viability (decreasing apoptosis or increasing cell number).

	muRZ for apoptosis						muRZ for cell number					
siGene-№	**VCaP_ChSM**	**VCaP_StdM**	**DuCaP**	**PC3**	**LNCaP**	**RWPE1**	**VCaP_ChSM**	**VCaP_StdM**	**DuCaP**	**PC3**	**LNCaP**	**RWPE1**
AREL1-06	-1.39	0.14	-0.19	-0.86	0.10	-0.29	0.73	0.91	0.22	0.38	-0.21	0.09
AREL1-07	-0.03	**2.54**	**2.50**	**2.01**	0.67	**7.70**	0.31	-0.04	-0.44	-0.90	-0.71	-1.60
AREL1-08	0.46	0.02	0.09	-0.91	-0.30	0.07	0.61	0.10	-0.04	1.07	0.30	1.73
AREL1-09	-0.61	-0.22	0.01	-0.15	-0.65	0.33	-0.15	-0.05	0.31	0.25	0.38	-0.16
CACUL1-09	0.78	0.77	**5.41**	0.02	1.19	**35.80**	-0.13	0.40	-0.11	-1.27	-0.70	**-2.29**
CACUL1-10	**11.47**	**19.01**	**4.65**	-0.67	**4.08**	1.62	1.73	-0.72	-1.27	-0.35	1.03	-0.72
CACUL1-11	0.80	0.24	0.89	1.02	-0.10	0.08	0.08	1.37	0.01	0.08	0.72	0.90
CACUL1-12	-0.54	-0.26	-0.36	-1.08	0.09	-1.11	0.47	0.24	0.35	0.67	-0.43	0.51
CAND1-09	**2.29**	0.13	0.09	-0.12	**2.67**	0.96	0.87	-0.40	1.21	0.14	-0.31	1.28
CAND1-10	**2.23**	**4.22**	**6.97**	**2.04**	**21.77**	**21.55**	0.34	1.01	-1.19	-1.71	-0.50	-1.95
CAND1-11	-0.78	0.50	**3.88**	0.12	0.37	-0.28	0.78	1.25	-1.15	-0.77	-0.68	-1.75
CAND1-12	0.62	-0.09	-0.08	**2.43**	0.12	-1.01	0.25	0.15	0.82	0.50	0.11	0.66
siAllStars	0.15	0.07	0.16	0.21	-0.03	0.14	-1.02	-0.13	0.04	-0.09	0.82	0.25
siCellDeath	**14.30**	**21.97**	0.57	**40.35**	**47.09**	**75.56**	-1.04	-1.82	-1.34	**-3.20**	-1.90	**-3.43**
siERG	-0.46	-0.25	**4.52**	1.85	1.59	**27.59**	-1.39	-0.93	-1.21	-1.62	-1.09	**-2.61**
CUL2-05	-0.30	1.48	**2.40**	-0.20	0.56	-0.70	1.40	-0.35	-0.18	0.22	-0.21	-0.24
CUL2-06	0.23	-0.26	**2.57**	-0.83	-0.50	0.29	-0.70	-0.53	-0.35	1.08	-0.73	-0.24
CUL2-07	0.75	**3.88**	-0.17	**8.55**	-1.43	**22.35**	-0.44	-0.45	0.14	-0.48	0.10	-1.93
CUL2-08	0.54	1.17	0.07	-1.26	1.28	-0.48	0.87	0.01	0.43	1.05	-0.03	0.76
CUL4B-05	-0.21	-0.94	-0.24	-0.14	-0.37	-0.97	1.10	0.94	0.69	1.21	0.04	0.96
CUL4B-06	0.36	1.05	-0.62	-0.38	0.02	-0.35	-0.30	-0.65	1.97	0.26	-0.62	0.51
CUL4B-07	-0.67	-1.13	-0.09	**2.19**	0.03	0.57	-0.41	1.49	0.89	0.54	-0.38	0.07
CUL4B-08	-1.20	-0.05	-0.40	-0.46	-0.31	-1.20	1.58	0.60	0.90	1.23	0.18	0.74
DCUN1D3-05	-1.41	0.45	**2.80**	0.77	-0.75	-0.81	0.63	0.22	-0.42	1.01	-0.02	-0.10
DCUN1D3-06	**4.02**	**19.39**	**8.63**	1.21	**6.06**	**34.89**	1.39	-0.16	-0.56	-0.66	0.97	**-2.56**
DCUN1D3-07	-0.49	1.47	-0.19	-0.27	-0.53	-0.84	0.84	1.11	0.43	0.84	-0.15	0.34
DCUN1D3-08	-0.13	-0.45	-0.83	-0.37	-0.72	-1.08	-0.17	0.52	1.63	-0.38	0.41	0.93
DCUN1D5-09	-1.19	0.13	-0.41	-0.18	-0.55	-0.79	0.89	-0.02	1.42	0.80	-0.16	0.69
DCUN1D5-10	-0.73	0.16	-0.06	-0.56	-0.24	-0.77	0.31	0.24	1.21	1.35	-0.26	0.67
DCUN1D5-11	0.75	0.35	1.32	0.21	**7.77**	1.07	-0.52	0.45	0.24	-0.47	-0.08	-0.84
DCUN1D5-12	**5.92**	**4.05**	**7.88**	1.93	**7.43**	0.40	1.14	1.91	-0.97	-0.03	-0.26	-0.70
HERC2-09	1.34	1.93	0.06	-0.30	**6.21**	1.82	0.80	-0.31	0.09	0.10	-0.08	-0.70
HERC2-10	0.74	0.31	0.33	0.82	1.40	0.17	0.03	-1.31	-0.37	-1.05	0.02	0.94
HERC2-11	-1.40	-0.87	-0.37	0.12	-0.36	0.20	-0.33	-0.27	0.15	-0.44	-0.99	0.81
HERC2-12	-1.03	-0.43	0.62	-0.01	-0.20	-0.73	0.25	0.32	-0.71	0.21	1.11	1.23

HERC5-06	**4.34**	**11.38**	0.84	**2.45**	0.70	**4.62**	-0.25	-0.67	-0.64	-0.51	-0.46	-1.92
HERC5-07	-1.43	0.31	1.27	-0.55	0.24	-0.87	0.14	-0.48	-0.50	0.86	0.65	0.58
HERC5-08	-0.40	0.44	-0.07	0.32	0.09	0.07	-0.06	-0.65	0.71	-0.35	0.29	0.41
HERC5-09	-0.18	-1.05	1.38	-0.29	0.54	-1.55	0.80	**3.02**	-0.45	-0.08	-1.08	0.76
RBX1-07	-0.27	0.26	0.64	-0.03	0.05	-0.28	0.89	0.03	0.26	0.19	-0.45	-0.67
RBX1-08	-0.74	-0.85	1.48	0.42	-0.38	0.03	0.58	0.64	-0.70	-0.31	-0.80	-0.91
RBX1-09	-0.90	-0.31	-0.03	**2.27**	0.11	0.19	-0.96	-0.56	-0.31	-1.38	-0.88	-1.30
RBX1-10	-0.96	-0.99	-1.04	0.51	0.01	0.17	0.33	1.03	1.82	-0.45	-0.89	-0.87
RNF25-05	-0.70	-0.13	0.54	-0.26	-0.18	-1.02	0.22	0.24	0.06	-0.36	-0.67	1.02
RNF25-06	-0.67	0.44	-0.54	-0.94	-0.51	-0.47	0.48	-0.19	0.54	1.08	0.08	0.41
RNF25-07	-0.38	-0.23	0.09	-0.35	-0.41	-0.25	1.57	-0.22	0.22	0.97	0.29	0.32
RNF25-08	-0.77	-0.46	-1.07	-0.43	-0.77	-0.79	-0.84	0.56	1.07	-1.00	0.54	1.17
SAG-05	0.13	-0.81	-0.84	-0.07	-0.40	-0.75	-0.59	0.86	1.72	0.26	0.03	1.19
SAG-06	0.06	-0.41	-0.12	-0.72	0.13	-0.80	1.06	0.10	0.20	0.81	-0.26	0.85
SAG-07	-1.59	-1.06	-0.02	-1.01	-0.26	-0.35	0.38	0.80	-0.41	-0.72	-0.78	-0.27
SAG-08	0.47	0.93	-0.10	0.10	-0.10	-0.26	0.33	0.39	0.19	0.85	0.58	0.54
SPOP-08	0.48	0.74	-0.61	-0.24	-0.29	-0.56	0.00	0.08	0.57	0.82	-0.90	0.15
SPOP-09	-0.72	-0.36	-0.19	-0.82	0.47	-0.74	0.38	0.80	-0.45	1.40	-1.35	0.58
SPOP-10	-0.17	1.14	0.12	-0.28	0.48	1.40	-0.05	-0.98	0.83	0.06	1.62	0.30
SPOP-11	-0.35	-1.22	1.21	-0.74	-0.70	-0.73	-0.17	**2.16**	-0.11	-0.54	-0.18	0.63
UBA3-05	-1.47	0.65	**3.12**	-0.15	0.40	-0.35	1.68	0.22	-0.70	1.25	-0.73	-0.42
UBA3-06	-0.54	-0.58	-0.49	-0.61	-0.20	-0.72	0.18	0.18	0.79	0.54	0.18	1.05
UBA3-07	0.77	1.54	-0.59	0.01	-0.49	-1.06	0.19	-0.37	0.43	0.16	-0.09	-0.33
UBA3-08	0.22	0.12	**4.90**	0.76	**2.71**	0.00	-0.63	0.08	-1.01	-0.41	-0.51	-0.97
UBE2A-05	-0.46	-0.48	-0.54	-0.49	-1.12	-0.48	0.41	1.32	0.69	-0.03	**6.73**	0.74
UBE2A-06	-0.77	-0.50	-0.39	-0.56	-0.73	-0.60	-0.17	1.52	0.53	1.07	0.15	0.58
UBE2A-07	-0.82	-0.77	-0.94	-0.79	-0.69	0.16	0.06	0.42	0.18	-0.32	-0.26	-0.55
UBE2A-08	-0.43	-0.81	0.01	-0.99	-1.25	-0.97	-0.07	-0.13	-0.53	-0.36	**6.85**	0.60
UBE2D2-06	-0.37	-0.37	-0.81	-0.45	0.01	0.45	-0.71	-1.06	1.26	-0.36	-0.91	0.65
UBE2D2-07	**3.31**	**9.36**	**7.63**	0.97	**3.32**	**4.20**	0.44	0.81	-1.03	-0.33	-0.70	-1.59
UBE2D2-08	-1.10	-0.53	0.79	0.85	0.59	1.35	0.02	-1.61	-0.69	0.07	-0.80	-0.45
UBE2D2-09	-0.20	-0.65	-0.52	**2.44**	-0.21	-0.17	0.31	0.94	1.32	-0.17	0.62	-0.10
UBE2F-09	-0.47	0.08	0.00	0.81	-0.03	0.07	0.61	-0.50	1.04	0.44	0.46	0.13
UBE2F-10	-0.57	-0.06	-0.61	0.17	-0.31	-0.38	-0.34	-0.64	0.84	0.15	0.14	0.29
UBE2F-11	-0.23	0.62	1.78	1.57	-0.81	1.87	-1.84	-1.76	-1.21	-1.03	1.78	-1.66
UBE2F-12	-0.70	-0.03	-0.33	-0.51	-0.68	-0.96	1.66	0.25	0.75	1.02	0.66	0.50
UBE2G1-06	0.24	-0.49	0.67	-0.79	-0.52	-0.49	-0.33	-0.59	-0.24	0.48	-0.35	0.67
UBE2G1-07	-0.67	-0.44	-0.31	-0.72	0.55	-0.76	0.43	0.51	0.89	1.04	-0.08	0.46
UBE2G1-08	-0.01	-0.84	0.65	-0.38	-0.93	-0.02	0.36	0.15	0.65	1.14	1.03	-0.50
UBE2G1-09	-0.07	-0.70	-0.52	0.14	-0.21	-0.30	-1.26	-0.31	0.32	0.63	1.98	-0.62
UBE2H-05	**5.54**	**13.95**	**4.35**	0.42	1.77	**2.19**	1.91	0.76	-0.51	1.27	0.48	0.05
UBE2H-06	-0.36	-0.68	-0.59	-0.12	-1.22	-0.18	0.90	0.68	0.89	0.54	**5.43**	0.37
UBE2H-07	0.76	1.90	-0.09	-0.96	-0.09	-0.42	0.57	1.62	0.64	1.25	1.54	0.49
UBE2H-08	0.91	-0.36	1.56	0.53	0.03	1.68	-0.52	0.52	-1.29	-1.12	1.12	-1.60

UBE2J1-05	-0.91	-0.77	-0.50	-0.43	-0.81	0.13	-0.22	0.11	0.07	-0.30	**3.80**	-0.38
UBE2J1-06	0.40	-0.15	**3.10**	**2.75**	**3.44**	1.25	0.89	1.07	-0.97	-0.02	0.64	-1.44
UBE2J1-07	-0.97	-0.10	1.14	0.12	0.26	**9.31**	1.47	-0.33	-1.16	0.14	-0.63	-1.64
UBE2J1-08	**4.13**	0.29	-0.22	-0.56	0.05	0.93	-0.72	-0.59	0.51	-0.38	0.20	0.37
UBE2QL1-09	-0.57	-0.36	-0.32	-0.53	-0.68	-0.77	0.34	-0.08	0.75	-0.12	0.12	0.02
UBE2QL1-10	1.80	-0.08	**2.97**	-0.80	-0.44	0.25	0.81	1.96	0.58	0.21	1.51	-1.11
UBE2QL1-11	-0.85	-1.21	-0.56	-0.11	-0.33	-1.06	0.42	0.20	0.73	1.33	1.04	0.53
UBE2QL1-12	1.25	**6.12**	**3.44**	-0.43	**10.99**	**2.32**	0.43	-0.16	-0.22	-1.34	-1.84	-1.79
UBE2S-05	**2.69**	1.07	0.38	0.35	-0.69	**4.92**	-0.59	0.45	-1.22	1.50	1.56	-1.84
UBE2S-06	-0.02	-0.50	-0.43	1.25	-0.37	0.82	0.38	0.31	-0.20	0.34	**5.58**	-0.15
UBE2S-07	0.28	1.46	1.45	0.32	0.35	-0.07	0.07	1.91	0.96	0.55	-0.08	-0.35
UBE2S-08	1.47	1.40	-0.69	0.20	0.18	0.70	-0.83	-0.97	0.89	-0.17	-0.21	-0.69
UBE2U-09	-0.94	-0.40	-0.35	0.41	-0.29	-0.54	0.94	1.00	0.94	0.45	0.63	0.37
UBE2U-10	**3.12**	**3.73**	1.34	**4.96**	**3.72**	**32.69**	0.47	-0.47	-1.11	-1.25	-0.18	-1.95
UBE2U-11	1.43	0.56	**3.41**	-0.61	-0.14	**2.50**	1.04	0.64	-0.80	1.23	-0.17	-1.09
UBE2U-12	**6.47**	**3.83**	1.00	1.71	**14.26**	**2.44**	0.65	-0.50	-0.74	-0.53	-1.22	-1.73
UBE2W-07	-0.40	-0.43	-1.04	1.11	-0.46	-0.10	-0.17	-0.89	1.43	0.27	0.05	-0.02
UBE2W-08	**5.60**	1.76	**4.22**	**2.20**	**7.27**	**6.11**	0.05	-0.82	-1.01	0.91	-0.14	-0.42
UBE2W-09	-0.24	-0.99	-0.55	-0.47	-0.37	-0.30	0.22	1.13	0.82	0.08	0.58	0.57
UBE2W-10	-0.87	0.12	-0.38	-0.90	-0.36	-0.36	0.55	-0.19	1.05	0.83	1.31	0.20
UBR1-06	0.07	0.05	0.41	-0.46	-0.46	-0.29	-1.05	0.25	0.17	0.17	0.93	-0.28
UBR1-07	-0.46	0.44	-0.50	0.31	0.46	0.37	1.50	1.30	0.27	1.01	0.25	-0.10
UBR1-08	**7.37**	**6.75**	0.18	**2.12**	0.95	0.47	-0.60	0.48	-0.48	-0.55	1.08	-1.30
UBR1-09	0.00	0.77	-0.83	-0.10	-0.09	-0.42	1.14	-0.15	0.36	0.75	-0.03	-0.26
UBR3-05	-0.31	-0.56	-0.89	-0.15	0.87	-1.00	-0.69	0.27	-0.19	-0.36	1.33	-0.46
UBR3-06	-0.85	-1.06	-0.87	-0.67	-0.40	-0.85	1.41	0.45	0.82	1.15	-0.12	1.20
UBR3-07	**6.34**	**7.20**	**5.41**	**17.59**	**9.09**	**5.38**	-0.35	-0.85	-0.87	-1.00	-0.18	-1.19
UBR3-08	1.12	**3.06**	-0.36	-0.32	-0.19	-0.17	-0.27	-0.92	0.26	-0.19	0.24	-0.27
UBR4-09	-0.46	-0.84	-0.85	0.08	0.63	0.04	-0.42	0.14	1.31	0.35	0.37	0.10
UBR4-10	1.29	-0.40	-0.86	-0.03	0.20	-0.07	0.86	0.35	1.32	0.27	0.10	0.52
UBR4-11	-0.44	-0.44	-0.74	-0.63	-0.28	-0.62	1.75	0.31	0.76	0.32	-0.30	0.64
UBR4-12	0.32	-0.35	0.42	-0.53	-0.15	0.86	1.12	**3.51**	0.13	0.39	1.73	-0.85
UBR5-06	-0.08	0.51	-0.18	-0.69	-0.85	-0.55	-0.31	-0.43	-0.16	0.17	0.09	-0.24
UBR5-07	-0.99	-0.81	-0.95	0.13	-0.37	-0.60	-1.08	0.37	0.91	**2.29**	0.00	0.59
UBR5-08	-0.12	-0.92	-0.81	0.31	-0.04	-0.90	0.02	0.52	0.76	0.09	-0.05	1.12
UBR5-09	**2.02**	**2.55**	**2.55**	**2.30**	**2.45**	**33.06**	-0.49	-1.35	-0.81	-1.96	-1.18	**-3.05**

Supplementary Table 7. Summary of secondary screens. Designations: numerics - number of hit siRNAs causing the same phenotype. 2 to 3: means 2 hit above the threshold, and 1 more just below the threshold. 1 (but 07): 1 hit with the 'major' phenotype, but siRNA with catalogue number 07 is a hit in the other direction. In red - hits decreasing viability, in green - increasing viability. Colon "Overall" describes the "major" phenotype caused by the gene inhibition: death – more apoptosis, survival – less apoptosis, ↓/↑ in cells – decrease or increase of cell number comparing to control.

Gene	Overall	Consensus	VCaP	VCaP (StdM)	DuCaP	PC3	LNCaP	RWPE1	Comment
UBE2U	death	**All**	3 (but 09)	2	3	2	2	3	Extremely clear phenotype
CAND1	death	**All**	2 (to 3)	1	2	2	2	2 (but 12)	Extremely clear phenotype
UBE2H	death	Except PC3 and LNCaP	2 to 3	2	2	0 (but 07)	1 (but 08)	2	Potentially ERG-specific?
CUL4B	survival AND ↑ in cells	All except LNCaP	1 AND 2	2 (but 06) AND 2	0 AND 3 to 4	0 (but 07) AND 2	0 and 0	2 AND 1 to 2	weak but clear
UBE2A	survival AND ↑ in cells	All	0 to 2 AND 0	0 to 2 AND 2	1 AND 0	1 to 2 AND 1	2 to 4 AND 2	1 AND 0	weak but clear
RBX1	survival OR ↓ in cells	Just VCaP	2 to 3	2	1 (but 08) OR 0	0 (but 09) OR 1	0 OR 2 to 3	0 OR 3	Opposite phenotype for LNCaP and RWPE1
CUL2	death	VCaP & DuCaP	0 to 1	3	2	1 (but 08 & 06)	1 (but 07)	1	No effect for VCaP in ChSM (ERG suppressed?)
DCUN1D5	death OR ↑in cells	opposite phenotypes	1 to 2 OR 2	1 OR 1	2 OR 2	1 OR 1 to 2	2 OR 0	1 OR 0 to 2	2 siRNAs cause mostly apoptosis, and 2 others cause mostly increase in cell death
UBE2QL1	death	VCaP & DuCaP	2 (but 11)	1 (but 11)	2	0	1	1 (but 11)	Only 1 siRNA is strong -> off-target? For others effect is unclear
CACUL1	death	All except PC3?	1 to 3	1 to 2	3	1 (but 12)	2	2 (but 12)	Specific for AR-sensitive cells?
AREL1	no effect	All							only si07 kills cells - off-target
UBE2S	death	VCaP RWPE1	2	3	1	1	0	2	Rather unclear
DCUN1D3	death	No	1 but (05)	2	2 (but 08)	1 to 2	1 (but 3?)	1 (but 07,08)	Only si06 definitely causes death -> off-target?
HERC2	no effect	all							Only si07 definitely causes death -> off-target?
HERC5	death	Just DuCaP	1 (but 07)	1 (but 09)	3	1	0	1 (but 07 & 09)	
RNF25	no effect	All							
SAG	no effect	All							Not very clear
SPOP	no effect	All							
UBA3	no effect	All							
UBE2D2	death	RWPE1	1 (but 08)	1	1	1 to 3	1	2	Only si06 definitely causes death -> off-target?
UBE2F	no effect	all							
UBE2G1	no effect	all							
UBE2J1	death	DuCaP & RWPE1	1 (but 07&05)	0	2	1	1	3	
UBE2W	No effect	all							Only si08 causes death - off-target?
UBR1	No effect	all							Only si08 causes death - off-target?
UBR3	No effect	all							Only si08 causes death - off-target?
UBR4	No effect	all							
UBR5	No effect	all							Only si08 causes death - off-target?

VI. REFERENCES

1. Abbas T, Dutta A. CRL4Cdt2: master coordinator of cell cycle progression and genome stability. Cell Cycle. 2011 Jan 15;10(2):241-9.

2. Abidi N, Xirodimas DP. Regulation of cancer-related pathways by protein NEDDylation and strategies for the use of NEDD8 inhibitors in the clinic. Endocr Relat Cancer. 2015 Feb;22(1):T55-70.

3. Abou Zeid N, Vallés AM, Boyer B. Serine phosphorylation regulates paxillin turnover during cell migration. Cell Commun Signal. 2006 Nov 22;4:8.

4. Abrahamsson P A, Lilja H. Partial characterization of a thyreoid stimulating hormone-like peptide neuroendocrme cell of the human prostate gland. Prostate (1989), 14:71-81

5. Agalliu I, Gern R, Leanza S, Burk RD. (2009) Associations of high-grade prostate cancer with BRCA1 and BRCA2 founder mutations. Clin Cancer Res 15, 1112-20

6. Aichem A, Kalveram B, Spinnenhirn V, Kluge K, Catone N, Johansen T, Groettrup M. The proteomic analysis of endogenous FAT10 substrates identifies p62/SQSTM1 as a substrate of FAT10ylation. J Cell Sci. 2012 Oct 1;125(Pt 19):4576-85.

7. Alimirah F, Chen J, Basrawala Z, Xin H, Choubey D. DU-145 and PC-3 human prostate cancer cell lines express androgen receptor: implications for the androgen receptor functions and regulation. FEBS Lett. 2006 Apr 17;580(9):2294-300.

8. Ammirante M, Luo JL, Grivennikov S, Nedospasov S, Karin M. B-cell-derived lymphotoxin promotes castration-resistant prostate cancer. Nature. 2010 Mar 11;464(7286):302-5.

9. An J, Wang C, Deng Y, Yu L, Huang H. Destruction of full-length androgen receptor by wild-type SPOP, but not prostate-cancer-associated mutants. Cell Rep. 2014 Feb 27;6(4):657-69.

10. An JY, Kim E, Zakrzewska A, Yoo YD, Jang JM, Han DH, Lee MJ, Seo JW, Lee YJ, Kim TY, de Rooij DG, Kim BY, Kwon YT. UBR2 of the N-end rule pathway is required for chromosome stability via histone ubiquitylation in spermatocytes and somatic cells. PLoS One. 2012;7(5):e37414.

11. Antony L, van der Schoor F, Dalrymple SL, Isaacs JT. Androgen receptor (AR) suppresses normal human prostate epithelial cell proliferation via AR/β-catenin/TCF-4 complex inhibition of c-MYC transcription. Prostate. 2014 Aug;74(11):1118-31.

12. Armah HB and Parwani AV. Atypical adenomatous hyperplasia (adenosis) of the prostate: a case report with review of the literature. (2008) Diagn Pathol, 3:34.

13. Attard G, Clark J, Ambroisine L, Fisher G, Kovacs G, Flohr P, Berney D, Foster CS, Fletcher A, Gerald WL, Moller H, Reuter V, De Bono JS, Scardino P, Cuzick J, Cooper CS; Transatlantic Prostate Group. Duplication of the fusion of TMPRSS2 to ERG sequences identifies fatal human prostate cancer. Oncogene. 2008 Jan 10;27(3):253-63.

14. Barbieri CE, Baca SC, Lawrence MS, Demichelis F, Blattner M, Theurillat JP, White TA, Stojanov P, Van Allen E, Stransky N, Nickerson E, Chae SS, Boysen G, Auclair D, Onofrio RC, Park K, Kitabayashi N, MacDonald TY, Sheikh K, Vuong T, Guiducci C, Cibulskis K, Sivachenko A, Carter SL, Saksena G, Voet D, Hussain WM, Ramos AH, Winckler W, Redman MC, Ardlie K, Tewari AK, Mosquera JM, Rupp N, Wild PJ,

Moch H, Morrissey C, Nelson PS, Kantoff PW, Gabriel SB, Golub TR, Meyerson M, Lander ES, Getz G, Rubin MA, Garraway LA. Exome sequencing identifies recurrent SPOP, FOXA1 and MED12 mutations in prostate cancer. Nat Genet. 2012 May 20;44(6):685-9.

15. Bardan R., Bucuras V., Dema A., Botoca M. Prostate Cancer: Epidemiology, Etiology, Pathology, Diagnosis and Prognosis. TMJ 2007, 57 (2 – 3):200-210

16. Barkley LR, Palle K, Durando M, Day TA, Gurkar A, Kakusho N, Li J, Masai H, Vaziri C. c-Jun N-terminal kinase-mediated Rad18 phosphorylation facilitates Polη recruitment to stalled replication forks. Mol Biol Cell. 2012 May;23(10):1943-54.

17. Bastus NC, Boyd LK, Mao X, Stankiewicz E, Kudahetti SC, Oliver RT, Berney DM, Lu YJ. Androgen-induced TMPRSS2:ERG fusion in nonmalignant prostate epithelial cells. Cancer Res. 2010 Dec 1;70(23):9544-8.

18. Bataineh ZM, Habbal O. Immunoreactivity of ubiquitin in human prostate gland. Neuro Endocrinol Lett. 2006 Aug;27(4):517-22.

19. Bedford L, Lowe J, Dick LR, Mayer RJ, Brownell JE. Ubiquitin-like protein conjugation and the ubiquitin-proteasome system as drug targets. Nat Rev Drug Discov. 2011 Jan;10(1):29-46.

20. Berg KD, Vainer B, Thomsen FB, Røder MA, Gerds TA, Toft BG, Brasso K, Iversen P. ERG protein expression in diagnostic specimens is associated with increased risk of progression during active surveillance for prostate cancer. Eur Urol. 2014 Nov;66(5):851-60.

21. Berger MF, Lawrence MS, Demichelis F, Drier Y, Cibulskis K, Sivachenko AY, Sboner A, Esgueva R, Pflueger D, Sougnez C, Onofrio R, Carter SL, Park K, Habegger L, Ambrogio L, Fennell T, Parkin M, Saksena G, Voet D, Ramos AH, Pugh TJ, Wilkinson J, Fisher S, Winckler W, Mahan S, Ardlie K, Baldwin J, Simons JW, Kitabayashi N, MacDonald TY, Kantoff PW, Chin L, Gabriel SB, Gerstein MB, Golub TR, Meyerson M, Tewari A, Lander ES, Getz G, Rubin MA, Garraway LA. (2011) The genomic complexity of primary human prostate cancer. Nature 470, 214-20.

22. Bergink S. and Jentsch S. (2009) Principles of ubiquitin and SUMO modifications in DNA repair. Nature 458, 461-7

23. Bernassola F, Karin M, Ciechanover A, Melino G. (2008) The HECT family of E3 ubiquitin ligases: multiple players in cancer development. Cancer Cell, 14(1):10-21.

24. Birdsey GM, Dryden NH, Amsellem V, Gebhardt F, Sahnan K, Haskard DO, Dejana E, Mason JC, Randi AM. Transcription factor Erg regulates angiogenesis and endothelial apoptosis through VE-cadherin. Blood. 2008 Apr 1;111(7):3498-506.

25. Birdsey GM, Shah AV, Dufton N, Reynolds LE, Osuna Almagro L, Yang Y, Aspalter IM, Khan ST, Mason JC, Dejana E, Göttgens B, Hodivala-Dilke K, Gerhardt H, Adams RH, Randi AM. The endothelial transcription factor ERG promotes vascular stability and growth through Wnt/β-catenin signaling. Dev Cell. 2015 Jan 12;32(1):82-96.

26. Birmingham A, Selfors LM, Forster T, Wrobel D, Kennedy CJ, Shanks E, Santoyo-Lopez J, Dunican DJ, Long A, Kelleher D, Smith Q, Beijersbergen RL, Ghazal P, Shamu CE. Statistical methods for analysis of high-throughput RNA interference screens. Nat Methods. 2009 Aug;6(8):569-75.

27. Borchert GM, Lanier W, Davidson BL. RNA polymerase III transcribes human microRNAs. Nat Struct Mol Biol. 2006 Dec;13(12):1097-101.

28. Boutros PC, Fraser M, Harding NJ, de Borja R, Trudel D, Lalonde E, Meng A, Hennings-Yeomans PH, McPherson A, Sabelnykova VY, *et al.*, Bristow RG. Spatial genomic heterogeneity within localized, multifocal prostate cancer. Nat Genet. 2015 May 25.

29. Bowerman B. Cytokinesis in the C. elegans embryo: regulating contractile forces and a late role for the central spindle. Cell Struct Funct. 2001 Dec;26(6):603-7.

30. Boysen G, Barbieri CE, Prandi D, Blattner M, Chae SS, Dahija A, Nataraj S, Huang D, Marotz C, Xu L, Huang J, Lecca P, Chhangawala S, Liu D, Zhou P, Sboner A, de Bono JS, Demichelis F, Houvras Y, Rubin MA. SPOP mutation leads to genomic instability in prostate cancer. Elife. 2015 Sep 16;4. pii: e09207

31. Broemer M, Tenev T, Rigbolt KT, Hempel S, Blagoev B, Silke J, Ditzel M, Meier P. Systematic in vivo RNAi analysis identifies IAPs as NEDD8-E3 ligases. Mol Cell. 2010 Dec 10;40(5):810-22.

32. Brower CS, Sato S, Tomomori-Sato C, Kamura T, Pause A, Stearman R, Klausner RD, Malik S, Lane WS, Sorokina I, Roeder RG, Conaway JW, Conaway RC. Mammalian mediator subunit mMED8 is an Elongin BC-interacting protein that can assemble with Cul2 and RBX1 to reconstitute a ubiquitin ligase. Proc Natl Acad Sci U S A. 2002 Aug 6;99(16):10353-8.

33. Brownell JE, Sintchak MD, Gavin JM, Liao H, Bruzzese FJ, Bump NJ, Soucy TA, Milhollen MA, Yang X, Burkhardt AL, Ma J, Loke HK, Lingaraj T, Wu D, Hamman KB, Spelman JJ, Cullis CA, Langston SP, Vyskocil S, Sells TB, Mallender WD, Visiers I, Li P, Claiborne CF, Rolfe M, Bolen JB, Dick LR. Substrate-assisted inhibition of ubiquitin-like protein-activating enzymes: the NEDD8 E1 inhibitor MLN4924 forms a NEDD8-AMP mimetic in situ. Mol Cell. 2010 Jan 15;37(1):102-11.

34. Burleson KM, Boente MP, Pambuccian SE, Skubitz AP. Disaggregation and invasion of ovarian carcinoma ascites spheroids. J Transl Med. 2006 Jan 24;4:6.

35. Caffrey DR, Zhao J, Song Z, Schaffer ME, Haney SA, Subramanian RR, Seymour AB, Hughes JD. siRNA off-target effects can be reduced at concentrations that match their individual potency. PLoS One. 2011;6(7):e21503

36. Caplen NJ, Parrish S, Imani F, Fire A, Morgan RA. Specific inhibition of gene expression by small double-stranded RNAs in invertebrate and vertebrate systems. Proc Natl Acad Sci U S A. 2001 Aug 14;98(17):9742-7.

37. Carter HB. Assessing Risk: Does This Patient Have Prostate Cancer? (Editorial). Journal of the National Cancer Institute. 2006, 98 (8): 506–7.

38. Carter P. Preparation of ligand-free human serum for radioimmunoassay by adsorption on activated charcoal. Clin Chem. 1978 Feb;24(2):362-4.

39. Carver BS, Tran J, Gopalan A, Chen Z, Shaikh S, Carracedo A, Alimonti A, Nardella C, Varmeh S, Scardino PT, Cordon-Cardo C, Gerald W, Pandolfi PP. Aberrant ERG expression cooperates with loss of PTEN to promote cancer progression in the prostate. Nat Genet. 2009 May;41(5):619-24.

40. Chairatvit K, Ngamkitidechakul C. Control of cell proliferation via elevated NEDD8 conjugation in oral squamous cell carcinoma. Mol Cell Biochem. 2007 Dec;306(1-2):163-9.

41. Chatterjee P, Choudhary GS, Alswillah T, Xiong X, Heston WD, Magi-Galuzzi C, Zhang J, Klein EA, Almasan A8 The TMPRSS2-ERG gene fusion blocks XRCC4-mediated non-homologous end-joining repair and radiosensitizes prostate cancer cells to PARP inhibition. Mol Cancer Ther. 2015 May 29.

42. Chen C, Seth AK, Aplin AE. Genetic and expression aberrations of E3 ubiquitin ligases in human breast cancer. Mol Cancer Res. 2006 Oct;4(10):695-707.

43. Chen C., Sun X, Guo P, Dong XY, Sethi P, Zhou W, Zhou Z, Petros J, Frierson HF Jr, Vessella RL, Atfi A, Dong JT. 2007 Ubiquitin E3 ligase WWP1 as an oncogenic factor in human prostate cancer. Oncogene 26, 2386-94.

44. Chen CD, Sawyers CL. NF-kappa B activates prostate-specific antigen expression and is upregulated in androgen-independent prostate cancer. Mol Cell Biol. 2002 Apr;22(8):2862-70.

45. Chen S, Wang C, Sun L, Wang DL, Chen L, Huang Z, Yang Q, Gao J, Yang XB, Chang JF, Chen P, Lan L, Mao Z, Sun FL. RAD6 promotes homologous recombination repair by activating the autophagy-mediated degradation of heterochromatin protein HP1. Mol Cell Biol. 2015 (a) Jan;35(2):406-16.

46. Chen S, Wang DL, Liu Y, Zhao L, Sun FL. RAD6 regulates the dosage of p53 by a combination of transcriptional and posttranscriptional mechanisms. Mol Cell Biol. 2012 Jan;32(2):576-87.

47. Chen TJ, Gao F, Yang T, Thakur A, Ren H, Li Y, Zhang S, Wang T, Chen MW. CDK-associated Cullin 1 promotes cell proliferation with activation of ERK1/2 in human lung cancer A549 cells. Biochem Biophys Res Commun. 2013 Jul 19;437(1):108-13.

48. Chen X, Wang Y, Zang W, Du Y, Li M, Zhao G. miR-194 targets RBX1 gene to modulate proliferation and migration of gastric cancer cells. Tumour Biol. 2015 (b) Apr;36(4):2393-401.

49. Chen Z, Shen BL, Fu QG, Wang F, Tang YX, Hou CL, Chen L. CUL4B promotes proliferation and inhibits apoptosis of human osteosarcoma cells. Oncol Rep. 2014 Nov;32(5):2047-53.

50. Chesire DR, Isaacs WB. Ligand-dependent inhibition of beta-catenin/TCF signaling by androgen receptor. Oncogene. 2002 Dec 5;21(55):8453-69.

51. Chiu YL, Rana TM. RNAi in human cells: basic structural and functional features of small interfering RNA. Mol Cell. 2002 Sep;10(3):549-61.

52. Chiu YT, Liu J, Tang K, Wong YC, Khanna KK, Ling MT. Inactivation of ATM/ATR DNA damage checkpoint promotes androgen induced chromosomal instability in prostate epithelial cells. PLoS One. 2012;7(12):e51108.

53. Cindolo L., Cantile M, Vacherot F, Terry S, de la Taille A.. (2007) Neuroendocrine differentiation in prostate cancer: from lab to bedside. Urol Int 79, 287-96.

54. Cogoni C, Macino G. Isolation of quelling-defective (qde) mutants impaired in posttranscriptional transgene-induced gene silencing in Neurospora crassa. Proc Natl Acad Sci U S A. 1997 Sep 16;94(19):10233-8.

55. Cole AJ, Clifton-Bligh R, Marsh DJ. Histone H2B monoubiquitination: roles to play in human malignancy. Endocr Relat Cancer. 2015 Feb;22(1):T19-33.

56. Conforti F, Yang AL, Piro MC, Mellone M, Terrinoni A, Candi E, Tucci P, Thomas GJ, Knight RA, Melino G, Sayan BS. PIR2/Rnf144B regulates epithelial homeostasis by mediating degradation of p21WAF1 and p63. Oncogene. 2013 Oct;32(40):4758-65.

57. Cooper GM. The Cell, 2nd edition. A Molecular Approach. Sunderland (MA): Sinauer Associates; 2000.

58. David JM, Rajasekaran AK. Dishonorable discharge: the oncogenic roles of cleaved E-cadherin fragments. Cancer Res. 2012 Jun 15;72(12):2917-23.

59. Davis NS. Determination of serotonin and 5-hydroxymdoleacetic acid in guinea pig and human prostate using HPLC. 1987, Prostate, 11:353-360

60. de Lange P, van Blokland R, Kooter JM, Mol JN. Suppression of flavonoid flower pigmentation genes in Petunia hybrida by the introduction of antisense and sense genes. Curr Top Microbiol Immunol. 1995;197:57-75.

61. De Marzo AM, Platz EA, Sutcliffe S, Xu J, Grönberg H, Drake CG, Nakai Y, Isaacs WB, Nelson WG. Inflammation in prostate carcinogenesis. Nat Rev Cancer. 2007 Apr;7(4):256-69.

62. de Miranda NF, Georgiou K, Chen L, Wu C, Gao Z, Zaravinos A, Lisboa S, Enblad G, Teixeira MR, Zeng Y, Peng R, Pan-Hammarström Q. Exome sequencing reveals novel mutation targets in diffuse large B-cell lymphomas derived from Chinese patients. Blood. 2014 Oct 16;124(16):2544-53.

63. Debacq-Chainiaux F, Erusalimsky JD, Campisi J, Toussaint O. Protocols to detect senescence-associated beta-galactosidase (SA-betagal) activity, a biomarker of senescent cells in culture and in vivo. Nat Protoc. 2009;4(12):1798-806.

64. Demichelis F, Fall K, Perner S, Andrén O, Schmidt F, Setlur SR, Hoshida Y, Mosquera JM, Pawitan Y, Lee C, Adami HO, Mucci LA, Kantoff PW, Andersson SO, Chinnaiyan AM, Johansson JE, Rubin MA. TMPRSS2:ERG gene fusion associated with lethal prostate cancer in a watchful waiting cohort. Oncogene. 2007 Jul 5;26(31):4596-9.

65. Denli A.M., Tops B.B., Plasterk R.H., Ketting R.F., Hannon G.J. Processing of primary microRNAs by the Microprocessor complex. Nature. 2004;432(7014):231-5.

66. Deshaies R. J. and Joazeiro C.A.P. (2009) RING domain E3 ubiquitin ligases. Annu Rev Biochem 78, 399–434;

67. Didier C, Broday L, Bhoumik A, Israeli S, Takahashi S, Nakayama K, Thomas SM, Turner CE, Henderson S, Sabe H, Ronai Z. RNF5, a RING finger protein that regulates cell motility by targeting paxillin ubiquitination and altered localization. Mol Cell Biol. 2003 Aug;23(15):5331-45.

68. Diniz MG, de Fatima Correia Silva J, de Souza FT, Pereira NB, Gomes CC, Gomez RS. Association between cell cycle gene transcription and tumor size in oral squamous cell carcinoma. Tumour Biol. 2015 Jul 9. [Epub ahead of print]

69. Don Chen J. Obstructing Androgen Receptor Activation in Prostate Cancer Cells through Posttranslational Modification by NEDD8. Application for grant. May 2009. Award Number: W81XWH-08-1-0143

70. Dong J, Wang XQ, Yao JJ, Li G, Li XG. Decreased CUL4B expression inhibits malignant proliferation of glioma in vitro and in vivo. Eur Rev Med Pharmacol Sci. 2015;19(6):1013-21.

71. Doronkin S, Djagaeva I, Beckendorf SK. The COP9 signalosome promotes degradation of Cyclin E during early Drosophila oogenesis. Dev Cell. 2003 May;4(5):699-710.

72. Doyle JM, Gao J, Wang J, Yang M, Potts PR. MAGE-RING protein complexes comprise a family of E3 ubiquitin ligases. Mol Cell. 2010 Sep 24;39(6):963-74.

73. Du D, Xu F, Yu L, Zhang C, Lu X, Yuan H, Huang Q, Zhang F, Bao H, Jia L, Wu X, Zhu X, Zhang X, Zhang Z, Chen Z. The tight junction protein, occludin, regulates the directional migration of epithelial cells. Dev Cell. 2010 Jan 19;18(1):52-63.

74. Duda DM, Scott DC, Calabrese MF, Zimmerman ES, Zheng N, Schulman BA. Structural regulation of cullin-RING ubiquitin ligase complexes. Curr Opin Struct Biol. 2011 Apr;21(2):257-64.

75. Duskova K, Vesely S. Prostate Specific Antigen. Current clinical application and future prospects. Biomed Pap Med Fac Univ Palacky Olomouc Czech Repub. 2014 Oct 2.

76. Edwards BK, Noone AM, Mariotto AB, Simard EP, Boscoe FP, Henley SJ, Jemal A, Cho H, Anderson RN, Kohler BA, Eheman CR, Ward EM. Annual Report to the Nation on the status of cancer, 1975-2010, featuring prevalence of comorbidity and impact on survival among persons with lung, colorectal, breast, or prostate cancer. Cancer. 2014 May 1;120(9):1290-314.

77. Eisenhaber B, Chumak N, Eisenhaber F, Hauser MT. The ring between ring fingers (RBR) protein family. Genome Biol. 2007;8(3):209.

78. Elbashir SM, Harborth J, Weber K, Tuschl T. Analysis of gene function in somatic mammalian cells using small interfering RNAs. Methods. 2002 Feb;26(2):199-213

79. Elledge S. Identification of Genes Required for the Survival of Prostate Cancer Cells. Annual report for Brigham and Women's Hospital, Boston. 2010 June

80. Enchev RI, Schulman BA, Peter M. Protein neddylation: beyond cullin-RING ligases. Nat Rev Mol Cell Biol. 2014 Dec 22;16(1):30-44.

81. Evans JC, McCarthy J, Torres-Fuentes C, Cryan JF, Ogier J, Darcy R, Watson RW, O'Driscoll CM. Cyclodextrin mediated delivery of NF-κB and SRF siRNA reduces the invasion potential of prostate cancer cells in vitro. Gene Ther. 2015 Oct;22(10):802-10.

82. Fan M, Bigsby RM, Nephew KP. The NEDD8 pathway is required for proteasome-mediated degradation of human estrogen receptor (ER)-alpha and essential for the antiproliferative activity of ICI 182,780 in ERalpha-positive breast cancer cells. Mol Endocrinol. 2003 Mar;17(3):356-65.

83. Fan M, Long X, Bailey JA, Reed CA, Osborne E, Gize EA, Kirk EA, Bigsby RM, Nephew KP. The activating enzyme of NEDD8 inhibits steroid receptor function. Mol Endocrinol. 2002 Feb;16(2):315-30.

84. Feldman B.J. and Feldman D. (2001) The development of androgen-independent prostate cancer. Nat Rev Cancer 1, 34-45.

85. Fiorini C, Gilleron J, Carette D, Valette A, Tilloy A, Chevalier S, Segretain D, Pointis G. Accelerated internalization of junctional membrane proteins (connexin 43, N-cadherin and ZO-1) within endocytic vacuoles: an early event of DDT carcinogenicity. Biochim Biophys Acta. 2008 Jan;1778(1):56-67.

86. Fire A, Xu S, Montgomery MK, Kostas SA, Driver SE, Mello CC. Potent and specific genetic interference by double-stranded RNA in Caenorhabditis elegans. Nature. 1998 Feb 19;391(6669):806-11.

87. Fletcher SJ, Iqbal M, Jabbari S, Stekel D, Rappoport JZ. Analysis of occludin trafficking, demonstrating continuous endocytosis, degradation, recycling and biosynthetic secretory trafficking. PLoS One. 2014 Nov 25;9(11):e111176.

88. Fletcher SJ, Poulter NS, Haining EJ, Rappoport JZ. Clathrin-mediated endocytosis regulates occludin, and not focal adhesion, distribution during epithelial wound healing. Biol Cell. 2012 Apr;104(4):238-56.

89. Florecki MM, Hartfelder K. Unconventional Cadherin Localization in Honey Bee Gonads Revealed Through Domain-Specific Apis mellifera E- and N-Cadherin Antibodies Indicates Alternative Functions. Insects. 2012, 3(4), 1200-1219

90. Fu B, Wang L, Ding H, Schwamborn JC, Li S, Dorf ME. TRIM32 Senses and Restricts Influenza A Virus by Ubiquitination of PB1 Polymerase. PLoS Pathog. 2015 Jun 9;11(6):e1004960.

91. Fu W, Hall JE, Schaller MD. Focal adhesion kinase-regulated signaling events in human cancer. Biomol Concepts. 2012 Jun;3(3):225-40.

92. Galluzzi L, Kepp O, Vander Heiden MG, Kroemer G. Metabolic targets for cancer therapy. Nature Reviews Drug Discovery 2013 12, 829–846

93. García-Flores M, Casanova-Salas I, Rubio-Briones J, Calatrava A, Domínguez-Escrig J, Rubio L, Ramírez-Backhaus M, Fernández-Serra A, García-Casado Z, López-Guerrero JA. Clinico-pathological significance of the molecular alterations of the SPOP gene in prostate cancer. Eur J Cancer. 2014 Nov;50(17):2994-3002.

94. Gavrilov K, Saltzman WM. Therapeutic siRNA: principles, challenges, and strategies. Yale J Biol Med. 2012 Jun;85(2):187-200.

95. Gleason DF. Classification of prostatic carcinomas. Cancer Chemother Rep 1966; 50(3):125-8.

96. Glickman MH, Ciechanover A. The ubiquitin-proteasome proteolytic pathway: destruction for the sake of construction. Physiol Rev. 2002 Apr;82(2):373-428.

97. Golubovskaya VM, Finch R, Cance WG. Direct interaction of the N-terminal domain of focal adhesion kinase with the N-terminal transactivation domain of p53. J Biol Chem. 2005 Jul 1;280(26):25008-21.

98. Golubovskaya VM, Finch R, Kweh F, Massoll NA, Campbell-Thompson M, Wallace MR, Cance WG. p53 regulates FAK expression in human tumor cells. Mol Carcinog. 2008 May;47(5):373-82.

99. Greenman C, Stephens P, Smith R, Dalgliesh GL, Hunter C, Bignell G, Davies H, Teague J, Butler A, Stevens C, Edkins S, O'Meara S, Vastrik I, Schmidt EE, Avis T, Barthorpe S, Bhamra G, Buck G, Choudhury B, Clements J, Cole J, Dicks E, Forbes S, Gray K, Halliday K, Harrison R, Hills K, Hinton J, Jenkinson A, Jones D, Menzies A, Mironenko T, Perry J, Raine K, Richardson D, Shepherd R, Small A, Tofts C, Varian J, Webb T, West S, Widaa S, Yates A, Cahill DP, Louis DN, Goldstraw P, Nicholson AG, Brasseur F, Looijenga L, Weber BL, Chiew YE, DeFazio A, Greaves MF, Green AR, Campbell P, Birney E, Easton DF, Chenevix-Trench G, Tan MH, Khoo SK, Teh BT, Yuen ST, Leung SY, Wooster R, Futreal PA, Stratton MR. Patterns of somatic mutation in human cancer genomes. Nature. 2007 Mar 8;446(7132):153-8.

100. Gregory CW, Hamil KG, Kim D, Hall SH, Pretlow TG, Mohler JL, French FS. 1998. Androgen receptor expression in androgen-independent prostate cancer is associated with increased expression of androgen-regulated genes. Cancer Res 58: 5718–5724.

101. Grieve AG, Rabouille C. Extracellular cleavage of E-cadherin promotes epithelial cell extrusion. J Cell Sci. 2014 Aug 1;127(Pt 15):3331-46.

102. Grosshans H, Slack FJ. Micro-RNAs: small is plentiful. J Cell Biol. 2002 Jan 7;156(1):17-21.

103. Gu G., Yuan J, Wills M, Kasper S. (2007) Prostate cancer cells with stem cell characteristics reconstitute the original human tumor in vivo. Cancer Res 67, 4807–15;

104. Guerrero-Santoro J, Kapetanaki MG, Hsieh CL, Gorbachinsky I, Levine AS, Rapić-Otrin V. The cullin 4B-based UV-damaged DNA-binding protein ligase binds to UV-damaged chromatin and ubiquitinates histone H2A. Cancer Res. 2008 Jul 1;68(13):5014-22.

105. Gupta S, Iljin K, Sara H, Mpindi JP, Mirtti T, Vainio P, Rantala J, Alanen K, Nees M, Kallioniemi O. FZD4 as a mediator of ERG oncogene-induced WNT signaling and epithelial-to-mesenchymal transition in human prostate cancer cells. Cancer Res. 2010 Sep 1;70(17):6735-45.

106. Haasnoot J, Westerhout EM, Berkhout B. Nat Biotechnol. 2007 Dec;25(12):1435-43. RNA interference against viruses: strike and counterstrike.

107. Hägglöf C, Hammarsten P, Strömvall K, Egevad L, Josefsson A, Stattin P, Granfors T, Bergh A. TMPRSS2-ERG expression predicts prostate cancer survival and associates with stromal biomarkers. PLoS One. 2014 Feb 5;9(2):e86824.

108. Hahn P, Dennig J, Bielke W, Kang J. United States Patent. Positive controls for expression modulating experiments. № US 8,470,998 B2. Date of patent: Jun. 25, 2013. Assignee: Qiagen GmbH

109. Hamilton AJ, Baulcombe DC. A species of small antisense RNA in posttranscriptional gene silencing in plants. Science. 1999 Oct 29;286(5441):950-2.

110. Hamilton G. Multicellular spheroids as an in vitro tumor model. Cancer Lett. 1998 Sep 11;131(1):29-34.

111. Han AL, Kumar S, Fok JY, Tyagi AK, Mehta K. Tissue transglutaminase expression promotes castration-resistant phenotype and transcriptional repression of androgen receptor. Eur J Cancer. 2014 Jun;50(9):1685-96.

112. Hanahan D. and Weinberg R.A. The Hallmarks of Cancer. (2000) Cell, Vol. 100, 57–70.

113. Härmä V, Virtanen J, Mäkelä R, Happonen A, Mpindi JP, Knuuttila M, Kohonen P, Lötjönen J, Kallioniemi O, Nees M. A comprehensive panel of three-dimensional models for studies of prostate cancer growth, invasion and drug responses. PLoS One. 2010 May 3;5(5):e10431.

114. Harper JW. Neddylating the guardian; Mdm2 catalyzed conjugation of NEDD8 to p53. Cell. 2004 Jul 9;118(1):2-4.

115. Hartsock A, Nelson WJ. Adherens and tight junctions: structure, function and connections to the actin cytoskeleton. Biochim Biophys Acta. 2008 Mar;1778(3):660-9.

116. Havens CG, Walter JC. Mechanism of CRL4(Cdt2), a PCNA-dependent E3 ubiquitin ligase. Genes Dev. 2011 Aug 1;25(15):1568-82.

117. Heinlein C.A. and Chang C. (2004) Androgen receptor in prostate cancer. Endocr Rev 25, 276-308

118. Herrmann J, Lerman L, Lerman A. Ubiquitin and ubiquitin-like proteins in protein regulation. Circ Res. 2007 May 11;100(9):1276-91.

119. Hjerpe R, Thomas Y, Chen J, Zemla A, Curran S, Shpiro N, Dick LR, Kurz T. Changes in the ratio of free NEDD8 to ubiquitin triggers NEDDylation by ubiquitin enzymes. Biochem J. 2012 Feb 1;441(3):927-36.

120. Hochstrasser M. (2009) Origin and function of ubiquitin-like proteins. Nature 458, 422-9.

121. Holohan C, Van Schaeybroeck S, Longley DB, Johnston PG. Cancer drug resistance: an evolving paradigm. Nat Rev Cancer. 2013 Oct;13(10):714-26

122. Hu H, Yang Y, Ji Q, Zhao W, Jiang B, Liu R, Yuan J, Liu Q, Li X, Zou Y, Shao C, Shang Y, Wang Y, Gong Y. CRL4B catalyzes H2AK119 monoubiquitination and coordinates with PRC2 to promote tumorigenesis. Cancer Cell. 2012 Dec 11;22(6):781-95.

123. Hu WS, Pathak VK. Design of retroviral vectors and helper cells for gene therapy. Pharmacol Rev. 2000 Dec;52(4):493-511.

124. Huang DT, Ayrault O, Hunt HW, Taherbhoy AM, Duda DM, Scott DC, Borg LA, Neale G, Murray PJ, Roussel MF, Schulman BA. E2-RING expansion of the NEDD8 cascade confers specificity to cullin modification. Mol Cell. 2009 Feb 27;33(4):483-95.

125. Huang G, Stock C, Bommeljé CC, Weeda VB, Shah K, Bains S, Buss E, Shaha M, Rechler W, Ramanathan SY, Singh B. SCCRO3 (DCUN1D3) antagonizes the neddylation and oncogenic activity of SCCRO (DCUN1D1). J Biol Chem. 2014 Dec 12;289(50):34728-42. doi: 10.1074/jbc.M114.585505.

126. Huang J, Xu LG, Liu T, Zhai Z, Shu HB. The p53-inducible E3 ubiquitin ligase p53RFP induces p53-dependent apoptosis. FEBS Lett. 2006 Feb 6;580(3):940-7.

127. Huggins C and Hodges CV. 2002. The Effect of Castration, of Estrogen and of Androgen Injection on Serum Phosphatases in Metastatic Carcinoma of the Prostate. Journal of Urology. Vol. 168, 9-12. (Reprint permission from Cancer Res, 1:293-297, 1941.)

128. Huotari J, Meyer-Schaller N, Hubner M, Stauffer S, Katheder N, Horvath P, Mancini R, Helenius A, Peter M. Cullin-3 regulates late endosome maturation. Proc Natl Acad Sci U S A. 2012 Jan 17;109(3):823-8.

129. Iioka H, Iemura S, Natsume T, Kinoshita N. Wnt signalling regulates paxillin ubiquitination essential for mesodermal cell motility. Nat Cell Biol. 2007 Jul;9(7):813-21.

130. Indovina P, Rainaldi G, Santini MT. Hypoxia increases adhesion and spreading of MG-63 three-dimensional tumor spheroids. Anticancer Res. 2008 Mar-Apr;28(2A):1013-22.

131. Isaacs J.T. and Coffey D.S. (1981) Adaptation versus selection as the mechanism responsible for the relapse of prostatic cancer to androgen ablation therapy as studied in the Dunning R-3327-H adenocarcinoma. Cancer Res 41, 5070-5.

132. Iwai K, Fujita H, Sasaki Y. Linear ubiquitin chains: NF-κB signalling, cell death and beyond. Nat Rev Mol Cell Biol. 2014 Aug;15(8):503-8.

133. Izant J., Weintraub H. Inhibition of thymidine kinase gene expression by antisense RNA: a molecular approach to genetic analysis. Cell 36, 1007–1015 (1984).

134. Jackson A, Burchard J, Schelter J, Chau N, Cleary M, Lim L, and Linsley PS. Widespread siRNA "off-target" transcript silencing mediated by seed region sequence complementarity. RNA. 2006 Jul; 12(7): 1179–1187.

135. Jemal A, Bray F, Center MM, Ferlay J, Ward E, Forman D. Global cancer statistics. CA Cancer J Clin. 2011 Mar-Apr;61(2):69-90.

136. Jia L, Li H, Sun Y. Induction of p21-dependent senescence by an NAE inhibitor, MLN4924, as a mechanism of growth suppression. Neoplasia. 2011 Jun;13(6):561-9.

137. Jia L, Soengas MS, Sun Y. ROC1/RBX1 E3 ubiquitin ligase silencing suppresses tumor cell growth via sequential induction of G2-M arrest, apoptosis, and senescence. Cancer Res. 2009 Jun 15;69(12):4974-82.

138. Jiang T, Tang HM, Wu ZH, Chen J, Lu S, Zhou CZ, Yan DW, Peng ZH. Cullin 4B is a novel prognostic marker that correlates with colon cancer progression and pathogenesis. Med Oncol. 2013;30(2):534.

139. Jin J, Li X, Gygi SP, Harper JW. Dual E1 activation systems for ubiquitin differentially regulate E2 enzyme charging. Nature. 2007 Jun 28;447(7148):1135-8.

140. Jin L, Pahuja KB, Wickliffe KE, Gorur A, Baumgärtel C, Schekman R, Rape M. Ubiquitin-dependent regulation of COPII coat size and function. Nature. 2012 Feb 22;482(7386):495-500.

141. Johansson J.E., Andrén O., Andersson S.O., Dickman P.W., Holmberg L., Magnuson A., Adami H.O. Natural history of early, localized prostate cancer. JAMA 2004;291(22):2713-9.

142. Kamarajan P, Kapila YL. An altered fibronectin matrix induces anoikis of human squamous cell carcinoma cells by suppressing integrin alpha v levels and phosphorylation of FAK and ERK. Apoptosis. 2007 Dec;12(12):2221-31.

143. Kamura T, Maenaka K, Kotoshiba S, Matsumoto M, Kohda D, Conaway RC, Conaway JW, Nakayama KI. VHL-box and SOCS-box domains determine binding specificity for Cul2-RBX1 and Cul5-Rbx2 modules of ubiquitin ligases. Genes Dev. 2004 Dec 15;18(24):3055-65.

144. Karagiannis GS, Schaeffer DF, Cho CK, Musrap N, Saraon P, Batruch I, Grin A, Mitrovic B, Kirsch R, Riddell RH, Diamandis EP. Collective migration of cancer-associated fibroblasts is enhanced by overexpression of tight junction-associated proteins claudin-11 and occludin. Mol Oncol. 2014 Mar;8(2):178-95.

145. Kasper S. (2009) Identification, characterization, and biological relevance of prostate cancer stem cells from clinical specimens. Urol Oncol 27,301-3.

146. Kawauchi T. Cell adhesion and its endocytic regulation in cell migration during neural development and cancer metastasis. Int J Mol Sci. 2012;13(4):4564-90.

147. Kesavan SV, Momey F, Cioni O, David-Watine B, Dubrulle N, Shorte S, Sulpice E, Freida D, Chalmond B, Dinten JM, Gidrol X, Allier C. High-throughput monitoring of major cell functions by means of lensfree video microscopy. Sci Rep. 2014 Aug 6;4:5942.

148. Ketting R.F., Fischer S.E., Bernstein E., Sijen T., Hannon G.J., Plasterk R.H. Dicer functions in RNA interference and in synthesis of small RNA involved in developmental timing in C. elegans. Genes Dev. 2001;15(20):2654-9.

149. Khvorova A, Reynolds A, Jayasena SD. Functional siRNAs and miRNAs exhibit strand bias. Cell. 2003 Oct 17;115(2):209-16.

150. Kiessling A, Hogrefe C, Erb S, Bobach C, Fuessel S, Wessjohann L, Seliger B. Expression, regulation and function of the ISGylation system in prostate cancer. Oncogene. 2009 Jul 16;28(28):2606-20.

151. Kim J, Guermah M, McGinty RK, Lee JS, Tang Z, Milne TA, Shilatifard A, Muir TW, Roeder RG. RAD6-Mediated transcription-coupled H2B ubiquitylation directly stimulates H3K4 methylation in human cells. Cell. 2009 (a) May 1;137(3):459-71.

152. Kim SH, Hwang KA, Shim SM, Choi KC. Growth and migration of LNCaP prostate cancer cells are promoted by triclosan and benzophenone-1 via an androgen receptor signaling pathway. Environ Toxicol Pharmacol. 2015 Mar;39(2):568-76.

153. Kim SH, Kim HJ, Kim S, Yim J. Drosophila Cand1 regulates Cullin3-dependent E3 ligases by affecting the neddylation of Cullin3 and by controlling the stability of Cullin3 and adaptor protein. Dev Biol. 2010 Oct 15;346(2):247-57.

154. Kim VN, Han J, Siomi MC. Biogenesis of small RNAs in animals. Nat Rev Mol Cell Biol. 2009 (b) Feb;10(2):126-39

155. Kim VN. RNA interference in functional genomics and medicine. J Korean Med Sci. 2003 Jun;18(3):309-18.

156. Kimchi-Sarfaty C, Brittain S, Garfield S, Caplen NJ, Tang Q, Gottesman MM. Efficient delivery of RNA interference effectors via in vitro-packaged SV40 pseudovirions. Hum Gene Ther. 2005 Sep;16(9):1110-5.

157. Klezovitch O, Risk M, Coleman I, Lucas JM, Null M, True LD, Nelson PS, Vasioukhin V. A causal role for ERG in neoplastic transformation of prostate epithelium. Proc Natl Acad Sci U S A. 2008 Feb 12;105(6):2105-10.

158. Knudsen K.E. and Penning T.M. (2010) Partners in crime: deregulation of AR activity and androgen synthesis in prostate cancer. Trends Endocrinol Metab 21, 315-24;

159. Koken MH, Hoogerbrugge JW, Jasper-Dekker I, de Wit J, Willemsen R, Roest HP, Grootegoed JA, Hoeijmakers JH. Expression of the ubiquitin-conjugating DNA repair enzymes HHR6A and B suggests a role in spermatogenesis and chromatin modification. Dev Biol. 1996 Jan 10;173(1):119-32.

160. Kong Y, Nan K, Yin Y. Identification and characterization of CAC1 as a novel CDK2-associated cullin. Cell Cycle. 2009 Nov 1;8(21):3552-61.

161. Korzeniewski N, Hohenfellner M, Duensing S. CAND1 promotes PLK4-mediated centriole overduplication and is frequently disrupted in prostate cancer. Neoplasia. 2012 Sep;14(9):799-806.

162. Kowalczyk AP, Nanes BA. Adherens junction turnover: regulating adhesion through cadherin endocytosis, degradation, and recycling. Subcell Biochem. 2012;60:197-222. doi: 10.1007/978-94-007-4186-7_9.

163. Krohn A, Freudenthaler F, Harasimowicz S, Kluth M, Fuchs S, Burkhardt L, Stahl P, C Tsourlakis M, Bauer M, Tennstedt P, Graefen M, Steurer S, Sirma H, Sauter G, Schlomm T, Simon R, Minner S. Heterogeneity and chronology of PTEN deletion and ERG fusion in prostate cancer. Mod Pathol. 2014 Dec;27(12):1612-20.

164. Kumar-Sinha C, Tomlins SA, Chinnaiyan AM. Recurrent gene fusions in prostate cancer. Nat Rev Cancer. 2008 Jul;8(7):497-511.

165. Kunapuli P, Somerville R, Still IH, Cowell JK. ZNF198 protein, involved in rearrangement in myeloproliferative disease, forms complexes with the DNA repair-associated HHR6A/6B and RAD18 proteins. Oncogene. 2003 May 29;22(22):3417-23.

166. Kuppens IE, Breedveld P, Beijnen JH, Schellens JH. Modulation of oral drug bioavailability: from preclinical mechanism to therapeutic application. Cancer Invest. 2005;23(5):443-64.

167. Laganà A, Shasha D, Croce CM. Synthetic RNAs for Gene Regulation: Design Principles and Computational Tools. Front Bioeng Biotechnol. 2014 Dec 11;2:65.

168. Lambert PF, Ludford-Menting MJ, Deacon NJ, Kola I, Doherty RR. The nfkb1 promoter is controlled by proteins of the Ets family. Mol Biol Cell. 1997 Feb;8(2):313-23.

169. Lapointe J, Li C, Higgins JP, van de Rijn M, Bair E, Montgomery K, Ferrari M, Egevad L, Rayford W, Bergerheim U, Ekman P, DeMarzo AM, Tibshirani R, Botstein D, Brown PO, Brooks JD, Pollack JR. Gene expression profiling identifies clinically relevant subtypes of prostate cancer. Proc Natl Acad Sci U S A. 2004 Jan 20;101(3):811-6.

170. Lausen J, Pless O, Leonard F, Kuvardina ON, Koch B, Leutz A. Targets of the Tal1 transcription factor in erythrocytes: E2 ubiquitin conjugase regulation by Tal1. Biol Chem. 2010 Feb 19;285(8):5338-46.

171. Lee J, Zhou P. Cullins and cancer. Genes Cancer. 2010 Jul;1(7):690-9.

172. Lee Y., Ahn C., Han J., Choi H., Kim J., Yim J., Lee J., Provost P., Rådmark O., Kim S., Kim V.N. The nuclear RNase III Drosha initiates microRNA processing. Nature. 2003;425(6956):415-9.

173. Lee YG, Korenchuk S, Lehr J, Whitney S, Vessela R, Pienta KJ. Establishment and characterization of a new human prostatic cancer cell line: DuCaP. In Vivo. 2001 Mar-Apr;15(2):157-62.

174. Lehmusvaara S, Erkkilä T, Urbanucci A, Waltering K, Seppälä J, Larjo A, Tuominen VJ, Isola J, Kujala P, Lähdesmäki H, Kaipia A, Tammela TLj, Visakorpi T. Chemical castration and anti-androgens induce differential gene expression in prostate cancer. J Pathol. 2012 Jul;227(3):336-45. doi: 10.1002/path.4027.

175. Leidecker O, Matic I, Mahata B, Pion E, Xirodimas DP. The ubiquitin E1 enzyme Ube1 mediates NEDD8 activation under diverse stress conditions. Cell Cycle. 2012 Mar 15;11(6):1142-50.

176. Leshem O, Madar S, Kogan-Sakin I, Kamer I, Goldstein I, Brosh R, Cohen Y, Jacob-Hirsch J, Ehrlich M, Ben-Sasson S, Goldfinger N, Loewenthal R, Gazit E, Rotter V, Berger R. TMPRSS2/ERG promotes epithelial to mesenchymal transition through the ZEB1/ZEB2 axis in a prostate cancer model. PLoS One. 2011;6(7):e21650.

177. Leung AK, Sharp PA. microRNAs: a safeguard against turmoil? Cell. 2007 Aug 24;130(4):581-5.

178. Leuschner PJ, Ameres SL, Kueng S, Martinez J. Cleavage of the siRNA passenger strand during RISC assembly in human cells. EMBO Rep. 2006 Mar;7(3):314-20.

179. Li C, Vagin VV, Lee S, Xu J, Ma S, Xi H, Seitz H, Horwich MD, Syrzycka M, Honda BM, Kittler EL, Zapp ML, Klattenhoff C, Schulz N, Theurkauf WE, Weng Z, Zamore PD. Collapse of germline piRNAs in the absence of Argonaute3 reveals somatic piRNAs in flies. Cell. 2009 May 1;137(3):509-21.

180. Li L, Wang M, Yu G, Chen P, Li H, Wei D, Zhu J, Xie L, Jia H, Shi J, Li C, Yao W, Wang Y, Gao Q, Jeong LS, Lee HW, Yu J, Hu F, Mei J, Wang P, Chu Y, Qi H, Yang M, Dong Z, Sun Y, Hoffman RM, Jia L. Overactivated neddylation pathway as a therapeutic target in lung cancer. J Natl Cancer Inst. 2014 May 22;106(6):dju083.

181. Li X, Lu D, He F, Zhou H, Liu Q, Wang Y, Shao C, Gong Y. Cullin 4B protein ubiquitin ligase targets peroxiredoxin III for degradation. J Biol Chem. 2011 Sep 16;286(37):32344-54.

182. Lilja H, Ulmert D, Vickers AJ. 2008. Prostate-specific antigen and prostate cancer: Prediction, detection and monitoring. Nat Rev Cancer 8: 268–278.

183. Lim ST, Chen XL, Lim Y, Hanson DA, Vo TT, Howerton K, Larocque N, Fisher SJ, Schlaepfer DD, Ilic D. Nuclear FAK promotes cell proliferation and survival through FERM-enhanced p53 degradation. Mol Cell. 2008 Jan 18;29(1):9-22.

184. Lim ST, Miller NL, Chen XL, Tancioni I, Walsh CT, Lawson C, Uryu S, Weis SM, Cheresh DA, Schlaepfer DD. Nuclear-localized focal adhesion kinase regulates inflammatory VCAM-1 expression. J Cell Biol. 2012 Jun 25;197(7):907-19.

185. Lima WF, Murray H, Nichols JG, Wu H, Sun H, Prakash TP, Berdeja AR, Gaus HJ, Crooke ST. Human Dicer binds short single-strand and double-strand RNA with high affinity and interacts with different regions of the nucleic acids. J Biol Chem. 2009 Jan 23;284(4):2535-48.

186. Lin C, Yang L, Tanasa B, Hutt K, Ju BG, Ohgi K, Zhang J, Rose DW, Fu XD, Glass CK, Rosenfeld MG. Nuclear receptor-induced chromosomal proximity and DNA breaks underlie specific translocations in cancer. Cell. 2009 Dec 11;139(6):1069-83.

187. Lin JJ, Milhollen MA, Smith PG, Narayanan U, Dutta A. NEDD8-targeting drug MLN4924 elicits DNA rereplication by stabilizing Cdt1 in S phase, triggering checkpoint activation, apoptosis, and senescence in cancer cells. Cancer Res. 2010 Dec 15;70(24):10310-20.

188. Lindholm PF, Bub J, Kaul S, Shidham VB, Kajdacsy-Balla A. The role of constitutive NF-kappaB activity in PC-3 human prostate cancer cell invasive behavior. Clin Exp Metastasis. 2000;18(6):471-9.

189. Liu C, Wang D, Wu J, Keller J, Ma T, Yu X. RNF168 forms a functional complex with RAD6 during the DNA damage response. J Cell Sci. 2013 May 1;126(Pt 9):2042-51.

190. Liu J, Zhang C, Wang XL, Ly P, Belyi V, Xu-Monette ZY, Young KH, Hu W, Feng Z. E3 ubiquitin ligase TRIM32 negatively regulates tumor suppressor p53 to promote tumorigenesis. Cell Death Differ. 2014 Nov;21(11):1792-804.

191. Llave C, Kasschau KD, Rector MA, Carrington JC. Endogenous and silencing-associated small RNAs in plants. Plant Cell. 2002 Jul;14(7):1605-19.

192. Luo J, Solimini NL, Elledge SJ. Principles of Cancer Therapy: Oncogene and Non-oncogene Addiction. Cell. 2009 Mar 6; 136(5): 823–837.

193. Luo WR, Wu AB, Fang WY, Li SY, Yao KT. Nuclear expression of N-cadherin correlates with poor prognosis of nasopharyngeal carcinoma. Histopathology. 2012 Aug;61(2):237-46. doi: 10.1111/j.1365-2559.2012.04212.x. Epub 2012 Mar 2.

194. Lykke-Andersen K, Schaefer L, Menon S, Deng XW, Miller JB, Wei N. Disruption of the COP9 signalosome Csn2 subunit in mice causes deficient cell proliferation, accumulation of p53 and cyclin E, and early embryonic death. Mol Cell Biol. 2003 Oct;23(19):6790-7.

195. Ma E., MacRae I.J., Kirsch J.F., Doudna J.A. Auto-inhibition of Human Dicer by its Internal Helicase Domain. Journal of Molecular Biology, 2008;380(1):237-243.

196. Ma T, Chen Y, Zhang F, Yang CY, Wang S, Yu X. RNF111-dependent neddylation activates DNA damage-induced ubiquitination. Mol Cell. 2013 Mar 7;49(5):897-907.

197. Maeda Y, Suzuki T, Pan X, Chen G, Pan S, Bartman T, Whitsett JA. CUL2 is required for the activity of hypoxia-inducible factor and vasculogenesis. J Biol Chem. 2008 Jun 6;283(23):16084-92.

198. Maine GN, Mao X, Komarck CM, Burstein E. COMMD1 promotes the ubiquitination of NF-kappaB subunits through a cullin-containing ubiquitin ligase. EMBO J. 2007 Jan 24;26(2):436-47.

199. Mancarella C, Casanova-Salas I, Calatrava A, Ventura S, Garofalo C, Rubio-Briones J, Magistroni V, Manara MC, López-Guerrero JA, Scotlandi K. ERG deregulation induces IGF-1R expression in prostate cancer cells and affects sensitivity to anti-IGF-1R agents. Oncotarget. 2015 Mar 27.

200. Mani RS, Tomlins SA, Callahan K, Ghosh A, Nyati MK, Varambally S, Palanisamy N, Chinnaiyan AM. Induced chromosomal proximity and gene fusions in prostate cancer. Science. 2009 Nov 27;326(5957):1230.29.

201. Markert EK, Mizuno H, Vazquez A, Levine AJ. Molecular classification of prostate cancer using curated expression signatures. Proc Natl Acad Sci U S A. 2011 Dec 27;108(52):21276-81.

202. Markson G, Kiel C, Hyde R, Brown S, Charalabous P, Bremm A, Semple J, Woodsmith J, Duley S, Salehi-Ashtiani K, Vidal M, Komander D, Serrano L, Lehner P, Sanderson CM. Analysis of the human E2 ubiquitin conjugating enzyme protein interaction network. Genome Res. 2009 Oct;19(10):1905-11.

203. Martinez VD, Vucic EA, Thu KL, Pikor LA, Hubaux R, Lam WL. Unique pattern of component gene disruption in the NRF2 inhibitor KEAP1/CUL3/RBX1 E3-ubiquitin ligase complex in serous ovarian cancer. Biomed Res Int. 2014;2014:159459.

204. Martinez VD, Vucic EA, Thu KL, Pikor LA, Lam S, Lam WL. Disruption of KEAP1/CUL3/RBX1 E3-ubiquitin ligase complex components by multiple genetic mechanisms: Association with poor prognosis in head and neck cancer. Head Neck. 2015 May;37(5):727-34.

205. Masuda Y, Suzuki M, Kawai H, Hishiki A, Hashimoto H, Masutani C, Hishida T, Suzuki F, Kamiya K. En bloc transfer of polyubiquitin chains to PCNA in vitro is mediated by two different human E2-E3 pairs. Nucleic Acids Res. 2012 Nov 1;40(20):10394-407.

206. McNeal JE. Cancer volume and site of origin of adenocarcinoma of the prostate: Relationship to local and distant spread. Hum Pathol 1992;23:258–66.

207. McNeal JE. Origin and development of carcinoma in the prostate. Cancer (1969), 23:24-34.

208. Meehan KL, Holland JW, Dawkins HJ. Proteomic analysis of normal and malignant prostate tissue to identify novel proteins lost in cancer. Prostate. 2002 Jan 1;50(1):54-63.

209. Meng W, Takeichi M. Adherens junction: molecular architecture and regulation. Cold Spring Harb Perspect Biol. 2009 Dec;1(6):a002899.

210. Merk F B, Ofner P, Kwan P W *et al*. Ultrastructural and biochemical expression of divergent differentiation in prostates of castrated dogs treated with estrogen and androgen. Lab Invest, 1982, 47:437

211. Merlet J, Burger J, Gomes JE, Pintard L. Regulation of cullin-RING E3 ubiquitin-ligases by neddylation and dimerization. Cell Mol Life Sci. 2009 Jun;66(11-12):1924-38.

212. Metzger MB, Hristova VA, Weissman AM. HECT and RING finger families of E3 ubiquitin ligases at a glance. J Cell Sci. 2012 Feb 1;125(Pt 3):531-7.

213. Metzger R, Heukamp L, Drebber U, Bollschweiler E, Zander T, Hoelscher AH, Warnecke-Eberz U. CUL2 and STK11 as novel response-predictive genes for neoadjuvant radiochemotherapy in esophageal cancer. Pharmacogenomics. 2010 Aug;11(8):1105-13.

214. Metzlaff M., O'Dell M., Cluster P.D., Flavell R.B. RNA-mediated RNA degradation and chalcone synthase A silencing in petunia. Cell. 1997;88(6):845-54.

215. Migliorini D., Bogaerts S, Defever D, Vyas R, Denecker G, Radaelli E, Zwolinska A, Depaepe V, Hochepied T, Skarnes WC, Marine JC. (2011) Cop1 constitutively regulates c-Jun protein stability and functions as a tumor suppressor in mice. J Clin Invest 121, 1329-43.

216. Milhollen MA, Traore T, Adams-Duffy J, Thomas MP, Berger AJ, Dang L, Dick LR, Garnsey JJ, Koenig E, Langston SP, Manfredi M, Narayanan U, Rolfe M, Staudt LM, Soucy TA, Yu J, Zhang J, Bolen JB, Smith PG. MLN4924, a NEDD8-activating enzyme inhibitor, is active in diffuse large B-cell lymphoma models: rationale for treatment of NF-kB-dependent lymphoma. Blood. 2010 Sep 2;116(9):1515-23.

217. Molochkov V.A., Ilyin I.I. Chronic urethrogenic prostatitis. Moscow. Publishing house: Medicine (1998), p.304. [book in russian]

218. Moschos SJ, Jukic DM, Athanassiou C, Bhargava R, Dacic S, Wang X, Kuan SF, Fayewicz SL, Galambos C, Acquafondata M, Dhir R, Becker D. Expression analysis of Ubc9, the single small ubiquitin-like modifier (SUMO) E2 conjugating enzyme, in normal and malignant tissues. Hum Pathol. 2010 Sep;41(9):1286-98.

219. Murakami T, Felinski EA, Antonetti DA. Occludin phosphorylation and ubiquitination regulate tight junction trafficking and vascular endothelial growth factor-induced permeability. J Biol Chem. 2009 Jul 31;284(31):21036-46

220. Murata T, Takayama K, Katayama S, Urano T, Horie-Inoue K, Ikeda K, Takahashi S, Kawazu C, Hasegawa A, Ouchi Y, Homma Y, Hayashizaki Y, Inoue S. miR-148a is an androgen-responsive microRNA that promotes LNCaP prostate cell growth by repressing its target CAND1 expression. Prostate Cancer Prostatic Dis. 2010 Dec;13(4):356-61.

221. Nagai S., Davoodi N, Gasser SM. (2011) Nuclear organization in genome stability: SUMO connections. Cell Res 21, 474-85.

222. Nai G, Marques M. Role of ROC1 protein in the control of cyclin D1 protein expression in skin melanomas. Pathol Res Pract. 2011 Mar 15;207(3):174-81.

223. Nakagawa T, Xiong Y. X-linked mental retardation gene CUL4B targets ubiquitylation of H3K4 methyltransferase component WDR5 and regulates neuronal gene expression. Mol Cell. 2011 Aug 5;43(3):381-91.

224. Napoli C, Lemieux C, Jorgensen R. Introduction of a Chimeric Chalcone Synthase Gene into Petunia Results in Reversible Co-Suppression of Homologous Genes in trans. Plant Cell. 1990 Apr;2(4):279-289.

225. Nelius T, Filleur S, Yemelyanov A, Budunova I, Shroff E, Mirochnik Y, Aurora A, Veliceasa D, Xiao W, Wang Z, Volpert OV. Androgen receptor targets NFkappaB and TSP1 to suppress prostate tumor growth in vivo. Int J Cancer. 2007 Sep 1;121(5):999-1008.

226. Ng CC, Arakawa H, Fukuda S, Kondoh H, Nakamura Y. p53RFP, a p53-inducible RING-finger protein, regulates the stability of p21WAF1. Oncogene. 2003 Jul 10;22(28):4449-58.

227. Nguyen N, Yi JS, Park H, Lee JS, Ko YG. Mitsugumin 53 (MG53) ligase ubiquitinates focal adhesion kinase during skeletal myogenesis. J Biol Chem. 2014 Feb 7;289(6):3209-16.

228. Nikolova-Krstevski V, Yuan L, Le Bras A, Vijayaraj P, Kondo M, Gebauer I, Bhasin M, Carman CV, Oettgen P. ERG is required for the differentiation of embryonic stem cells along the endothelial lineage. BMC Dev Biol. 2009 Dec 23;9:72.

229. Oh C, Park S, Lee EK, Yoo YJ. Downregulation of ubiquitin level via knockdown of polyubiquitin gene Ubb as potential cancer therapeutic intervention. Sci Rep. 2013;3:2623.

230. Okuda H, Saitoh K, Hirai S, Iwai K, Takaki Y, Baba M, Minato N, Ohno S, Shuin T. The von Hippel-Lindau tumor suppressor protein mediates ubiquitination of activated atypical protein kinase C. J Biol Chem. 2001 Nov 23;276(47):43611-7.

231. Okumura F, Matsuzaki M, Nakatsukasa K, Kamura T. The Role of Elongin BC-Containing Ubiquitin Ligases. Front Oncol. 2012 Feb 3;2:10.

232. Oved S, Mosesson Y, Zwang Y, Santonico E, Shtiegman K, Marmor MD, Kochupurakkal BS, Katz M, Lavi S, Cesareni G, Yarden Y. Conjugation to NEDD8 instigates ubiquitylation and down-regulation of activated receptor tyrosine kinases. J Biol Chem. 2006 Aug 4;281(31):21640-51.

233. Palvimo JJ, Reinikainen P, Ikonen T, Kallio PJ, Moilanen A, Jänne OA. Mutual transcriptional interference between RelA and androgen receptor. J Biol Chem. 1996 Sep 27;271(39):24151-6.

234. Pan L, Wang S, Lu T, Weng C, Song X, Park JK, Sun J, Yang ZH, Yu J, Tang H, McKearin DM, Chamovitz DA, Ni J, Xie T. Protein competition switches the function of COP9 from self-renewal to differentiation. Nature. 2014 Oct 9;514(7521):233-6.

235. Parsons JT, Horwitz AR, Schwartz MA. Cell adhesion: integrating cytoskeletal dynamics and cellular tension. Nat Rev Mol Cell Biol. 2010 Sep;11(9):633-43.

236. Pawar RD, Lin TL, Cui W, Aljitawi OS. N-Cadherin Immunoexpression In Patients With Acute Myeloid Leukemia. Blood 2013; 122(21):4976

237. Pawlowski JE, Ertel JR, Allen MP, Xu M, Butler C, Wilson EM, Wierman ME. Liganded androgen receptor interaction with beta-catenin: nuclear co-localization and modulation of transcriptional activity in neuronal cells. J Biol Chem. 2002 Jun 7;277(23):20702-10. Epub 2002 Mar 26.

238. Perner S, Svensson MA, Hossain RR, Day JR, Groskopf J, Slaughter RC, Jarleborn AR, Hofer MD, Kuefer R, Demichelis F, Rickman DS, Rubin MA. ERG rearrangement metastasis patterns in locally advanced prostate cancer. Urology. 2010 Apr;75(4):762-7.

239. Petsko GA, Ringe D. Protein Structure and Function. New Science Press, 2004

240. Pierce NW, Lee JE, Liu X, Sweredoski MJ, Graham RL, Larimore EA, Rome M, Zheng N, Clurman BE, Hess S, Shan SO, Deshaies RJ. Cand1 promotes assembly of new SCF complexes through dynamic exchange of F box proteins. Cell. 2013 Mar 28;153(1):206-15.

241. Pintard L, Kurz T, Glaser S, Willis JH, Peter M, Bowerman B Neddylation and deneddylation of CUL-3 is required to target MEI-1/Katanin for degradation at the meiosis-to-mitosis transition in C. elegans. Curr Biol. 2003 May 27;13(11):911-21.

242. Piper RC, Katzmann DJ. Biogenesis and function of multivesicular bodies. Annu Rev Cell Dev Biol. 2007;23:519-47.

243. Piskounova E, Agathocleous M, Murphy MM, Hu Z, Huddlestun SE, Zhao Z, Leitch AM, Johnson TM, DeBerardinis RJ, Morrison SJ. Oxidative stress inhibits distant metastasis by human melanoma cells. Nature. 2015 Oct 14.

244. Pratt AJ, MacRae IJ. The RNA-induced silencing complex: a versatile gene-silencing machine. J Biol Chem. 2009 Jul 3;284(27):17897-901. doi: 10.1074/jbc.R900012200.

245. Raikwar NS, Vandewalle A, Thomas CP. Nedd4-2 interacts with occludin to inhibit tight junction formation and enhance paracellular conductance in collecting duct epithelia. Am J Physiol Renal Physiol. 2010 Aug;299(2):F436-44.

246. Rastogi A, Tan SH, Mohamed AA, Chen Y, Hu Y, Petrovics G, Sreenath T, Kagan J, Srivastava S, McLeod DG, Sesterhenn IA, Srivastava S, Dobi A, Srinivasan A. Functional antagonism of TMPRSS2-ERG splice variants in prostate cancer. Genes Cancer. 2014 Jul;5(7-8):273-84.

247. Rayet B, Gélinas C. Aberrant rel/nfkb genes and activity in human cancer. Oncogene. 1999 Nov 22;18(49):6938-47.

248. Reiter R.E., de Kernion J.B. Epidemiology, etiology and prevention of prostate cancer. In: Walsh PC, Vaughan ED, Retik AB, Wein A (Eds.) Campbell's Urology, 8th Ed., Philhadelphia: Saunders, 2002.

249. Renaudin X, Guervilly JH, Aoufouchi S, Rosselli F. Proteomic analysis reveals a FANCA-modulated neddylation pathway involved in CXCR5 membrane targeting and cell mobility. J Cell Sci. 2014 Aug 15;127(Pt 16):3546-54. doi: 10.1242/jcs.150706.

250. Reyes-Turcu F., Ventii KH, Wilkinson KD. (2009) Regulation and cellular roles of ubiquitin-specific deubiquitinating enzymes. Annu Rev Biochem 78, 363-97

251. Reynolds A, Leake D, Boese Q, Scaringe S, Marshall WS, Khvorova A. Rational siRNA design for RNA interference. Nat Biotechnol. 2004 Mar;22(3):326-30.

252. Riabinska A, Daheim M, Herter-Sprie GS, Winkler J, Fritz C, Hallek M, Thomas RK, Kreuzer KA, Frenzel LP, Monfared P, Martins-Boucas J, Chen S, Reinhardt HC. Therapeutic targeting of a robust non-oncogene addiction to PRKDC in ATM-defective tumors. Sci Transl Med. 2013 Jun 12;5(189):189ra78.

253. Rolland T, Taşan M, Charloteaux B, Pevzner SJ, Zhong Q, Sahni N, Yi S, Lemmens I, Fontanillo C, Mosca R7, Kamburov A, Ghiassian SD, Yang X, Ghamsari L, Balcha D, Begg BE, Braun P, Brehme M, Broly MP, Carvunis AR, Convery-Zupan D, Corominas R, Coulombe-Huntington J, Dann E, Dreze M, Dricot A, Fan C, Franzosa E, Gebreab F, Gutierrez BJ, Hardy MF, Jin M, Kang S, Kiros R, Lin GN, Luck K, MacWilliams A, Menche J, Murray RR, Palagi A, Poulin MM, Rambout X, Rasla J, Reichert P, Romero V, Ruyssinck E, Sahalie JM1, Scholz A, Shah AA, Sharma A, Shen Y, Spirohn K, Tam S, Tejeda AO, Trigg SA, Twizere JC, Vega K, Walsh J, Cusick ME, Xia Y, Barabási AL, Iakoucheva LM, Aloy P, De Las Rivas J, Tavernier J, Calderwood MA, Hill DE, Hao T, Roth FP, Vidal M. A proteome-scale map of the human interactome network. Cell. 2014 Nov 20;159(5):1212-26.

254. Rubin MA. ETS rearrangements in prostate cancer. Asian J Androl. 2012 May;14(3):393-9. doi: 10.1038/aja.2011.145.

255. Russell RC, Ohh M. NEDD8 acts as a 'molecular switch' defining the functional selectivity of VHL. EMBO Rep. 2008 May;9(5):486-91.

256. Sadeghi L, Siggens L, Svensson JP, Ekwall K. Centromeric histone H2B monoubiquitination promotes noncoding transcription and chromatin integrity. Nat Struct Mol Biol. 2014 Mar;21(3):236-43.

257. Safferling K, Sütterlin T, Westphal K, Ernst C, Breuhahn K, James M, Jäger D, Halama N, Grabe N. Wound healing revised: a novel reepithelialization mechanism revealed by in vitro and in silico models. J Cell Biol. 2013 Nov 25;203(4):691-709.

258. Salon C, Brambilla E, Brambilla C, Lantuejoul S, Gazzeri S, Eymin B. Altered pattern of Cul-1 protein expression and neddylation in human lung tumours: relationships with CAND1 and cyclin E protein levels. J Pathol. 2007 Nov;213(3):303-10.

259. Sarkaria I, O-charoenrat P, Talbot SG, Reddy PG, Ngai I, Maghami E, Patel KN, Lee B, Yonekawa Y, Dudas M, Kaufman A, Ryan R, Ghossein R, Rao PH, Stoffel A, Ramanathan Y, Singh B. Squamous cell carcinoma related oncogene/DCUN1D1 is highly conserved and activated by amplification in squamous cell carcinomas. Cancer Res. 2006 Oct 1;66(19):9437-44.

260. Sawh AN, Duchaine TF. Turning Dicer on its head. Nat Struct Mol Biol. 2012 Apr 4;19(4):365-6.

261. Schwechheimer C. The COP9 signalosome (CSN): an evolutionary conserved proteolysis regulator in eukaryotic development. Biochim Biophys Acta. 2004 Nov 29;1695(1-3):45-54.

262. Schweizer L, Rizzo CA, Spires TE, Platero JS, Wu Q, Lin TA, Gottardis MM, Attar RM. The androgen receptor can signal through Wnt/beta-Catenin in prostate cancer cells as an adaptation mechanism to castration levels of androgens. BMC Cell Biol. 2008 Jan 24;9:4.

263. Sertic S, Evolvi C, Tumini E, Plevani P, Muzi-Falconi M, Rotondo G. Non-canonical CRL4A/4B(CDT2) interacts with RAD18 to modulate post replication repair and cell survival. PLoS One. 2013;8(3):e60000.

264. Sharifi HJ, Furuya AK, Jellinger RM, Nekorchuk MD, de Noronha CM. Cullin4A and cullin4B are interchangeable for HIV Vpr and Vpx action through the CRL4 ubiquitin ligase complex. J Virol. 2014 Jun;88(12):6944-58.

265. Shchebet A, Karpiuk O, Kremmer E, Eick D, Johnsen SA. Phosphorylation by cyclin-dependent kinase-9 controls ubiquitin-conjugating enzyme-2A function. Cell Cycle. 2012 Jun 1;11(11):2122-7.

266. Shen MM, Abate-Shen C. Molecular genetics of prostate cancer: new prospects for old challenges. Genes Dev. 2010 Sep 15;24(18):1967-2000.

267. Shipitsin M, Small C, Choudhury S, Giladi E, Friedlander S, Nardone J, Hussain S, Hurley AD, Ernst C, Huang YE, Chang H, Nifong TP, Rimm DL, Dunyak J, Loda M, Berman DM, Blume-Jensen P. Identification of proteomic biomarkers predicting prostate cancer aggressiveness and lethality despite biopsy-sampling error. Br J Cancer. 2014 Sep 9;111(6):1201-12.

268. Shoval I, Ludwig A, Kalcheim C. Antagonistic roles of full-length N-cadherin and its soluble BMP cleavage product in neural crest delamination. Development. 2007 Feb;134(3):491-501. Epub 2006 Dec 21.

269. Sidow A, Spies N. Concepts in solid tumor evolution. Trends Genet. 2015 Apr;31(4):208-14.

270. Siegel R., Naishadham D., Jemal A. Cancer Statistics, 2012 // CA: A Cancer Journal for Clinicians, 62(1):10–29.

271. Smith C.J. Watson C.F., Bird C.R., Ray J., Schuch W., Grierson D.. Expression of a truncated tomato polygalacturonase gene inhibits expression of the endogenous gene in transgenic plants. Mol Gen Genet. 1990;224(3):477-81.

272. Sobel RE, Sadar MD. Cell lines used in prostate cancer research: a compendium of old and new lines--part 1. J Urol. 2005 Feb;173(2):342-59.

273. Solanas G, Cortina C, Sevillano M, Batlle E. Cleavage of E-cadherin by ADAM10 mediates epithelial cell sorting downstream of EphB signalling. Nat Cell Biol. 2011 Jul 31;13(9):1100-7.

274. Song H, Hollstein M, Xu Y. p53 gain-of-function cancer mutants induce genetic instability by inactivating ATM. Nat Cell Biol. 2007 May;9(5):573-80.

275. Song JJ, Smith SK, Hannon GJ, Joshua-Tor L. Crystal structure of Argonaute and its implications for RISC slicer activity. Science. 2004 Sep 3;305(5689):1434-7

276. Song LN, Herrell R, Byers S, Shah S, Wilson EM, Gelmann EP. Beta-catenin binds to the activation function 2 region of the androgen receptor and modulates the effects of the N-terminal domain and TIF2 on ligand-dependent transcription. Mol Cell Biol. 2003 Mar;23(5):1674-87.

277. Sorokin AV, Kim ER, Ovchinnikov LP. Proteasome system of protein degradation and processing. Biochemistry (Mosc). 2009 Dec;74(13):1411-42.

278. Soucy TA, Smith PG, Milhollen MA, Berger AJ, Gavin JM, Adhikari S, Brownell JE, Burke KE, Cardin DP, Critchley S, Cullis CA, Doucette A, Garnsey JJ, Gaulin JL, Gershman RE, Lublinsky AR, McDonald A, Mizutani H, Narayanan U, Olhava EJ, Peluso S, Rezaei M, Sintchak MD, Talreja T, Thomas MP, Traore T, Vyskocil S, Weatherhead GS, Yu J, Zhang J, Dick LR, Claiborne CF, Rolfe M, Bolen JB,

Langston SP. An inhibitor of NEDD8-activating enzyme as a new approach to treat cancer. Nature. 2009 Apr 9;458(7239):732-6.

279. Souphron J, Waddell MB, Paydar A, Tokgöz-Gromley Z, Roussel MF, Schulman BA. Structural dissection of a gating mechanism preventing misactivation of ubiquitin by NEDD8's E1. Biochemistry. 2008 Aug 26;47(34):8961-9.

280. Sowalsky AG, Ye H, Bubley GJ, Balk SP. Clonal progression of prostate cancers from Gleason grade 3 to grade 4. Cancer Res. 2013 Feb 1;73(3):1050-5.

281. St John J, Powell K, Conley-Lacomb MK, Chinni SR. TMPRSS2-ERG Fusion Gene Expression in Prostate Tumor Cells and Its Clinical and Biological Significance in Prostate Cancer Progression. J Cancer Sci Ther. 2012 Apr 26;4(4):94-101.

282. Stark JR, Perner S, Stampfer MJ, Sinnott JA, Finn S, Eisenstein AS, Ma J, Fiorentino M, Kurth T, Loda M, Giovannucci EW, Rubin MA, Mucci LA. Gleason Score and Lethal Prostate Cancer: Does 3 + 4 = 4 + 3? (2009) Journal of Clinical Oncology, 27(21):3459-3464

283. Stewart A, Ham C, Zachary I. The focal adhesion kinase amino-terminal domain localises to nuclei and intercellular junctions in HEK 293 and MDCK cells independently of tyrosine 397 and the carboxy-terminal domain. Biochem Biophys Res Commun. 2002 Nov 22;299(1):62-73.

284. Stewart, B. W., Wild, C. P. World Cancer Report 2014. International Agency for Research on Cancer, World Health Organization. 2014.

285. Stickle NH, Chung J, Klco JM, Hill RP, Kaelin WG Jr, Ohh M. pVHL modification by NEDD8 is required for fibronectin matrix assembly and suppression of tumor development. Mol Cell Biol. 2004 Apr;24(8):3251-61.

286. Sun C, Dobi A, Mohamed A, Li H, Thangapazham RL, Furusato B, Shaheduzzaman S, Tan SH, Vaidyanathan G, Whitman E, Hawksworth DJ, Chen Y, Nau M, Patel V, Vahey M, Gutkind JS, Sreenath T, Petrovics G, Sesterhenn IA, McLeod DG, Srivastava S. TMPRSS2-ERG fusion, a common genomic alteration in prostate cancer activates C-MYC and abrogates prostate epithelial differentiation. Oncogene. 2008 Sep 11;27(40):5348-53.

287. Swanson TA, Krueger SA, Galoforo S, Thibodeau BJ, Martinez AA, Wilson GD, Marples B. TMPRSS2/ERG fusion gene expression alters chemo- and radio-responsiveness in cell culture models of androgen independent prostate cancer. Prostate. 2011 Oct 1;71(14):1548-58.

288. Tai YL, Chen LC, Shen TL. Emerging roles of focal adhesion kinase in cancer. Biomed Res Int. 2015;2015:690690.

289. Tan SH, Furusato B, Fang X, He F, Mohamed AA, Griner NB, Sood K, Saxena S, Katta S, Young D, Chen Y, Sreenath T, Petrovics G, Dobi A, McLeod DG, Sesterhenn IA, Saxena S, Srivastava S. Evaluation of ERG responsive proteome in prostate cancer. Prostate. 2014 Jan;74(1):70-89.

290. Taylor BS, Schultz N, Hieronymus H, Gopalan A, Xiao Y, Carver BS, Arora VK, Kaushik P, Cerami E, Reva B, Antipin Y, Mitsiades N, Landers T, Dolgalev I, Major JE, Wilson M, Socci ND, Lash AE, Heguy A, Eastham JA, Scher HI, Reuter VE, Scardino PT, Sander C, Sawyers CL, Gerald WL. Integrative genomic profiling of human prostate cancer. Cancer Cell. 2010 Jul 13;18(1):11-22.

291. Thiery JP. Epithelial-mesenchymal transitions in tumour progression. Nat Rev Cancer. 2002 Jun;2(6):442-54.

292. Thompson I, Pauler D, Goodman P, Tangen C, Lucia M, Parnes H, Minasian L, Ford L, Lippman S, Crawford E, Crowley J, Coltman C. Prevalence of prostate cancer among men with a prostate-specific antigen level ≤4.0 ng per milliliter. 2004, N Engl J Med 350 (22): 2239–46

293. Tian TV, Tomavo N, Huot L, Flourens A, Bonnelye E, Flajollet S, Hot D, Leroy X, de Launoit Y, Duterque-Coquillaud M. Identification of novel TMPRSS2:ERG mechanisms in prostate cancer metastasis: involvement of MMP9 and PLXNA2. Oncogene. 2014 Apr 24;33(17):2204-14

294. Tomari Y, Matranga C, Haley B, Martinez N, Zamore PD. A protein sensor for siRNA asymmetry. Science. 2004 Nov 19;306(5700):1377-80.

295. Tomlins S.A., Laxman B, Varambally S, Cao X, Yu J, Helgeson BE, Cao Q, Prensner JR, Rubin MA, Shah RB, Mehra R, Chinnaiyan AM. Role of the TMPRSS2-ERG gene fusion in prostate cancer. Neoplasia, 2008. 10, 177-88.

296. Tomlins SA, Laxman B, Dhanasekaran SM, Helgeson BE, Cao X, Morris DS, Menon A, Jing X, Cao Q, Han B, Yu J, Wang L, Montie JE, Rubin MA, Pienta KJ, Roulston D, Shah RB, Varambally S, Mehra R, Chinnaiyan AM. Distinct classes of chromosomal rearrangements create oncogenic ETS gene fusions in prostate cancer. Nature. 2007 **(a)** Aug 2;448(7153):595-9.

297. Tomlins SA, Mehra R, Rhodes DR, Cao X, Wang L, Dhanasekaran SM, Kalyana-Sundaram S, Wei JT, Rubin MA, Pienta KJ, Shah RB, Chinnaiyan AM. Integrative molecular concept modeling of prostate cancer progression. Nat Genet. 2007 **(b)** Jan;39(1):41-51.

298. Tomlins SA, Rhodes DR, Perner S, Dhanasekaran SM, Mehra R, Sun XW, Varambally S, Cao X, Tchinda J, Kuefer R, Lee C, Montie JE, Shah RB, Pienta KJ, Rubin MA, Chinnaiyan AM. Recurrent fusion of TMPRSS2 and ETS transcription factor genes in prostate cancer. Science. 2005 Oct 28;310(5748):644-8.

299. Tommer Ravid, Mark Hochstrasser. Degradation signal diversity in the ubiquitin-proteasome system. Nat Rev Mol Cell Biol. Sep 2008; 9(9): 679–690.

300. Traweger A, Fang D, Liu YC, Stelzhammer W, Krizbai IA, Fresser F, Bauer HC, Bauer H. The tight junction-specific protein occludin is a functional target of the E3 ubiquitin-protein ligase itch. J Biol Chem. 2002 Mar 22;277(12):10201-8.

301. Truica CI, Byers S, Gelmann EP. Beta-catenin affects androgen receptor transcriptional activity and ligand specificity. Cancer Res. 2000 Sep 1;60(17):4709-13.

302. Tuschl T, Borkhardt A. Small interfering RNAs: a revolutionary tool for the analysis of gene function and gene therapy. Mol Interv. 2002 Jun;2(3):158-67.

303. Tuschl T, Zamore PD, Lehmann R, Bartel DP, Sharp PA. Targeted mRNA degradation by double-stranded RNA in vitro. Genes Dev. 1999 Dec 15;13(24):3191-7.

304. Ui-Tei K, Nishi K, Takahashi T, Nagasawa T. Thermodynamic Control of Small RNA-Mediated Gene Silencing. Front Genet. 2012 Jun 4;3:101.

305. Urbinati G, Ali HM, Rousseau Q, Chapuis H, Desmaële D, Couvreur P, Massaad-Massade L. Antineoplastic Effects of siRNA against TMPRSS2-ERG Junction Oncogene in Prostate Cancer. PLoS One. 2015 May 1;10(5):e0125277.

306. Vallenius T. Actin stress fibre subtypes in mesenchymal-migrating cells. Open Biol. 2013 Jun 19;3(6):130001.

307. Valluy J, Bicker S, Aksoy-Aksel A, Lackinger M, Sumer S, Fiore R, Wüst T, Seffer D, Metge F, Dieterich C, Wöhr M, Schwarting R, Schratt G. A coding-independent function of an alternative Ube3a transcript during neuronal development. Nat Neurosci. 2015 May;18(5):666-73. doi: 10.1038/nn.3996.

308. van Bokhoven A, Caires A, Maria MD, Schulte AP, Lucia MS, Nordeen SK, Miller GJ, Varella-Garcia M. Spectral karyotype (SKY) analysis of human prostate carcinoma cell lines. Prostate. 2003 **(a)** Nov 1;57(3):226-44.

309. van Bokhoven A, Varella-Garcia M, Korch C, Johannes WU, Smith EE, Miller HL, Nordeen SK, Miller GJ, Lucia MS. Molecular characterization of human prostate carcinoma cell lines. Prostate. 2003 **(b)** Nov 1;57(3):205-25.

310. van der Krol AR, Mur LA, Beld M, Mol JN, and Stuitje AR. Flavonoid genes in petunia: addition of a limited number of gene copies may lead to a suppression of gene expression. Plant Cell. 1990 Apr; 2(4): 291–299.

311. van Kerkhof P, Westgeest M, Hassink G, Strous GJ. SCF(TrCP) acts in endosomal sorting of the GH receptor. Exp Cell Res. 2011 Apr 15;317(7):1071-82.

312. van Wijk SJ, de Vries SJ, Kemmeren P, Huang A, Boelens R, Bonvin AM, Timmers HT. A comprehensive framework of E2-RING E3 interactions of the human ubiquitin-proteasome system. Mol Syst Biol. 2009;5:295.

313. Varambally S., Yu J, Laxman B, Rhodes DR, Mehra R, Tomlins SA, Shah RB, Chandran U, Monzon FA, Becich MJ, Wei JT, Pienta KJ, Ghosh D, Rubin MA, Chinnaiyan AM.. (2005) Integrative genomic and proteomic analysis of prostate cancer reveals signatures of metastatic progression. Cancer Cell 8, 393-406

314. Veldscholte J, Berrevoets CA, Ris-Stalpers C, Kuiper GG, Jenster G, Trapman J, Brinkmann AO, Mulder E. The androgen receptor in LNCaP cells contains a mutation in the ligand binding domain which affects steroid binding characteristics and response to antiandrogens. J Steroid Biochem Mol Biol. 1992 Mar;41(3-8):665-9.

315. Vermeulen A., Behlen L., Reynolds A., Wolfson A., Marshall W.S., Karpilov J., Khvorova A. The contributions of dsRNA structure to Dicer specificity and efficiency. RNA. 2005;11:674-682.

316. Vierstra RD. The Expanding Universe of Ubiquitin and Ubiquitin-Like Modifiers. Plant Physiol. Sep 2012; 160(1): 2–14.

317. Vilgelm AE, Chumakov SP, Prasolov VS. RNA interference: biology and perspectives of application in biomedicine and biotechnology. [Article in Russian] Mol Biol (Mosk). 2006 May-Jun;40(3):387-403.

318. Vitari A.C., Leong KG, Newton K, Yee C, O'Rourke K, Liu J, Phu L, Vij R, Ferrando R, Couto SS, Mohan S, Pandita A, Hongo JA, Arnott D, Wertz IE, Gao WQ, French DM, Dixit VM. (2011) COP1 is a tumour suppressor that causes degradation of ETS transcription factors. Nature 474, 403-6.

319. Wang J, Cai Y, Shao LJ, Siddiqui J, Palanisamy N, Li R, Ren C, Ayala G, Ittmann M. Activation of NF-κB by TMPRSS2/ERG Fusion Isoforms through Toll-Like Receptor-4. Cancer Res. 2011 Feb 15;71(4):1325-33

320. Wang J, Cai Y, Yu W, Ren C, Spencer DM, Ittmann M. Pleiotropic biological activities of alternatively spliced TMPRSS2/ERG fusion gene transcripts. Cancer Res. 2008 Oct 15;68(20):8516-24.

321. Wang L, Li Y, Yang X, Yuan H, Li X, Qi M, Chang YW, Wang C, Fu W, Yang M, Zhang J, Han B. ERG-SOX4 interaction promotes epithelial-mesenchymal transition in prostate cancer cells. Prostate. 2014 May;74(6):647-58.

322. Wang Q., Li W, Zhang Y, Yuan X, Xu K, Yu J, Chen Z, Beroukhim R, Wang H, Lupien M, Wu T, Regan MM, Meyer CA, Carroll JS, Manrai AK, Jänne OA, Balk SP, Mehra R, Han B, Chinnaiyan AM, Rubin MA, True L, Fiorentino M, Fiore C, Loda M, Kantoff PW, Liu XS, Brown M. (2009) Androgen receptor regulates a distinct transcription program in androgen-independent prostate cancer. Cell 138, 245-56.

323. Wang W, Liu Z, Qu P, Zhou Z, Zeng Y, Fan J, Liu Y, Guo Y, Qiu J. Knockdown of regulator of cullins-1 (ROC1) expression induces bladder cancer cell cycle arrest at the G2 phase and senescence. PLoS One. 2013 May 8;8(5):e62734.

324. Wang Z.A. and Shen M.M. Revisiting the concept of cancer stem cells in prostate cancer. Oncogene 2011. 30, 1261-71.

325. Watson IR, Blanch A, Lin DC, Ohh M, Irwin MS. Mdm2-mediated NEDD8 modification of TAp73 regulates its transactivation function. J Biol Chem. 2006 Nov 10;281(45):34096-103.

326. Watson IR, Irwin MS, Ohh M. NEDD8 pathways in cancer, Sine Quibus Non. Cancer Cell. 2011 Feb 15;19(2):168-76.

327. Wei D, Li H, Yu J, Sebolt JT, Zhao L, Lawrence TS, Smith PG, Morgan MA, Sun Y. Radiosensitization of human pancreatic cancer cells by MLN4924, an investigational NEDD8-activating enzyme inhibitor. Cancer Res. 2012 Jan 1;72(1):282-93.

328. Wei D, Sun Y. Small RING Finger Proteins RBX1 and RBX2 of SCF E3 Ubiquitin Ligases: The Role in Cancer and as Cancer Targets. Genes Cancer. 2010 Jul;1(7):700-7.

329. Wertz I.E., O'Rourke KM, Zhou H, Eby M, Aravind L, Seshagiri S, Wu P, Wiesmann C, Baker R, Boone DL, Ma A, Koonin EV, Dixit VM. (2004) De-ubiquitination and ubiquitin ligase domains of A20 downregulate NF-kappaB signalling. Nature 430, 694-9.

330. Willis A, Jung EJ, Wakefield T, Chen X. Mutant p53 exerts a dominant negative effect by preventing wild-type p53 from binding to the promoter of its target genes. Oncogene. 2004 Mar 25;23(13):2330-8.

331. Wu L, Zhao JC, Kim J, Jin HJ, Wang CY, Yu J. ERG is a critical regulator of Wnt/LEF1 signaling in prostate cancer. Cancer Res. 2013 Oct 1;73(19):6068-79

332. Wyatt AW, Mo F, Wang K, McConeghy B, Brahmbhatt S, Jong L, Mitchell DM, Johnston RL, Haegert A, Li E, Liew J, Yeung J, Shrestha R, Lapuk AV, McPherson A, Shukin R, Bell RH, Anderson S, Bishop J, Hurtado-Coll A, Xiao H, Chinnaiyan AM, Mehra R, Lin D, Wang Y, Fazli L, Gleave ME, Volik SV, Collins CC. Heterogeneity in the inter-tumor transcriptome of high risk prostate cancer. Genome Biol. 2014 Aug 26;15(8):426.

333. Xiao F, Kim YC, Snyder C, Wen H, Chen PX, Luo J, Becirovic D, Downs B, Cowan KH, Lynch H, Wang SM. Genome instability in blood cells of a BRCA1+ breast cancer family. BMC Cancer. 2014 May 19;14:342. doi: 10.1186/1471-2407-14-342.

334. Xie L, Xiao K, Whalen EJ, Forrester MT, Freeman RS, Fong G, Gygi SP, Lefkowitz RJ, Stamler JS. Oxygen-regulated beta(2)-adrenergic receptor hydroxylation by EGLN3 and ubiquitylation by pVHL. Sci Signal. 2009 Jul 7;2(78):ra33.

335. Xin H, Lin W, Sumanasekera W, Zhang Y, Wu X, Wang Z. The human RAD18 gene product interacts with HHR6A and HHR6B. Nucleic Acids Res. 2000 Jul 15;28(14):2847-54.

336. Xirodimas DP, Saville MK, Bourdon JC, Hay RT, Lane DP. Mdm2-mediated NEDD8 conjugation of p53 inhibits its transcriptional activity. Cell. 2004 Jul 9;118(1):83-97.

337. Xu J, Li L, Yu G, Ying W, Gao Q, Zhang W, Li X, Ding C, Jiang Y, Wei D, Duan S, Lei Q, Li P, Shi T, Qian X, Qin J, Jia L. The neddylation-cullin 2-RBX1 E3 ligase axis targets tumor suppressor RhoB for degradation in liver cancer. Mol Cell Proteomics. 2015 Mar;14(3):499-509

338. Xu J, Ma M, Purcell WM. Characterisation of some cytotoxic endpoints using rat liver and HepG2 spheroids as in vitro models and their application in hepatotoxicity studies. II. Spheroid cell spreading inhibition as a new cytotoxic marker. Toxicol Appl Pharmacol. 2003 Jun 1;189(2):112-9.

339. Yadav SS, Li J, Lavery HJ, Yadav KK, Tewari AK. Next-generation sequencing technology in prostate cancer diagnosis, prognosis, and personalized treatment. Urol Oncol. 2015 Jun;33(6):267.e1-267.e13.

340. Yang D, Li L, Liu H, Wu L, Luo Z, Li H, Zheng S, Gao H, Chu Y, Sun Y, Liu J, Jia L. Induction of autophagy and senescence by knockdown of ROC1 E3 ubiquitin ligase to suppress the growth of liver cancer cells. Cell Death Differ. 2013 Feb;20(2):235-47.

341. Yang X, Zhou J, Sun L, Wei Z, Gao J, Gong W, Xu RM, Rao Z, Liu Y. Structural basis for the function of DCN-1 in protein Neddylation. J Biol Chem. 2007 Aug 24;282(34):24490-4.

342. Yang Y, Liu R, Qiu R, Zheng Y, Huang W, Hu H, Ji Q, He H, Shang Y, Gong Y, Wang Y. CRL4B promotes tumorigenesis by coordinating with SUV39H1/HP1/DNMT3A in DNA methylation-based epigenetic silencing. Oncogene. 2015 Jan 2;34(1):104-18.

343. Yao WT1, Wu JF2, Yu GY2, Wang R3, Wang K4, Li LH5, Chen P5, Jiang YN2, Cheng H6, Lee HW7, Yu J7, Qi H8, Yu XJ6, Wang P3, Chu YW9, Yang M8, Hua ZC4, Ying HQ10, Hoffman RM11, Jeong LS7, Jia LJ2. Suppression of tumor angiogenesis by targeting the protein neddylation pathway Cell Death Dis. 2014 Feb 13;5:e1059.

344. Yeh S, Niu Y, Miyamoto H, Chang T, Chang C. Differential Roles of Androgen Receptor in Prostate Development and Cancer Progression. 2009. Androgen Action in Prostate Cancer. Book chapter, pp 73-89

345. Yi J, Lu G, Li L, Wang X, Cao L, Lin M, Zhang S, Shao G. DNA damage-induced activation of CUL4B targets HUWE1 for proteasomal degradation. Nucleic Acids Res. 2015 May 19;43(9):4579-90.

346. Yi JS, Park JS, Ham YM, Nguyen N, Lee NR, Hong J, Kim BW, Lee H, Lee CS, Jeong BC, Song HK, Cho H, Kim YK, Lee JS, Park KS, Shin H, Choi I, Lee SH, Park WJ, Park SY, Choi CS, Lin P, Karunasiri M, Tan T, Duann P, Zhu H, Ma J, Ko YG. MG53-induced IRS-1 ubiquitination negatively regulates skeletal myogenesis and insulin signalling. Nat Commun. 2013;4:2354.

347. Yoshimoto M, Ding K, Sweet JM, Ludkovski O, Trottier G, Song KS, Joshua AM, E Fleshner N, Squire JA, Evans AJ. PTEN losses exhibit heterogeneity in multifocal prostatic adenocarcinoma and are associated with higher Gleason grade. Mod Pathol. 2012 Sep 28.

348. Yu J, Yu J, Mani RS, Cao Q, Brenner CJ, Cao X, Wang X, Wu L, Li J, Hu M, Gong Y, Cheng H, Laxman B, Vellaichamy A, Shankar S, Li Y, Dhanasekaran SM, Morey R, Barrette T, Lonigro RJ, Tomlins SA, Varambally S, Qin ZS, Chinnaiyan AM. An integrated network of androgen receptor, polycomb, and TMPRSS2-ERG gene fusions in prostate cancer progression. Cancer Cell. 2010 May 18;17(5):443-54.

349. Yu ZK, Gervais JL, Zhang H. Human CUL-1 associates with the SKP1/SKP2 complex and regulates p21(CIP1/WAF1) and cyclin D proteins. Proc Natl Acad Sci U S A. 1998 Sep 15;95(19):11324-9.

350. Yuan J, Han B, Hu H, Qian Y, Liu Z, Wei Z, Liang X, Jiang B, Shao C, Gong Y. CUL4B activates Wnt/β-catenin signalling in hepatocellular carcinoma by repressing Wnt antagonists. J Pathol. 2015a Apr;235(5):784-95.

351. Yuan J, Jiang B, Zhang A, Qian Y, Tan H, Gao J, Shao C, Gong Y. Accelerated hepatocellular carcinoma development in CUL4B transgenic mice. Oncotarget. 2015b Jun 20;6(17):15209-21.

352. Yuan WC, Lee YR, Lin SY, Chang LY, Tan YP, Hung CC, Kuo JC, Liu CH, Lin MY, Xu M, Chen ZJ, Chen RH. K33-Linked Polyubiquitination of Coronin 7 by Cul3-KLHL20 Ubiquitin E3 Ligase Regulates Protein Trafficking. Mol Cell. 2014 May 22;54(4):586-600.

353. Yun J, Kim YI, Tomida A, Choi CH. Regulation of DNA topoisomerase IIalpha stability by the ECV ubiquitin ligase complex. Biochem Biophys Res Commun. 2009 Nov 6;389(1):5-9.

354. Zammarchi F, Boutsalis G, Cartegni L. 5' UTR control of native ERG and of Tmprss2:ERG variants activity in prostate cancer. PLoS One. 2013;8(3):e49721.

355. Zarif JC, Lamb LE, Schulz VV, Nollet EA, Miranti CK. Androgen receptor non-nuclear regulation of prostate cancer cell invasion mediated by Src and matriptase. Oncotarget. 2015 Mar 30;6(9):6862-76.

356. Zhai W, Yao XD, Xu YF, Peng B, Zhang HM, Liu M, Huang JH, Wang GC, Zheng JH. Transcriptome profiling of prostate tumor and matched normal samples by RNA-Seq. Eur Rev Med Pharmacol Sci. 2014;18(9):1354-60.

357. Zhang J, Hu MM, Wang YY, Shu HB. TRIM32 protein modulates type I interferon induction and cellular antiviral response by targeting MITA/STING protein for K63-linked ubiquitination. J Biol Chem. 2012 Aug 17;287(34):28646-55.

358. Zhang L, Altuwaijri S, Deng F, Chen L, Lal P, Bhanot UK, Korets R, Wenske S, Lilja HG, Chang C, Scher HI, Gerald WL. NF-kappaB regulates androgen receptor expression and prostate cancer growth. Am J Pathol. 2009 Aug;175(2):489-99.

359. Zhang S, Zhao H, Darzynkiewicz Z, Zhou P, Zhang Z, Lee EY, Lee MY. A novel function of CRL4(Cdt2): regulation of the subunit structure of DNA polymerase δ in response to DNA damage and during the S phase. J Biol Chem. 2013 Oct 11;288(41):29550-61. doi: 10.1074/jbc.M113.490466. Epub 2013 Aug 2.

360. Zhao Y, Xiong X, Jia L, Sun Y. Targeting Cullin-RING ligases by MLN4924 induces autophagy via modulating the HIF1-REDD1-TSC1-mTORC1-DEPTOR axis. Cell Death Dis. 2012 Sep 6;3:e386.

361. Zheng Q, Zhao LY, Kong Y, Nan KJ, Yao Y, Liao ZJ. CDK-associated Cullin 1 can promote cell proliferation and inhibit cisplatin-induced apoptosis in the AGS gastric cancer cell line. World J Surg Oncol. 2013 Jan 13;11:5.

362. Zong Y, Xin L, Goldstein AS, Lawson DA, Teitell MA, Witte ON. ETS family transcription factors collaborate with alternative signaling pathways to induce carcinoma from adult murine prostate cells. Proc Natl Acad Sci USA. 2009 Jul 28;106(30):12465-70.

363. Zou Y, Mi J, Cui J, Lu D, Zhang X, Guo C, Gao G, Liu Q, Chen B, Shao C, Gong Y. Characterization of nuclear localization signal in the N terminus of CUL4B and its essential role in cyclin E degradation and cell cycle progression. J Biol Chem. 2009 Nov 27;284(48):33320-32.

364. Zuo W, Huang F, Chiang YJ, Li M, Du J, Ding Y, Zhang T, Lee HW, Jeong LS, Chen Y, Deng H, Feng XH, Luo S, Gao C, Chen YG. c-Cbl-mediated neddylation antagonizes ubiquitination and degradation of the TGF-β type II receptor. Mol Cell. 2013 Feb 7;49(3):499-510.

Summary
The major aim of cancer therapy is to specifically suppress malignant neoplasm without detriment to normal cells. Modern therapeutic approaches exploit characteristic hallmarks of cancer cells, which render them susceptible to certain types of assault such as DNA damage, and mitotic and oxidative stress. Recently, the ubiquitin-proteasome system (UPS) has emerged as one of the principal cancer targets. In this work, a systematic approach, based on cascade organization, is described for screening the UPS. The effect of RNAi knockdown of individual UPS components on the viability of PCa cells was evaluated, with major focus on the TMPRSS:ERG-positive cell line, VCaP, as a model of the prevalent phenotype of prostate cancer. Seven genes have been identified to be particularly important for the functioning of PCa cells. Among them, UBE2U was the strongest hit. This thesis provides the first evidence for UBE2U involvement in prostate carcinogenesis and describes initial characterization of UBE2U as a potential drug target.
The prevalence of the components of the CRL/NEDD8 pathway in the hits (four out of seven) suggests the importance of neddylation to PCa biology. Two of these hits, CUL2 and RBX1, being specific to TMPRSS2:ERG-positive cells, were potentially ERG-dependent. This study reveals the crucial role of the CRL-exchange factor, CAND1, in particular, when neddylation is compromised. Knockdown of CAND1 induces apoptosis in VCaP cells which is further potentiated by neddylation-specific inhibitor MLN4924. CAND1 is, therefore, a novel potential drug target. Furthermore, this study has found that the inhibition of the CRL/NEDD8 pathway in PCa cells has a complex outcome that strongly depends on cellular context. The MLN4924 inhibitor induced apoptosis in all tested cell lines, though TMPRSS2:ERG positive cells were significantly more resistant. This study demonstrates that the increased resistance of VCaP cells reflects the plasticity of cancer cells is provided by the sophisticated interaction network ERG:NF-kB:c-Myc:Wnt/β-cat:AR. Partial inhibition of neddylation triggered transcriptional reprogramming of the VCaP cells, leading to cell quiescence and inhibition of proliferation-dependent apoptosis. This was a result of the re-activation of the AR program and the induction of a differentiation-like state. We conclude that the CRL/NEDD8 pathway regulates one of the cancer transcriptional networks which underlie cancer cell plasticity. This knowledge may help in the search for better treatments for TMPRSS2:ERG-positive cancers.
Finally, it was observed that neddylation inhibition changed the membrane properties and the morphology of VCaP cells. This was accompanied by dose-dependent changes in the level and localization of several membrane-associated proteins, including occludin, N-cadherin, paxillin and FAK. We thus conclude that CRL/NEDD8 pathway might be involved in the sorting/trafficking of membrane proteins. This part of the work requires further investigation, since gaining an understanding of its underlying mechanisms would be of general importance and may uncover a new role of the CRL/NEDD8 pathway in the regulation of cellular functions.
General conclusions:
1.We have obtained a comprehensive dataset on the involvement of all the human E1-E2 UPS components in the regulation of viability of PCa cells.
2.Our work has revealed new potential drug targets for PCa treatment: UBE2U and CAND1.
3.We have demonstrated the role of CRL/NEDD8 pathway in the regulation of cancer cell plasticity and morphology.